Lancaster University

Faculty of Health & Medicine

Division of Biomedical & Life Sciences

Neuroprotective effects of incretin mimetics upon chronic endoplasmic reticulum (ER) stress

Implications for novel therapeutic pathways and opportunities in Alzheimer's disease

Theodora Panagaki

PharmD, MSc

This thesis is submitted in fulfilment of the requirements for

the Degree of Doctor of Philosophy

June 2018

Declaration of Authorship

I, Theodora Panagaki, hereby declare that the current thesis, titled as ‘Neuroprotective effects of incretin mimetics upon chronic endoplasmic reticulum (ER) stress’, along with the presented work in it is my own. I confirm that:

- Any part of the current thesis has not been previously submitted for the award of a higher degree at Lancaster University or any other educational institution.
- Parts of the current thesis that have been published are clearly identified in the Chapter page
- Where I have consulted the published work of others, this is always clearly attributed.
- I have acknowledged all main sources of help.

Signed: ***T.Panagaki***

Date: 13 June 2018

"Imagine for a moment that we are nothing but the product of billions of years of molecules coming together and ratcheting up through natural selection, that we are composed only of highways of fluids and chemicals sliding along roadways within billions of dancing cells, that trillions of synaptic conversations hum in parallel, that this vast egglike fabric of micron-thin circuitry runs algorithms undreamt of in modern science, and that these neural programs give rise to our decision making, loves, desires, fears, and aspirations."

Dave Eagleman, *Incognito: The Secret Lives of the Brain*

Contents

List of Figures

List of Tables

Abstract

Growing evidence suggests that incretin mimetics exert neuroprotective and neurorestorative effects across a range of experimental models of neuronal degeneration. In a recent pilot clinical trial, Liraglutide rescued the decline of the cerebral glucose consumption in Alzheimer's disease (AD) patients, signifying improved energy metabolism in brain areas previously correlated with cognitive decline and disease progression. However, the exact underlying mechanism of action remains unclear. Chronic endoplasmic reticulum (ER) stress has emerged as a hub for the aberrant proteostasis underlying the onset and progression of neuronal degeneration that renders it a pivotal therapeutic target for AD. Herein, I examined the neuroprotective effects of Liraglutide along with the signalling network against the persistent and calcium-dependent ER stress in the human proliferating SH-SY5Y neuroblastoma cells. I report that Liraglutide modulated the ER stress response and elicited ER proteostasis and autophagy machinery homeostasis to restore the hyperactivity of the antioxidant Nrf2 factor and halt the impaired cell viability and proliferation. Mechanistically, Liraglutide engaged the Akt pathway and normalised the signal transducer and activator of transcription 3 (STAT3) activity to favour adaptive responses and shift cell fate towards survival under chronic stress conditions.

These findings have motivated me to replicate the phenotype in human post-mitotic neurones from the LUHMES cell line. I have further addressed the neuroprotective and restorative effects of a novel dual incretin against the chronic and calcium-dependent ER

stress. Novel dual incretin analogues have recently been developed and have displayed superior anti-hyperglycaemic and insulinotropic efficacy compared to Liraglutide, rendering them potent candidates for the treatment of diabetes mellitus type 2. Consistently, I showed that the chronic incretin treatment modulated the ER stress response and promoted homeostasis of the ER chaperones and autophagy machinery to rescue the excessive synapse damage and death of post-mitotic neurones. The incretin mimetics restored the suppressed Akt and signal transducer and activator of transcription 3 (STAT3) signalling to resolve the impaired activity of the antioxidant Nrf2 factor and confer trophic signals for neuronal repair following chronically persistent ER stress.

Finally, I have assessed the effects of the dual incretin in the $APP_{swe}/PS1_{\Delta E9}$ mouse model for AD at the age of 10 months and compared them to Liraglutide and the glucose-dependent insulinotropic peptide (GIP) mono-therapy. Once-a-day intraperitoneal administration of $25\,\mathrm{nmol\,kg^{-1}}$ of the dual incretin for two months halted the spatial cognitive decline and synapse damage of this murine model. It remarkably decreased the plaque deposition and gliosis over the $APP_{swe}/PS1_{\Delta E9}$ mouse cortex and hippocampus too. The attenuation of the AD-like pathology reflected the resolution of ER stress and restoration of autophagy impairments, both lying downstream of the rectified Akt signalling.

Collectively, the findings presented in the current thesis endorsed the beneficial effects of the incretin signalling in the neuronal degeneration management and further deepened our understanding of the incretin neuropharmacology.

Abbreviations

Aβ	Amyloid β
AD	Alzheimer's disease
ADAM10	Disintegrin and metalloproteinase domain-containing protein 10
AICD	APP intracellular domain
AMPK	5' Adenosine monophosphate–activated protein kinase
APP	Amyloid precursor protein
ARE/EpRE	Antioxidant/electrophilic response element
ASK1	Apoptotic signalling kinase 1
Asp	Aspartic acid
ATF4	Activating transcription factor 4
ATF6	Activating transcription factor 6
Atg	Autophagy-related
ATP	Adenosine triphosphate
BACE1	β-site APP cleaving enzyme-1
BAD	Bcl2 – associated death promoter
BAK	Bcl2 – homologous antagonist/killer protein
BAX	Bcl2 – associated X protein
Bcl2	B cell lymphoma 2
Bcl-X_L	B cell lymphoma extra large

BDNF	Brain-derived neurotrophic factor
BFA	Brefeldin-A
BID	BH3 interacting-domain death agonist
BIM	Bcl2 – interacting mediator of cell death
BiP/Grp78	78-kDa Glucose-related protein
BrdU	5-bromo- 2'-deoxyuridine
BSA	Bovine serum albumin
cAMP	Adenosine-3',5'-cyclic monophosphate
CASP	Caspase
Chop/GADD153	CAAT/enhancer-binding protein (C/EBP) homologous protein
CST	Cell Signaling Technology
CTCF	Corrected total cell fluorescence
DA	GLP1/GIP dual agonist
DAB	(3,3'-diaminobenzidine
db-cAMP	N^6 2'-O-Dibutyryl cAMP sodium salt
DMSO	Dimethyl sulfoxide
ECE1	Endothelin converting enzyme 1
ECE2	Endothelin converting enzyme 2
eIF2α	Eukaryotic translation initiator factor 2α
ER	Endoplasmic reticulum
ERAD	ER-associated degradation
ERK1/2	Extracellular signal–regulated kinases 1/2
ERO1α	ER oxidoreductin 1α protein
FAD	Familial AD
FBS	Foetal bovine serum

FGF	Fibroblast growth factor
FTDP-17	Frontotemporal dementia and parkinsonism linked to chromosome 17
FTLD	Frontotemporal lobar degeneration
GADD34	Growth arrest and DNA damage-inducible protein
GDNF	Glial cell-derived neurotrophic factor
GFAP	Glial fibrillary acidic protein
GIP	Glucose-dependent insulinotropic polypeptide
GRP94	94-kDa Glucose-related protein
GLP1	Glucagon-like peptide-1
GSK3β	Glycogen synthase kinase 3β
GVD	Granulovacuolar degeneration
H_2O_2	Hydrogen peroxide
HPLC	High performance liquid chromatography
HRP	Horseradish peroxidase
Hsp27	27-kDa Heat-shock protein
Hsp72	72-kDa Heat-shock protein
IBA1	Ionized calcium-binding adapter molecule 1
IgG	Immunoglobulin G
IKK	IκB kinase
IP_3R	Inositol 1,4,5-trisphosphate receptor
IRE1	Inositol-required 1
JNK	c-Jun N-terminal kinase
Keap1	Kelch-like ECH-associated protein 1
LIRA	Liraglutide
LIXI	Lixisenatide

LDH	Lactate dehydrogenase
LUHMES	Lund human mesencephalic
MALDI–TOF	Matrix-assisted laser desorption/ionisation time-of-flight mass spectrometry
MAPK	Mitogen-activated protein kinase
MT	Microtubule
mTOR	Mammalian target of rapamycin
MW	Molecular weight
N/A	Not applicable
NFκB	κ-light-chain-enhancer of the activated B cell
NGF	Nerve growth factor
NMDA-R	N-methyl-D-aspartate receptor
NOX	Nicotinamide adenine dinucleotide phosphate-oxidase
Nrf2	Nuclear respiratory factor 2
ns	Non significant
NTFs	Neurofibrillary Tangles
PARP	Poly (ADP-ribose) polymerase
PBS	Phosphate buffered saline
PDI	Protein disulphide isomerase
PEN-2	Enhancer of presenilin-2
PERK	Protein kinase RNA-like ER kinase
PFA	Para-formaldehyde
PKA	Protein kinase A
PKB	Protein kinase B, also known as Akt
PKR	Double-stranded RNA-dependent protein kinase
PP1	Protein phosphatase 1

PRAS40	Proline-rich Akt substrate protein of 40kDa
PSD95	Post synaptic density protein 95
PS	Presenilin
PUMA	p53 up-regulated modulator of apoptosis
p70S6K	p70 S6 kinase
ROS	Reactive oxygen species
RIDD	IRE1 dependent decay
rpS6	Ribosomal protein S6
RyRs	Ryanodine receptors
SEM	Standard error
Ser	Serine
SERCA	SarcoER calcium ATPase
SNPs	Single nucleotide polymorphisms
STAT	Signal transducer and activator of transcription
TBS	Tris buffered saline
TBT–T	TBS with 0.05% Tween® 20
TG	Thapsigargin
Thr	Threonine
TNF	Tumour necrosis factor
TRAF2	TNF receptor-associated factor 2
Tyr	Tyrosine
UPR	Unfolded protein response
VDAC	Voltage-dependent anion channel
XBP1	X box-binding protein 1
XTT	2,3-Bis-(2-methoxy-4-nitro-5-sulphophenyl)-2H-tetrazolium-5-carboxanilide

WT	Wild-type

Chapter 1

Introduction

1.1 Alzheimer's disease

Alzheimer's disease (AD) is a devastating neurodegenerative disorder characterised by gradual cognitive, behavioural and functional decline. It typically manifests with episodic-memory impairments that halt the acquisition of new long-term memories and obscure the recollection of recent events, including autobiographical. Episodic-memory impairments persist over the disease course and are further accompanied by an increasing deterioration in diverse cognitive domains related to language, spatial orientation and memory, reasoning, judgment, problem-solving and the processing of longer-term declarative memory from the patient's former years, among others. As such, the patient progressively becomes incapable of looking after and even articulating their own daily needs. Abnormal behaviour consisting of social withdrawal, depressive dysphoria, aimless and restless activity, and aggression often accompanies the patient's clinical profile. AD ultimately culminates in death, with a median survival of 12 years following its onset.[78]

AD currently afflicts more than 46.8 million worldwide, with a newly diagnosed case every 3 seconds. It affects individuals of all races and ethnic groups, occurring slightly more often in women than in men. Ageing represents the principal risk factor for the disease development. The incidence doubles every five years over 65 years of age and approach one in three over 85 years of age.[242] Regrettably, there is neither a remission in the disease progress nor are there any disease-stabilising agents currently available. Existing therapeutic options solely promote a temporary symptomatic relief.[42,97,125] Furthermore, the AD multi-factorial aetiology is widely recognised, though the molecular intricacies that stimulate the central nervous system derangements remain elusive. Indeed, only a small percentage of cases ($< 5\%$) stem from mutations in three genes – the amyloid precursor protein (APP), presenilin (PS)-1 and PS2 – that cause an early-onset (< 60 years of age) autosomal dominant AD (also termed as familial AD).[125] Meanwhile, epidemiological studies indicate that AD will become even more prevalent with a prognosis of 131.5 million cases worldwide by the mid-century, raising a substantial health concern and economic burden on society.[242] As such, an improved understanding of AD aetiopathogenesis along with the discovery of disease-modifying drugs are now the pharmacological research priorities.[42,97,125]

Histopathologically, the AD brain features the accumulation of two classes of highly-insoluble, densely-packed filaments – the extracellular amyloid plaques (also, termed as "senile" plaques) and the intracellular neurofibrillary tangles (NTFs). The latter is composed of an abnormally hyper-phosphorylated and aggregated form of the τ protein. Normally, τ is a highly-soluble microtubule-associated protein (MAP) abundant in axons. There, it regulates the assembly and stability of microtubules and thereby the organelle and vesicle transport between the neural compartments. Aberrant phosphorylation of τ renders it insoluble whilst diminishing its affinity for the microtubules. As such, hyper-phosphorylated τ accumulates into the somatodendritic compartment where it self-associates into paired, helically-wound structures of 10 to 20 nm in diameter coalescing into insoluble tangles. The senile plaques primarily consist of a 4.3 kDa β-amyloid peptide (Aβ) that originates from the sequential proteolytic cleavage of the APP protein by the β-site APP-cleaving enzyme 1 (BACE 1; also known as β-secretase 1) and γ-secretase complex.[246] At physiologic levels, Aβ modulates the synaptic strength to prevent neuronal hyperactivity upon stimulation. Neuronal activation triggers the biosynthesis and secretion of Aβ peptide that seems to function as a negative feedback mechanism for vesicle release and neurotransmission at the excitatory synapse.[141] However, the defective proteostasis that governs AD favours and exacerbates the accumulation of Aβ. This in turn can readily self-aggregate into lower-molecular-weight oligomers (2–6 peptides) forming further intermediate assemblies. Alternatively, accumulated Aβ peptides can coalesce themselves into higher-molecular-weight fibrils acquiring β-pleated structures to formulate the insoluble fibres of the advanced amyloid plaques. The size of the Aβ aggregated form determines its toxicity, with the soluble oligomeric and intermediate assemblies exerting the highest neurotoxic effect.[246] Both the amyloid plaques and NTFs represent the pathognomonic features required for the disease diagnosis during the *post-mortem* brain examination. Nevertheless, it would be misleading to create the impression that these are the only lesions occurring in the AD brain. In fact, multiple structural and functional alterations ensue – *e.g.,* oxidative stress, cell energy deprivation,[75, 238] dysregulated calcium signalling,[20, 96] deficient proteasome-mediated and autophagy-mediated clearance of damaged proteins and organelles,[219, 220] aberrant gliosis, and abnormal inflammatory responses.[92, 188, 202] Altered cholinergic function and glutamatergic signalling – deriving from the impaired synthesis of the neurotransmitter acetylcholine and the defective glial-mediated glutamate re-uptake in the synaptic cleft, respectively – along with the subsequent over-activation of the N-methyl-D-aspartate (NMDA) receptor calcium channel occur in the AD brain.[234, 291] In addition to the cholinergic and glutamatergic dysfunction, the AD brain displays reduced levels of noradrenergic and serotonergic markers[39, 291] and the suppressed expression of the brain-derived neurotrophic factor (BDNF) and nerve growth factor (NGF). The survival of the neurones and glial cells, memory formation and behavioural plasticity all rely on the availability of neurotrophic factors.[246] Decreased expression and membranous distribution of the insulin receptor along with a compromised insulin signalling occur in the AD brain too.[254, 280, 288] The insulin signalling is essential to neuronal survival, the regulation of synapse population and postsynaptic plasticity.[54] These lesions altogether culminate in the aberrant synaptic damage and neuronal death in numerous brain areas and especially in those for higher-order cognitive processing, *i.e.*, the basal forebrain and hippocampus.[54, 56, 75, 96, 202, 238, 246, 262] Synapse dysfunction is the most potent clinical correlate of the cognitive decline[262] while the excessive neuronal loss potentiates atrophy of the AD brain that may weigh the one-third of the brain from an age-matched, non-demented individual at the time of death.[246,278]

1.1.1 Towards an ER-centric approach

Determining the molecular mechanisms by which the various pathological alterations compromise the neuronal function and integrity and potentiate disease symptomatology has been a long-standing goal of the AD research. Intriguingly, the aberrant deposition of misfolded proteins, compromised clearance of damaged organelles and proteins, neuroinflammation, defective calcium dynamics, mitochondrial dysfunction, excitotoxicity, and synapse degeneration converge into the occurrence of chronic stress of the endoplasmic reticulum (ER).[20,30,111,224,235,258] The ER is a dynamic membrane system that, in neurones, extends from the soma to the entire dendrite arbour, including some dendritic spines, and to the axon.[249] It is the cardinal sub-cellular compartment for the protein synthesis and quality control of nearly one-third of the total proteome,[111,235,261] including the APP[301] and insulin.[173] In fact, it is highly enriched in molecular chaperones and foldases that assist proper folding and maturation of proteins entering the secretory pathway while the unique ER oxidising environment pivotally impacts the activity of protein disulphide isomerases (PDIs).[261] Oxidised PDIs catalyse the formation and re-arrangement of disulphide cross-links between cysteine residues that in turn determine the stability and function of proteins destined for secretion or membrane display.[27,261] The ER is additionally central to the biosynthesis of lipids, autophagosomes and peroxisomes[111,235,261] and the major calcium storage depot in the cell.[284] Calcium release from the ER mediates neurotransmitter exocytosis at the pre-synapse whilst potentiating gene transcription and modulating membrane excitability and dendritic spine structure for post-synaptic plasticity.[152,201,284] Upon release, the sarcoplasmic/ER calcium ATP–ase (SERCA) channel buffers calcium re-uptake from the cytosol into the ER to replenish the local calcium stores,[284] which are critical for protein folding reactions and chaperone function. For instance, the 78-kDa glucose-regulated protein (GRP78, also termed as BiP), calnexin and calreticulin are calcium-dependent chaperones that slow folding reactions and stabilise folding intermediates to prevent their aggregation within the organelle lumen.[261]

Many physiological and pathological stimuli can alter the protein folding process at the ER triggering a rise in the unfolded or misfolded protein load in its lumen, a cellular state referred to as ER stress.[261] In turn, the cell activates an adaptive signalling network, known as the unfolded protein response (UPR). The UPR initially aims to reinforce proper protein folding, attenuate protein influx into the ER, stimulate ER-membrane expansion and thereby restore normal ER function. It further modulates the cell degradation machinery to eliminate the abnormal protein load and re-establish proteostasis. Non-native conformers can be eliminated through the ER-associated protein degradation (ERAD) pathway, in which the unfolded proteins are retro-translocated to the cytosol and subjected to ubiquitylation and proteasome-mediated degradation. Larger protein aggregates and dysfunctional organelles are sequestered in double-membrane vacuoles (autophagosomes) and subsequently fused with lysosomes for degradation. However, upon stress chronicity, the UPR adapts its dynamics and shifts cell fate towards apoptosis.[109,111,261]

Apoptosis may serve a physiological role in eliminating cells unresponsive to the UPR.[111] However, in AD, the engagement of the apoptotic signalling is more likely to drive degeneration, in which synapse is the initiation point.[111,224,258] Indeed, the persistent accumulation of Aβ and phosphorylated τ provokes a chronic ER disturbance and stress that depletes synapse components and dampens synaptic functioning.[79,224] Pharmacological and genetic attenuation of chronic ER stress has successfully restored pathognomonic features and behavioural impairments of diverse animal models of neuronal degeneration, including AD.[111,235] Recent evidence further indicates that the UPR network may regulate τ

phosphorylation and Aβ metabolism. As such, therapeutic interventions which resolve the UPR towards a balance between protein generation and degradation and promote ER homeostasis may significantly benefit the Alzheimer's clinical outcome.[30,235] Following by more and more UPR markers detected in the *post-mortem* brain samples from affected patients[99,119,120,160,283,314] and animal models of AD,[3,13,90,253,267] the relationship between ER stress and AD currently attracts increasing attention. In the following sections, I provide a comprehensive overview of the signalling network activated upon ER stress and discuss recent advances that mechanistically link ER stress to the AD onset and progression.

1.2 The UPR signalling network

The UPR engages two central components, a group of specialised stress sensors and transcription factors that re-programme gene expression and enable either adaptation to stress or the induction of apoptosis. Protein kinase RNA-like ER kinase (PERK), activating transcription factor 6 (ATF6) and inositol-requiring enzyme 1 (IRE1) are the three signalling effectors of the UPR (**Figure 1.1**). Under homeostatic, non-stressful conditions, the N-termini of IRE1 and PERK and the C-terminus of ATF6 are bound to BiP within the organelle lumen and maintained at an inactive state. Upon ER stress, the unfolded or misfolded proteins accumulate and sequester BiP from the intra-luminal domains of the UPR effectors, triggering their activation.

PERK is a *Ser/Thr* protein kinase of which the catalytic core shares substantial homology to the eukaryotic translation initiation factor 2α (eIF2α). Upon BiP sequestration, PERK self-dimerises in the ER membranes, inducing its auto-phosphorylation and kinase domain activation. Activated PERK in turn phosphorylates eIF2α at the serine 51 (Ser 51) residue that downstream impedes the delivery of the initiator methionyl-tRNA to the ribo-

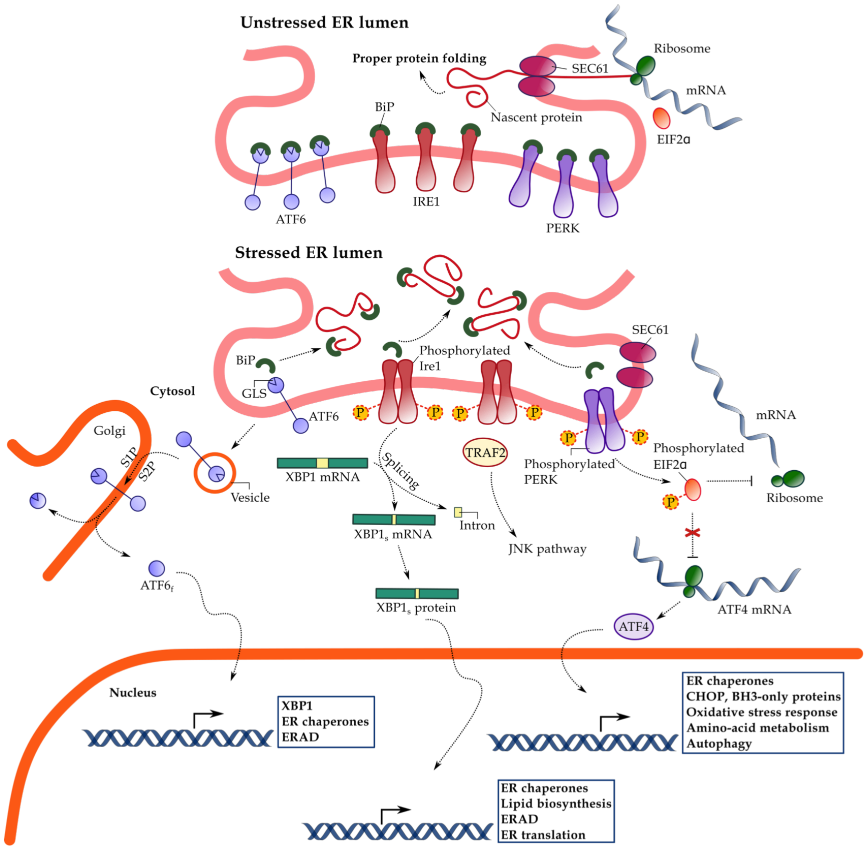

Figure 1.1: **The UPR signalling in mammals.** Accumulation of non-native conformers in the endoplasmic reticulum (ER) lumen initiates the unfolded protein response (UPR). Protein kinase RNA-like ER kinase (PERK), activating transcription factor 6 (ATF6) and inositol-requiring enzyme 1 (IRE1) are the three main signalling branches that mediate the UPR. Under ER stress, ATF6 translocates to Golgi where resident site-1 protease (S1P) and S2P cleave the factor to generate an active cytosolic ATF6 fragment (ATF6f). ATF6f functions as a transcription factor to induce the expression of genes encoding ER chaperones, ER-associated protein degradation (ERAD) components and the X-box protein 1 (XBP1). Activated PERK phosphorylates the eukaryotic translation initiation factor 2α (eIF2α) that represses global protein translation, except for the translation of ATF4 mRNA. Once translated and emigrated to the nucleus, ATF4 stimulates the expression of genes for protein quality and redox control, autophagy and amino acid metabolism. ATF4 additionally regulates the expression of the CAAT/enhancer-binding protein (C/EBP) homologous protein (Chop) that functions as a node of a feedback mechanism for the de-phosphorylation of eIF2α and re-initiation of protein synthesis. Active IRE1 induces the splicing of XBP1 mRNA, leading to the expression of an active transcription factor XBP1s. The latter up-regulates a gene transcription programme for protein quality control, ERAD and lipid biosynthesis. Besides XBP1, IRE1 endoribonuclease activity identifies and degrades a subset of mRNAs localised to ER membrane through the regulated IRE1 dependent decay (RIDD) pathway. IRE1 regulates ERAD, autophagy and apoptosis through XBP1-independent pathways; it recruits the TNF (tumour necrosis factor) receptor-associated factor 2 (TRAF2) that lies upstream of the activation of Jun-N-terminal kinase (JNK) signalling.

some and ceases global protein translation. The inhibition of protein synthesis initially aims to attenuate the overload of nascent proteins in the organelle lumen and promote cell survival. Paradoxically, these conditions favour the translation of a specific subset of mRNAs, including the mRNA encoding transcription factor ATF4. ATF4 is a basic region-leucine zipper (bZIP) transcription factor of the mammalian ATF/CREB family and regulates expression of genes involved in amino acid metabolism, autophagy and antioxidant responses. However, not all ATF4-induced genes are anti-apoptotic; in fact, PERK/ATF4 arm stimulates the transcription of CAAT/enhancer-binding protein (C/EBP) homologous protein (Chop; also termed as growth-arrest, DNA-damage 153 – GADD153) which, as detailed later, is an important mediator of the apoptotic UPR signalling.[109,261] PERK can additionally potentiate the bZIP Cap 'n' Collar transcription factor nuclear respiratory factor 2 (Nrf2) to favour adaptive responses following ER stress. Normally, Nrf2 is mainly localised to the cytoplasm in a complex with the Kelch-like ECH-associated protein 1 (Keap1), an ubiquitin ligase substrate adaptor that targets Nrf2 for degradation. Activated PERK can directly phosphorylate Nrf2 at Ser 40 and trigger its dissociation from the Keap1 complex. Nrf2 can then rapidly translocate into nucleus where it dimerises with other transcription factors, *e.g.,* the small musculoaponeurotic fibrosarcoma proteins. The heterodimer in turn binds to the antioxidant/electrophilic response element (ARE/EpRE) and stimulates the transcription of genes encoding antioxidant proteins, detoxifying enzymes, proteasome subunits, and autophagic components.[230]

IRE1 is a type I transmembrane protein with an ER luminal dimerisation domain and a cytoplasmic domain with Ser/Thr kinase and endoribonuclease (RNAase) activities. It exists in two isoforms – the IRE1α and IRE1β – that solely differ in tissue expression. IRE1α ubiquitously expresses while the IRE1β expression is predominant in the intestinal epithelial cells. When released by BiP, IRE1 similarly undergoes self-oligomerisation in the ER membranes and trans-autophosphorylation to activate its RNAase domain. The latter excises a 26-nucleotide intron from the X-box protein 1 (XBP1) mRNA. This splicing reaction shifts the reading frame of the mRNA and renders it competent for translation to produce the 41-kDa spliced XBP1 protein. Spliced XBP1 is a stable and active bZiP transcription factor that regulates the expression of UPR target genes involved in the retrograde transport of unfolded proteins from the ER to the cytosol, ERAD, autophagy, and ER biogenesis, among others.[109,110] Besides XBP1, the IRE1 RNAase can identify and target a subset of ER membrane-localised mRNAs to the regulated IRE1-dependent decay (RIDD) pathway for degradation and thus attenuate the protein influx into the organelle lumen upon ER stress (discussed in detail by Hetz, C. *et al.*[110]). The cytoplasmic kinase domain of the phosphorylated IRE1 recruits the TNF (tumour necrosis factor) receptor-associated factor 2 (TRAF2) and activates the apoptotic signalling kinase 1 (ASK1) and IκB kinase (IKK) to modulate autophagy and inflammatory responses, respectively. ASK1 lies upstream the activation of the 'alarm stress pathways', the Jun-N-terminal kinase (JNK) and p38 mitogen-activated protein kinase (MAPK) cascades while IKK is the major activator of the nuclear factor κ-light-chain-enhancer of the activated B cell (NFκB) signalling.[110] The IRE1α/TRAF2/ASK1/JNK1 might also activate the Nrf2 pathway.[298] However, the exact impact of these downstream UPR signalling cascades in the context of ER stress remains partially understood and most of the reports monitor these kinases as stress markers only.[110]

Following the release from the BiP complex, ATF6 translocates to the Golgi complex. Golgi-resident site-1 and site-2 proteases cleave the factor at the juxtamembrane site and generate an active cytosolic ATF6 fragment. The latter emigrates to the nucleus where it activates gene transcription programmes for cell adaptation, including the up-regulation of ERAD components and the PDI and BiP chaperones of the ER quality control machinery. Active ATF6 can bind to the promoter and enhance the expression of XBP1 whilst dimerising with the spliced XBP1 to instigate specific patterns of gene expression.[109–111]

1.2.1 The UPR signalling network during the apoptosis phase

When the intensity or duration of the stress stimuli exceeds the buffering capacity of the UPR, the pathway adapts its signalling dynamics towards a disproportionate activity of its effectors and a 'terminal UPR' signalling. Although the molecular intricacies switching from survival towards cell suicide remain enigmatic and may differ among the cell types, 'terminal UPR' engages proteases, kinases, transcription factors, and B-cell lymphoma-2 (Bcl-2) family components to induce the intrinsic and extrinsic pathways of apoptosis.[109,111,210]

The predominant 'terminal UPR' signalling node is the bZiP transcription factor Chop[109,111] that lies downstream of the sustained activation of PERK/ATF4 arm.[169] Chop co-operates with ATF4 to transcriptionally activate GADD34 expression. GADD34 regulates global protein translation under stress conditions. It forms a functional complex with protein phosphatase 1 (PP1) to de-phosphorylate eIF2α and thereby re-initiate protein synthesis. This phenomenon, however, within persistently stressed cells can lead to ATP depletion, exacerbate unfolded protein overload in the ER lumen, and induce oxidative stress and altogether cell death.[100] Furthermore, Chop up-regulates the ER-oxidoreductin 1α protein (ERO1α)[109,111,303] that harnesses the oxidising power of the molecular oxygen to oxidise the active cysteinyl-thiol groups in PDI, enabling the latter to introduce disulphide bonds to folding substrates and to maintain the thiol-disulphide exchange and PDI capacity for the bond isomerisation within nascent polypeptides.[27] As such, the Chop-induced up-regulation of ERO1α expression perturbs oxidative folding and therefore redox conditions within the ER lumen.[191] It additionally triggers the inositol-1,4,5-trisphosphate receptor (IP_3R)-mediated calcium efflux into cytosol,[163] which in turn can detrimentally influence mitochondrial function and multiple pathways upstream of the ‘core’ (intrinsic) apoptosis machinery.[144,303] Indeed, a significant fraction of IP_3Rs is localised to highly specialised tethers that physically connect ER cisternae to mitochondria (mitochondrial-associate membrane, abbreviated as MAM) and regulate calcium dynamics at the ER-mitochondrion interface. In that sense, a massive calcium release into the mitochondria can potentiate the production of reactive oxygen species (ROS), cytochrome C release, caspase (CASP) cascade (*e.g.*, CASP3, CASP9) and autophagy fail.[274,303]

In addition to ERO1α, Chop downstream precludes the transcription of the pro-survival Bcl-2 protein whilst favouring the expression of Bcl2-interacting mediator of cell death (BIM) and p53 up-regulated modulator of apoptosis (PUMA). Such an imbalance between pro-survival versus anti-apoptotic Bcl-2 components provokes the oligomerisation and activation of the pro-apoptotic Bcl2-associated X protein (BAX) and Bcl2-homologous antagonist/killer protein (BAK) in the mitochondrial membranes. BAX impedes the interaction of the anti-apoptotic Bcl-X_L protein with IP_3Rs, perturbing ER calcium release and stimulating the intrinsic (mitochondrial-dependent) apoptotic machinery.[109,144,303] Perturbed calcium dynamics can further induce the proteolytic (activating) cleavage of the ER-resident CASP12.[211] Active CASP12 also potentiates a downstream caspase cascade that executes the degradation of the poly (ADP-ribose) polymerase (PARP) to assure the fulfilment and irreversibility of the apoptotic process.[147,203,212] Besides the modulation of redox signalling and core apoptosis machinery, Chop can limit autophagy through the transcriptional regulation of autophagy-related (Atg) components for phagophore elongation and maturation into the autophagosome[16,17] that may, in turn, exacerbate defective proteostasis reinforcing cell suicide.[30,274] Apart from Chop, the PERK arm induces the expression of death receptor 5 (DR5) to engage the extrinsic apoptosis pathway and trigger CASP8 activation for cell death execution.[184]

Chronic ER stress may provoke the transition from the IRE1 homo-dimeric form to higher-order oligomeric structures, pivotally determining the 'switch' from adaptive towards the apoptosis phase. Sustained RIDD activity can deplete essential chaperones for protein folding and maturation, exacerbating the abnormal protein load within the organelle lumen and worsening ER stress. Aberrant IRE1 RNAase activity selectively diminishes microRNAs that normally suppress the pro-inflammatory and pro-death targets,[109] such as the pro-oxidant thioredoxin-interacting protein (TXNIP) and CASP2, culminating in their up-regulation.[162] Increased TXNIP engages CASP1 activity for inflammasome complex formation and thus signals to the programmed-lytic cell death pathway.[162] Finally, the sustained IRE1 kinase activity can induce apoptotic signalling cascade through the downstream activation of ASK1/JNK. The latter deranges the expressions levels of the Bcl-2 family components towards the pro-apoptotic factors, such as BIM.[109,144,303] Activated MAPKs may also phosphorylate Chop at Ser78 or Ser81 and thereby reinforce the apoptotic and transcriptional activity of this factor at a post-translational level.[194,304]

1.3 The ER stress in AD

1.3.1 The UPR component in the Alzheimer's brain

The UPR activation has repeatedly been detected in the *post-mortem* brain samples from affected patients[99,119,120,160,283,314] and animal models of AD.[3,13,90,253,267] Increased BiP expression and phosphorylation of IRE1α, PERK and eIF2α occur in morphologically intact neurones of the cortex and hippocampus at the early disease stages,[99,119,120] preceding the overt amyloid deposition in the AD brain.[99,121] Meanwhile, the up-regulation of pro-apoptotic UPR components, including Chop expression and CASP12 proteolysis occurs at the late disease stages (Braak stage *VI*), signifying the occurrence of persistent ER stress in the AD brain.[160,314] In addition to UPR effectors and pro-apoptotic components, the

AD frontal cortex features the elevated expression of *HERP1* gene, which lies downstream of the UPR network and encodes a protein with an N-terminal ubiquitin-like domain that interacts with the ERAD system.[257] Interestingly, HERP1 up-regulation occurs in brain areas enriched in amyloid plaques.[257] Furthermore, the expression of a spectrum of chaperones, including the 72-kDa heat-shock protein (Hsp72), GRP94, PDI, and calreticulin, is abnormally elevated in the AD brain and cerebrospinal fluid[99,170,296,313] with the Hsp72 exclusively localised in neuritic plaques and NTFs.[99] Correspondingly, aged Tg2576 mice expressing a mutant form of APP (isoform 695) exhibit signs of the UPR activation, including abnormal eIF2α phosphorylation and BiP expression.[253] Likewise, the brain of the $APP_{swe}/PS1_{\Delta E9}$ mouse model – that over-expresses the Swedish mutation of APP together with the PS1 exon 9 deletion – features the elevated BiP and Chop expressions along with enhanced activity of the ER-resident CASP12.[13]

Although all these reports validate the activation of the UPR in the AD brain, it remains elusive what triggers the UPR in neurones. Amyloid plaques and tangles do not localise in the ER. However, numerous studies have demonstrated that the cell exposure to the Aβ oligomers and fibrils triggers ER stress in neuronal-like cell lines, primary neuronal cultures and, organotypic hippocampal slices. The ER dysfunction is evident by the increased PERK and eIF2α phosphorylation, deranged XBP1 mRNA splicing, and the up-regulation of Chop, BiP, and PDI in these studies,[3,33,34,36,74,128,143,153,218,264] reminiscent of the UPR profile in the *post-mortem* AD brain samples. Neural cells from pluripotent stem cells of sporadic and familial AD cases spontaneously manifest the ER-stress response, attributed to the intracellular accumulation of Aβ oligomers.[151] Aβ oligomers interact with the NR2B subunit of NMDA receptor that in turn induce an early rise of calcium levels in the cytosol of the primary hippocampal rat neurones. This increment stimulates the activation of nicotinamide adenine dinucleotide phosphate-oxidase (NOX) and concomitant production of superoxide radicals, resulting in ER calcium depletion and the UPR induction.[49] Aβ

peptides can additionally flux toxic amounts of calcium into the cytoplasm through the voltage-gated calcium channel (VGCC) in human neuroblastoma cells and mouse cortical neurones,[65] as well as by forming and inserting ion-channel-like structures with high cation conductivity in the planar bilayer membrane too.[5] Notably, such pores exist in the neuronal cell membrane from AD patients.[129] Aβ oligomers further disrupt the calcium content within the ER lumen, as a consequence of the enhanced calcium release through the IP_3Rs and ryanodine receptors (RyRs) in cultured neurones.[73] In addition to neurones, Aβ oligomers perturb the calcium homeostasis to provoke ER stress and excessive gliosis in cortical and hippocampal astrocytes from primary rat cultures and organotypic slices from the triple-transgenic mouse model of the AD,[3] signifying a common mechanism for the UPR activation between neuronal and glial cells.

1.3.1.1 The UPR as an executioner of the Aβ-derived degenerative & apoptotic signals

Mechanistically, the ER stress appears to mediate the neurotoxic effects of Aβ (reviewed in[72,143]). More than a decade ago, a pioneering study in the UPR field showed that the Aβ-induced apoptosis requires the specific activation of the ER resident CASP12. As such, CASP12 knockdown renders cortical neurones resistant to Aβ toxicity, when compared to the wild-type ones.[212] Subsequent studies have confirmed this finding[247,277] and further revealed that Aβ requires CASP12 to induce degeneration of the pre-synapse with decrements in local mitochondrial function and availability of cytoskeletal and synaptic-vesicle components.[207,247] ER stress signals to mitochondrion and perturbs its function and membrane potential to engage the mitochondrial apoptotic machinery in response to Aβ.[46–48,74] Mitochondrial dysfunction in turn enhances susceptibility to Aβ-induced ER stress and ultimately favour cell suicide.[47] Furthermore, the oligomeric Aβ application in the distal axone induces PERK phosphorylation and the subsequent local synthesis of ATF4. The latter translocates to the neuronal cell body and transmits the neurodegeneration signal through the somatic up-regulation of Chop expression. Locally synthesised ATF4 can further potentiate axonal damage via a cell-non-autonomous mechanism that propagates among neurones. In animal models over-expressing mutant APP and PSEN1 (5XFAD mouse model) or intra-ventricularly injected with the Aβ peptide, ER stress engages the MAPK signalling cascade, including JNK, to induce apoptosis and cognitive impairments.[90,314] Indeed, the pharmacological restoration of ER stress rescues the aberrant apoptosis and MAPK kinase activation in the hippocampus of the intra-ventricularly Aβ-injected animals.[90] JNK ablation from 5XFAD mouse model alleviates memory deficits and amyloid pathology in the hippocampus and cortex and switch neuronal fate towards survival.[314] Similarly, the UPR resolution coincides with a decreased intra-neuronal Aβ immunoreactivity, enhanced expression of plasticity-related proteins and restored spine density in the hippocampus of the Tg2576 mouse model of AD at the age of 12 and 16 months.[253]

However, it is debatable whether the ER stress is a constant mediator of the neurotoxic signals of the Aβ peptide. For instance, a normal expression and activity of the UPR effectors and pro-apoptotic components (*e.g.,* caspase 12 and Chop) characterise the brain from 17-month old Tg2576 mice,[160] contradicting the earlier findings. Furthermore, the extracellular accumulation of Aβ does not impact the XBP1 mRNA splicing, PERK phosphorylation and *CHOP* transcription in primary cortical neurones. Instead, it induces neuronal apoptosis through an UPR-independent mechanism.[319] Differentiated neuroblastoma cells treated with Aβ oligomers manifest only a 'mild' ER stress, with a subtle UPR induction in a fraction of cells when a fluorescent ER stress indicator employed but completely undetectable in biochemical studies.[35] A subsequent study has demonstrated that the Aβ treatment preferentially activates the PERK/eIF2α arm of the UPR network in neuroblastoma cells, constituting an early response to the peptide.[161] These researchers further suggest that this early stimulation of PERK/eIF2α signalling and increased BiP expression both function to resolve the Aβ-induced ER-stress and preclude apoptosis.[161]

1.3.1.2 The UPR as a link to early τ pathology

Aberrant τ phosphorylation and accumulation characterises a group of increasingly prevalent disorders that are classified as tauopathies, including AD. Although the underlying mechanism for τ hyper-phosphorylation in tauopathies remains elusive, recent evidence implicates ER stress to the early stages of τ pathology.[66,118] In the AD brain, phosphorylated PERK immunoreactivity occurs in hippocampal neurones with diffuse phosphorylated τ whilst being almost absent in tangle-bearing neurones, signalling for the UPR activation at an early stage of the neurofibrillary degeneration.[119] A more recent autopsy study has addressed the UPR activation in sporadic tauopathies, including progressive supranuclear palsy and Pick's disease and familial cases with frontotemporal dementia and parkinsonism linked to chromosome 17 (FTDP-17) that carry mutations in *MAPT* gene encoding τ. Phosphorylated PERK and IRE1α are abundant in hippocampal neurones and glia of frontotemporal lobar degeneration with tau pathology (FTLD-tau) cases and young carriers of *MAPT* mutation, but completely undetectable in other FTLD subtypes negative for τ pathology.[217] Moreover, a genome-wide study has correlated single nucleotide polymorphisms (SNPs) in the gene coding for PERK with enhanced risk for sporadic tauopathies.[113] Decreased XBP1 expression levels enhance CASP activity, neuronal apoptosis and neurotoxicity of tau in a *Drosophila* model of tauopathy.[180] Altogether, these findings demonstrate a pathogenic link between the UPR and tau accumulation and aggregation though little is known of their relationship, especially in AD.

Mechanistically, the UPR network may mediate the crosstalk between Aβ and τ.[252] In primary cortical neurones, Aβ oligomers potentiate the glycogen synthase kinase 3β (GSK3β) and trigger τ phosphorylation, coinciding with BiP up-regulation and CASP12 proteolytic cleavage.[252] GSK3β is a well-documented tau-targeting kinase for the NFT formation.[179] Meanwhile, the UPR abolishes the inhibitory phosphorylation of GSK3β at the serine 9 residue (Ser9) and thus induces the kinase activity.[26,178,200,232,276,287] Intriguingly, immunoprecipitation studies have revealed a substantial elevation in the binding levels of BiP to τ (mainly phosphorylated) and GSK3β under ER stress conditions both *in vivo* and *in vitro*, implicating this chaperone in the GSK3β-dependent τ phosphorylation.[178] Altogether, these findings support that the ER stress is intimately related to tau pathology. However, the mechanistic insights of this relationship necessitate clarification.

1.3.2 The UPR as a component of the Alzheimer's pathogenesis

Accumulating evidence supports that Aβ is a key trigger for the Alzheimer's pathogenesis while the regulation of metabolic pathways for its generation may lie downstream of the UPR signalling network.[72] Gene transcription programmes for the protein quality-control machinery, X-box proteins, and calcineurin regulatory subunits are differentially modulated during the initial and intermediate stages of Aβ deposition in the hippocampus and cortex of AD mice, pointing towards a close link between the ER stress and amyloidogenesis.[263] O'Connor *et al.* have recently proposed that the Aβ accumulation occurs downstream of the PERK/eIF2α stress-response pathway and *vice versa*.[222] In this model, the energy deprivation upon cellular stress promotes the phosphorylation of PERK and eIF2α that in turn favour the translation of a subset of stress-responsive proteins, including BACE1. The enhanced synthesis of these proteins initially drives adaptive responses and aims towards the cell survival. However, chronic cellular stress along with the persistent PERK signalling and abnormal BACE1 levels culminates in the excessive Aβ generation. The latter in turn triggers neuronal dysfunction and stress, feeding back and reinforcing the PERK/eIF2α stress-response pathway.[222] Contrarily, PERK haploinsufficiency precludes the abnormal BACE1 elevation and rescues the excessive Aβ production and deposition in the brain of the 5XFAD mouse model.[58] In non-neuronal cells, the PERK arm modulates the PS1 transcription to augment the γ secretase activity[226] and to channel APP towards the amyloidogenic processing.[174] Notably, the observed Aβ accumulation solely reflects the excessive amyloidogenesis, without intricacies of the Aβ degradation machinery or APP transcription upon prolonged ER stress.[174]

Furthermore, an oligomerisation-prone pool of Aβ manifests within the ER lumen, concomitant with a prolonged ER stress and the halted axonal transport. Specifically, under arrested axonal transport, the APP, Fe65[1] and the motor protein kinesin-1 accumulate in the neurone soma and form a complex within the ER lumen. The APP:Fe65:kinesin1 complex recruits the active JNK that downstream phosphorylates APP at Thr 668. Phosphorylated APP is preferentially cleaved through the amyloidogenic pathway to release Aβ in the ER lumen.[208] In HEK293 and COS-7 cell lines, the E693δ mutation in APP results in the accumulation of Aβ oligomers in the ER lumen, which correlates to the abnormal BiP expression, eIF2α phosphorylation, caspase 4 activation, and DNA fragmentation.[218] Similarly, the *in-vivo* expression of the E693δ mutant APP stimulates the Aβ accumulation within the ER that coincides with the aberrant BiP and HRD1 expression in hippocampal neurones and culminates in neuronal loss.[297] The HRD1 is an ERAD ubiquitin ligase that resides in the ER and protects against the ER stress-induced apoptosis.[142] Most importantly, HRD1 interacts with APP and promotes the ubiquitination and degradation of this protein to preclude Aβ generation. As such, the HRD1 suppression accelerates the APP accumulation and Aβ generation accompanied by ER stress and apoptosis.[142] In addition to HRD1, BiP can interact with APP and alter its localisation along the secretory pathway,

[1] an APP-binding protein involved in APP trafficking

which in turn may impact maturation and proteolytic processing of the protein.[311] Altogether, these findings highlight the prominent role of the UPR network in the regulation of APP metabolism though its mechanistic insights necessitate further clarification.

A genome-wide screening study has revealed that several AD-related genes integrate into the transcription network governed by the spliced XBP1.[2] Besides the regulation of the transcription programme for UPR adaptive responses, the spliced XBP1 binds to genes encoding *subunits of* γ *secretase complex* (PS, nicastrin and the enhancer of PS2), *adaptor proteins* for the APP trafficking and processing (ubiquilin 1, MINT3 and Fe65), *the ERAD-associated protein HERP1* for APP degradation, and *two candidate proteins* potentially implicated in tau phosphorylation (cyclin-dependent kinase 5, abbreviated as Cdk5, and Cdk5 regulatory subunit associated protein 3).[2] Taken together, the XBP1 appears to orchestrate major mechanisms for the Alzheimer's onset and progression. However, there are no functional studies currently available to validate this hypothesis. Intriguingly, a recent screening study has further revealed that the XBP1 regulates the gene expression of the disintegrin and metalloproteinase domain-containing protein 10 (ADAM10), the physiological α secretase.[251] In particular, the spliced XBP1 variant dose-dependently augments the ADAM10 expression synergistically with the insulin signalling and promotes non-amyloidogenic processing of APP in neuronal cell lines. In the $\mathrm{APP}_{swe}/\mathrm{PS1}_{\Delta E9}$ and 5XFAD brain, the dynamics of the XBP1 metabolism is inversely correlated to the temporal and spatial of pathological protein accumulation. The early stages of the AD-like pathology of these murine models feature augmented levels of the spliced XBP1 and ADAM10 that both decrease up to 50% with the animal ageing and the development of the AD-like phenotype. Correspondingly, in the *post-mortem* brain samples from AD cases, active XBP1 strongly correlates with ADAM10 mRNA levels, with their expression dramatically diminishing in frontal cortex and subtly decreasing in the temporal cortex.[251] Furthermore, a single nucleotide polymorphism (–116C/G) within the XBP1 promoter increases the risk for the Alzheimer's onset and progression in the Chinese population, with the CC genotype accelerating the cognitive decline compared to the G-carrier genotypes.[176] Subsequent *in-vitro* studies have demonstrated that this polymorphism compromises the expression of spliced XBP1, defecting the ER-stress response and raising the risk for bipolar disorder.[139] However, it remains unknown whether the same mechanism underlies the increased susceptibility of the Chinese population carrying this polymorphism to the Alzheimer's development, as well as whether this polymorphism is present in other populations too.

1.4 Towards a growth factor approach for resolving UPR and defective proteostasis in AD

Ageing represents the principal risk factor for the onset of neurodegenerative disorders, including the AD. Mechanistically, it attenuates the cellular capacity to engage adaptive responses like the UPR, autophagy and heat-shock response under stress conditions that seems to coincide with a impaired insulin-related growth factor signalling.[85] The resistance and deficiency of insulin and insulin-like growth factor signalling parallel the disease progression in the AD brain.[54,55] Correspondingly, pharmacological down-regulation and genetic depletion of the brain insulin receptors manifest abnormal protein accumulation, cognitive impairments and neuronal degeneration *in vivo*, reminiscent of the AD pathology.[55] Suppressed insulin receptor substrate-1 lies downstream of the ER stress, which may act synergistically with pro-inflammatory signals to compromise insulin signalling in the AD brain and promote synapse and cognitive dysfunction.[183] Altogether, a cross-talk between growth factor signalling and proteostasis network seems to exist and offer a potential approach for halting or preventing the AD progression.[55,85]

The glucagon-like peptide-1 (GLP-1) is an insulinotropic incretin hormone synthesised by the L-type cells of the gastroenteropancreatic endocrine system and released upon food ingestion. It stimulates insulin gene transcription, proinsulin biosynthesis and the glucose-dependent postprandial insulin secretion whilst inhibiting glucagon secretion, gastric emptying and acid secretion. It additionally promotes the proliferation of islet cells and differentiation of pancreatic ductal cells into insulin-producing cells and impedes β-cell apoptosis, culminating in the expansion of β-cell mass.[10] Currently, three GLP-1 analogues, Exenatide (Byetta®), Liraglutide (Victoza®) and Lixisenatide (Luxymia®) are on the market for type 2 Diabetes Mellitus (T2DM) treatment. Besides their glucose-dependent pancreatic effects, these insulin-stimulating/releasing agents cross the blood-brain barrier and exert neurotrophic and cell-survival signals.[10,116] For instance, chronic intraperitoneal administration of Liraglutide has preserved normal population and activity of cortical and hippocampal synapses, impeded hippocampal atrophy, halted excessive Aβ accumulation and deposition, and mitigated excessive gliosis to rescue spatial cognitive decline in the APP$_{swe}$/PS1$_{\Delta E9}$ mouse model for AD and the senescence-accelerated mouse prone 8 (SAMP8) model for age-related sporadic AD.[116] In line with the *in-vivo* findings, Liraglutide and Exenatide have favoured survival over apoptotic signalling to impede cytotoxicity and death of hippocampal and primary cortical neurones and neuronal-like cells chronically exposed to excitotoxic insults[91,166,236,316] and Aβ oligomers.[237,244,316] In a pilot clinical trial, Liraglutide has rescued the decline of the cerebral glucose consumption in AD patients that signifies energy metabolism in brain areas previously correlated with cognitive decline and disease progression.[86]

Correspondingly, the stable analogue of the glucose-dependent insulinotropic polypeptide (GIP), $_D$Ala^2-GIP has alleviated neuroinflammatory responses, oxidative stress and cerebral amyloid plaque load to attenuate the poor cognitive performance of the APP$_{swe}$/PS1$_{\Delta E9}$

mouse model.[63,70] These effects have been further correlated to enhanced synaptogenesis and restored synaptic plasticity events in the cortex and hippocampus of the middle-aged and aged $APP_{swe}/PS1_{\Delta E9}$ mice upon chronic $_{D}Ala^{2}$-GIP treatment.[70]

Recently, novel GLP-1/GIP Dual Agonist analogues have been developed and displayed superior anti-hyperglycaemic and insulinotropic efficacy compared to the GLP-1 monotherapy, rendering them potent candidates for T2DM treatment.[76] Pilot pre-clinical studies have further demonstrated the neurotrophic and restorative effects of the dual incretin against hallmark, disease-related pathological lesions in a mouse model of mild traumatic brain injury (TBI),[289] a rat model of streptozotocin-induced diabetes and neurodegeneration,[269] and of the 1–methyl-4–phenyl-1,2,3,6–tetrahydropyridine (MPTP) and 6-hydroxydopamine (6-OHDA) rodent models of Parkinson's disease (PD).[31,133,136,320]

The neuroprotective and restorative effects of incretin mimetics lie downstream of the induction of the GLP-1 and GIP receptors.[10,116] Indeed, GLP-1 receptor (GLP-1R) over-expression in hippocampus augments spatial learning and memory performance *in vivo* that are blocked by the presence of a GLP-1R antagonist.[64] Conversely, GLP-1R-deficient mice feature suppressed hippocampal synaptic plasticity[1] accompanied by decrements in the associative contextual[64] and spatial learning[1] and increased susceptibility to kainic acid-induced seizures and neuronal degeneration in the hippocampus.[64] Similarly, the depletion of the GIP receptor (GIP-R) impairs the proliferation of hippocampal progenitor cells in the murine brain[221] whereas the pharmacological stimulation or over-expression of the receptor modulates the synaptic strength to ease spatial memory formation.[62,69] GLP-1 and GIP receptors are widely expressed in the human and rodent brain and coupled to the Gα-protein. Upon activation, the latter stimulates the adenyl cyclase that lies upstream of the Akt and extracellular signal-regulated 1 and 2 (ERK1/2) signalling pathways to confer survival and trophic signals intracellularly.[10,116] But, what happens next? Does the incretin signalling regulate the proteostasis machinery and favour cell adaptive responses to rescue pathognomonic features of protein misfolding disorders, such as the AD, and thereby elicit synapse homeostasis and improved cognitive functioning? Furthermore, does the incretin signalling involve other signal transduction nodes apart from the Akt and ERK1/2 kinases to impact neuronal fate?

1.4.1 Thesis aims

In the light of these questions, the present thesis addressed:

- The neuroprotective effects of Liraglutide against the persistent and calcium-dependent ER stress in the human proliferating SH-SY5Y neuroblastoma cells. To accomplish this, markers of the UPR response, protein quality-control chaperones and autophagy components were assessed in correlation to cell viability and proliferation. A functional protein microarray was further employed to scan for the intracellular signalling 'pool' mediating the survival and restorative signals downstream of the GLP-1R stimulation (Chapter 3).
- The replication of the phenotype in human post-mitotic neurones from the LUHMES cell line and its further correlation to the expression of plasticity-related synaptic proteins (Chapter 4).
- The neuroprotective and restorative effects of a novel dual incretin against the chronic and calcium-dependent ER stress along with underlying intracellular signalling cascade in human post-mitotic neurones from the LUHMES cell line (Chapter 4).
- The verification of the efficacy of the dual incretin in the cognitive performance, synapse homeostasis and cerebral proteostasis in the middle-aged $APP_{swe}/PS1_{\Delta E9}$ mouse model for AD.

Chapter 2

Materials & Methods

Partly Published in *Scientific Reports* 7(1) : 16158, 2017

2.1 Materials

Cell proliferation kit II [2,3-Bis-(2-methoxy-4-nitro-5-sulphophenyl)-2H-tetrazolium-5-carboxanilide (XTT)], cell proliferation ELISA 5-bromo-2'-deoxyuridine (BrdU) kit and Cytotoxicity Detection Kit^{PLUS} [lactate dehydrogenase (LDH)] were purchased from Roche Diagnostics Ltd (West Sussex, UK). The ER Stress Antibody Sampler kit (#9956), Bcl-2 (D17C4) monoclonal antibody (#3498), phospho-Bcl-2 (Ser70) (5H2) monoclonal antibody (#2827), BH3 interacting-domain death agonist (BID; Human Specific) polyclonal antibody (#2002), voltage-dependent anion channel (VDAC; D73D12) monoclonal antibody (#4661), beclin-1 (D40C5) monoclonal antibody (#3495), Atg3 monoclonal antibody (#3415), Atg7 monoclonal antibody (#8558), LC3B polyclonal antibody (#2775), post-synaptic density protein 95 (PSD95; D27E11) XP® monoclonal antibody (#3450), cleaved caspase 3 (CASP3; Asp175) polyclonal antibody (#9661), Phospho-GSK-3β (Ser9) (D85E12) XP® monoclonal antibody (#5558), phospho-Akt (Thr308) (D25E6) XP® monoclonal antibody (#13038), phospho-ERK1/2 (Thr202 /Tyr204) (D13.14.4E) XP® monoclonal antibody (#4370), β-Actin (8H10D10) monoclonal antibody (#3700), horseradish peroxidase (HRP)-linked secondary antibodies against the corresponding species IgG of the primary antibodies (#7074 & #7076), PathScan® Intracellular Signaling Array kit (#7323), PathScan® Sandwich ELISA lysis buffer (1X; #7018), and Protease/Phosphatase Inhibitor Cocktail (100X) were purchased from Cell Signaling Technology (New England Biolabs UK Ltd, Hertfordshire, UK). Phospho-IRE1 (S724) polyclonal antibody (ab48187), ATF6 [1-7] polyclonal antibody (ab122897), ATF6 polyclonal antibody (ab37149), caspase 12 (CASP12) polyclonal antibody (ab62484), Nrf2 [EP1808Y] (ab62352) monoclonal antibody, synaptophysin polyclonal antibody (ab7837), glial fibrillary acidic protein (GFAP) polyclonal antibody (ab7260), and normal goat serum were purchased from Abcam (Cambridgeshire, UK). β-Amyloid polyclonal antibody (71-5800) was purchased from Thermo Fisher Scientific (Renfrewshire, UK). Ionised calcium-binding adapter molecule 1 (IBA-1) polyclonal antibody (016-20001) was obtained by Wako Pure Chemicals GmbH (North Rhine-Westphalia, Germany).

Quick Start™ Bradford protein assay kit was obtained from BIO-RAD Laboratories Ltd (Hertfordshire, UK). Amersham ECL Prime western blotting detection reagent kit was obtained from GE Healthcare Life Sciences (Buckinghamshire, UK). Invitrogen™ goat anti-rabbit IgG H & L Alexa Fluor® 488 secondary antibody (A11034), Invitrogen™ iBlot® 2 Dry Blotting System, iBlot™ 2 Transfer Stacks with integrated nitrocellulose transfer membranes, precast polyacrylamide Bolt™ 4-12% gradient Bis-Tris Plus gels, and Restore™ PLUS Western Blot stripping buffer were purchased from Fisher Scientific UK Ltd (Leicestershire, UK). Bovine serum albumin (BSA), tris buffered saline (TBS; pH 8.0) supplemented or not with 0.05% Tween® 20, phosphate buffered saline (PBS; pH 7.4), phosphate buffer (0.1 M, pH 7.4), fibronectin from human plasma (0.1%), poly-L-ornithine solution ($MW = 30,000 - 70,000$; $0.1\,\mathrm{mg\,mL^{-1}}$), N^6 2'-O-Dibutyryl cAMP (adenosine-3',5'-cyclic monophosphate) sodium salt, tetracycline hydrochloride (BioReagent, suitable for cell culture), dimethyl sulphoxide (DMSO; anhydrous, $\geq$ 99.9%), isopropyl alcohol, heparin sodium salt from porcine intestinal mucosa, sucrose, ethylene glycol (anhydrous, $\geq$ 99.8%), glycerol for molecular biology ($\geq$ 99%), hydrogen peroxide solution (50%), and para-formaldehyde were obtained from Sigma-Aldrich Corporation (Dorset, UK). Human recombinant glial-derived neurotrophic factor (GDNF) was obtained from R&D Systems (Bio-Techne Ltd, Oxfordshire, UK). VECTASTAIN® Elite® ABC-HRP Kit (Peroxidase, Rabbit IgG), Vector® DAB Peroxidase (HRP) Substrate kit, VECTASHIELD antifade mounting medium with DAPI, and VectaMount AQ aqueous mounting medium were purchased from Vector Laboratories Ltd (Cambridgeshire, UK). Other materials and reagents for cell culture, western blotting, immunocytochemistry and histology were purchased from Fisher Scientific UK Ltd (Leicestershire, UK), unless otherwise stated.

Name	Shortened Name	Amino acid sequence	MW (Da)	Reference
Liraglutide	LIRA	HAEGTFTSDVSSYLEGQAA[Lys-γE-C16 acyl]EFIAWLVRGRG–OH	3751.26	76
$_{D}$Ala^{2}-GIP	D-Ala-GIP	Y $_{D}$Ala^{2}EGTFISDYSIAMDKIHQQDF VNWLLAQKGKKNDWKHNITQ–OH	4983.6	112
GLP-1/GIP Dual Agonist	DA	Y**X**EGTFTSDYSIYLDKQAA**X**EFVN WLLAGGPSSGAPPPS[Lys-C16]–NH_2	4234.63	76

Table 2.1: **Names, amino acid sequence and molecular weight (MW) of the incretin mimetics used in the current thesis**. Wherein the sequences, the **"X"** symbol stands for aminoisobutyric acid.

2.2 Peptides

The incretin mimetics were purchased from Chinapeptides Co., Ltd and Biochem Ltd (Shanghai, China). The purity of the peptides was analysed by reverse-phase high performance liquid chromatography (HPLC) and characterised using matrix-assisted laser desorption/ionisation time-of-flight (MALDI–TOF) mass spectrometry. The purity of the peptides tested was $\geq 96\%$ in accord with the manufacturers' reports. The amino acid sequence of the peptides tested in the current thesis is described in **Table 2.1**. Peptides were maintained in powdered, desiccated form at $-80\,^{\circ}$C and reconstituted in Gibco® Water for Injection for Cell Culture to the required concentration for each experimental setup at the beginning of each study.

2.3 Methods for neuronal cell lines

2.3.1 Human neuroblastoma SH-SY5Y cell line

2.3.1.1 Cell culture

The human neuroblastoma SH-SY5Y is a thrice sub-clone of the parental SH-N-SH cell line, which was originally derived from a metastatic bone marrow biopsy of a 4-year-old female neuroblastoma patient with sympathetic adrenergic ganglial origin in the early 1970's.[21] The SH-SY5Y cell line (ATCC® CRL-2266™) was obtained from LGC Standards (Middlesex, UK) and cultivated in Dulbecco's modified eagle medium/nutrient mixture F-12 (DMEM / F-12, 1 : 1; 1X) Glutamax™, supplemented with 10% heat-inactivated foetal bovine serum (FBS), 100 IU ml^{-1} of Penicillin and 100 µg ml^{-1} of Streptomycin (hereinafter referred to as complete growth medium). Cells were maintained at 37 °C in a humidified incubator with 5% CO_2 and 95% air. Culture medium was renewed every 3 to 4 days.

2.3.1.2 Subculturing procedure

SH-SY5Y cells were subcultured when 80–90% confluent and grown up to 15 passages to avoid senescence. Initially, the spent culture medium was discarded and the cell monolayer was gently rinsed with Hank's balanced salt solution (HBSS) that was formulated without calcium and magnesium. Subsequently, the cell monolayer was incubated with the TrypLE™ Select CTS™ dissociation reagent at 37 °C for $\sim 2 - 3$ min. Cells were collected by centrifugation at $200 \times g$ for 5 min using Allegra™ X-30R centrifuge (Beckman Coulter, Buckinghamshire, UK) and suspended in complete growth medium. Viable cells were counted and seeded at the desired cell density for the assays using the Countess™ Automated Cell Counter (Thermo Fisher Scientific, Renfrewshire, UK). The latter is based on the standard trypan blue exclusion technique, in which dead cells are selectively permeable to the dye and stained blue. Alternatively, SH-SY5Y cells were seeded at 1 : 10 ratio.

2.3.1.3 Handling procedure for frozen cells & cryopreservation

Upon receipt, the vial containing frozen SH-SY5Y cell suspension was thawed by gentle agitation in a 37 °C water bath. The contents of the vial were subsequently transferred to a centrifuge tube containing 9.0 mL of the complete growth medium and spun at $200 \times g$ for 5 min using Allegra™ X-30R centrifuge. Cell pellet was re-suspended in 1.0 mL of the complete growth medium. Cells were seeded in a T25 Nunc™ Cell Culture Treated EasY Flask at 1 : 5 ratio and maintained in a humidified incubator with 5% CO_2 and 95% air till reach 80–90% confluence. Cells were subcultured twice to allow cell recovery from the stress of freeze/thaw cycle and gradually cultivated in T175 Nunc™ Cell Culture Treated EasY Flasks at 1 : 10 ratio to acquire high cell density. SH-SY5Y cell line stocks were prepared at passage 3 by re-suspending the collected cell pellet in 10.0 mL of Gibco™ Recovery™ Cell Culture Freezing Medium to yield $2 \times 10^6\ cells$/mL. The aforementioned suspension was equally aliquoted in 10 Nunc™ cell culture cryogenic tubes. The cryogenic tubes were stored in a Thermo Scientific™ Mr. Frosty™ Freezing Container with isopropyl alcohol at −80 °C overnight and subsequently transferred to a liquid nitrogen tank for long-term storage. Upon recovery of the SH-SY5Y cell line stocks, we followed the same handling procedure like upon receipt.

2.3.1.4 Cell treatments

The ER stressor used in the present thesis was the naturally-occurring sesquiterpene lactone thapsigargin, which selectively inhibits sarcoplasmic/ER Ca^{2+}–ATPase (SERCA) and depletes the ER calcium stores.[292] Thapsigargin was received as a colourless solid film, solubilised in 100% DMSO at a concentration of 1 mM, aliquoted and stored at −20 °C until used. For the experiments, thapsigargin stock preparations were serially diluted in serum-free culture medium at final working concentrations of 10 to 1000 nM, containing $\leq 0.1\%$ DMSO. 0.1% DMSO did not affect cell viability as assessed in preliminary experiments in SH-SY5Y cells [**Figure S1**].

Liraglutide was received as white lyophilised (freeze-dried) powder, reconstituted in Gibco® Water for Injection for Cell Culture to a concentration of 1 mg ml^{-1}, aliquoted and stored at −20 °C until used. For the experiments, Liraglutide stock preparations were diluted in serum-free culture medium to a final working concentration of 100 nM. The concentration was selected on the basis of previous experiments in which our group has established optimal working concentrations for the neuroprotective and anti-apoptotic effects of Liraglutide.[134,265]

2.3.1.5 Cell viability, proliferation and cytotoxicity assessment

Cell viability, proliferation and cytotoxicity were determined using Cell proliferation kit II (XTT), cell proliferation ELISA BrdU (colorimetric) kit and Cytotoxicity Detection Kit$^{\mathrm{PLUS}}$ (LDH), respectively. The assays were formatted in Nunc™ MicroWell™ flat-bottomed 96-well plates. SH-SY5Y cells were seeded at a density of 2×10^4 cells per well for 24 h. The cells were subsequently serum starved in serum-free medium for 8 h and stressed with different concentrations of thapsigargin for 16 h, in the presence or absence of 100 nM of Liraglutide. All cell treatments were performed in sextuplicate per plate per experiment. Following the cell treatments, 50 µL of XTT labelling reagent and 1 µL of electron coupling reagent was added to each well, yielding final XTT concentration of 0.3 mg mL^{-1}. Cells were incubated with the XTT labelling mixture for 6 h at 37 °C in a humidified incubator with 5% CO_2 and 95% air. Plates were then gently shaken for 5 min on a Microtitre plate shaker (Stuart, Staffordshire, UK) and absorbance was measured at 492 and 690 nm (reference wavelength) in an Infinite® 200 PRO microplate reader (Tecan, Berkshire, UK). The assay rests on the cleavage of the yellow tetrazolium salt XTT into an orange, water-soluble formazan product by metabolically active cells (mitochondrial dehydrogenase enzyme activity). Thus, absorbance values are proportional to the number of viable cells in the respective microcultures.

Alternatively, SH-SY5Y cells were incubated with 10 µM BrdU labelling solution for 6 h at 37 °C in a humidified incubator with 5% CO_2 and 95% air. The pyridine analogue BrdU was incorporated, in place of thymidine, into the newly synthesised DNA strands of proliferating cells. BrdU incorporation was detected by immunoperoxidase staining and a subsequent colorimetric substrate reaction as per manufacturer's protocol. Plates were read at 450 and 690 nm (reference wavelength) using Infinite® 200 PRO microplate reader. Developed colour and absorbance values reflect the amount of DNA synthesis, and hereby the number of proliferating cells in the respective microcultures.

Cytotoxicity Detection Kit^{PLUS} was used to quantify LDH activity. LDH is a stable cytoplasmic enzyme present in all cells and rapidly released into the culture supernatant upon plasma membrane damage. The assay involves a coupled enzymatic reaction that results in the formation of a red, water-soluble formazan product during a limited time period. The amount of colour developed is proportional to the number of damaged/lysed cells in the respective microcultures. As per manufacturer's instructions, following the cell treatments, 50 µL of the cell supernatant was collected and incubated with the provided reaction mixture for 30 min at room temperature. The reaction was terminated by adding the Stop Solution from the kit and absorbance was measured at 490 and 650 nm (reference wavelength).

2.3.1.6 Immunocytochemistry

1×10^5 cells per well were grown on the Millicell EZ SLIDE eight-well glass chamber slides for 24 h. Following serum starvation for 8 h, cells were stressed with 100 nM of thapsigargin for 16 h, in the presence or absence of 100 nM of Liraglutide. Thereafter, cells were washed once with 1X PBS, fixed with 4% para-formaldehyde for 10 min and permeabilised in 0.3% Triton-X-100 for 5 min at room temperature. Cells were blocked in 10% normal goat serum and incubated with the primary antibody against Nrf2 (1 : 500) or ATF6 (1 : 200) overnight at 4 °C. Primary antibody was diluted in 1% BSA in 1X PBS supplemented with 0.3% Triton-X-100. Following primary antibody incubation, cells were washed three times in 1X PBS for 5 min each and incubated with goat anti-rabbit IgG H & L Alexa Fluor® 488 secondary antibody (1 : 1000) for 1 h at room temperature. Specimens were cover-slipped with Vectashield Antifade Mounting Medium with DAPI and sealed with nail polish. Zeiss LSM510 Meta Laser Scanning confocal microscope was used for cell imaging and eight pictures were captured at 40X magnification per experimental group per experiment for quantification. Image J software (National Institutes of Health, Bethesda, Maryland, USA) was used to quantify Nrf2 corrected total cell fluorescence in the cell nucleus. Image acquisition and processing were performed in a blinded fashion.

2.3.1.7 Sample collection and protein extraction

2×10^6 cells were grown at 75 cm^2 Nunc™ Cell Culture Treated EasYFlasks for 24 h. Following serum starvation for 8 h, cells were stressed with 100 nM of thapsigargin for 16 h, in the presence or absence of 100 nM of Liraglutide. Thereafter, cells were washed once with ice-cold 1X PBS and harvested in 1X PathScan® Sandwich ELISA cell lysis buffer supplemented with protease/phosphatase inhibitor cocktail (1X). After two freeze/thaw cycles, whole-cell lysate was collected and total protein was extracted by centrifugation at $\sim 16000 \times g$ at 4 °C for 15 min. The Quick start™ Bradford protein assay was conducted to estimate the protein concentration of the samples, as described in **subsection 2.3.3**. Protein samples of whole-cell lysate were aliquoted and stored at −80 °C till processed for western blotting (**subsection 2.3.4**) and PathScan® sandwich immunoassay (**subsection 2.3.5**).

2.3.2 Lund Human Mesencephalic (LUHMES) cell line

2.3.2.1 Cell culture

The Lund human mesencephalic (LUHMES) cell line is a sub-clone of the tetracycline-controlled, v-myc-over-expressing foetal human mesencephalic-derived cell line MESC2.10, established and characterised at Lund University (Lund, Sweden).[181,182] The LUHMES cell line (ATCC® CRL-2927™) was obtained from LGC Standards. Proliferating LUHMES cells were cultivated in Advanced DMEM / F-12 supplemented with 1X Glutamax™, 1X N-2 supplement and 40 ng mL^{-1} basic recombinant human fibroblast growth factor (bFGF) (hereinafter referred to as complete growth medium for the LUHMES cell line) in culture vessels, which were sequentially pre-coated with 50 µg mL^{-1} poly-L-ornithine and 1 g mL^{-1} fibronectin to promote cell attachment. Cells were maintained at 37 °C in a humidified incubator with 5% CO_2 and 95% air. Culture medium was renewed every 1 to 2 days.

2.3.2.2 Coating procedure for culture vessels

Nunc™ Cell Culture Treated EasY Flasks, Nunc™ MicroWell™ flat-bottomed 96-well plates and Millicell EZ SLIDE eight-well glass chamber slides were pre-coated overnight with 50 µg mL^{-1} poly-L-ornithin at room temperature. Following the removal of the poly-L-ornithin solution, the culture vessels were rinsed three times with Gibco® Water for Injection for Cell Culture and allowed to air-dry uncapped in a biological safety cabinet.

Subsequently, Nunc™ Cell Culture Treated EasY Flasks, Nunc™ MicroWell™ flat-bottomed 96-well plates and Millicell EZ SLIDE eight-well glass chamber slides were coated with $1\,\mathrm{g\,mL^{-1}}$ fibronectin for 3 h at 37 °C. Post the incubation, fibronectin solution was removed and culture vessels were rinsed three times with Gibco® Water for Injection for Cell Culture. Culture vessels were then allowed to air-dry uncapped in a biological safety cabinet. When dry, culture vessels containing culture medium were placed for at least 30 min in the incubator to allow the medium to reach its normal pH (7.0–7.6) and avoid excessive alkalinity of medium during cell handling procedures. Alternatively, pre-coated Nunc™ Cell Culture Treated EasY Flasks were sealed with Parafilm® M film under aseptic conditions and kept in 4 °C up to a week. Poly-L-ornithin and fibronectin were diluted at the required concentration in Gibco® Water for Injection for Cell Culture and HBSS solution, respectively, immediately before used.

2.3.2.3 Subculturing procedure

Proliferating LUHMES cells were subcultured when 70–80% confluent and grown up to passage 10 to avoid senescence and loss of pluripotency. Initially, the spent culture medium was discarded and the cell monolayer was gently rinsed with Dulbecco's phosphate-buffered saline (DPBS) that was formulated without calcium and magnesium. Subsequently, the cell monolayer was incubated with the TrypLE™ Select CTS™ dissociation reagent at 37 °C for ~ 5 min. Cells were collected by centrifugation at $200 \times g$ for 7 min using Allegra™ X-30R centrifuge and suspended in complete growth medium for LUHMES cell line. Viable cells were counted and seeded at the desired cell density for the differentiation procedure using the Countess™ Automated Cell Counter that utilises the standard trypan blue exclusion technique. Alternatively, proliferating LUHMES cells were seeded at $1:10$ ratio.

2.3.2.4 Handling procedure for frozen cells & cryopreservation

Upon receipt, the vial containing frozen LUHMES cell suspension was thawed by gentle agitation in a 37 °C water bath. The contents of the vial were subsequently transferred to a centrifuge tube containing 9.0 mL Advanced DMEM/F12 medium supplemented with 1X Glutamax™ and 1X N-2 supplement. The tube was subsequently spun at $200 \times g$ for 7 min using Allegra™ X-30R centrifuge. Cell pellet was re-suspended in 1.0 mL of the complete growth medium for the LUHMES cell line. Proliferating cells were seeded in a pre-coated T25 Nunc™ Cell Culture Treated EasY Flask at 1 : 5 ratio and maintained in a humidified incubator with 5% CO_2 and 95% air till reach 70–80% confluence. Proliferating cells were subcultured twice to allow cell recovery from the stress of freeze/thaw cycle and gradually cultivated in pre-coated T175 Nunc™ Cell Culture Treated EasY Flasks at 1 : 10 ratio to acquire high cell density. LUHMES cell line stocks were prepared at passage 3 by re-suspending the collected cell pellet in 10.0 mL of cryopreservation medium to yield $2 \times 10^6\, cells/\mathrm{mL}$; cryopreservation medium consisted of 70% complete growth medium for LUHMES cell line, 20% of heat-inactivated FBS and 10% DMSO. The aforementioned suspension was equally aliquoted in 10 Nunc™ cell culture cryogenic tubes. The cryogenic tubes were stored in a Thermo Scientific™ Mr. Frosty™ Freezing Container with isopropyl alcohol at −80 °C overnight and subsequently transferred to a liquid nitrogen tank for long-term storage. Upon recovery of the LUHMES cell line stocks, we followed the same handling procedure like upon receipt.

2.3.2.5 Differentiation procedure

Differentiation procedure was conducted as previously described[260] and summarised in **Figure 2.1**. Briefly, 1×10^7 proliferating LUHMES cells were seeded into pre-coated T175 Nunc™ Cell Culture Treated EasY Flasks in the appropriate complete growth medium.

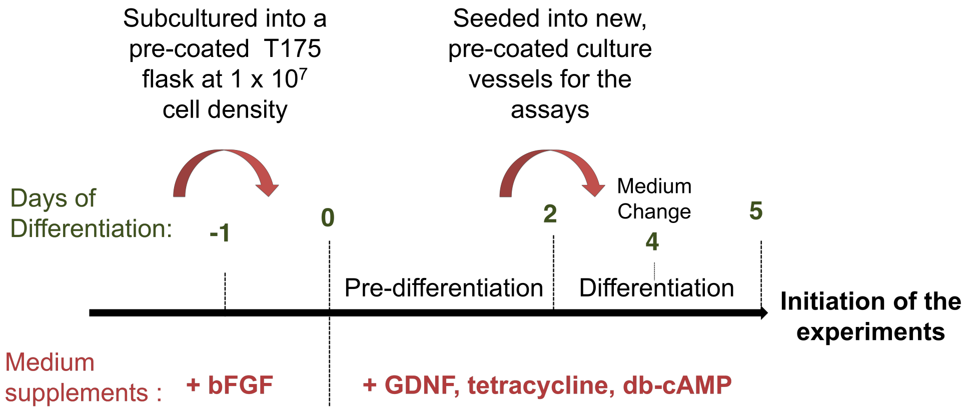

Figure 2.1: **Two-step differentiation procedure for conversion of proliferating LUHMES cells into post-mitotic neuronal cells, as previously established by Scholz, Diana *et al.*[260] and described in subsubsection 2.3.2.5**. For the list of the abbreviations used, please refer to the corresponding **chapter** .

Twenty-four hours post seeding, spent medium was discarded and replaced with the differentiation medium that defines day 0 (d 0) of the differentiation procedure. Differentiation medium consisted of Advanced DMEM/F12 medium supplemented with 1X Glutamax™, 1X N-2 supplement, $2\,\mathrm{ng\,mL^{-1}}$ human recombinant GDNF, 1 mM N^6 2'-O-Dibutyryl cAMP sodium salt and $1\,\mathrm{\mu g\,mL^{-1}}$ tetracycline hydrochloride. Two days post the initiation of the differentiation, cell monolayer were gently rinsed with DPBS that was formulated without calcium and magnesium. Subsequently, the cell monolayer was incubated with the TrypLE™ Select CTS™ dissociation reagent at 37 °C for ∼ 5 min. Pre-differentiated LUHMES cells were collected by centrifugation at $200 \times g$ for 7 min using Allegra™ X-30R centrifuge, suspended in differentiation medium, and seeded into pre-coated Nunc™ MicroWell™ flat-bottomed 96-well plates, T75 Nunc™ Cell Culture Treated EasY Flasks or into Millicell EZ SLIDE eight-well glass chamber slides at the required cell density for each assay. Differentiation process continued for additional 3 d to allow cells to morphologically and biochemically mature into post-mitotic neuronal cells. Differentiation medium was changed at d 4 of the differentiation procedure. All experiments were conducted after 5 d of differentiation.

2.3.2.6 Cell treatments

Thapsigargin was received as a colourless solid film, solubilised in 100% DMSO at a concentration of 1 mM, aliquoted and stored at −20 °C until used. For the experiments, thapsigargin stock preparations were serially diluted in differentiation medium at final working concentrations of 10 to 1000 nM, containing ≤ 0.1% DMSO. DMSO concentration up to 0.33% has no impact on LUHMES cell viability and neurite outgrowth.[282]

Liraglutide and GLP-1/GIP Dual Agonist were received as white lyophilised (freeze-dried) powders, reconstituted in Gibco® Water for Injection for Cell Culture to a concentration of 1 mg ml^{-1}, aliquoted and stored at −20 °C until used. For the experiments, Liraglutide and GLP-1/GIP Dual Agonist stock preparations were diluted in differentiation medium to a final working concentration of 100 nM. The concentration was selected on the basis of previous experiments in which our group has established optimal working concentrations for the neuroprotective and anti-apoptotic effects of incretin mimetics.[134,232,265]

2.3.2.7 Cell viability and cytotoxicity assessment

Pre-differentiated LUHMES cells were seeded at a density of 2×10^4 cells per well into pre-coated Nunc™ MicroWell™ flat-bottomed 96-well plates. Cells were maintained in the differentiation medium for additional 3 d. Between d 5 to d 6 of differentiation, LUHMES cells were stressed with different concentrations of thapsigargin for 16 h, in the presence or absence of 100 nM of Liraglutide or 100 nM of GLP-1/GIP Dual Agonist. All cell treatments were performed at least in sextuplicate per experiment. Following the treatment incubation period, cell viability and cytotoxicity were determined with the Cell proliferation kit II (XTT) and Cytotoxicity Detection Kit$^{\mathrm{PLUS}}$ (LDH), respectively, as per the protocols described in the **subsubsection 2.3.1.5**.

2.3.2.8 Immunocytochemistry

1×10^5 pre-differentiated LUHMES cells per well were seeded into pre-coated Millicell EZ SLIDE eight-well glass chamber slides and maintained in the differentiation medium for additional 3 d. Between d 5 to d 6 of differentiation, LUHMES cells were stressed with 100 nM of thapsigargin for 16 h, in the presence or absence of 100 nM of Liraglutide or 100 nM of GLP-1/GIP Dual Agonist. All cell treatments were performed in duplicate per experiment. Thereafter, neurones were fixed, permeabilised and labelled for Nrf2, as per the protocol described in **subsubsection 2.3.1.6**.

2.3.2.9 Sample collection and protein extraction

2×10^6 pre-differentiated LUHMES cells were seeded into pre-coated T75 cm^2 Nunc™ Cell Culture Treated EasYFlasks™ and maintained in the differentiation medium for additional 3 day. Between d 5 to d 6 of differentiation, LUHMES cells were stressed with 100 nM of thapsigargin for 16 h, in the presence or absence of 100 nM of Liraglutide or 100 nM of GLP-1/GIP Dual Agonist. Thereafter, cells were washed once with ice-cold 1X PBS and harvested in 1X PathScan® Sandwich ELISA cell lysis buffer supplemented with protease/phosphatase inhibitor cocktail (1X). After two freeze/thaw cycles, whole-cell lysate was collected and total protein was extracted by centrifugation at $\sim 16000 \times g$ at 4 °C for 15 min. The Quick start™ Bradford protein assay was conducted to estimate the protein concentration of the samples, as described in **subsection 2.3.3**. Protein samples of whole-cell lysate were aliquoted and stored at −80 °C till processed for western blotting (**subsection 2.3.4**) and PathScan® sandwich immunoassay (**subsection 2.3.5**).

2.3.3 Bradford protein assay

The Quick start™ Bradford protein assay was conducted to estimate the protein concentration of the whole-cell lysate samples and performed as per the manufacturer's protocol. The assay was formatted in Nunc™ MicroWell™ flat-bottomed 96-well plates during which the BSA served as the protein standard. 5 µL of 0.125, 0.25, 0.5, 0.75, 1, 1.5 and 2 $mg\,mL^{-1}$ of BSA along with 20 µL of double-distilled water and 150 µL of Coomassie Brilliant Blue G-250 dye were added in a 96-well plate. The plate was then gently shaken for 5 min on a Microtitre plate shaker and absorbance was measured at 595 nm in an Infinite® 200 PRO microplate reader. The same procedure was followed for the whole-cell lysate protein samples, which were previously diluted with double-distilled water at 1 : 7 ratio. Bradford protein assay rests on the absorbance shift of the protonated red cationic form ($A_{max} = 470\,nm$) of Coomassie Brilliant Blue G-250 dye into its stable deprotonated blue form ($A_{max} = 595\,nm$) upon binding to proteins.[154] Thus, absorbance values at 595 nm are proportional to the content (concentration) of protein present in the sample.[154] Absorbance versus the concentration of the BSA standard solutions was plotted for the preparation of the standard curve. The standard curve was subsequently used to estimate the protein concentration of the whole-cell lysate samples.

2.3.4 Western blotting

Protein of whole-cell lysate (4 µg) was reduced and denaturated by boiling in lithium dodecyl sulfate (LDS) sample buffer containing 50 mM dithiothreitol (DTT) at 95 °C for 5 min. Replicate protein samples were separated on Bolt™ 4 – 12% gradient Bis-Tris gel and blotted onto nitrocellulose membranes using iBlot® 2 Dry Blotting System. Blots were washed once in 1X TBS for 5 min, blocked in 5% w/v skimmed milk or 5% BSA (when the total or phosphorylated form of a protein was detected, respectively) for 1 h at room temperature, and probed with the primary antibodies overnight at 4 °C. The primary antibodies used for the *in-vitro* studies are summarised in **Table 2.2**. All the primary antibodies used were diluted in 5% BSA in 1X TBS with 0.05% Tween® 20 (TBS–T; pH 8) at 1 : 1000 ratio, unless otherwise specified in **Table 2.2**. All the primary antibodies used were generated in rabbit, except for the antibodies against Chop, ATF6 and β-actin that were raised in mice. Following primary antibody incubation, blots were washed three times in 1X TBS–T for 5 min each and incubated with the HRP-linked secondary antibodies against the corresponding species IgG (1 : 2000) for 1 h at room temperature. Blots were developed using Amersham ECL Prime western blotting detection reagent kit as per manufacturer's instructions. ChemiDoc™ MP Imaging System with Image Lab™ software (BIO-RAD Laboratories Ltd, Hertfordshire, UK) used to image chemiluminescent bands and perform densitometric analysis. β-Actin protein was served as the loading control to which relative peak intensities of the examined markers were normalised. To re-probe, blots were incubated in Restore™ PLUS stripping buffer for 20 min at 37 °C with gentle agitation and subsequently washed three times in TBS for 5 min each. Chemiluminescent detection to ensure the removal of the original signal preceded blot re-incubation with another primary antibody of interest.

2.3.5 PathScan® sandwich immunoassay

The PathScan® Intracellular Signaling Array kit is a sandwich-based, glass slide array for the simultaneous detection of 18 signalling molecules when phosphorylated or cleaved, as shown in **Figure 2.2**. The PathScan® Intracellular Signaling Array kit was used in accord with the manufacturer's protocol. Briefly, 100 µL Array Blocking Buffer was added to each well of the the antibody array slide and incubated for 15 min at room temperature. Thereafter, protein of whole-cell lysate (0.3 mg mL^{-1}) was placed onto each well and incubated overnight at 4 °C with gentle agitation. The following day, all the wells were washed three times in 1X Array Wash Buffer for 5 min each, and probed with 1X Detection Antibody

Target	Blocking Buffer	Dilution Ratio	Isotype	Cell Line Used SH-SY5Y	LUHMES	Manufacturer	Catalog No.
β-Actin	5% w/v skimmed milk	$1:10^4$	Mouse IgG	✓	✓	CST	#3700
ATF6[1-7]	5% w/v skimmed milk	1 : 500	Mouse IgG	✓	✓	Abcam	ab122897
Atg3	5% w/v skimmed milk	1 : 1000	Rabbit IgG	✓	✓	CST	#3415
Atg7	5% w/v skimmed milk	1 : 1000	Rabbit IgG	✓	✓	CST	#8558
Bcl-2	5% w/v skimmed milk	1 : 1000	Rabbit IgG	✓	✓	CST	#3498
BID	5% w/v skimmed milk	1 : 1000	Rabbit IgG	✓	✓	CST	#2002
BiP	5% w/v skimmed milk	1 : 1000	Rabbit IgG	✓	✓	CST	#9956
beclin-1	5% w/v skimmed milk	1 : 1000	Rabbit IgG	✓	✓	CST	#3495
Calnexin	5% w/v skimmed milk	1 : 1000	Rabbit IgG	✓	✓	CST	#9956
CASP12	5% w/v skimmed milk	1 : 2000	Rabbit IgG	✓	✓	Abcam	ab62484
Chop	5% w/v skimmed milk	1 : 1000	Mouse IgG	✓	✓	CST	#9956
Ero1-Lα	5% w/v skimmed milk	1 : 1000	Rabbit IgG	✓	✓	CST	#9956
IRE1α	5% w/v skimmed milk	1 : 1000	Rabbit IgG	✓	✓	CST	#9956
LC3B	5% w/v skimmed milk	1 : 1000	Rabbit IgG	✓	✓	CST	#2775
PDI	5% w/v skimmed milk	1 : 1000	Rabbit IgG	✓	✓	CST	#9956
Phospho-Bcl-2 (Ser70)	5% w/v BSA	1 : 1000	Rabbit IgG	✓	✓	CST	#2827
Phospho-IRE1 (Ser724)	5% w/v BSA	1 : 1000	Rabbit IgG	✓	✓	Abcam	ab48187
PSD95	5% w/v/ skimmed milk	1 : 1000	Rabbit IgG		✓	CST	#3450
Synaptophysin	5% w/v skimmed milk	1 : 1000	Rabbit IgG		✓	Abcam	ab7837

Table 2.2: **List of the primary antibodies used in the *in-vitro* immunoblotting studies**. For the list of the abbreviations used, please refer to the corresponding **chapter** .

Cocktail for 1 h at room temperature with gentle agitation. Streptavidin-conjugated HRP along with LumiGLO®/Peroxide Reagent were used to visualise the bound antibody cocktail by chemiluminescence. ChemiDoc ™ MP Imaging System with Image Lab™ software was used to capture images of the slide. The Protein Array Analyzer[32] for Image J was used for the densitometric analysis. The relative peak intensities of the examined signalling molecules were normalised to the corresponding values of the positive and negative controls of the array.

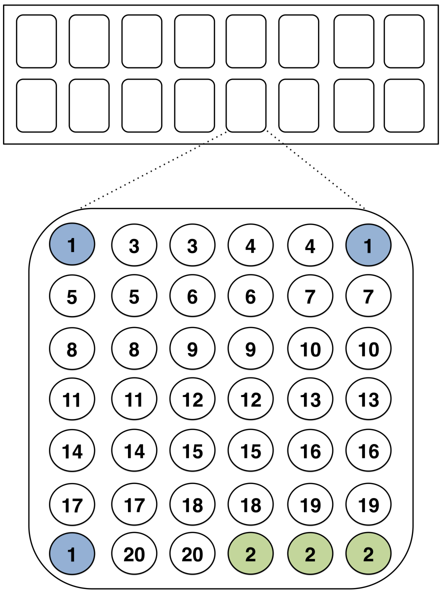

#	Target	Modification Site	Modification Type
1	Positive Control	N/A	N/A
2	Negative Control	N/A	N/A
3	ERK1/2	Thr 202/Tyr 204	Phosphorylation
4	Stat1	Tyr 701	Phosphorylation
5	Stat3	Tyr 705	Phosphorylation
6	Akt	The 308	Phosphorylation
7	Akt	Ser 4731	Phosphorylation
8	AMPKα	Thr 172	Phosphorylation
9	rpS6	Ser 235/236	Phosphorylation
10	mTOR	Ser 2448	Phosphorylation
11	HSP27	Ser 78	Phosphorylation
12	BAD	Ser 112	Phosphorylation
13	p70S6K	Thr 389	Phosphorylation
14	PRAS40	Thr 246	Phosphorylation
15	p53	Ser 15	Phosphorylation
16	p38	Thr 180/Tyr 182	Phosphorylation
17	SAPK/JNK	Thr 183/Tyr 185	Phosphorylation
18	PARP	Asp 214	Cleavage
19	CASP3	Asp 175	Cleavage
20	GSK3β	Ser 9	Phosphorylation

Figure 2.2: **Array of the intracellular signalling targets included in the slide-based Pathscan® sandwich immunoassay.** For the list of the abbreviations used, please refer to the corresponding **chapter** .

2.3.6 Statistics

All the results were expressed as the mean ± standard error (SEM) of at least three independent experiments for each group. Differences among the means were considered significant if $p \leq 0.05$. The assumption of normality was examined by performing the Kolmogorov-Smirnov test. Data was processed with one-way ANOVA analysis, followed by *post hoc* Bonferroni's multiple-comparison t-tests to identify differences among groups of unstressed and stressed conditions. The effects of Liraglutide and GLP-1/GIP Dual Agonist were studied by two-way ANOVA, followed by *post hoc* Bonferroni's multiple-comparison t-tests. Statistical calculations were performed in GraphPad Prism 5 (GraphPad Software Inc., San Diego, USA) for Mac OS X software.

2.4 *In-vivo* Methods

2.4.1 Animals

$APP_{swe}/PS1_{\Delta E9}$ male mice with a C57 black 6 (C57BL/6) background were obtained from the Jackson Laboratory (Maine, US). Wild-type (WT) C57BL/6 female mice were obtained from Charles River UK, Ltd (Kent, UK). Heterozygous $APP_{swe}/PS1_{\Delta E9}$ males were bred with WT females C57BL/6 in the Lancaster University animal unit. Their offspring were ear punched and genotyped for the APP sequence (Forward "GAATTCCGACATGACTCAGG", Reverse: "GTTCTGCTGCATCTTGGACA") by polymerase chain reaction with sequence specific primers (PCR-SSP). Animal genotyping was performed by *Dr.* Simon Gengler and for detailed protocol, please refer to Gengler *et al.*[87] Genotyping results were confirmed by the histological staining of amyloid-β plaques in mouse brains at the end of the study (**subsection 2.4.6**). Mice negative for the transgene in PCR-SSP served as WT controls while their littermates positive for the transgene served as the experimental groups in our study. Animals of both genders were used in our study and single housed in individually ventilated cages (IVC's) in a temperature-controlled colony room ($21 \pm 2\,°C$). Animals were housed in an enriched environment with standard nesting material, NestPak® bedding material, chewing stick and non-toxic polycarbonate play tunnel. They were under a 12 h light/dark cycle, with the lights coming on at 07.00 AM. Food and water were provided *ad libitum*. Daily handling of the animals for two weeks preceded the initiation of the treatments when the mice were 10 month old. Animals were administered Saline (0.9% Sodium Chloride), Liraglutide, ${}_{D}$Ala^2-GIP or GLP-1/GIP Dual Agonist once daily via the intraperitoneal (i.p.) route at a dose of $25\,\mathrm{nmol\,kg^{-1}\,d^{-1}}$ for incretin mimetics and of $10\,\mathrm{mL\,kg^{-1}\,d^{-1}}$ for Saline. Daily dose was selected based on previous experiments that demonstrate the neuroprotective and neurorestorative effects of incretin mimetics in the $APP_{swe}/PS1_{\Delta E9}$ animal model[87,195–198] and in accordance to Good Practice Guidelines for the administration of substances in laboratory animals.[61,81,205] Animals were monitored for their body weight weekly over the treatment period. Mice received the treatments for 8 weeks prior to the commencement of behavioural tasks for assessment of animals' exploratory behaviour, anxiety, learning and memory. All procedures were carried out during the light phase of the cycle, with at least an hour gap from the light/dark transition.

Experimental protocols and research purposes were approved and licensed by the UK Home Office (PPL70/8250). Animal handling and experiments were conducted in accordance to the Animal (scientific procedures) Act of 1986.

2.4.2 Open field test

Exploratory behaviour and anxiety were assessed in the open field test 8 weeks post initiation of the treatment with Liraglutide, $_{D}$Ala^2-GIP and GLP-1/GIP Dual Agonist, as previously described.[94] The open field test was conducted in a grey-coloured, circular aluminium arena (58 cm in diameter) surrounded by a continuous 31-cm-high wall. The open field apparatus was illuminated by a 60-W light bulb fixed to the ceiling, 2.1 m above the centre of the arena. Prior to the commencement of the behavioural task, mice were acclimated to the experimental room for 20 min. Each mouse was placed into the centre of the open field and allowed to explore freely the apparatus for 10 min, with the experimenter out of the animal's sight. A Python-based video tracking/analyser system software (developed by *Dr.* Simon Gengler) interfaced with a monochrome digital camera (Point Grey, ClearView Imaging, Oxfordshire, UK) was used to automatically detect, record and pro-

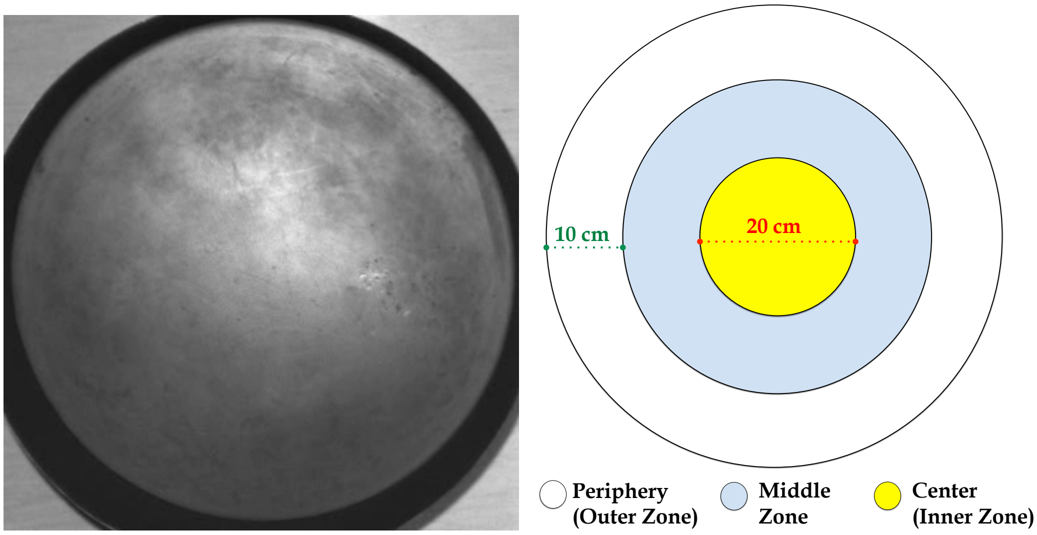

(a) (b)

Figure 2.3: **Example of the overhead camera view of the open field arena recognised by the Python-based video tracking software prior to tracking procedures (a) and an illustration of the zone overlay (b) used to process and interpret open field tracking data.**

cess mouse movements in the arena. Each generated track represented the total distance travelled over the course session and analysed for the time spent, velocity and path length in the centre (inner zone with a radius of 10 cm) and periphery (outer zone with a radius of 10 cm) of the open field [**Figure 2.3**]. Rearing (when the mouse raises its forepaws, stands on its hind paws and extends its head upwards) and grooming (when the mouse licked/scratched its fur, washed its face, and/or licked its genitalia) events were recorded manually during each session. Behavioural scoring was performed blind to animal genotype and treatment. Upon task completion, the mouse was gently removed from the open field and returned back to its home cage. Any faecal boil deposits were manually counted and removed, and the apparatus was thoroughly cleaned with 70% ethyl alcohol to eliminate residual olfactory cues.

2.4.3 Morris water maze task

Morris water maze was employed to evaluate spatial learning and reference memory[204] 8 weeks post initiation of the treatment with Liraglutide, $_{D}$Ala^{2}-GIP and GLP-1/GIP Dual Agonist. It describes a swimming-based cognitive paradigm for rodents that encompasses the acquisition and spatial localisation of relevant visual cues which are processed, consolidated, retained and then retrieved in order to successfully navigate and thus locate a hidden platform to escape the water.[59,204] The Morris water maze task was conducted in a circular white plastic pool with a diameter of 150 cm and a depth of 60 cm. The pool was filled with water at $22 \pm 1\,°C$ to preclude animal hypothermia and at that depth in which the escape platform (10 cm in diameter; made of clear plexiglass) was submerged 1 cm below the water surface. The water was opacified with a non-toxic white dye that rendered the escape platform invisible. The water maze apparatus was illuminated by four 60-W light bulbs fixed on the floor surrounding the pool. Extra-maze visual cues were added in the sidewalls of the apparatus and fixed at positions triangulating the centre of the pool.

Two principal axes of the maze were designated, with each axis bisecting the apparatus perpendicular to one another and creating an imaginary " + ". The ends of each axis demarcates four cardinal points along the circumference of the apparatus – North (N), South (S), East (E), and West (W) [**Figure 2.4**], which did not relate to true magnetic compass directions. Instead, they relied on the experimenter's position, with S being the experimenter's position, N being opposite to S point, and E and W being to the experimenter's right and left, respectively.[300] These points served as starting positions for the mice in the water maze. Having further divided the maze in that way created four equal quadrants for platform positioning [**Figure 2.4**] and animal tracking analysis. Swimming activity of each mouse was monitored with a monochrome digital camera (The Imaging Source Europe GmbH, Bremen, Germany) which was mounted overhead (2.1 m above the centre of the apparatus) and relayed video signals to a Python-based, water-maze tracking/analyser system software (developed by *Dr.* Simon Gengler).

The Morris water maze task initiated a day post the completion of the open field task and lasted 17 days. It consisted of three phases, the visible-platform training, the spatial acquisition and the spatial reversal phase, as described below. On each day of testing, all mice were acclimated to the experimental room for 20 min prior to the commencement of the task. At the end of each trial, over the testing period, mice were gently removed from the pool, returned to their home cages, and placed under a 60-W infrared heat lamp for 1–2 min; mice were visually inspected to ensure thorough dryness. All testing was conducted at roughly the same time each day in order to minimise variability in performance due to time of day.

2.4.3.1 Visible-platform training

Mice were initially trained to locate an escape platform which was cued with a flag, rendering it visible. If an animal did not locate the platform within 60 s, it was gently guided onto platform and allowed to re-orient to the distal visual cues for 30 s before being removed by the pool. Visible-platform training was performed to detect any potent sensorimotor and motivational/emotional defects which could significantly impact the upcoming spatial acquisition phase.[59] For that purpose, path length and the amount of time required to locate the platform along with the swim velocity and thigmotactic behaviour were recorded over a 60-s trial; thigmotactic behaviour was evaluated by the swim time along the perimeter of the pool, defined as a peripheral zone with a radius of 10 cm in the tracking/analyser system software. Mice were assigned to the visible-platform training for 4 consecutive days. Over the training course, animals run in total 9 trials, with one trial on the first day, two trials

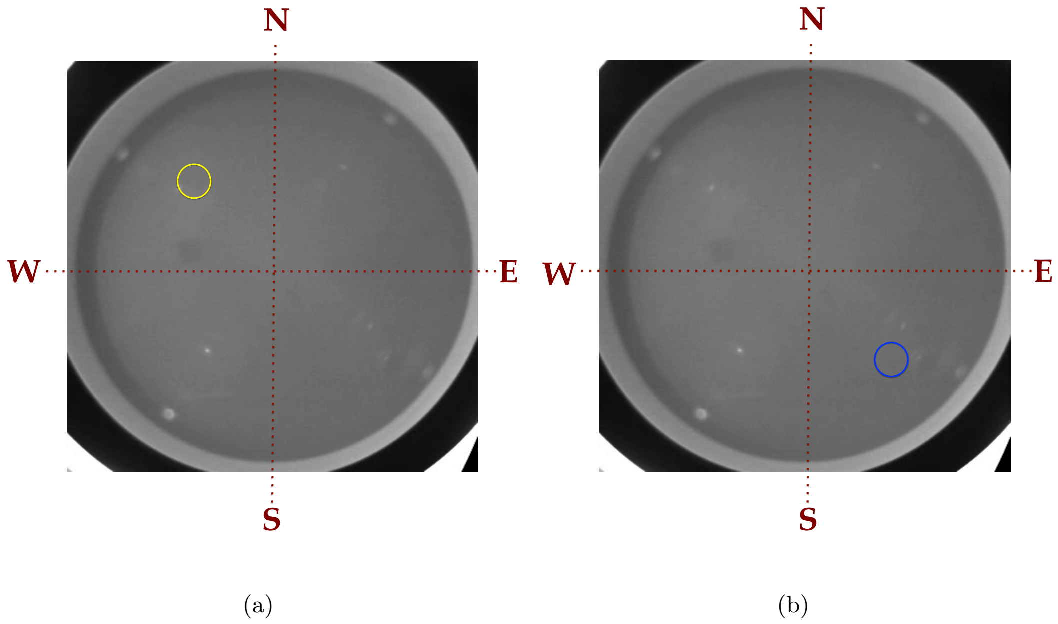

Figure 2.4: **Example of the overhead camera view of the Morris water maze recognised by the Python-based video tracking software prior to tracking procedures, along with the used cardinal points that divided the maze into four equal quadrants for platform positioning, in the spatial acquisition (a) and reversal acquisition (b) phases.**

on the second day, three trials on third and fourth day. Pairs of trials were separated by an inter-trial interval of approximately 30 min. The position of the cued, visible platform and the starting position of each mouse were randomly alternated to avoid animal habituation to a specific area of the pool.

2.4.3.2 Spatial Acquisition

Mice were next trained to locate an invisible escape platform fixed on a target position in the northwest quadrant and 30 cm away from the wall of the apparatus [**Figure 2.4(a)**]. Animals were allowed to search for the invisible escape platform for 60 s and gently guided onto the platform if they did not manage to locate it within that time interval. Animals run 3 trials per day with an inter-trial interval of approximately 30 min. Animal starting position was randomised among the trials per day. Acquisition phase continues for 9 additional days for a total of 30 training trials. Swim time and path travelled to locate the platform along with the swim velocity and thigmotactic behaviour were recorded during each trial; the daily mean swim time (hereinafter referred to as escape latency) and path length to locate the platform were monitored to evaluate spatial learning.[300] A retention probe trial was held on the 11th day to assess spatial reference memory. The escape platform was removed and the swimming pattern of each mouse was recorded in a single trial of 60 s. The percentage of the swim time spent in the quadrant that formerly contained the platform along with the average distance of each mouse from the centre of platform were considered as indexes of memory retention.[83,204]

2.4.3.3 Spatial reversal

A day after the retention probe trial, the escape platform was placed back to the maze but relocated to the opposite, southeast quadrant and fixed 30 cm away from the wall of the apparatus [**Figure 2.4(b)**]. Mice were subjected to a set of 3 trials per day for 5 additional days for a total of 15 trials. Spatial reversal training was conducted similarly to the spatial acquisition training. The spatial reversal phase was aimed to study animals' cognitive flexibility to extinguish their initial learning of the platform's position and acquire a direct path to the new goal position.[300] As in the acquisition phase, at the end of the reversal learning, a reversal probe trial was given 24 h later. The percentage of the swim time spent in the quadrant that formerly contained the platform along with the average distance of each mouse from the centre of platform were similarly considered as measures of memory retention.[83,204]

2.4.4 Novel object recognition task

Recognition memory – a form of declarative memory that refers to the ability to identify a previously encountered object as familiar,[279] was assessed in the novel object recognition

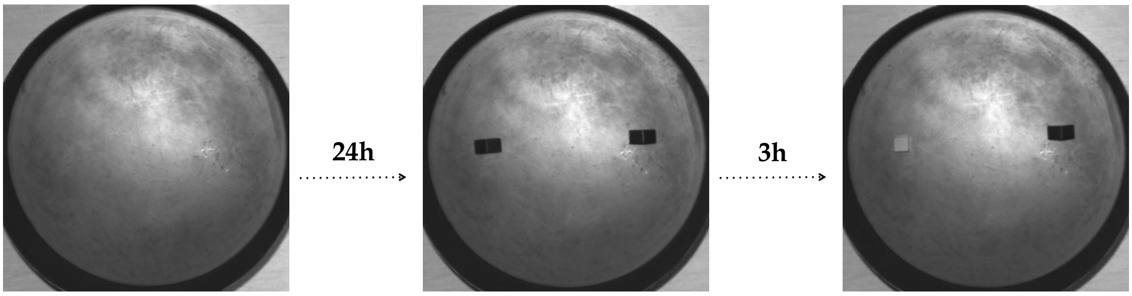

(a) (b) (c)

Figure 2.5: **Example of the overhead camera view of the open field arena recognised by the Python-based video tracking software prior to tracking procedures in the habituation (a), acquisition (b) and the retention (c) trial of the novel object recognition task, along with the inter-trial time intervals.**

task 11 weeks post initiation of the treatment with Liraglutide, ${}_{D}$Ala^2-GIP and GLP-1/GIP Dual Agonist. The task was conducted in the open field apparatus, which was illuminated by 60-W light bulb fixed to the ceiling, 2.1 m above the centre of the arena. The objects used in the present study were green wooden cubes (2.5 cm $\times$ 2.5 cm $\times$ 2.5 cm) and blue wooden triangle blocks (5 cm $\times$ 3 cm $\times$ 3 cm).

The task procedure consisted of three phases – habituation, acquisition and the testing phase [**Figure 5.6**]. In particular, each mouse initially habituated to the open field arena for 10 min, in the absence of the objects. A single acquisition session followed 24 h later, during which each mouse was placed in the familiar arena that at the time contained two identical objects (two triangle blocks or two cubes), and allowed to explore the enriched environment for 10 min. After a retention interval of 3 h, each mouse was assigned to re-explore the familiar arena in the presence of an object identical to previously encountered one and a novel object to evaluate its intermediate-term recognition memory over a 10-min trial. During the acquisition and testing phase, the two objects were positioned in symmetrical sites along the circular arena, 10 cm away from the wall. Novel and familiar object location was counterbalanced within each animal group to prevent bias for a particular area of the apparatus. Similarly, the type of object served as novel was counterbalanced within each animal group, although C57BL/6 and $APP_{swe}/PS1_{\Delta E9}$ mice have displayed equal preference for the green wooden cube and blue wooden triangle block during pilot studies in our laboratory. On each day of testing, all mice were acclimated to the room for 20 min prior to the commencement of the task. At the end of each session, the subject mouse was gently removed from the apparatus and returned back to its home cage. The apparatus and the objects were then thoroughly cleaned with 70% ethyl alcohol to eliminate residual olfactory cues.

During each session, animal activity was recorded with a monochrome digital camera (Point Grey, ClearView Imaging, Oxfordshire, UK) that was mounted on the ceiling, 2.1 m above the centre of the open field arena. The camera was interfaced with a Python-based video tracking/analyser system software (developed by *Dr.* Simon Gengler) that allowed us the automatic detection of the exploration time allotted in each object during the acquisition and retention trials. A mouse was considered to explore an object when its nose was directed towards the object at a distance ≤ 2 cm.[4] Data was processed for the calculation of the *Recognition Index* that describes the percent ratio of the amount of time spent in exploring the familiar or novel object over the total time spent in object exploration during the retention trial course.[4] Recognition index for the novel object was then compared to the corresponding index for the familiar object within each animal group; novelty preference signified task acquisition and recognition memory retrieval.[4] The velocity and total path length were also recorded and compared among the groups to determine whether lack of motivation or emotional defects interfered with the object recognition task acquisition and memory testing.

2.4.5 Brain tissue collection

Following behavioural tasks, animals were transcardially perfused under deep urethane anaesthesia (i.p. injected) with sterile-filtered PBS (1X) supplemented with $20\,\mathrm{IU\,mL^{-1}}$ of heparin. Brains were removed from the skull and sagittally dissected into the two hemispheres. Collected right hemispheres were processed for immunohistochemical studies, as described in **subsection 2.4.6**. Left hemispheres were snap frozen in liquid nitrogen and stored at -80 °C till processed further for homogenisation and protein extraction (**subsection 2.4.7**).

2.4.6 Histology

Upon collection, the right hemispheres were immersion-fixed in 4% parafolmadehyde for 48 h at 4 °C. They were subsequently cryoprotected into 30% sucrose in PBS solution 4 °C, till sunk to the bottom. Brain tissue was embedded on the specimen stage using Tissue-Tek® O.C.T. compound, snap frozen with Ice-It™ Freezing Spray and sectioned in the coronal plane at 40 µm on a Leica cryostat (Leica Microsystems Ltd, Buckinghamshire, UK). Sections were sampled in accordance to stereological rules,[23] with the first one retained randomly and every 12^{th} section afterward, rendering 7–12 coronal sections throughout the neocortex and limbic system per animal for quantitative analysis. Sections were maintained in 30% ethylene glycol and 25% glycerol in 0.1 M phosphate buffer (pH 7.4) at -20 °C till processed for immunohistochemical assessment of amyloid-β plaques and neuroinflammation. We evaluated neuroinflammation by monitoring the immunoreactivity of IBA-1protein, which is involved in membrane ruffling and phagocytosis of activated microglia,[131,225] along with the immunoreactivity of GFAP, the hallmark intermediate filament protein of astrocytes with a profound role in of reactive astrogliosis and glial scar formation.[114,275] We performed avidin-biotin-peroidase complex (ABC) staining method

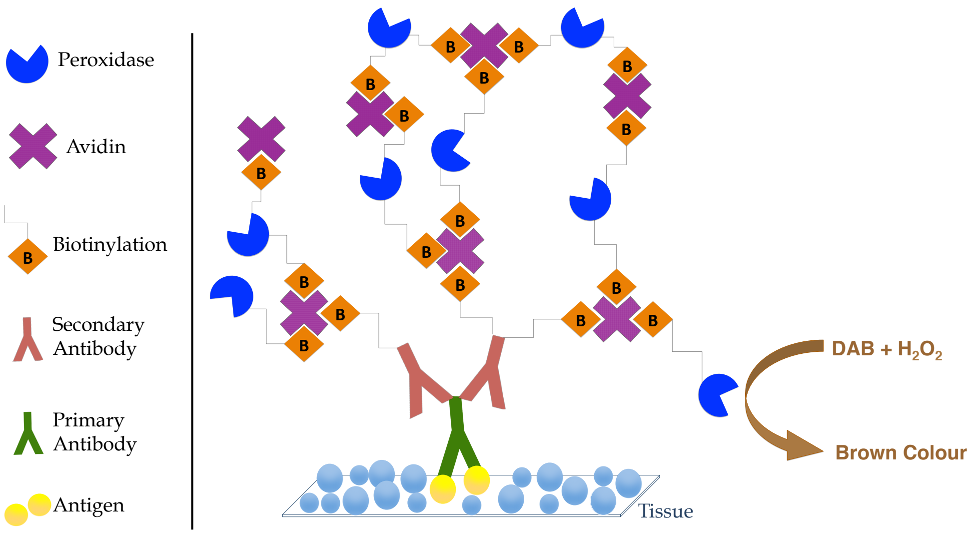

Figure 2.6: **Illustration for the molecular interactions of the avidin-biotin-peroxidase complex (ABC) staining method that rests on the covalent and irreversibly binding between the egg-white glycoprotein, avidin and the vitamin, biotin**. By labelling the secondary antibody with biotin, the tissue antigen of interest can be irreversibly linked to avidin-biotinylated reporter enzyme (*i.e.*, peroxidase) complex, which can be detected by the addition of the chromogen, 3,3–diaminobenzidine (DAB) in the presence of hydrogen peroxide (H_2O_2). As each avidin has multiple biotin-binding sites on its tetravalent molecule, it forms lattice complexes containing multiple copies of the reporter enzyme and resulting into the amplification of the signal of the target antigen.[25]

for detecting and amplifying each target antigen signal, as described in the following paragraph and illustrated in **Figure 2.6**.

Upon thawing, the sections were washed three times in 1X TBS for 10 min each and subsequently incubated with pre-warmed 0.05 M trisodium citrate (pH 9) at 90 °C for 30 min to enhance antigen recognition. When cooled down to room temperature, the sections were washed three times in 1X TBS for 10 min each and incubated with 0.6% hydrogen peroxide for 30 min with gentle agitation at room temperature to quench endogenous peroxidase activity. Following three washes in 1X TBS for 10 min each, the sections were treated with 0.3% Triton-X 100 for 10 min with gentle agitation at room temperature to promote cell permeabilisation. Non-specific antibody binding was prevented by blocking the sections in 5% normal goat serum in TBS for 30 min with gentle agitation at room temperature. The sections were then incubated with the primary antibody against GFAP, IBA-1 or Aβ overnight at 4 °C. All primary antibodies were diluted in 2% normal goat serum in 1X TBS with 0.4% Triton-X 100 at 1 : 500, 1 : 2000 and 1 : 250 ratio for GFAP, IBA-1 or Aβ, respectively. All primary antibodies were generated in rabbit. Following primary antibody incubation, the sections were washed three times in 1X TBS for 10 min each and incubated with a biotinylated goat secondary antibody to rabbit IgG (1 : 360) for 90 min at 4 °C with gentle agitation. Post secondary antibody incubation and three washes in 1X TBS to remove the unbound antibody, tissue was incubated with pre-formed ABC reagent (VECTASTAIN® Elite® ABC-HRP Kit) for 90 min at 4 °C with gentle agitation. The ABC reagent was prepared as per manufacturer's instructions 30 min before use that allowed biotinylated horseradish peroxidase to irreversibly link to the multiple biotin-binding sites available in each tetravalent avidin molecule. Biotinylated peroxidase enzyme and avidin were mixed at the manufacturer's recommended ratio that favoured the formation of lattice enzyme-avidin complexes in the solution though preventing avidin saturation. The remaining biotin-binding sites on the avidin molecule could bind to the biotinylated antibody that had been already bound to the tissue. As a result, a greater concentration of peroxidase localised at the antigen site, increasing sensitivity[25] [**Figure 2.6**]. Following ABC incubation, the sections were washed three times in 1X TBS for 10 min each and flooded with Vector® DAB (3,3–diaminobenzidine) peroxidase substrate working solution, freshly prepared as per manufacturer's instructions. Colour development ceased after 7-8 min by washing the sections three times in tap water for 10 min each. Sections were mounted on silanized slides and cover-slipped using VectaMount AQ aqueous mounting medium. Nikon Eclipse E 600 polarising microscope equipped with Zeiss AxioCam ICc 1 was used for image acquisition. Three micrographs at random points over the cortex along with 2–3 micrographs over the hippocampus were captured at 10X magnification per section per slide per animal group for quantification. Image J was used to quantify the percentage of stained area on each micrograph. The captured micrographs were converted in 8-bit black and white images and automatically segmented into stained and unstained surface areas by the MultiThresholder Image J plug-in, employing maximum entropy thresholding.[256] Image acquisition and processing were performed in a blinded fashion.

2.4.7 Brain tissue homogenisation and protein extraction

Left hemispheres were homogenised by mechanical shearing with a Wheaton™ Dounce tissue grinder in pre-cooled 1X PBS supplemented with protease/phosphatase inhibitor cocktail (1X) on ice. For every 100 mg of tissue, we added 500 µL of the homogenising buffer to acquire 20% *w/v* homogenate. Following a freeze/thaw cycle, homogenate was mixed at 1 : 1 ratio with pre-cooled 1X PathScan® Sandwich ELISA cell lysis buffer supplemented with protease/phosphatase inhibitor cocktail (1X), sonicated for 5 min (30 s ON/30 s OFF – 5 cycles) in an ultrasonic water bath (Ultrawave, South Glamorgan, UK) and gently agitated in a roller shaker (Stuart, Staffordshire, UK) for 1 h at 4 °C to complete cell lysis. Protein was extracted by centrifugation at $\sim 16000 \times g$ for 15 min at 4 °C. The Quick start™ Bradford protein assay was conducted to estimate the protein concentration of the samples, as described in **subsection 2.3.3**. Protein samples of brain whole cell lysate were aliquoted and stored at −80 °C till processed for western blotting.

2.4.8 Western blotting

Protein of mouse brain whole cell lysate (20 µg) was reduced and denaturated by boiling in lithium dodecyl sulfate (LDS) sample buffer containing 50 mM dithiothreitol (DTT) at 95 °C for 5 min. Protein samples were separated on Bolt™ 4 – 12% gradient Bis-Tris gel and blotted onto nitrocellutlose membranes using iBlot® 2 Dry Blotting System. Blots were washed once in 1X TBS for 5 min, blocked in 5% w/v skimmed milk and probed with the primary antibodies against BiP, IRE1α, Chop, ATF6, CASP12, VDAC, beclin-1, Atg3, Atg7, LC3B, synaptophysin, PSD95, or β-actin overnight at 4 °C. Alternatively, blots were blocked in 5% BSA and probed with the primary antibodies against phospho-IRE1 (Ser724), phospho-Akt (Thr308), phospho-ERK1/2 (Thr202/Tyr204) or phospho-GSK3β(Ser9) overnight at 4 °C. All the primary antibodies used were diluted in 5% BSA in 1X TBS with 0.05% Tween® 20 (TBS–T; pH 8) at 1 : 1000 ratio, except for ATF6, CASP12 and β-actin which were diluted at 1 : 500, 1 : 2000 and 1 : 10^4 ratio, respectively. All the primary antibodies used were generated in rabbit, except for the antibodies against Chop and β-actin that were raised in mice. Following primary antibody incubation, blots were washed three times in 1X TBS–T for 5 min each and incubated with the HRP-linked secondary antibodies against the corresponding species IgG (1 : 2000) for 1 h at room temperature. Blots were developed using Amersham ECL Prime western blotting detection reagent kit as per manufacturer's instructions. ChemiDoc™ MP Imaging System with Image Lab™ software used to image chemiluminescent bands and perform densitometric analysis. β-Actin protein was served as the loading control to which relative peak intensities of the examined markers were normalised. To re-probe, blots were incubated in Restore™ PLUS stripping buffer for 20 min at 37 °C with gentle agitation and subsequently washed three times in TBS for 5 min each. Chemiluminescent detection to ensure the removal of the original signal preceded blot re-incubation with another primary antibody of interest.

2.4.9 Statistics

All the results were expressed as the mean ± standard error (SEM) of 9–15 animals for the behavioural studies or 6–8 animals for the histological and biochemical studies per group. Differences among the means were considered significant if $p \leq 0.05$. The assumption of normality was examined by performing the Kolmogorov-Smirnov test. The animal-weight data and Morris water maze acquisition endpoints were analysed by repeated measures two-way ANOVA, followed by *post hoc* Bonferroni's multiple comparison t-test at each time point. Morris water maze probe-trial and open-field data was analysed by one-way ANOVA, followed by *post hoc* Bonferroni's multiple comparison t-test (if the significance level reached). The exploration time allotted in each object during the acquisition of the novel object recognition paradigm along the recognition indexes for the familiar and novel object during the retention trial were processed with Student's *t* test and one-way ANOVA analysis to determine differences within each group and among the groups, respectively. Histological data was analysed by the Kruskal-Wallis test, followed by *post hoc* Dunn's multiple comparison test. Immunoblotting data was processed with one-way ANOVA, followed by *post hoc* Bonferroni's multiple comparison t-test (if the significance level reached). Statistical calculations were performed in GraphPad Prism 5 (GraphPad Software Inc., San Diego, USA) for Mac OS X software.

Chapter 3

Liraglutide restored chronic ER stress, autophagy impairments and apoptotic signalling in SH-SY5Y cells

Published in *Scientific Reports* 7(1) : 16158, 2017

3.1 Introduction

Neuronal injury owing to chronic stress of the endoplasmic reticulum (ER) is increasingly being recognised as a common contributor to amyotrophic lateral sclerosis (ALS), Alzheimer's disease (AD), Parkinson's disease (PD), ischaemic stroke and traumatic brain injury (TBI).[30,111,213,235,312] Shared among these seemingly dissimilar neurological disorders is the presence of intracellular and/or extracellular conditions that perturb signalling and handling of calcium, protein folding processes and autophagic machinery, generating a vicious circle of chronic ER stress.[30,111,213,235,312] The ER is a multifunctional signalling organelle that orchestrates calcium homeostasis and metabolic processes, including gluconeogenesis and the biosynthesis of autophagosomes in the cell. It additionally is the fundamental intracellular compartment for the synthesis, maturation, quality control and delivery of the secretory and membrane proteins.[108] Much physiological and pathological stimuli can alter the protein folding at the ER, triggering a rise in the unfolded or misfolded protein load in the organelle lumen, a cellular state referred to as ER stress.[261] In turn, the cell activates an adaptive signalling network, known as the unfolded protein response (UPR). The UPR essentially engages the three ER-resident transmembrane stress transducers – protein kinase RNA-like ER kinase (PERK), activating transcription factor 6 (ATF6) and inositol-requiring enzyme 1 (IRE1) – to safeguard proteostasis through attenuation of global protein synthesis and transcriptional induction of genes functioning as ER chaperones, and degrade the abnormal through the proteasome (ER-associated degradation) and lysosome-mediated autophagy.[108,109,111] However, under persistent and unsurmountable ER stress, the UPR adapts its dynamics and drives cells towards suicide through diverse but often overlapping mechanisms, including the induction of proteases, kinases, the transcription of CAAT/enhancer-binding protein (C/EBP) homologous protein (Chop) and Bcl-2 family members along with their mediators.[108,109] It is therefore intuitive that therapeutic interventions which resolve UPR and promote a balance between protein generation and degradation crucial for proteostasis may significantly benefit the clinical outcome of acute and chronic neurodegenerative disorders.[30,213,235,312] In this regard, we have focused our research efforts on investigating the restorative effects of the neuroprotective glucagon-like peptide 1 (GLP-1) analogue Liraglutide against chronic ER stress and autophagy dysfunction in SH-SY5Y neuroblastoma cell line.

The incretin hormone GLP-1 is best known for regulating glucose homeostasis and insulin signalling and biosynthesis in response to food ingestion. As such, GLP-1 mimetics are currently approved for the treatment of type 2 diabetes mellitus (T2DM). Apart from their glucose-dependent pancreatic effects, GLP-1 mimetics cross the blood brain barrier and modulate multiple cellular processes within the central nervous system (CNS), including synaptogenesis, neuronal energetics, memory formation and inflammatory responses.[6,115] For instance, intraperitoneal administration of Liraglutide has rescued cognitive and synaptic plasticity deficits, halted excessive synaptic loss, enhanced mitochondria biogenesis and clearance of aggregated proteins and/or mitigated microglia activation and inflammation in a transgenic APP/PS1 mouse model of AD,[195,198] in a 1-methyl-4-phenyl-1,2,3,6-tetrahydropyridine (MPTP) model of PD,[177] in a transgenic mouse model of dementia-related tauopathy,[101] in a rat model of middle cerebral artery occlusion,[259,327] and in a mouse model of mild TBI.[166] In line with the *in-vivo* data, Liraglutide and other GLP-1 mimetics have protected cultured neurones and neuronal cell lines from hypoxia, oxidative stress and excitotoxic injury.[134,166,167,236,265] Notably, in a pilot clinical trial, Liraglutide has rescued the decline of cerebral glucose consumption in AD patients, which signifies energy metabolism in brain areas that have been correlated with cognitive decline in AD and therefore disease progression.[86] Additionally, a pilot open-label clinical trial of the GLP-1 analogue Exenatide has demonstrated persistent improvements in cognitive and motor function of Parkinson's patients.[8,9] A recently-published phase II placebo-controlled double-blind trial has similarly shown that Exenatide halts PD progression and thus confirmed the aforementioned preliminary data.[7] The neuroprotective effects of GLP-1 mimetics lie downstream of the induction of the GLP-1 receptors (GLP-1Rs).[6,115] Indeed, GLP-1R overexpression in hippocampus augments spatial learning and memory performance *in vivo*, effects that are blocked in the presence of a GLP-1R antagonist.[64] Conversely, GLP-1R-deficient mice feature impaired hippocampal synaptic plasticity[1] accompanied by decrements in associative contextual[64] and spatial learning,[1] and increased susceptibility to kainic acid-induced seizures and neuronal degeneration in the hippocampus,[64] as compared to wild-type controls. GLP-1Rs are widely expressed in the brain and mediate survival and trophic signals via the Gα-protein, culminating into the stimulation of adenyl cyclase, Akt and mitogen-activated protein kinase (MAPK) pathways.[6,115] However, whether GLP-1R agonists regulate highly conserved cellular mechanisms, such as the UPR and protein quality control machinery, and engage additional signalling pathways to the aforementioned to promote neuronal survival and tissue repair remains largely unexplored.

The present study demonstrated that the chronic Liraglutide treatment modulated the UPR signalling, restored ER proteostasis and promoted autophagic machinery homeostasis in the proliferating SH-SY5Y human neuroblastoma cells. The stimulation of the GLP-1R potentiated the Akt activity, as expected, while restored the suppressed activity of signal transducer and activator of transcription 3 (STAT3) to normalise the abnormal activity of the antioxidant defensive Nrf2 factor and shift cell fate towards survival upon chronically persistent ER stress. These observations endorse the beneficial effects of the incretin mimetics in neurodegenerative disorders whilst deepening the current understanding of the underlying signalling and mechanism, as outlined in the following sections.

3.2 Liraglutide rescued thapsigargin-induced cytotoxicity and cell-growth arrest

First, the cytoprotective effect of Liraglutide in the SH-SY5Y human neuroblastoma cells from chronic ER stress by thapsigargin elucidated. Thapsigargin is a naturally occurring sesquiterpene lactone that selectively inhibits sarcoplasmic/ER Ca^{2+}–ATPase (SERCA), triggering a transient increase in the cytosolic calcium and depleting ER calcium stores.[292] Cells were treated with 0, 10, 100 and 1000 nM of thapsigargin in the presence or absence of 100 nM Liraglutide for 16 h, and processed for XTT, BrdU and LDH assays to assess cell viability, proliferation and cytotoxicity, respectively. One-way ANOVA analysis revealed overall significant differences in cell viability [$F_{(7,442)} = 79.59$, $p \leq 0.001$], proliferation [$F_{(7,355)} = 48.98$, $p \leq 0.001$] and cytotoxicity [$F_{(7,436)} = 255.2$, $p \leq 0.001$]. *Post-hoc* analysis with Bonferroni correction demonstrated that thapsigargin impaired cell viability in a dose-dependent fashion; it triggered an approximately 7%, 20% ($p \leq 0.001$) and 50% ($p \leq 0.001$) decline in the number of viable, metabolically active cells that were accordingly challenged with 10, 100 and 1000 nM of the stressor, with respect to control conditions [**Figure 3.1(a)**]. A dose-dependent cell growth arrest and membrane perturbation accompanied the suppressed cell viability. Specifically, the percentage of proliferating cells approximately decreased by 30% ($p \leq 0.001$), 50% ($p \leq 0.001$) and 60% ($p \leq 0.001$) in the micro-cultures exposed to 10, 100 and 1000 nM of thapsigargin, respectively, when compared to the control conditions [**Figure 3.1(b)**]. Conversely, LDH release progressively increased by 8%, 30% ($p \leq 0.001$) and 120% ($p \leq 0.001$) in the supernatant of the micro-cultures received the aforementioned stressor doses [**Figure 3.1(c)**]. Two-way ANOVA analysis demonstrated that Liraglutide co-treatment significantly rescued the abnormal LDH activity [$F_{(3,436)} = 16.91$, $p \leq 0.001$] and ameliorated cell-viability [$F_{(3,442)} = 8.14$,

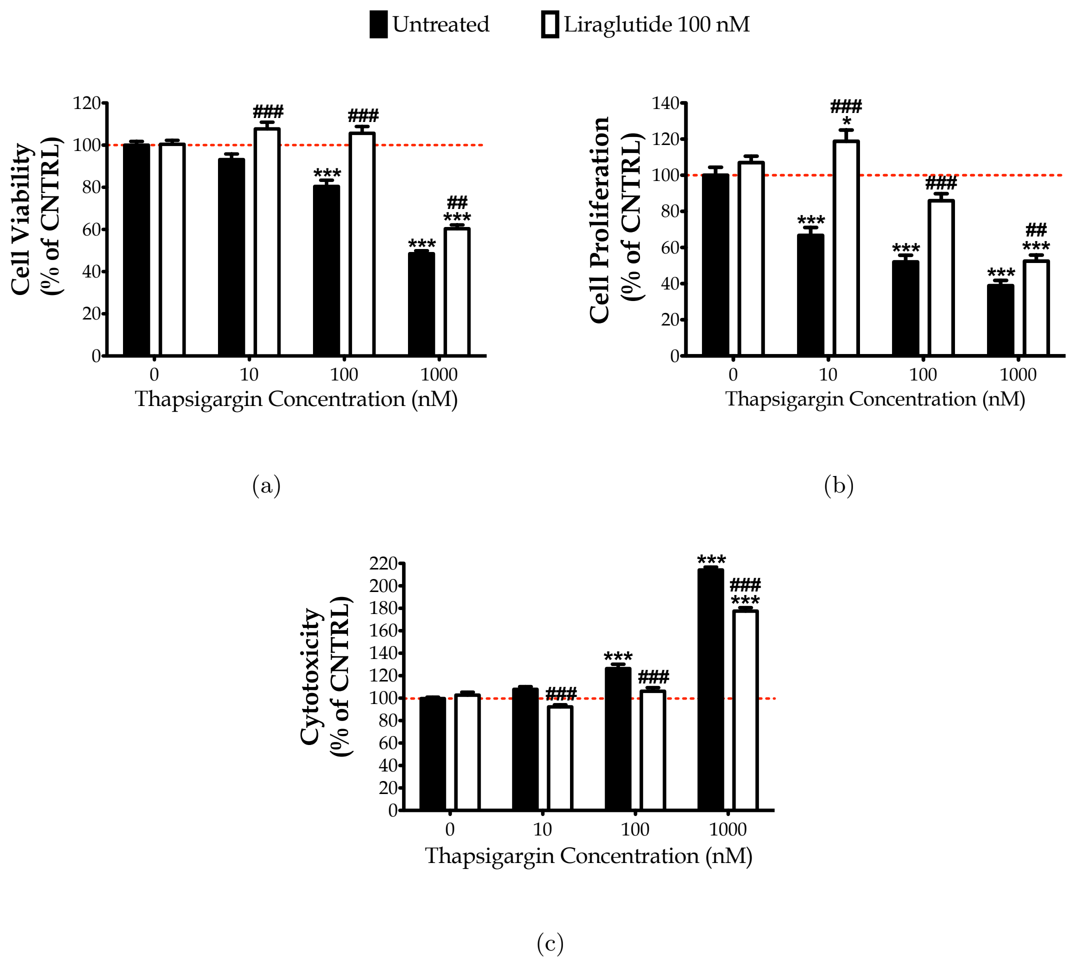

Figure 3.1: **Liraglutide restored abnormal cytotoxicity and ameliorated impaired viability and proliferation in the neuroblastoma SH-SY5Y cell line upon persistent ER stress.** Twenty-four hours post seeding, SH-SY5Y cells were serum starved for 8 h and treated with 0, 10, 100 and 1000 nM of thapsigargin for 16 h, in the presence or absence of 100 nM Liraglutide. Cells were then assayed for XTT metabolisation [**(a)**] and BrdU incorporation [**(b)**] to assess cell viability and proliferation, respectively. Cell supernatant was collected and processed for LDH activity [**(c)**] to determine cytotoxicity. Each bar represents the mean ± SEM from four independent experiments. All cell treatments were performed in sextuplicate per plate per experiment. Data is expressed as a percentage of the control (CNTRL; unstressed/untreated conditions). Data was analysed by one- and two-way ANOVA, followed by *post hoc* Bonferroni's multiple comparison t-test ($^{*}p \leq 0.05$ & $^{***}p \leq 0.001$ compared to CNTRL; $^{\sharp\sharp}p \leq 0.01$ & $^{\sharp\sharp\sharp}p \leq 0.001$ compared to the corresponding thapsigargin-treated cells). Red dashed line corresponds to the CNTRL levels.

$p \leq 0.001$] and proliferation [$F_{(3,355)} = 11.75$, $p \leq 0.001$] impairments following chronic SERCA inhibition [**Figure 3.1**]. Interestingly, Liraglutide approximately induced a 25% and 35% rise in the number of metabolically active and proliferating cells when stressed with 100 nM of thapsigargin, and restored the cell density nearly back to control levels [**Figures 3.1(a)–3.1(b)**]. Similarly, Liraglutide co-treatment normalised the abnormal LDH activity in the SH-SY5Y micro-cultures received 100 nM of thapsigargin [**Figure 3.1(c)**]. Therefore, the concentration of 100 nM of thapsigargin stress, where Liraglutide fully restores cell physiology, was considered for the subsequent biochemical studies .

3.3 Liraglutide resolved the UPR and restored homeostasis in the protein folding machinery of ER

Cells were treated with 0 and 100 nM of thapsigargin in the presence or absence of 100 nM Liraglutide for 16 h, and processed for immunoblotting analysis of hallmark ER stress-related signalling molecules. One-way ANOVA analysis demonstrated overall significant differences in the binding immunoglobulin protein (BiP) [$F_{(3,28)} = 27.90$, $p \leq 0.001$], full-length ATF6 [$F_{(3,28)} = 6.267$, $p \leq 0.01$], IRE1α activation [$F_{(3,27)} = 8.683$, $p \leq 0.001$], Chop [$F_{(3,28)} = 20.66$, $p \leq 0.001$], and active caspase 12 (CASP12) [$F_{(3,28)} = 4.185$, $p \leq 0.05$]. Chronic thapsigargin treatment triggered a 1.5-fold increase in BiP expression [**Figure 3.2(a)**] indicating ER stress,[159] as well a significant increase in the full-length ATF6 levels ($p \leq 0.01$) too [**Figure 3.2(d)**]. Upon ER stress, ATF6 translocates to Golgi where it undergoes proteolytic cleavage at a juxtamembrane site. The latter generates an active cytosolic 50-kDa ATF6 fragment that migrates into the nucleus.[261] Although this proteolytic fragment was not consistently observed in the four immunoblotting experiments analysed (data not shown), confocal imaging revealed a nuclear accumulation of ATF6 following chronic thapsigargin treatment in SH-SY5Y cells [**Figure 3.2(c)**] that signified its activation. Chronic thapsigargin treatment significantly precluded the activating phosphorylation of IRE1α at the serine 724 residue (Ser724) ($p \leq 0.001$), as compared to control conditions [**Figure 3.2(b)**]. It additionally potentiated a 10-fold increase in Chop

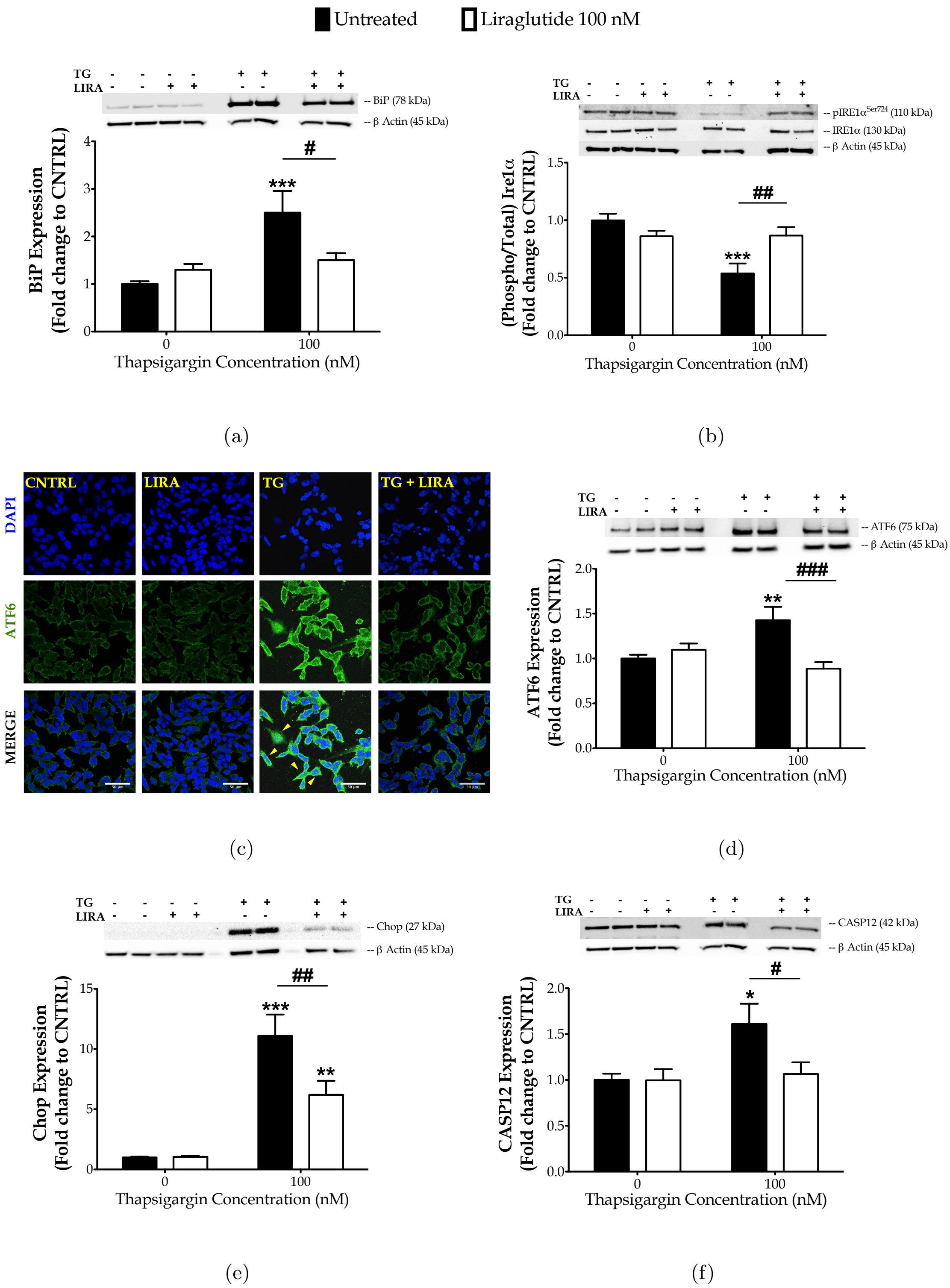
Untreated
Liraglutide 100 nM
TG
LIRA
-- BiP (78 kDa)
-- β Actin (45 kDa)
BiP Expression
(Fold change to CNTRL)
Thapsigargin Concentration (nM)
(a)
-- pIRE1α Ser724 (110 kDa)
-- IRE1α (130 kDa)
-- β Actin (45 kDa)
(Phospho/Total) Ire1α
(Fold change to CNTRL)
Thapsigargin Concentration (nM)
(b)
CNTRL
LIRA
TG
TG + LIRA
DAPI
ATF6
MERGE
(c)
-- ATF6 (75 kDa)
-- β Actin (45 kDa)
ATF6 Expression
(Fold change to CNTRL)
Thapsigargin Concentration (nM)
(d)
-- Chop (27 kDa)
-- β Actin (45 kDa)
Chop Expression
(Fold change to CNTRL)
Thapsigargin Concentration (nM)
(e)
-- CASP12 (42 kDa)
-- β Actin (45 kDa)
CASP12 Expression
(Fold change to CNTRL)
Thapsigargin Concentration (nM)
(f)

Figure 3.2: **Liraglutide resolved UPR in the neuroblastoma SH-SY5Y cell line.** Twenty-four hours post seeding, SH-SY5Y cells were serum starved for 8 h and treated with 0 or 100 nM of thapsigargin (TG) for 16 h, in the presence or absence of 100 nM Liraglutide (LIRA). Cells were harvested, and the expression levels of BiP [**(a)**], phosphorylated and total IRE1α [**(b)**], ATF6 [**(d)**], Chop [**(e)**], and caspase 12 (CASP12) [**(f)**] proteins were determined by western blotting. β-Actin was used as the loading control to all western blot analyses. Each bar represents the mean $\pm$ SEM from four independent experiments. Data is expressed as fold change to the control (CNTRL; unstressed/untreated conditions). Data was analysed by one- and two-way ANOVA, followed by *post hoc* Bonferroni's multiple comparison t-test ($^{*}p \leq 0.05$, $^{**}p \leq 0.01$ & $^{***}p \leq 0.001$ compared to CNTRL; $^{\sharp}p \leq 0.05$, $^{\sharp\sharp}p \leq 0.01$ & $^{\sharp\sharp\sharp}p \leq 0.001$ compared to the corresponding thapsigargin-treated cells). [**(d)**] Representative pictures of SHSY5Y cells immunolabelled for ATF6 following thapsigargin and Liraglutide treatments. Scale bars: 50 µm.

($p \leq 0.001$) and almost doubled the active CASP12 fragment at 42 kDa ($p \leq 0.05$) [**Figure 3.2(e)–3.2(f)**]. Intriguingly, Liraglutide normalised the abnormal BiP [**Figure 3.2(a)**] and ATF6 [**Figure 3.2(d)**] protein expressions. It rescued IRE1α [**Figure 3.2(b)**] and ATF6 activation [**Figure 3.2(c)**]. Moreover, Liraglutide co-treatment normalised abnormal CASP12 activity [**Figure 3.2(f)**] and significantly ameliorated the ectopic Chop expression by halving protein levels of this transcription factor ($p \leq 0.01$) [**Figure 3.2(e)**].

It was pertinent to ask at that point whether the modulation of the UPR corresponded to a restoration of ER protein quality control machinery. One-way ANOVA demonstrated overall significant differences in the ER oxidoreductase 1α (Ero1-Lα) [$F_{(3,28)} = 3.668$, $p \leq 0.05$] and calnexin [$F_{(3,28)} = 11.62$, $p \leq 0.001$] but not in the expression of protein disulphide isomerase (PDI) [$F_{(3,28)} = 1.053$, $p = 0.3846$]. *Post-hoc* analysis showed that chronic thapsigargin treatment exacerbated Ero1-Lα protein levels ($p \leq 0.05$) whilst suppressing calnexin by approximately 60% ($p \leq 0.001$). Notably, Liraglutide co-treatment normalised aberrant protein expression of Ero1-Lα and calnexin, as illustrated in **Figure 3.3**.

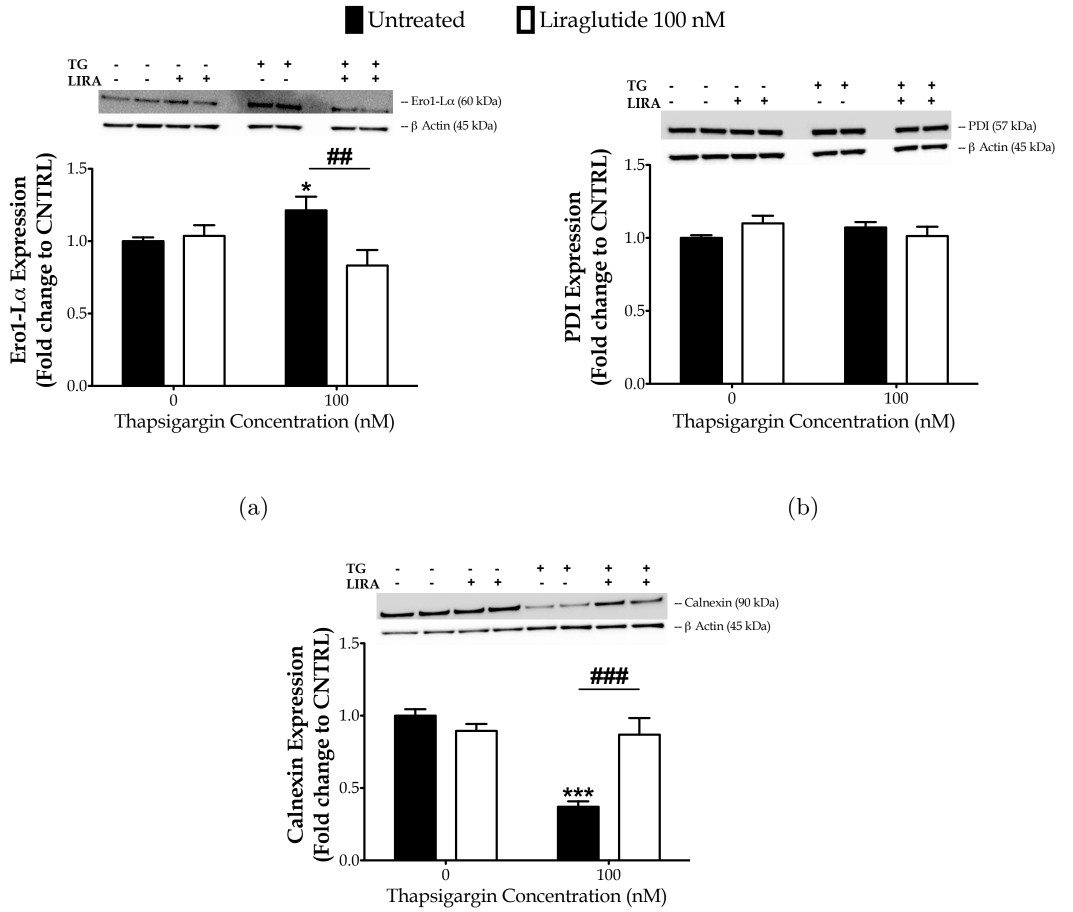

(c)

Figure 3.3: **Liraglutide promoted ER proteostasis in the neuroblastoma SH-SY5Y cell line upon persistent ER stress.** Twenty-four hours post seeding, SH-SY5Y cells were serum starved for 8 h and treated with 0 or 100 nM of thapsigargin for 16 h, in the presence or absence of 100 nM Liraglutide. Cells were harvested, and the expression of ER oxidoreductase 1 alpha (Ero1-Lα) [**(a)**], protein disulphide isomerase [PDI; **(b)**] and of calnexin [**(c)**] were determined by western blotting. β-Actin was used as the loading control to all western blot analyses. Each bar represents mean $\pm$ SEM from four independent experiments. Data is expressed as fold change to the control (CNTRL; unstressed/untreated conditions). Data was analysed by one- and two-way ANOVA, followed by *post hoc* Bonferroni's multiple comparison t-test ($^{*}p \leq 0.05$ & $^{***}p \leq 0.001$ compared to CNTRL; $^{\sharp\sharp}p \leq 0.01$ & $^{\sharp\sharp\sharp}p \leq 0.001$ compared to the corresponding thapsigargin-treated cells).

3.4 Liraglutide rescued thapsigargin-induced autophagy impairments

ER-localised blocking of calcium flux has been previously shown to perturb autophagosome biogenesis[67] and fusion with lysosome,[84] culminating into autophagy arrest[67,84] that can,

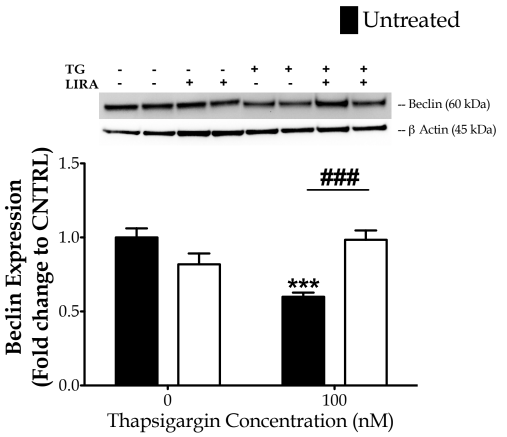

(a)

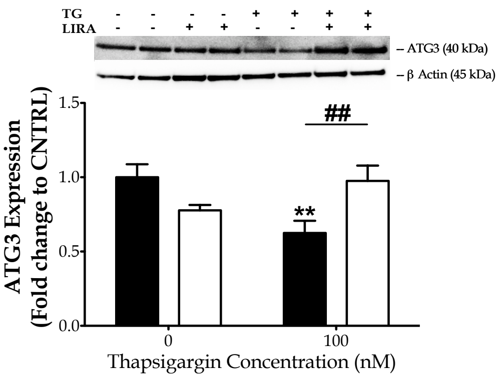

(b)

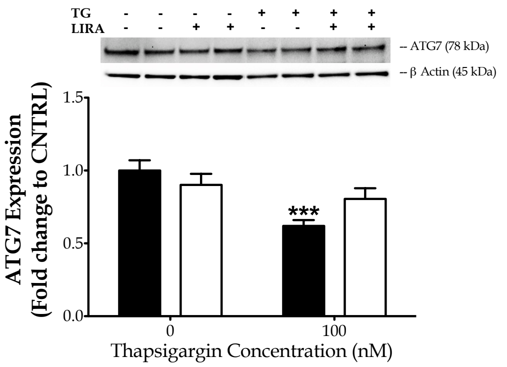

(c)

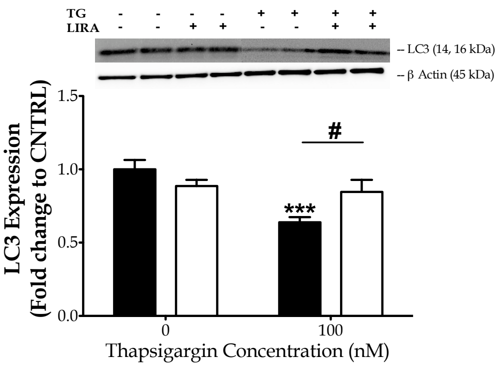

(d)

Figure 3.4: **Chronic disturbance of ER calcium homeostasis diminished "core" Atg proteins required for autophagosome formation. Liraglutide rescued autophagy impairments in the neuroblastoma SH-SY5Y cell line upon persistent ER stress.** Twenty-four hours post seeding, SH-SY5Y cells were serum starved for 8 h and treated with 0 or 100 nM of thapsigargin for 16 h, in the presence or absence of 100 nM Liraglutide. Cells were harvested, and the expression of beclin-1 [**(a)**], ATG3 [**(b)**], ATG7 [**(c)**] and of LC3 [**(d)**] were determined by western blotting. β-Actin was used as the loading control to all western blot analyses. Each bar represents mean ± SEM from four independent experiments. Data is expressed as fold change to the control (CNTRL; unstressed/untreated conditions). Data was analysed by one- and two-way ANOVA, followed by *post hoc* Bonferroni's multiple comparison t-test ($^{**}p \leq 0.01$ & $^{***}p \leq 0.001$ compared to CNTRL; $^{\sharp}p \leq 0.05$, $^{\sharp\sharp}p \leq 0.01$ & $^{\sharp\sharp\sharp}p \leq 0.001$ compared to the corresponding thapsigargin-treated cells).

in turn, elicit or enhance ER stress.[274] Thus, the present study investigated the expression of a set of autophagy-related (Atg) proteins following chronic thapsigargin and Liraglutide treatment [**Figure 3.4**]. Protein expression of beclin-1 [$F_{(3,28)} = 10.02$, $p \leq 0.001$], Atg3 [$F_{(3,28)} = 4.78$, $p \leq 0.01$], Atg7 [$F_{(3,28)} = 5.977$, $p \leq 0.01$], and LC3 [$F_{(3,28)} = 6.557$,

$p \leq 0.01$] significantly differed among groups, as evident by one-way ANOVA analysis. *Post-hoc* analysis demonstrated that chronic thapsigargin treatment significantly suppressed beclin-1 ($p \leq 0.001$) [**Figure 3.4(a)**], Atg3 ($p \leq 0.01$) [**Figure 3.4(b)**], Atg7 ($p \leq 0.001$) [**Figure 3.4(c)**], and LC3 ($p \leq 0.001$) [**Figure 3.4(d)**] protein expression. Two-way ANOVA analysis indicated that Liraglutide co-treatment significantly alleviated the impairments in beclin-1 ($F_{(1,28)} = 23.07$, $p \leq 0.001$), Atg3 ($F_{(1,28)} = 12.52$, $p \leq 0.01$) and LC3 ($F_{(1,28)} = 7.43$, $p \leq 0.05$). Additionally, there was a trend of improvement by Liraglutide on the decreased Atg7 expression following thapsigargin treatment [$F_{(1,28)} = 4.59$, $p \leq 0.05$], though it did not reach statistical significance when compared to the corresponding stress conditions in *post-hoc* analysis [**Figure 3.4(c)**].

3.5 Liraglutide normalised aberrant nuclear accumulation of Nrf2 following ER stress and autophagy dysfunction

Immunocytochemical analysis of the nuclear levels of the transcription factor Nrf2 was employed to link defective proteostasis to the antioxidant (defensive) response of the proliferating SH-SY5Y cells. Under basal conditions, Nrf2 is mainly localised to cytoplasm in a complex with the Kelch-like ECH-associated protein 1 (Keap1). Keap1 is an ubiquitin ligase substrate adaptor that targets Nrf2 for degradation.[186] Consistently, unstressed SH-SY5Y cells display a faint Nrf2-positive immunostaining that mainly resides in the peri-nuclear area [red arrows; **Figure 3.5(a)**]. However, in response to cellular stress, Nf2 dissociates from Keap1 and rapidly translocates into nucleus to confer its transcriptional activity.[186] Accordingly, chronic thapsigargin treatment induced nuclear accumulation of Nrf2 (*post hoc*; $p \leq 0.05$) that was normalised by Liraglutide co-treatment [yellow arrows; **Figure 3.5**].

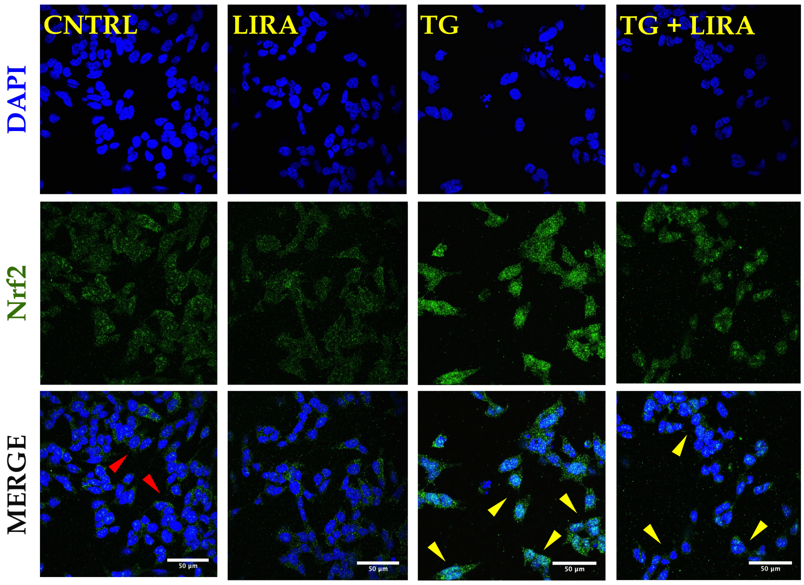

(a)

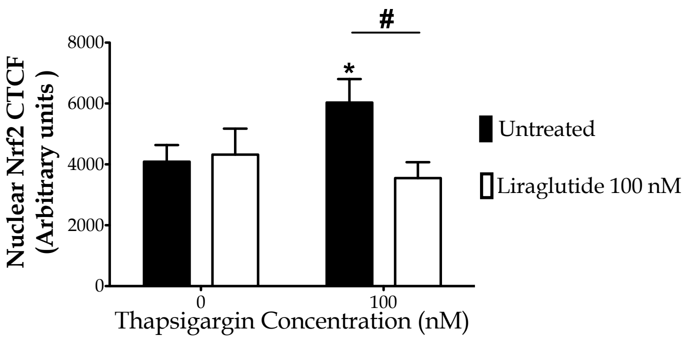

(b)

Figure 3.5: **Liraglutide restored aberrant signalling of the nuclear factor erythroid 2-related factor 2 (Nrf2) in the neuroblastoma SH-SY5Y cell line upon chronic ER stress.** Twenty-four hours post seeding, SH-SY5Y cells were serum starved for 8 h and treated with 0 or 100 nM of thapsigargin (TG) for 16 h, in the presence or absence of 100 nM Liraglutide (LIRA). Cells were (para-formaldehyde)-fixed, immunolabelled for Nrf2 and processed for confocal imaging at 40X magnification, as shown in the representative image panel [**(a)**]. Eight pictures were captured per experimental group per experiment for quantification. Image J was used to quantify corrected total cell fluorescence (CTCF) of the nuclear Nrf2 staining [**(b)**]. Each bar represents mean ± SEM from three independent experiments. Data was analysed by one- and two-way ANOVA, followed by *post hoc* Bonferroni's multiple comparison t-test ($^{*}p \leq 0.05$ compared to CNTRL; $^{\sharp}p \leq 0.05$ compared to the corresponding thapsigargin-treated cells). Scale bars: 50 µm.

3.6 Liraglutide restored impaired STAT3 activity and activates Akt signalling to ameliorate thapsigargin-induced apoptosis

Sandwich-based antibody array was employed for investigating the signalling network that underlied the cross-talk among the different sub-cellular compartments and mediated the prominent neuroprotective/restorative effects of Liraglutide [**Figures 3.6 & 3.7, Table S1**]. Disturbance of ER calcium homeostasis significantly precluded the activating phosphorylation of the extracellular signal-regulated kinase 1/2 (ERK1/2) at threonine 202 (Thr202) and tyrosine 204 (Tyr204) residues ($p \leq 0.05$) and of Stat3 at Tyr705 ($p \leq 0.01$), as shown in **Figures 3.6(b) & 3.6(f)**, respectively. It additionally induced the glycogen synthase kinase 3β (GSK3β) activity [**Figure 3.6(d)**] by halving the inhibitory phosphorylation of the kinase at the serine 9 (Ser9) residue ($p \leq 0.001$ whilst significantly impeding the phosphorylation of the stress-responsive p53 at Ser15 ($p \leq 0.05$) [**Figure 3.6(e)**]. All these alterations in the signalling molecules correlated to a two-fold increase ($p \leq 0.001$) in the cleaved poly (ADP-ribose) polymerase (PARP) [**Figure 3.6(h)**] that assured the fulfilment and irreversibility of the apoptotic process[228] upon the 16-h time course of thapsigargin treatment in SH-SY5Y cells. Liraglutide rescued STAT3 activation ($p \leq 0.05$) [**Figure 3.6(f)**] but did not alleviate ERK1/2 impairments [**Figure 3.6(b)**]. Moreover, Liraglutide restored GSK3β [**Figure 3.6(d)**] and p53 [**Figure 3.6(e)**] activity to the baseline levels, and significantly provoked Akt phosphorylation at Thr308 ($p \leq 0.05$) under chronic thapsigargin treatment [**Figure 3.6(c)**]. Liraglutide significantly attenuated the ectopic PARP proteolysis ($p \leq 0.05$) upon unmitigated UPR and autophagy impairments that signifies cytoprotection, though it remained significantly elevated when compared to control conditions ($p \leq 0.05$) in *post-hoc* analysis [**Figure 3.6(h)**].

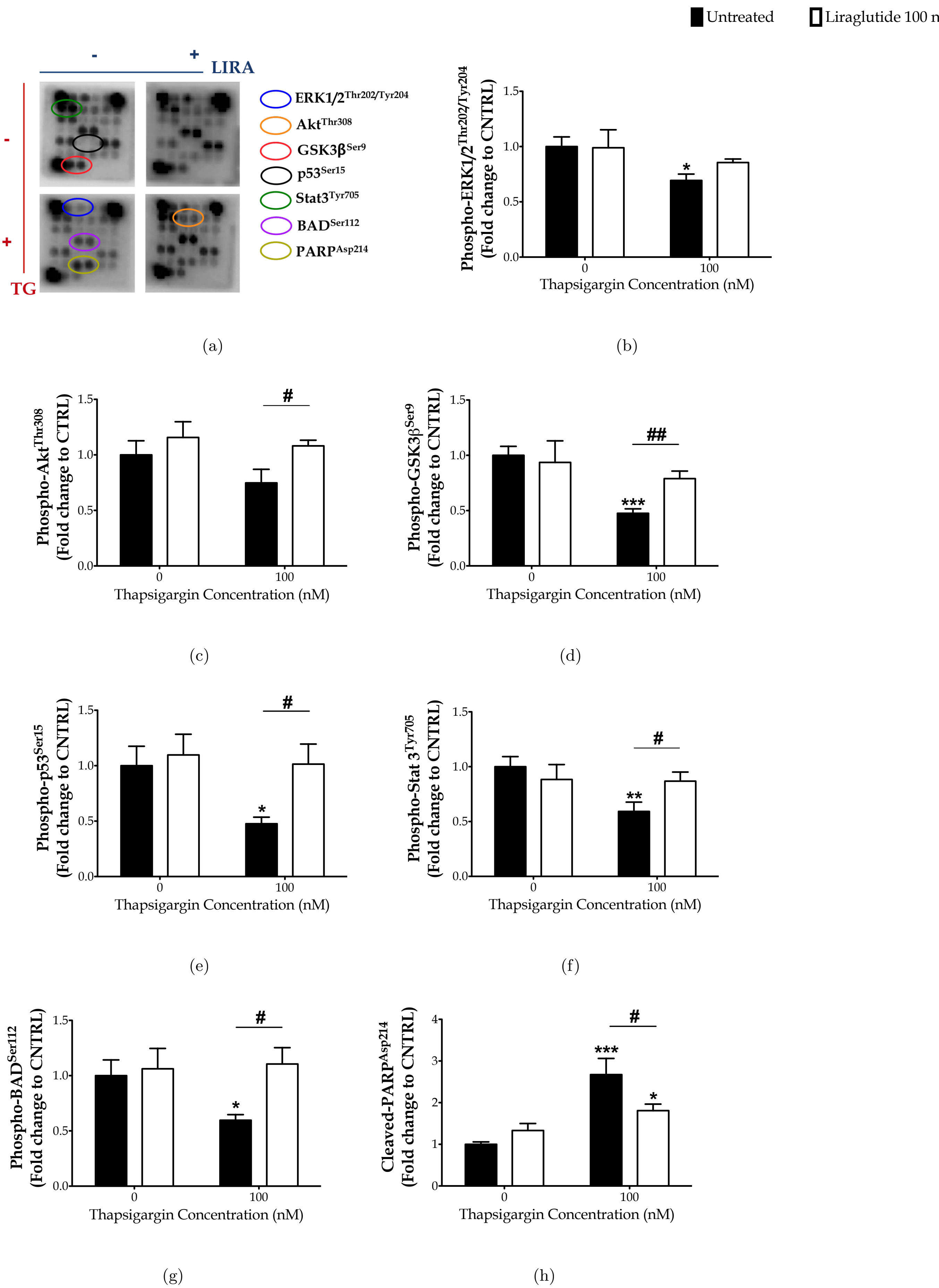
Untreated
Liraglutide 100 n
LIRA
-
+
-
+
TG
ERK1/2Thr202/Tyr204
AktThr308
GSK3βSer9
p53Ser15
Stat3Tyr705
BADSer112
PARPAsp214
(a)
Phospho-ERK1/2Thr202/Tyr204 (Fold change to CNTRL)
0.0
0.5
1.0
1.5
*
0
100
Thapsigargin Concentration (nM)
(b)
Phospho-AktThr308 (Fold change to CTRL)
0.0
0.5
1.0
1.5
#
0
100
Thapsigargin Concentration (nM)
(c)
Phospho-GSK3βSer9 (Fold change to CNTRL)
0.0
0.5
1.0
1.5
##
***
0
100
Thapsigargin Concentration (nM)
(d)
Phospho-p53Ser15 (Fold change to CNTRL)
0.0
0.5
1.0
1.5
#
*
0
100
Thapsigargin Concentration (nM)
(e)
Phospho-Stat 3Tyr705 (Fold change to CNTRL)
0.0
0.5
1.0
1.5
#
**
0
100
Thapsigargin Concentration (nM)
(f)
Phospho-BADSer112 (Fold change to CNTRL)
0.0
0.5
1.0
1.5
#
*
0
100
Thapsigargin Concentration (nM)
(g)
Cleaved-PARPAsp214 (Fold change to CNTRL)
0
1
2
3
4
#
***
*
0
100
Thapsigargin Concentration (nM)
(h)

Figure 3.6: **Chronic disturbance of ER calcium homeostasis induced PARP cleavage, diminished inhibitory phosphorylation of the pro-apoptotic BAD protein and of the multifunctional GSK3β kinase, and impaired ERK and STAT3 signalling to promote genotoxicity and apoptosis. Liraglutide rescued PARP cleavage and activation of STAT3 and p53 kinases. It additionally induced Akt phosphorylation that relieved BAD and GSK3β activity to promote cell survival in the neuroblastoma SH-SY5Y cell line upon persistent ER stress.** Twenty-four hours post seeding, SH-SY5Y cells were serum starved for 8 h and treated with 0 or 100 nM of thapsigargin for 16 h, in the presence or absence of 100 nM Liraglutide. Cells were harvested, and 0.3 mg mL^{-1} protein of whole-cell lysate was processed with the PathScan® sandwich immunoassay. All protein samples per experiment were processed in duplicate. Each bar represents mean ± SEM from four independent experiments. Data is expressed as fold change to the control (CNTRL; unstressed/untreated conditions). Data was analysed by one- and two-way ANOVA, followed by *post hoc* Bonferroni's multiple comparison t-test ($^{*}p \leq 0.05$, $^{**}p \leq 0.01$ & $^{***}p \leq 0.001$ compared to CNTRL; $^{\sharp}p \leq 0.05$ & $^{\sharp\sharp}p \leq 0.01$ compared to the corresponding thapsigargin-treated cells).

It is well documented that the majority of pro-death signals emerging from UPR regulate the expression and activity of pro- and anti-apoptotic proteins of BCL-2 family.[108,109] Consistently, we report that persistent ER-localised blocking of calcium flux diminishes the inhibitory phosphorylation of the pro-apoptotic BAD at Ser112 ($p \leq 0.05$) [**Figure 3.6(g)**], accompanied by a significant de-phosphorylation of the survival-agonist Bcl-2 at Ser70 ($p \leq 0.01$) [**Figure 3.7(a)**]. Liraglutide normalises aberrant BAD [**Figure 3.6(g)**] and Bcl-2 [**Figure 3.7(a)**] phosphorylation patterns and further down-regulates the normal expression of the full-length BH3 interacting-domain death agonist (BID) [**Figure 3.7(b)**].

3.7 Discussion

Neuronal injury owing to chronic and unmitigated ER stress has been increasingly correlated with a range of neurodegenerative disorders while UPR activation and dysregulation has been repeatedly found in *post-mortem* brain samples from affected patients and animals of AD, PD, ALS, HD, and experimental stroke.[30,111,213,235,312] Pharmacological and genetic manipulation approaches have unravelled promising mechanisms that link ER stress

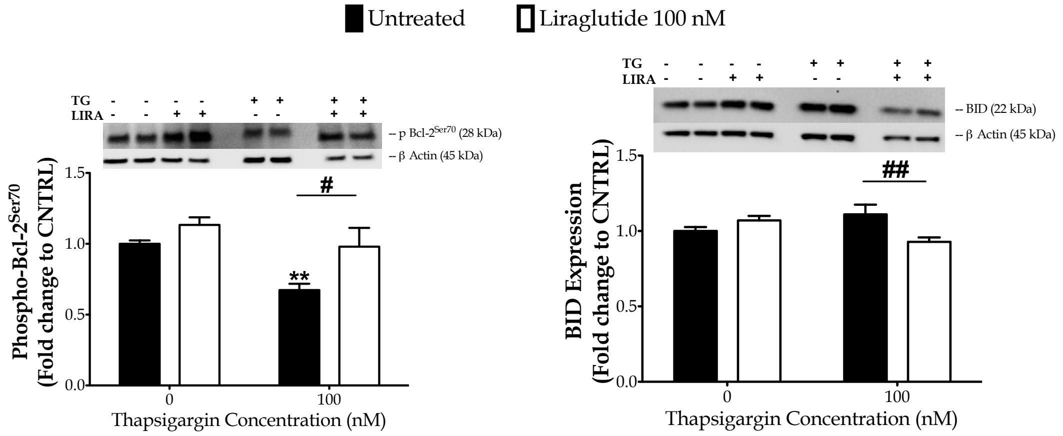

(a) (b)

Figure 3.7: **Liraglutide restored impaired Bcl-2 phosphorylation at serine 70 whilst down-regulating the BID protein levels in the neuroblastoma SH-SY5Y cell line upon persistent ER stress.** Twenty-four hours post seeding, SH-SY5Y cells were serum starved for 8 h and treated with 0 or 100 nM of thapsigargin for 16 h, in the presence or absence of 100 nM Liraglutide. Cells were harvested, and Bcl-2 phosphorylation [**(a)**] and BID expression [**(b)**] were determined by western blotting. β-Actin was used as the loading control to all western blot analyses. Each bar represents the mean $\pm$ SEM from four independent experiments. Data is expressed as fold change to the control (CNTRL; unstressed/untreated conditions). Data was analysed by one- and two-way ANOVA, followed by *post hoc* Bonferroni's multiple comparison t-test ($^{**}p \leq 0.01$ compared to CNTRL; $^{\sharp}p \leq 0.05$ & $^{\sharp\sharp}p \leq 0.01$ compared to the corresponding thapsigargin-treated cells).

to neurodegenerative processes. In particular, AD features the accumulation of amyloid-β (Aβ) peptides in the brain, which underlies neuronal dysfunction and cognitive decline. Aβ primarily perturbs the cellular redox status and abnormally increases the amount of calcium that can be released by the ER, triggering ER stress, mitochondrial dysfunction and thereby neuronal toxicity and astrogliosis *in vivo*.[30,235] Accordingly, α-Synuclein, the molecular determinant of PD pathobiology, alters the interactions between ER and mitochondria, which triggers an aberrant increase in the mitochondrial calcium content and compromises mitochondrial membrane potential, autophagic function and cellular bioenergetics.[229] Recent studies have further revealed that α-synuclein preferentially accumulates within the ER\microsomes, where it aggregates in toxic oligomeric formations in mouse and human brain with α–synucleinopathy. Those oligomeric forms have been further associated with the onset of chronic ER stress and disease progression.[44,45] UPR and ER calcium dynamics seem to additionally govern neuronal injury progression in HD,[286,299] TBI and following stroke.[213] Therefore, resolution of chronic ER stress can benefit acute and chronic neurodegenerative disorders that feature diverse aetiologies and clinical manifestations,[213,235,312] whilst prolonged perturbation of ER calcium homeostasis may offer an integrated cellular model to simulate neurodegenerative processes for drug discovery.

GLP-1 analogues, which are currently approved for T2DM treatment, have been repeatedly shown to exert neurotrophic/ restorative effects in a range of animal models of AD, PD, ALS, TBI and experimental stroke.[29,87,101,103,126,127,166,167,177,195,196,198,259,271,285,323,327] Importantly, GLP-1 mimetics, such as Liraglutide has rescued the AD-related reduction in cortical activity and energy utilisation,[86] and a recently phase II clinical trial testing Exenatide has impeded PD progression.[7] The underlying biochemical processes are manifold. Incretin mimetics have prevented aberrant apoptosis of (hippocampal and primary cortical and dopaminergic) neurones and SH-SY5Y neuroblastoma cells exposed to hypoxia, excitotoxic insults, neurotoxins (*e.g.*, hydrogen peroxide and oxidopamine) and thapsigargin-induced ER stress.[91,166,167,316] Liraglutide pre-treatment favours cell survival over apoptotic signalling to promote cytoprotection from persistent mitochondria dysfunction in SH-SY5Y cells.[265] Similarly, post-treatment with GLP-1R agonists rescues aberrant cytotoxicity and impaired viability, and further enhances cell survival signalling to protect SH-SY5Y neuroblastoma cells from chronic rotenone-induces oxidative stress.[134] In the present study, we have addressed the neuroprotective/restorative effects of Liraglutide, along with the underlying molecular mechanisms and signalling network after prolong perturbation of ER calcium homeostasis. Consistently, we report that Liraglutide impedes the increase in the number of SH-SY5Y cells with compromised plasma membrane and mitochondrial dysfunction induced by thapsigargin, and promotes cell proliferation in a stressor dose-dependent manner.

Thapsigargin is a specific, almost irreversible inhibitor of the SERCA channel, triggering a transient increase in the cytosolic calcium and depleting ER calcium stores.[292] Calcium depletion in the ER precludes the activity of calcium-dependent chaperones to potentiate the accumulation of unfolded/misfolded proteins within the organelle lumen and thereby ER stress.[261] In response, the cell activates the UPR network that integrates signals about the chronicity and severity of the stress stimuli and culminates into disproportionate activation of PERK, ATF6 and IRE1α signalling to determine cell fate.[108,109,169] Particularly, chronic ER stress augments PERK arm to amplify the transcription and translation of the pro-apoptotic transcription factor Chop,[169] whilst suppressing IRE1α signalling[164,169] to possibly attenuate the survival and neurotrophic effects of the downstream spliced X-box binding protein 1(XBP-1) and sensitise the cells to ER stress.[109] It can additionally enhance ATF6 activity to reinforce Chop expression and thus amplify the apoptotic component of the UPR.[109,169] Consistently, the present study demonstrated that chronic thapsigargin treatment up-regulated ATF6 which accumulated in the cell nuclei and signified its activation, whilst almost abolishing the activating phosphorylation of IRE1α at Ser724. Chronic thapsigargin treatment triggered an ectopic expression of Chop that correlated to calnexin deficiency and ERO1α excess in SH-SY5Y neuroblastoma cells. Calnexin silencing has been previously reported to sensitise cardiomyocytes to ER stress and favour apoptosis through Chop up-regulation and calcium dysregulation.[24] Furthermore, induction of the oxidoreductase ERO1α downstream of Chop perturbs the ER redox state[191] that in turn stimulates inositol-1,4,5-trisphosphate receptor (IP_3R)-mediated calcium efflux into cytosol.[163] The latter could influence multiple pathways upstream of the core apoptosis machinery and, most importantly, mitochondrial function.[144,303] In addition to Chop, persistent ER stress can activate the ER-resident CASP12 to further promote cell suicide. CASP12 provokes a downstream caspase cascade that leads to PARP degradation and therefore programmed cell death initiation,[147,203,212] as reflected in our results too. Intriguingly, Liraglutide co-treatment normalised BiP induction along with ATF6 and IRE1α signalling in thapsigargin-treated SH-SY5Y cells. It additionally mitigated abnormal Chop expression and CASP12 activity, restored calnexin and ERO1α expression, and alleviated PARP degradation. These biochemical traits further related to the restoration of SH-SY5Y cell viability and proliferation. Collectively, the currently presented findings suggest that GLP-1R activation resolved the induction of UPR effectors and pro-apoptotic mediators and promoted chaperone homeostasis in the ER lumen to restores cell proteostasis following persistent neuronal ER stress.

Acute SERCA channel inhibition has been shown to preclude autophagosome formation[67] and fusion with lysosomes,[84] resulting into autophagy arrest.[67,84] Autophagy fail along with deregulated UPR seem to drive the imbalance between protein generation and degradation that underlies the onset and progression of neuronal degeneration.[30,274,312] Autophagy is a tightly regulated pathway that allows cells to eliminate harmful or damaged components through catabolism and recycling to maintain nutrient and energy homeostasis. As such, autophagy constitutes a crucial mechanism for preserving structures and functioning of sub-cellular organelles, including ER and mitochondria, when it operates at basal levels, and for cell survival in response to stress.[30,274,312] Several studies have shown that Liraglutide promotes autophagy and thereby cell survival in liver, pancreas and SH-SY5Y cells.[105,134,137,266,294,302,326] Contrarily, Zhao *et al.* have demonstrated a cytoprotective effect of Liraglutide by inhibiting autophagy in renal tubular epithelial cells.[325] Similarly, Liraglutide has prevented oxidative stress-induced axonal injury by halting excessive autophagy in retinal ganglion cells.[187] Excessive autophagic flux can exert detrimental effects by aberrantly degrading endogenous inhibitors of apoptosis and Atg components, and lead to cell death. That dual role has been further attributed to autophagy under ER stress conditions.[274]

Herein, apoptotic ER stress correlated with a substantial decrement in the protein levels of beclin-1 that determines the initiation and formation of phagophore. Suppressed IRE1α and Bcl-2 phosphorylation may have underlay beclin-1 impairments following the prolonged thapsigargin-treatment in SH-SY5Y cells. Previous studies have revealed that, among the three UPR arms, the induction of pro-survival autophagy after ER stress requires IRE1 signalling.[223] The latter mediates the phosphorylation of Bcl-2, which results in its dissociation from and to the release of beclin-1.[175] In addition, spliced XBP1, lying downstream of IRE1 arm, has been previously shown to bound to the promoter of beclin-1 and induce its transcription.[192] In addition to beclin-1, chronic ER calcium dyshomeostasis culminated in Atg3, Atg7 and LC3 protein deficiency that may have resulted from the ectopic Chop expression. Chop has been previously shown to limit autophagy through the transcriptional control of a dozen of Atg genes involved in phagophore elongation and maturation into the autophagosome, and thereby to stimulate apoptosis upon persistent ER stress.[16,17] Autophagy dysfunction along with persistent ER stress can further trigger the excess accumulation of the autophagy adaptor protein p62,[89] which contains a Keap1-binding motif similar to Nrf2.[149] Accumulation of p62 leads to Keap1 sequestration and inactivation and thereby promotes aberrant nuclear Nrf2 localisation and transcription of Nrf2 target genes.[149] Although the Nrf2 transcription programme has been recognised as one of the main antioxidant defensive mechanisms for cytoprotection,[186] that constitutive Nrf2 activation along with autophagy preclusion has been previously shown to drive the hepatic injury observed in Atg7-knockout mice.[149] Accordingly, the currently presented findings pointed towards the Nrf2 hyper-activation, which coincided with a deficiency in the "core" Atg components during the prolong ER calcium perturbation, and therefore indicated that a regulated Nrf2 activation could benefit cellular defensive responses to stress. Strikingly, Liraglutide co-treatment ameliorated Atg3, Atg7, beclin-1, and LC3 expression impairments and further normalised aberrant Nrf2 and Bcl-2 activity in thapsigargin-treated SH-SY5Y cells. Taken together, the observations herein highlighted that the GLP-1R activation promoted homeostasis of both ER and autophagic machinery for cell adaptation and survival upon unmitigated neuronal ER stress.

Mechanistically, Liraglutide rectified the impaired STAT3 signalling and engaged Akt pathway to exert its neuroprotective/restorative effects upon persistent ER stress. STAT3 is a latent transcription factor that is primarily activated by the phosphorylation of a single tyrosine residue, Tyr705, in response to the stimulation of cytokine and growth factor receptors,[214, 241] including GLP-1R.[272] Once activated, STAT3 dimerises and enters the nucleus to orchestrate – alone or in cooperation with other factors – transcriptional programmes for neuronal/glial survival, proliferation and differentiation.[214] Suppressed STAT3 activity has been previously found in the hippocampus of *post-mortem* brain samples from AD patients and transgenic mice.[41] Chiba *et al.* have further demonstrated that Aβ inactivates hippocampal JAK2 (Janus kinase 2)/STAT3 axis to provoke the basal forebrain cholinergic dysfunction and spatial working memory deficits *in vivo*, linking STAT3 pathway to neurodegenerative processes.[41] It has been additionally recognised that ER stress perturbs JAK-signal transducers and STAT3 signalling to mediate acute-phase neuroinflammatory responses[199] and leptin resistance in the brain[123] or to drive apoptosis that underlies suppressed hepatic gluconeogenesis[146] in periphery. Although the mechanistic interplay among UPR, STAT3 signalling and GLP-1R in the context of cell fate and neuronal degeneration remains unknown, STAT3 has been recently emerged as a multifaceted determinant for autophagy.[241] For instance, nuclear STAT3 can transcriptionally induce the anti-apoptotic Bcl-2 expression and consequently inhibit autophagy.[317] However, that phenotype was not prominent on the findings presented herein; no changes in total Bcl-2 levels occurred following chronic thapsigargin and/or Liraglutide treatments in SH-SY5Y cells [**Figure S2**]. Intriguingly, Atg3 promoter has been recently shown to contain a STAT3-responsive element,[172] which may have explained the restorative effects of Liraglutide against the thapsigargin-induced Atg3 deficiency, though this hypothesis requires further investigation.

Akt (also known as protein kinase B – PKB) is a serine/threonine kinase member of the AGC protein kinase family with a profound function in growth, proliferation, intermediate metabolism and cell survival,[189,189,190] and a pivotal effector of the anti-apoptotic GLP-1R signalling.[265] In response to the phosphoinositide 3-kinase (PI3K) stimulation, Akt is recruited to the cell membrane where it can undergo phosphorylation at the threonine 308 (Thr308) residue by PDK1 and at the serine 473 (Ser473) residue by mTORC2. Phosphorylation of Thr308 site critically determines Akt activation while the phosphorylation of both aforementioned sites is required for the maximal kinase activity.[189,190] Herein, Liraglutide significantly increased the phosphorylation levels of Akt at Thr308, which signified kinase activation. Activated Akt phosphorylates multiple targets in the cytoplasm, nucleus, mitochondria and ER membrane to regulate adaptive responses and cell fate under diverse insults, including ER and oxidative stress and DNA damage.[122,124,189,190] Among others, Akt phosphorylates and inhibits the death-agonist BAD that becomes rapidly dephosphorylated upon apoptotic stimuli,[189] as prominent in our findings too. Active (dephosphorylated) BAD binds to the survival-agonist Bcl-x_L or Bcl-2 at the mitochondria that provokes Bax and Bak oligomerisation and perturbs mitochondrial membrane permeabilisation to favour the point-of-no-return of apoptotic cell death.[40,306,328] However, the restoration of BAD phosphorylation downstream of growth factor signalling raises the mitochondrial threshold for apoptosis that renders the cells less vulnerable to death signals,[53] as evident in our results too.

In addition to BAD, Akt phosphorylates and inhibits the GSK3β, a major protein kinase that drives neurodegenerative processes in AD[179] and neuronal apoptosis following ER stress.[26,200,276,287] Indeed, accumulating evidence from diverse neuronal cell lines, primary neuronal cultures, and ER insults has demonstrated that the UPR abolishes the inhibitory phosphorylation of GSK3β at Ser9[26,200,276,287] to promote Chop expression and switch from pro-survival to pro-death signalling during ER stress,[200] as reflected in our results too. Moreover, it has been previously reported that PERK engages GSK3β to phosphorylate the p53 tumour suppressor protein at Ser315 and Ser376 and favour nuclear export and proteosomal degradation of p53 upon ER stress.[12,245] p53 is transcription factor of which activation serves to organise cellular responses with apoptosis, cell cycle arrest, senescence, DNA repair, cell metabolism, or autophagy depending on the nature and degree of stress insult, environmental context, and cell type. The regulation of p53 is complex and involves post-translational modifications – *e.g.,* phosphorylation and acetylation – at multiple sites that impact its cellular localisation, stability and transcriptional activity.[155] We assessed the phosphorylated levels of p53 at Ser15 that facilitates p53 nuclear accumulation and stabilisation by halting the ability of the E3 ubiquitin-protein ligase Mdm2 to interact with and target p53 for proteosomal degradation.[270,324] Herein, chronic ER stress precluded the phosphorylation of p53 at Ser15 that favoured p53 destabilisation in accord with previously reported observations.[12,245] The de-stabilisation of p53 herein most likely lay downstream of the decreased activity of ERK1/2, which has been previously shown to regulate the phosphorylation of this transcription factor at Ser15 in SH-SY5Y cells.[227] Although Liraglutide did not alleviate the impaired ERK1/2 phosphorylation, it potentiated Akt signalling which can engage the atypical p53-related protein kinase and thus phosphorylate p53 at Ser15 in human cell lines[68] to restore p53 stabilisation following cellular stress.[22] Intriguingly, recent evidence demonstrates that Akt phosphorylates and inhibits PERK,[206] which may offer an additional mechanistic link on how Liraglutide confered its restorative effects on p53, though necessitates further experimentation.

Though not examined in the present study, Liraglutide may have restored calcium homeostasis to elicit neuroprotection upon chronic thapsigargin treatment. Previous studies have demonstrated that GLP-1R induction potentiates cyclic AMP (cAMP) production[236] and regulates calcium responses,[91,265] which underlie protection of hippocampal neurones and SH-SY5Y neuroblastoma cells from excitotoxicity[91] and oxidative stress-induced[265] apoptosis, respectively. Furthermore, cAMP increase by GLP-1R stimulation potentiates protein kinase A (PKA) that downstream induces SERCA function to promote cytoprotection in insulin-resistant macrophages[168] and high glucose-treated cardiomyocytes.[318] Accordingly, PKA pharmacological inhibition blocks the GLP-1R-mediated anti-apoptotic effects. Contrarily, the adenylate cyclase activator, Forskolin mimics the GLP-1R-induced cardioprotection upon hyperglycaemia.[318] cAMP has been additionally shown to potentiate cAMP-regulated guanine nucleotide exchange factors (also known as Epac) that regulate calcium dynamics in response to GLP-1R stimulation.[117]

In conclusion, the findings discussed herein demonstrated the neuroprotective/restorative effects of Liraglutide upon unmitigated neuronal ER stress. They further unravelled a complex signalling network through which Liraglutide regulated UPR outcome, elicited autophagy machinery homeostasis and shifted cell fate from apoptosis to survival, endorsing the beneficial effects of the GLP-1R stimulation and signalling in neurodegenerative disorders and deepening our understanding of the underlying mechanism.

Chapter 4

Incretin signalling restored chronic ER stress, autophagy impairments and Nrf2 activation to promote neuroprotection and synapse homeostasis

Submitted for publication

4.1 Introduction

The Alzheimer's disease (AD) neuropathological cascade begins years prior to the onset of cognitive and brain-structural impairments. It alters the proteostasis network and calcium dynamics, gradually favouring the aberrant deposition of misfolded proteins and synapse degeneration.[20,30,111,224,235,258] The buffering capacity and integrity of these processes lie in the homeostasis of the endoplasmic reticulum (ER)[20,111,235] a dynamic membrane system that extends from the soma to the entire dendrite arbour, including some dendritic spines, and the axon of the neurone.[249] The ER is the fundamental sub-cellular compartment for the protein synthesis and quality control of approximately one-third of the total proteome.[111,235,261] It additionally is the major calcium storage depot in the cell.[284] Calcium release from the ER mediates neurotransmitter exocytosis at the pre-synapse whilst potentiating gene transcription and modulating membrane excitability and dendritic spine structure for post-synaptic plasticity.[152,201,284] Upon release, the sarcoplasmic/ER calcium ATP–ase (SERCA) channel buffers calcium re-uptake from the cytosol into the ER to replenish the local calcium stores.[284]

A potential depletion of ER calcium stores will preclude the functionality of local molecular chaperones that closely monitor and assist folding, maturation and the delivery of secretory and membrane proteins. As such, the former results in a rise of the unfolded or misfolded protein load within the organelle lumen, a cellular state defined as ER stress.[261] In turn, the cell activates an adaptive signalling network, known as the unfolded protein response (UPR). The UPR engages the three ER-resident transmembrane stress transducers – the protein kinase RNA-like ER kinase (PERK), activating transcription factor 6 (ATF6) and inositol-requiring enzyme 1 (IRE1), which initially attenuate global protein synthesis, potentiate the transcription of chaperone proteins, and degrade the abnormal protein load through the proteasome (ER-associated degradation) and lysosome-mediated autophagy to safeguard proteostasis.[109,111,261] However, upon stress chronicity, the UPR adapts its dynamics and shifts cell fate towards apoptosis[109] through diverse but often overlapping mechanisms, including autophagy fail, aberrant kinase activity, the transcription of CAAT/enhancer-binding protein (C/EBP) homologous protein (Chop), caspase cascade, and Bcl-2 family members along with their mediators, which altogether drive neuronal degeneration and cognitive decline in AD.[30,111,224,235,258] Noteworthy is that β-amyloid (Aβ) – the Alzheimer's pathognomonic signature[246] – perturbs calcium dynamics and abnormally increases the amount of calcium released by the ER that culminates into ER stress, mitochondrial fragmentation, synapse/neuronal toxicity and astrogliosis *in vivo*.[30,207,235,247] Accordingly, the ER calcium perturbation seems to govern the Aβ production[95,240] and accelerate its aggregation.[130] It is therefore intuitive that therapeutic interventions which resolve the UPR towards a balance between protein generation and degradation and promote ER homeostasis may significantly benefit the Alzheimer's clinical outcome[30,235] while the ER calcium perturbation may offer an integrative cellular model to simulate AD-related neuropathological processes for drug discovery. In this light, the present study addressed the restorative effects of the glucagon-like peptide 1 (GLP-1) analogue, Liraglutide and a novel dual incretin analogue on the synapse damage, cytotoxicity and impaired proteostasis upon persistent and calcium-dependent ER stress in post-mitotic neurones from the human LUHMES cell line.

The incretin hormone, GLP-1 is best known for regulating glucose homeostasis and insulin biosynthesis and secretion in response to food ingestion. The GLP-1 mimetics, Liraglutide and Exenatide are currently approved for the treatment of type 2 diabetes mellitus (T2DM). Besides their glucose-dependent pancreatic effects, the GLP-1 mimetics cross the blood-brain barrier and exert neurotrophic and cell survival signals.[10,116] For instance, chronic intraperitoneal administration of Liraglutide has preserved normal population and activity of cortical and hippocampal synapses, impeded hippocampal atrophy, halted excessive Aβ

accumulation and deposition, and mitigated excessive gliosis to rescue spatial cognitive decline in the $APP_{swe}/PS1_{\Delta E9}$ mouse model for AD[195,197,198] and the senescence-accelerated mouse prone 8 (SAMP8) model for age-related sporadic AD.[102] In line with the *in-vivo* findings, Liraglutide and Exenatide have favoured survival over apoptotic signalling to impede cytotoxicity and death of hippocampal and primary cortical neurones and neuronal-like cells chronically exposed to excitotoxic insults[91,166,236,316] and Aβ oligomers.[237,244,316] In a pilot clinical trial, Liraglutide has rescued the decline of the cerebral glucose consumption in AD patients that signifies energy metabolism in brain areas previously correlated with cognitive decline and disease progression.[86]

Recently, novel dual incretin analogues have been developed and displayed superior anti-hyperglycaemic and insulinotropic efficacy compared to the GLP-1 mono-therapy, rendering them potent candidates for T2DM treatment.[76] Pilot pre-clinical studies have further demonstrated the neurotrophic and restorative effects on hallmark, disease-related pathological lesions of the dual incretin in a mouse model of mild traumatic brain injury,[289] the rat model of streptozotocin-induced diabetes and neurodegeneration,[269] and neurotoxin-based rodent models of Parkinson's disease (PD).[31,133,136,320] The neuroprotective effects of the incretin mimetics lie downstream of the induction of the GLP-1 and GIP (glucose-dependent insulinotropic polypeptide) receptors that are widely expressed in the human and rodent brain and coupled to Gα-protein. Upon activation, the latter stimulates adenyl cyclase, Akt and mitogen-activated protein kinase (MAPK) pathways to mediate survival and trophic signals.[10,116] However, it remains poorly explored whether the incretin signalling engages supplementary pathways and regulates mechanisms or responses for proteostasis, such as the UPR and the machinery of protein quality control and autophagy, to elicit synapse homeostasis and neuronal survival.

Herein, chronic incretin treatment modulated the UPR output and promoted homeostasis of the ER chaperones and autophagy to halt excessive synapse damage and neuronal death upon chronic and calcium-dependent ER stress. The stimulation of the GIP and/or GLP-1 receptors downstream rectified the aberrant activity of the antioxidant and defensive nuclear factor erythroid 2-related factor 2 (Nrf2) and the signal transducer and activator of transcription 3 (STAT3) along with the Akt pathway to exert neuroprotection and proteostasis. The present study confirmed my recently published findings in the proliferating neuroblastoma SH-SY5Y cells[232] and for the first time correlated the incretin-induced resolution of the ER stress with the synapse homeostasis to endorse the beneficial effects of incretin mimetics on neurodegenerative disorders.

4.2 Liraglutide and the novel GLP-1/GIP Dual Agonist ameliorate thapsigargin-induced neuronal toxicity

First, the neuroprotective effect of Liraglutide and the novel GLP-1/GIP Dual Agonist on chronic ER stress by thapsigargin elucidated. Thapsigargin is a naturally-occurring sesquiterpene lactone that selectively inhibits the SERCA channel, triggering a transient increase in the cytosolic calcium and depleting the ER calcium stores.[292] LUHMES cells were pre-differentiated for 2 d and re-plated in 96-well plates where the differentiation process continued for additional 3 d. On d 5–6, the post-mitotic neurones were treated with 0, 10, 100 and 1000 nM of thapsigargin in the presence or absence of 100 nM Liraglutide or of 100 nM GLP-1/GIP Dual Agonist for 16 h. Neuronal cultures were subsequently processed for XTT and LDH assays to assess cell viability and cytotoxicity, respectively. One-way ANOVA analysis revealed overall significant differences in cell viability [$F_{(11,333)} = 63.48$, $p \leq 0.001$] and cytotoxicity [$F_{(11,351)} = 18.40$, $p \leq 0.001$]. *Post-hoc* analysis with Bonferroni correction demonstrated that thapsigargin impaied cell viability in a dose-dependent fash-

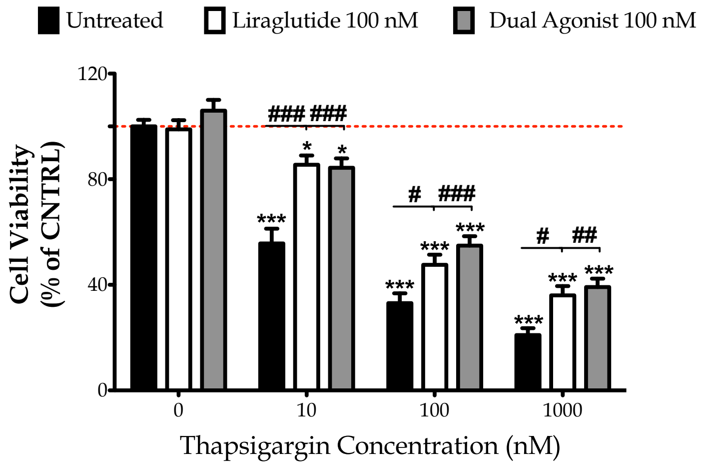

(a)

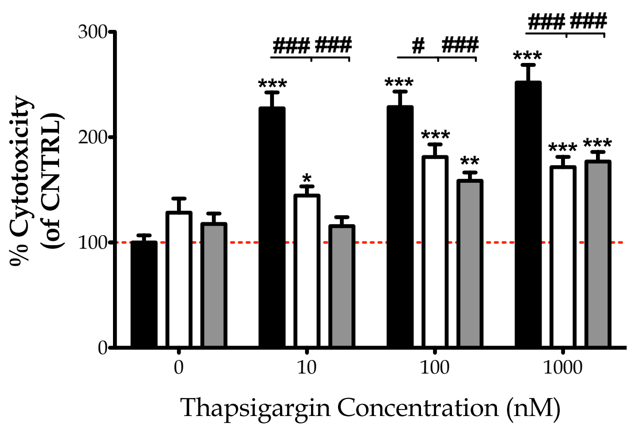

(b)

Figure 4.1: **Incretin mimetics ameliorated neuronal toxicity upon persistent ER stress.** On d 5–6 of the differentiation period, post-mitotic neurones from the human LUHMES cell line were treated with 0, 10, 100 and 1000 nM of thapsigargin in the presence or absence of 100 nM Liraglutide or of 100 nM novel GLP-1/GIP Dual Agonist for 16 h. Neuronal cultures were then assayed for the XTT metabolisation [**(a)**] to assess cell viability. Cell supernatant was collected and processed for the LDH activity [**(b)**] to determine cytotoxicity. Each bar represents mean ± SEM from four independent experiments. All cell treatments were performed at least in sextuplicate per experiment. Data is expressed as a percentage of the control (CNTRL; unstressed/untreated conditions). Data was analysed by one- and two-way ANOVA, followed by *post hoc* Bonferroni's multiple comparison t-test ($^{*}p \leq 0.05$, $^{**}p \leq 0.01$ & $^{***}p \leq 0.001$ compared to CNTRL; $^{\sharp}p \leq 0.05$, $^{\sharp\sharp}p \leq 0.01$ & $^{\sharp\sharp\sharp}p \leq 0.001$ compared to the corresponding thapsigargin-treated neurones). Red dashed line corresponds to CNTRL levels.

ion; it provoked an approximately 44%($p \leq 0.001$), 67% ($p \leq 0.001$) and 79% ($p \leq 0.001$) decline in the number of viable and metabolically active neurones that were accordingly challenged with 10, 100 and 1000 nM of the stressor with respect to control conditions

[**Figure 4.1(a)**]. A significant membrane perturbation accompanied the suppressed cell viability, with the LDH release gradually increasing by 127%($p \leq 0.001$), 130% ($p \leq 0.001$) and 152% ($p \leq 0.001$) in the supernatant of micro-cultures that had received the aforementioned stressor doses [**Figure 4.1(b)**]. Two-way ANOVA analysis indicated that Liraglutide co-treatment significantly rescued the abnormal LDH activity ($F_{(3,235)} = 8.604$, $p \leq 0.001$) and ameliorated cell viability impairments ($F_{(3,222)} = 5.837$, $p \leq 0.001$) following chronic SERCA inhibition [**Figure 4.1**]. Similarly, the novel GLP-1/GIP Dual Agonist co-treatment significantly rescued the abnormal LDH activity ($F_{(3,232)} = 10.87$, $p \leq 0.001$) and attenuated impaired cell viability ($F_{(3,220)} = 3.262$, $p \leq 0.05$) following chronic SERCA inhibition [**Figure 4.1**]. Both incretin mimetics approximately induced a 30% rise in the number of metabolically active neurones and almost halve the abnormal LDH activity in the micro-cultures exposed to 10 nM of thapsigargin, rendering them the strongest effects noted in cell physiology assays. Nevertheless, the concentration of 100 nM of thapsigargin stress was selected for the biochemical studies to maintain consistency between the cell lines used in the present thesis.

4.3 Liraglutide and the novel GLP-1/GIP Dual Agonist attenuated the UPR and restored homeostasis in the ER protein folding machinery

Neurones were treated with 0 and 100 nM of thapsigargin in the presence or absence of 100 nM Liraglutide or GLP-1/GIP Dual Agonist for 16 h, and processed for immunoblotting analysis of hallmark ER stress-related signalling molecules. One-way ANOVA analysis demonstrated overall significant differences in BiP [$F_{(5,42)} = 21.82$, $p \leq 0.001$], full-length ATF6 [$F_{(5,42)} = 5.046$, $p \leq 0.01$], IRE1α activation [$F_{(5,42)} = 9.166$, $p \leq 0.001$], Chop [$F_{(5,42)} = 295.6$, $p \leq 0.001$], and caspase 12 [CASP12; $F_{(5,42)} = 3.018$, $p \leq 0.05$]. Chronic

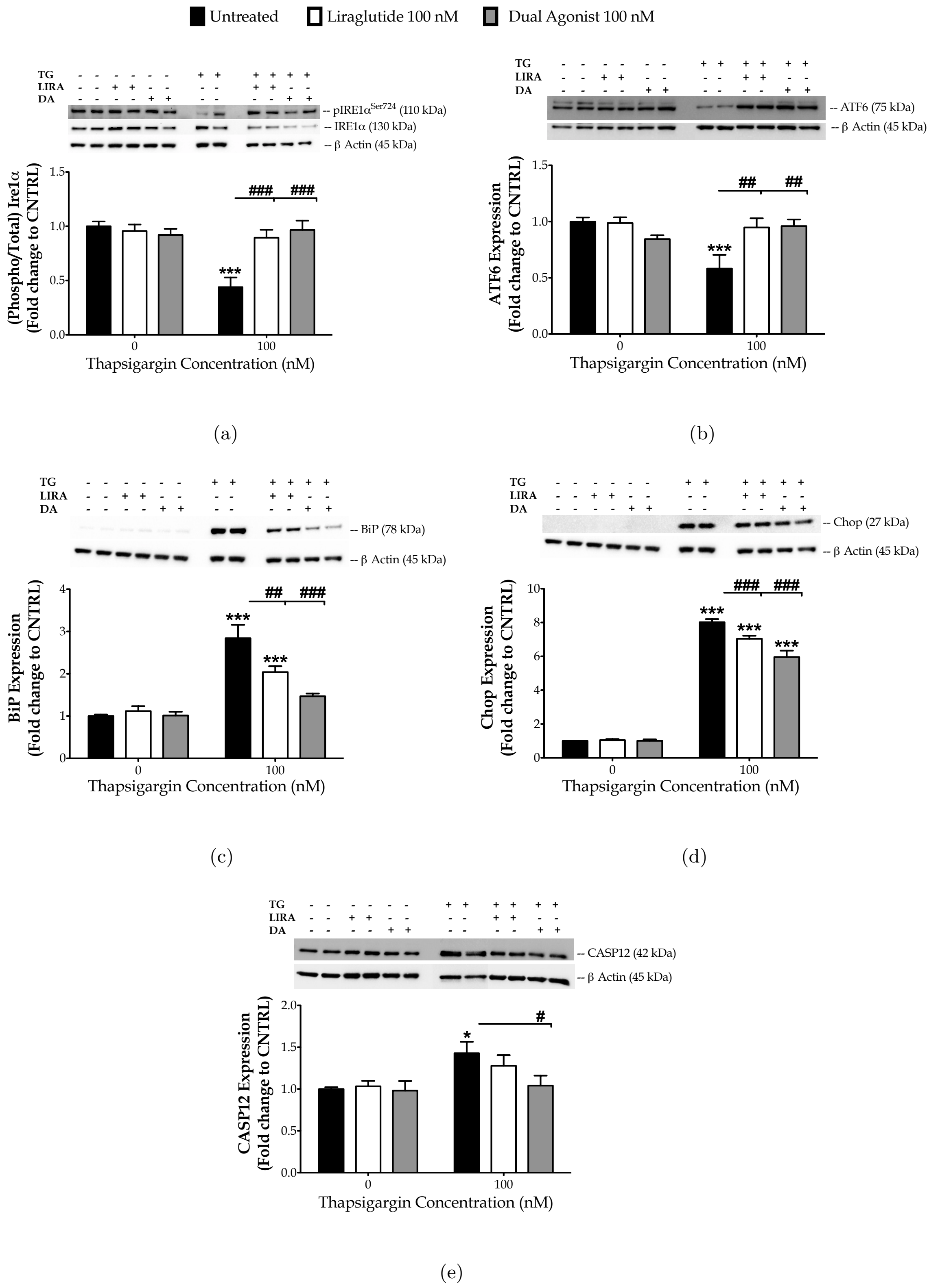

Figure 4.2: **Incretin mimetics resolve the unfolded protein response (UPR) in human post-mitotic neurones.** On d 5–6 of the differentiation period, post-mitotic neurones from the human LUHMES cell line were treated with 0 and 100 nM of thapsigargin (TG) in the presence or absence of 100 nM Liraglutide (LIRA) or of 100 nM novel GLP-1/GIP Dual Agonist (DA) for 16 h. Neurones were then harvested, and the expression levels of total and phosphorylated IRE1α [**(a)**], ATF6 [**(b)**], BiP [**(c)**], Chop [**(d)**], and caspase 12 (CASP12) [**(e)**] proteins

were determined by western blotting. β-Actin was used as the loading control to all western blot analyses. Each bar represents mean $\pm$ SEM from four independent experiments. Data is expressed as fold change to the control (CNTRL; unstressed/untreated conditions). Data was analysed by one- and two-way ANOVA, followed by *post hoc* Bonferroni's multiple comparison t-test ($^{*}p \leq 0.05$, $^{**}p \leq 0.01$ & $^{***}p \leq 0.001$ compared to CNTRL; $^{\sharp}p \leq 0.05$, $^{\sharp\sharp}p \leq 0.01$ & $^{\sharp\sharp\sharp}p \leq 0.001$ compared to the corresponding thapsigargin-treated neurones).

thapsigargin treatment potentiated a two-fold increase in BiP expression [**Figure 4.2(a)**] that signified ER stress.[159] It almost halveds the ATF6 protein levels ($p \leq 0.001$) [**Figure 4.2(c)**] and significantly precluded the activating phosphorylation of IRE1α at the serine 724 residue (Ser724) ($p \leq 0.001$) [**Figure 4.2(b)**]. A seven-fold rise in the levels of the pro-apoptotic transcription factor Chop ($p \leq 0.001$) [**Figure 4.2(c)**] along with an increased expression of the active CASP12 fragment at 42 kDa by half ($p \leq 0.05$) [**Figure 4.2(d)**] accompanied the biochemical profiles of the chronically-treated neurones. Notably, Liraglutide restored the ATF6 protein expression ($p \leq 0.01$) and IRE1α phosphorylated levels ($p \leq 0.001$) [**Figures 4.2(b)–4.2(c)**]. It rescued the ectopic protein expression of BiP ($p \leq 0.01$) [**Figure 4.2(a)**] and Chop ($p \leq 0.001$) [**Figure 4.2(d)**], though their levels remained significantly elevated when compared to control conditions ($p \leq 0.001$). There is also a trend of improvement by Liraglutide on CASP12 activation following thapsigargin treatment, with $p \gg 0.05$ in comparison to control conditions. However, it did not reach the statistical significance when compared to the corresponding stress conditions in *post-hoc* analysis [**Figure 4.2(e)**]. Similarly, two-way ANOVA analysis demonstrated significant effects of the GLP-1/GIP Dual Agonist co-treatment significantly in the expression of BiP ($F_{(1,28)} = 16.80$, $p \leq 0.001$) and ATF6 ($F_{(1,28)} = 13.66$, $p \leq 0.001$), as well as in the activation of IRE1α ($F_{(1,28)} = 18.12$, $p \leq 0.001$) upon chronic SERCA channel inhibition. Intriguingly, the dual incretin normalised the aberrant BiP and ATF6 expressions and IRE1α phosphorylation, as illustrated in **Figure 4.2**. It further attenuated

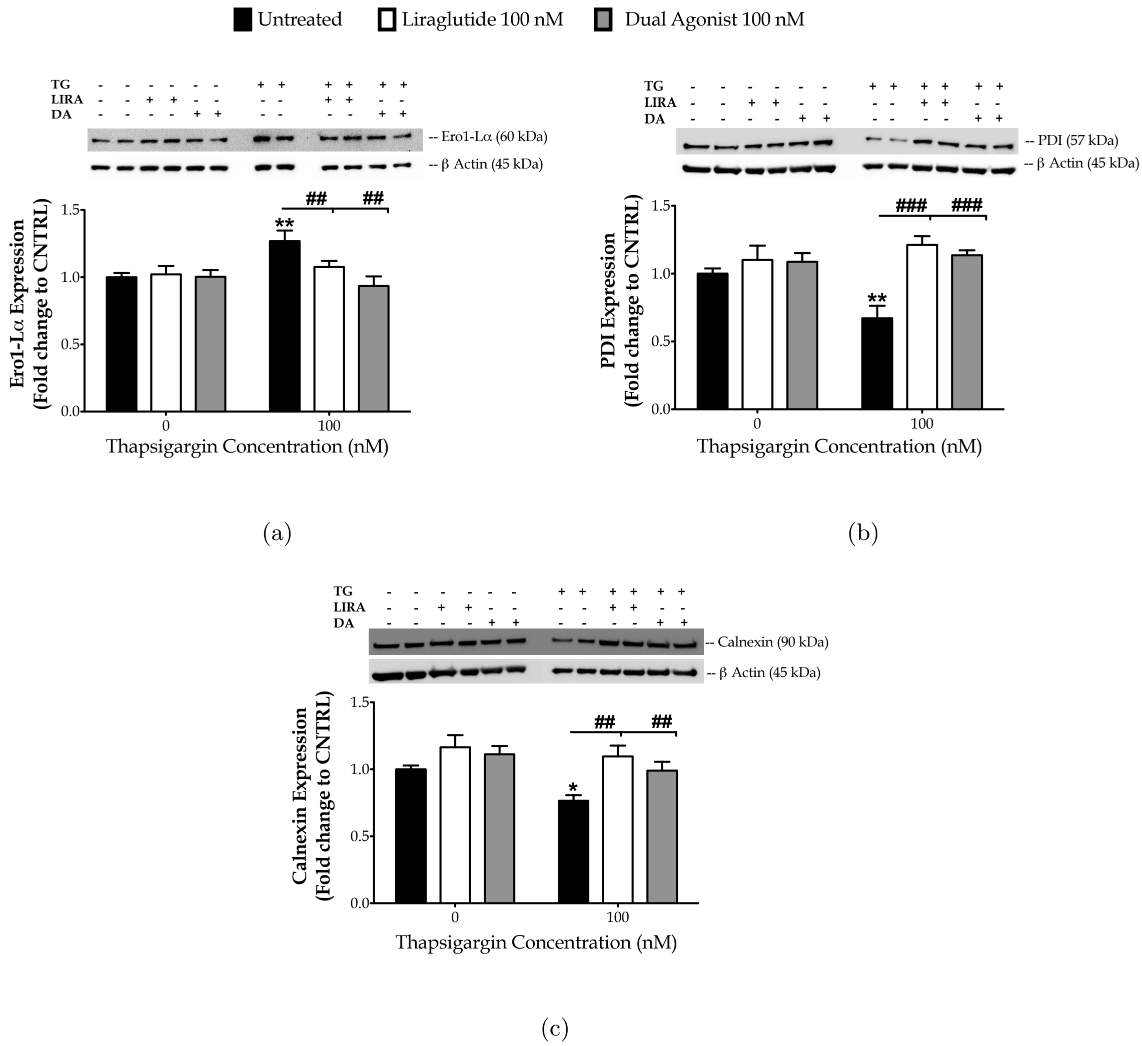

Figure 4.3: **Incretin mimetics promoted ER proteostasis in post-mitotic neurones upon persistent ER stress.** On d 5–6 of the differentiation period, post-mitotic neurones from the LUHMES cell line were treated with 0 and 100 nM of thapsigargin (TG) in the presence or absence of 100 nM Liraglutide (LIRA) or of 100 nM novel GLP-1/GIP Dual Agonist (DA) for 16 h. Neurones were then harvested, and the expression of ER oxidoreductase 1α [Ero1-Lα; **(a)**], protein disulphide isomerase [PDI; **(b)**] and of calnexin [**(c)**] were determined by western blotting. β-Actin was used as the loading control to all western blot analyses. Each bar represents mean $\pm$ SEM from four independent experiments. Data is expressed as fold change to the control (CNTRL; unstressed/untreated conditions). Data was analysed by one- and two-way ANOVA, followed by *post hoc* Bonferroni's multiple comparison t-test ($^{*}p \leq 0.05$, $^{**}p \leq 0.01$ & $^{***}p \leq 0.001$ compared to CNTRL; $^{\sharp\sharp}p \leq 0.01$ & $^{\sharp\sharp\sharp}p \leq 0.001$ compared to the corresponding thapsigargin-treated neurones).

the ectopic Chop expression by a two-fold decrease in its protein levels ($p \leq 0.001$) and restored CASP12 activation back to control levels ($p \leq 0.05$) [**Figure 4.2**].

Next, the expression levels of the major components of the ER protein quality machinery ER-residing protein endoplasmic oxidoreductin-1 (Ero1-Lα), protein disulphide isomerase (PDI) and calnexin were assessed [**Figure 4.3**] . One-way ANOVA analysis revealed overall significant differences in Ero1-Lα [$F_{(5,42)} = 3.914$, $p \leq 0.01$[, PDI [$F_{(5,42)} = 7.163$, $p \leq 0.001$], and calnexin [$F_{(5,42)} = 4.820$, $p \leq 0.01$]. *Post-hoc* analysis demonstrates that chronic thapsigargin treatment significantly up-regulated Ero1-Lα protein levels ($p \leq 0.01$) whilst suppressing PDI and calnexin by 30% ($p \leq 0.01$) and 25% ($p \leq 0.05$), respectively. Notably, Liraglutide and the GLP-1/GIP Dual Agonist co-treatments reversed the abnormal protein expressions of Ero1-Lα, PDI, and calnexin, as illustrated in **Figure 4.3**.

4.4 Liraglutide and the novel GLP-1/GIP Dual Agonist rescue thapsigargin-induced autophagy impairments

Autophagy is a tightly regulated pathway for the elimination of harmful or damaged components through catabolism and recycling to maintain nutrient and energy homeostasis. It constitutes a crucial mechanism for preserving structures and functioning of sub-cellular organelles, including ER and mitochondria, when operates at basal levels, and for cell survival in response to stress.[30,274,312] Acute ER-localised blocking of calcium flux perturbs autophagosome biogenesis[67] and fusion with lysosome,[84] culminating in autophagy arrest.[67,84] Accordingly, we have previously reported that persistent SERCA inhibition diminishes "core" Atg proteins for the autophagosome formation and maturation in the neuroblastoma SH-SY5Y cell line.[232] Similarly, one-way ANOVA demonstrated overall significant differences in the neuronal protein expression of beclin-1 [$F_{(5,42)} = 16.07$, $p \leq 0.001$], Atg3 [$F_{(5,42)} = 14.65$, $p \leq 0.001$], Atg7 [$F_{(5,42)} = 9.285$, $p \leq 0.001$] and of LC3 [$F_{(5,42)} = 7.903$, $p \leq 0.001$] among groups. Chronic thapsigargin treatment particularly suppressed the protein expression of beclin-1 ($p \leq 0.001$) [**Figure 4.4(a)**] that determines the phagophore as-

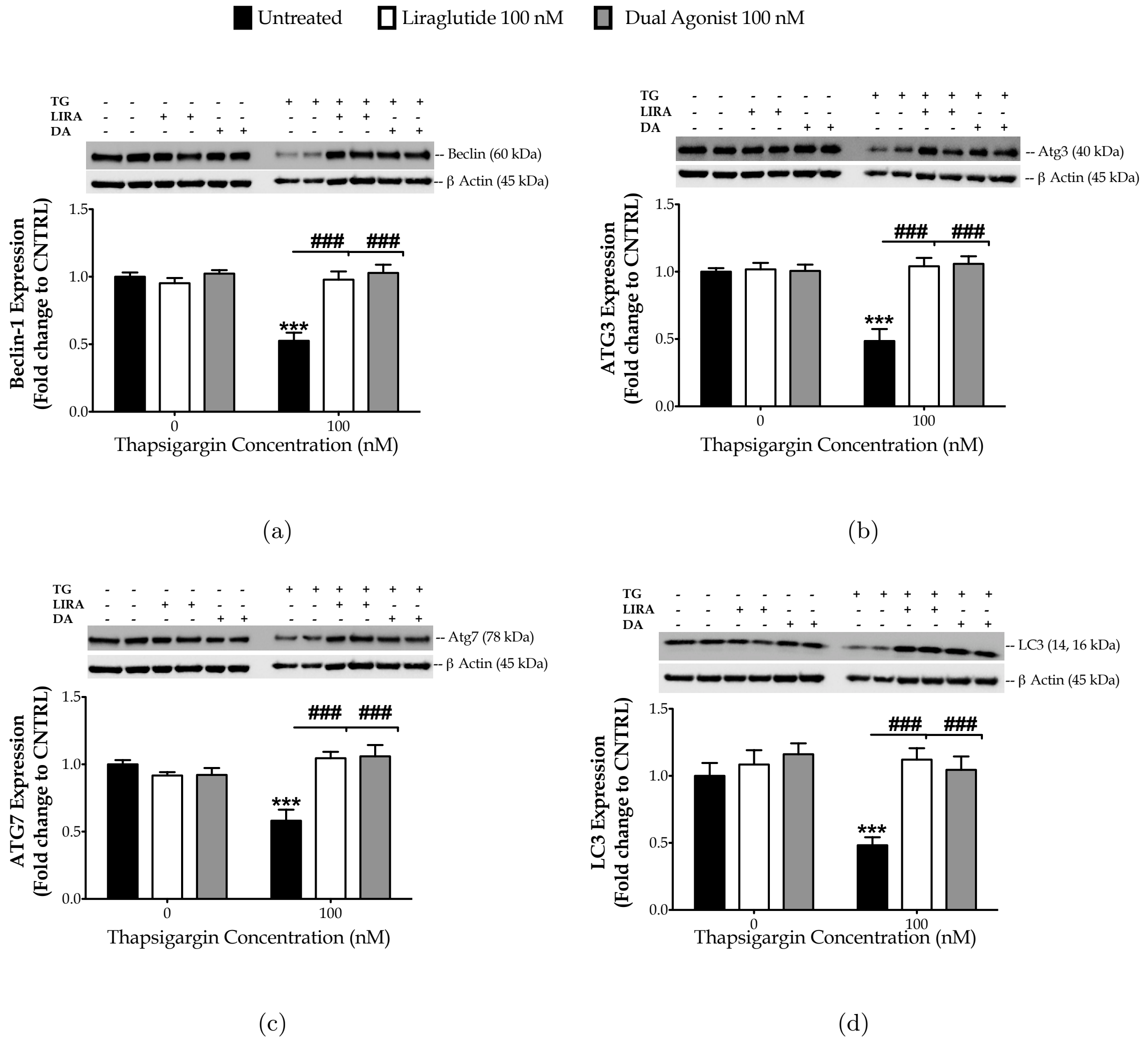

Figure 4.4: **Incretin mimetics rescued the suppressed expression of "core" Atg proteins required for autophagosome formation in post-mitotic neurones upon persistent ER stress.** On d 5–6 of the differentiation period, post-mitotic neurones from the LUHMES cell line were treated with 0 and 100 nM of thapsigargin (TG) in the presence or absence of 100 nM Liraglutide (LIRA) or of 100 nM novel GLP-1/GIP Dual Agonist (DA) for 16 h. Neurones were harvested, and the expression of beclin-1 [**(a)**], ATG3 [**(b)**], ATG7 [**(c)**] and of LC3 [**(d)**] were determined by western blotting. β-Actin was used as the loading control to all western blot analyses. Each bar represents mean ± SEM from four independent experiments. Data is expressed as fold change to the control (CNTRL; unstressed/untreated conditions). Data was analysed by one- and two-way ANOVA, followed by *post hoc* Bonferroni's multiple comparison t-test ($^{***}p \leq 0.001$ compared to CNTRL; $^{\sharp\sharp\sharp}p \leq 0.001$ compared to the corresponding thapsigargin-treated neurones).

sembly.[30] It further decreased the protein levels of Atg3 ($p \leq 0.001$) [**Figure 4.4(b)**], Atg7 ($p \leq 0.001$) [**Figure 4.4(c)**], and LC3 ($p \leq 0.001$) [**Figure 4.4(d)**], which all regulate the elongation and maturation of phagophore into autophagosome.[30] Two-way ANOVA analysis revealed that the Liraglutide co-treatment rescued the impaired expression of beclin-1

$[F_{(1,28)} = 25.76,\ p \leq 0.001]$, Atg3 $[F_{(1,28)} = 19.69,\ p \leq 0.001]$, Atg7 $[F_{(1,28)} = 28.21,\ p \leq 0.001]$, and LC3 $[F_{(1,28)} = 9.815,\ p \leq 0.01]$ following chronic SERCA inhibition. The GLP-1/GIP Dual Agonist significantly impacted the beclin-1 $[F_{(1,28)} = 25.68,\ p \leq 0.001]$, Atg3 $[F_{(1,28)} = 23.14,\ p \leq 0.001]$, Atg7 $[F_{(1,28)} = 17.86,\ p \leq 0.001]$, and LC3 protein expressions $[F_{(1,28)} = 5.483,\ p \leq 0.05]$ following chronic thapsigargin treatment, and more specifically restored their levels back to control. Therefore, the stimulation of the GIP and/or GLP-1 receptor modulated regulatory steps for the autophagosome formation to rescue autophagy impairments following chronically persistent ER stress, as illustrated in **Figure 4.4**.

4.5 Liraglutide and the novel GLP-1/GIP Dual Agonist rescued thapsigargin-induced neuronal synaptic damage

Proteostasis is a crucial determinant for the formation, maintenance and function of synapses, which govern neuronal connectivity and information processing in the brain.[79,249] Indeed, the UPR dysregulation along with autophagy impairments provoked synaptic damage in human post-mitotic neurones, as illustrated in **Figure 4.5**. One-way ANOVA analysis demonstrated significant differences in the protein levels of the hallmark scaffolding protein for dendritic spine morphogenesis and synaptic plasticity, PSD95[80] $[F_{(5,42)} = 14.51,\ p \leq 0.001]$ and of the major pre-synaptic vesicle protein, synaptophysin $[F_{(5,42)} = 4.250,\ p \leq 0.01]$ among the groups, with the chronic thapsigargin treatment remarkably suppressing their expression. Notably, Liraglutide reversed the thapsigargin-induced impairments in PSD95 (*post hoc*; $p \leq 0.001$) and synaptophysin (*post hoc*; $p \leq 0.05$). Similarly, the GLP-1/GIP Dual Agonist significantly impacted the expression of PSD95 $[F_{(1,28)} = 19.70,\ p \leq 0.001]$ and synaptophysin $[F_{(1,28)} = 7.562,\ p \leq 0.05]$ to maintain synapse integrity upon chronic thapsigargin treatment [**Figure 4.5**].

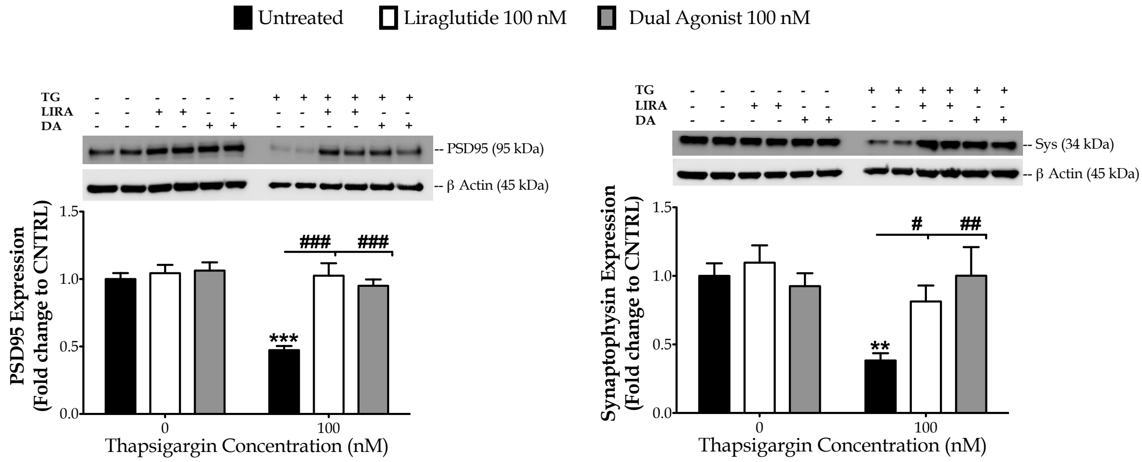

(a)

(b)

Figure 4.5: **Incretin mimetics promote synapse homeostasis upon persistent ER stress.** On d 5–6 of the differentiation period, post-mitotic neurones from the LUHMES cell line were treated with 0 and 100 nM of thapsigargin (TG) in the presence or absence of 100 nM Liraglutide (LIRA) or of 100 nM novel GLP-1/GIP Dual Agonist (DA) for 16 h. Neurones were then harvested, and the expression of post-synaptic density protein 95 [PSD95; **(a)**] and synaptophysin [Sys; **(b)**] were determined by western blotting. β-Actin was used as the loading control to all western blot analyses. Each bar represents mean ± SEM from four independent experiments. Data is expressed as fold change to the control (CNTRL; unstressed/untreated conditions). Data was analysed by one- and two-way ANOVA, followed by *post hoc* Bonferroni's multiple comparison t-test ($^{**}p \leq 0.01$ & $^{***}p \leq 0.001$ compared to CNTRL; $^{\sharp}p \leq 0.05$, $^{\sharp\sharp}p \leq 0.01$ & $^{\sharp\sharp\sharp}p \leq 0.001$ compared to the corresponding thapsigargin-treated neurones).

4.6 Liraglutide and the novel GLP-1/GIP Dual Agonist restored impaired Nrf2 nuclear content upon aberrant UPR and autophagy

Immunocytochemical analysis of the nuclear levels of the transcription factor Nrf2 was next performed to evaluate the antioxidant defensive signalling for neuroprotection upon aberrant proteostasis following chronic thapsigargin treatment. Normally, Nrf2 is expressed throughout the neurone soma with a predominant expression in the nucleus,[250] as prominent in our immunocytochemical analysis too [**Figure 4.6(a)**]. Contrarily, degenerating neurones featured a decreased nuclear Nrf2 content that signified the impaired activity of the transcription factor.[250] Accordingly, herein, thapsigargin-treated neurones displayed a

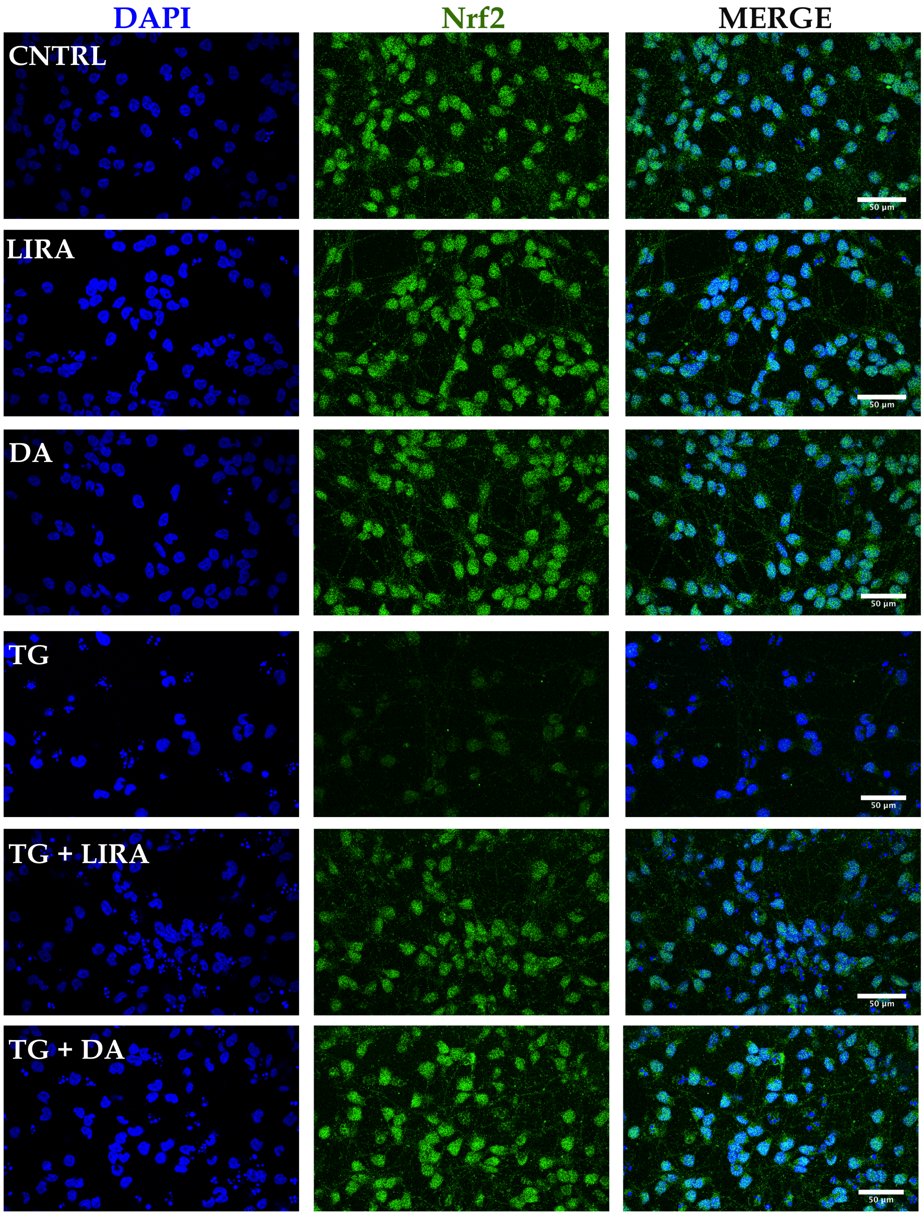

DAPI
Nrf2
MERGE
CNTRL
LIRA
DA
TG
TG + LIRA
TG + DA

(a)

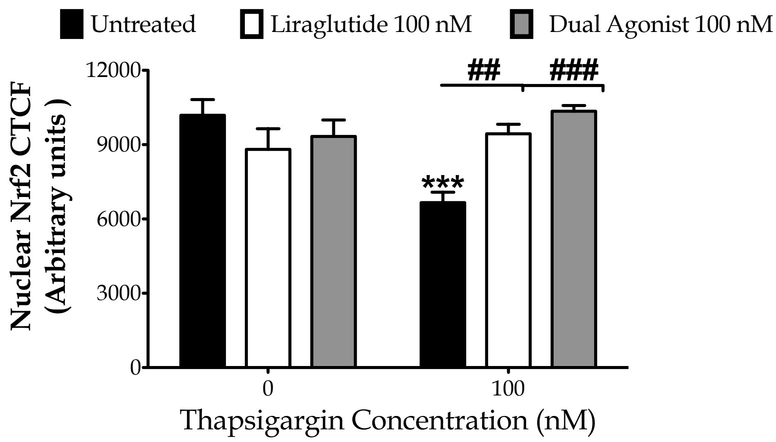

Untreated
Liraglutide 100 nM
Dual Agonist 100 nM
Nuclear Nrf2 CTCF (Arbitrary units)
12000
9000
6000
3000
0
***
##
###
0
100
Thapsigargin Concentration (nM)

(b)

Figure 4.6: **Incretin mimetics restore the impaired signalling of the nuclear factor erythroid 2-related factor 2 (Nrf2) in post-mitotic neurones upon chronically persistent ER stress.** On d 5–6 of the differentiation period, post-mitotic neurones from the LUHMES cell line were treated with 0 and 100 nM of thapsigargin (TG) in the presence or absence of 100 nM Liraglutide (LIRA) or of 100 nM novel GLP-1/GIP Dual Agonist (DA) for 16 h. All cell treatments were performed in duplicate per experiment. Neurones were (paraformaldehyde)-fixed, immunolabelled for Nrf2 and processed for confocal imaging at 40X magnification, as shown in the representative images [**(a)**]. Six pictures were captured per treatment sample per experiment for quantification. Image J was used to quantify corrected total cell fluorescence (CTCF) of the nuclear Nrf2 staining [**(b)**]. Each bar represents mean ± SEM from three independent experiments. Data was analysed by one- and two-way ANOVA, followed by *post hoc* Bonferroni's multiple comparison t-test ($^{***}p \leq 0.001$ compared to CNTRL; $^{\sharp\sharp}p \leq 0.01$ & $^{\sharp\sharp\sharp}p \leq 0.001$ compared to the corresponding thapsigargin-treated neurones). Scale bars: 50 µm.

faint Nrf2-immunopositive staining, particularly in the nuclear area [**Figure 4.6(a)**]. One-way ANOVA analysis demonstrated significant differences in the nuclear Nrf2 content among the groups [$F_{(5,192)} = 4.635$, $p \leq 0.001$]. Two-way ANOVA analysis revealed that Liraglutide [$F_{(1,122)} = 11.57$, $p \leq 0.001$] and the GLP-1/GIP Dual Agonist [$F_{(1,128)} = 17.30$, $p \leq 0.001$] co-treatments significantly modulated the Nrf2 nuclear content and notably normalised it, as illustrated in **Figure 4.6**.

4.7 Liraglutide and the novel GLP-1/GIP Dual Agonist restored STAT3, Akt and mTOR signalling to favour neuroprotection and synapse homeostasis upon persistent ER stress

Functional protein micro-array was employed for scanning for the signalling network that underlay the cross-talk among the different sub-cellular compartments and mediated the neuroprotective/restorative effects of incretin mimetics [**Figures 4.7 & 4.8, Table S2**]. The persistent disturbance of ER calcium homeostasis significantly precluded the activating phosphorylation of STAT3 at the tyrosine residue 705 ($p \leq 0.01$) and of Akt at the serine

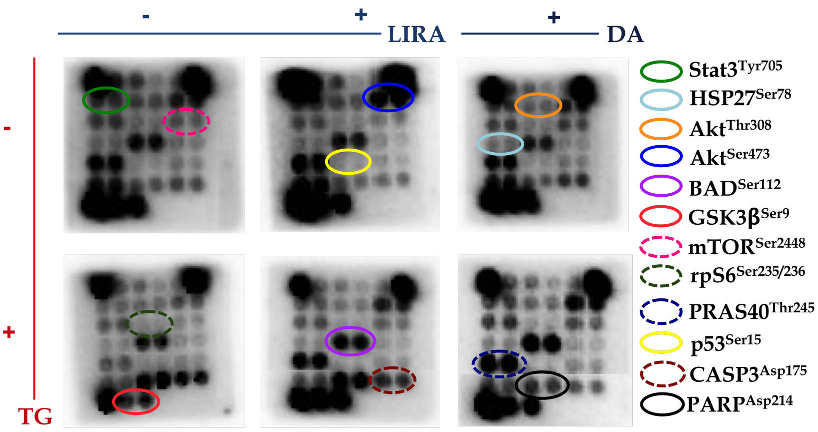

-
+
LIRA
+
DA
-
+
TG
Stat3Tyr705
HSP27Ser78
AktThr308
AktSer473
BADSer112
GSK3βSer9
mTORSer2448
rpS6Ser235/236
PRAS40Thr245
p53Ser15
CASP3Asp175
PARPAsp214

(a)

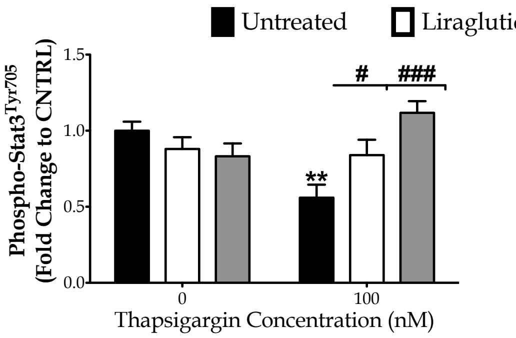

Untreated
Liraglutide 100 nM
Dual Agonist 100 nM
Phospho-Stat3Tyr705 (Fold Change to CNTRL)
1.5
1.0
0.5
0.0
0
100
Thapsigargin Concentration (nM)
**
#
###

(b)

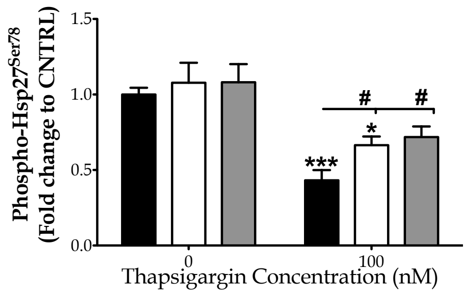

Phospho-Hsp27Ser78 (Fold change to CNTRL)
1.5
1.0
0.5
0.0
0
100
Thapsigargin Concentration (nM)
***
*
#
#

(c)

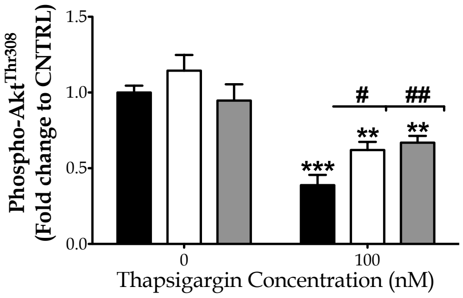

Phospho-AktThr308 (Fold change to CNTRL)
1.5
1.0
0.5
0.0
0
100
Thapsigargin Concentration (nM)
***
**
**
#
##

(d)

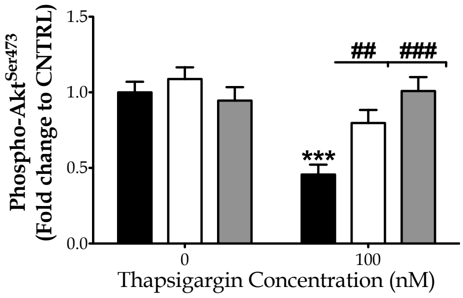

Phospho-AktSer473 (Fold change to CNTRL)
1.5
1.0
0.5
0.0
0
100
Thapsigargin Concentration (nM)
***
##
###

(e)

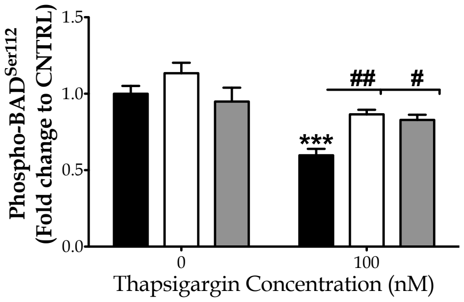

Phospho-BADSer112 (Fold change to CNTRL)
1.5
1.0
0.5
0.0
0
100
Thapsigargin Concentration (nM)
***
##
#

(f)

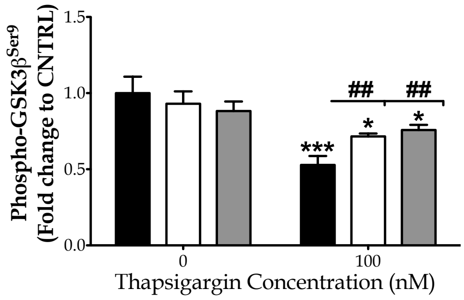

Phospho-GSK3βSer9 (Fold change to CNTRL)
1.5
1.0
0.5
0.0
0
100
Thapsigargin Concentration (nM)
***
*
*
##
##

(g)

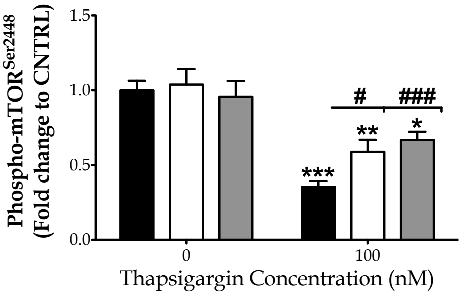

(h)

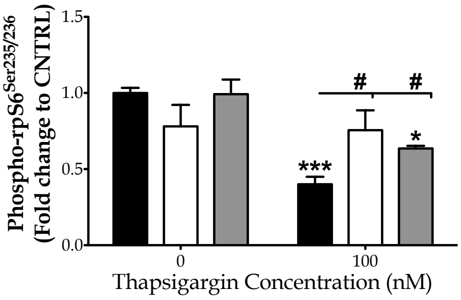

(i)

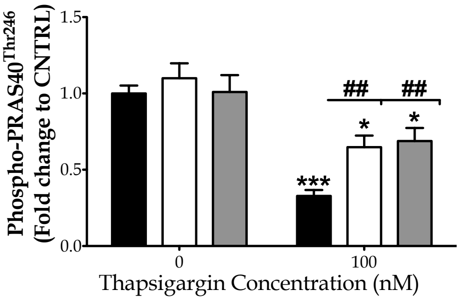

(j)

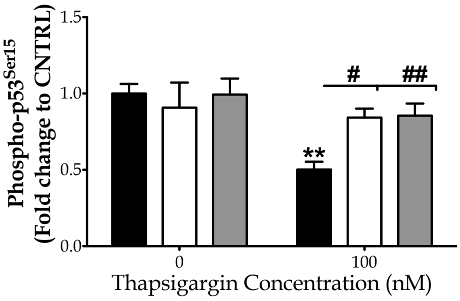

(k)

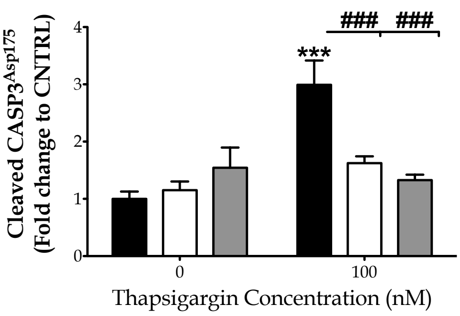

(l)

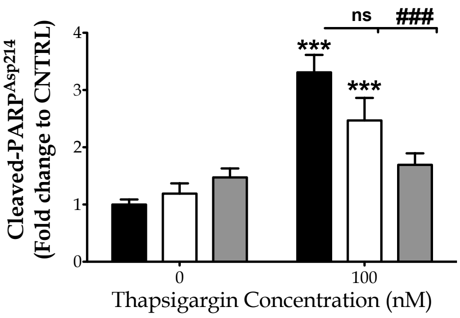

(m)

Figure 4.7: **Incretin mimetics rescued the suppressed Akt and STAT3 signalling to halt the ectopic poly (ADP-ribose) polymerase (PARP) and caspase 3 (CASP3) cleavage and thus favoured neuronal survival and homeostasis upon chronically persistent ER stress.** On d 5–6 of the differentiation period, post-mitotic neurones from the LUHMES cell line were treated with 0 and 100 nM of thapsigargin (TG) in the presence or absence of 100 nM Liraglutide (LIRA) or of 100 nM novel GLP-1/GIP Dual Agonist (DA) for 16 h. Neurones were then harvested, and $0.3\,\mathrm{mg\,mL^{-1}}$ protein of whole-cell lysate was processed with the PathScan® sandwich immunoassay. All protein samples per experiment were processed in duplicate. Each bar represents mean ± SEM from four independent experiments. Data is expressed as fold change to the control (CNTRL; unstressed/untreated conditions). Data was analysed by one- and two-way ANOVA, followed by *post hoc* Bonferroni's multiple comparison t-test ($^{*}p \leq 0.05$, $^{**}p \leq 0.01$ & $^{***}p \leq 0.001$ compared to CNTRL; $^{\sharp}p \leq 0.05$, $^{\sharp\sharp}p \leq 0.01$, $^{\sharp\sharp\sharp}p \leq 0.001$, & $^{ns}p \gg 0.05$ compared to the corresponding thapsigargin-treated neurones).

473 ($p \leq 0.001$) and threonine 308 ($p \leq 0.001$) residues, as illustrated in **Figures 4.7(b)–4.7(d)**. The preclusion of Akt activation correlated with a nearly three-fold decrease in the phosphorylation of the proline-rich Akt substrate of 40 kDa (PRAS40) kinase at Thr246 ($p \leq 0.001$) and of the mammalian target of rapamycin (mTOR) at Ser2448 ($p \leq 0.001$) that was further accompanied by a 60%-reduction in ribosomal protein S6 (rpS6) activation ($p \leq 0.001$) in post-mitotic neurones chronically challenged with 100 nM of thapsigargin [**Figures 4.7(g)–4.7(j)**]. Persistent SERCA inhibition additionally impeded the phosphorylation of the stress-responsive p53 [**Figure 4.7(k)**] and heat shock protein 27 (HSP27) [**Figure 4.7(i)**] at Ser15 ($p \leq 0.01$) and Ser78 ($p \leq 0.001$), respectively, whilst engaging the glycogen synthase kinase 3β [GSK3β; **Figure 4.7(e)**] by halving the inhibitory phosphorylation of the kinase at the serine 9 residue ($p \leq 0.001$). All these alterations in the signalling molecules associated with a two-fold increase ($p \leq 0.001$) in cleaved caspase 3 [CASP3; **Figure 4.7(l)**] that executed the proteolytic cleavage of the poly (ADP-ribose) polymerase (PARP) at the aspartic acid residue 214 (Asp214) [**Figure 4.7(m)**] to assure the fulfilment and irreversibility of the apoptotic process[228] upon a 16-h time course of thapsigargin treatment in post-mitotic neurones from the human LUHMES cell line.

Notably, Liraglutide restored neuronal STAT3 activation upon persistent ER stress, as evident by two-way ANOVA analysis [$F_{1,28} = 5.908$, $p \leq 0.05$] and illustrated in **Figure 4.7(b)**. It significantly attenuated the suppressed Akt phosphorylation at Ser473 ($p \leq 0.01$) and Thr308 ($p \leq 0.05$) [**Figures 4.7(c)–4.7(d)**] that further correlated with an improved PRAS40 kinase activation [**Figure 4.7(j)**]. Liraglutide additionally ameliorated the mTOR-pathway impairments by restoring the protein levels of the phosphorylated mTOR at Ser2448 ($p \leq 0.05$) and its downstream target rpS6 at Ser235/236 ($p \leq 0.05$) [**Figures 4.7(g)–4.7(h)**]. Liraglutide further rescued the aberrant neuronal GSK3β [**Figure 4.7(e)**], p53 [**Figure 4.7(k)**] and HSP27 [**Figure 4.7(i)**] activity under chronic thapsigargin treatment. The aforementioned improvements in the signalling network downstream of the GLP-1 receptor induction correlated with a normalisation of the active (cleaved) CASP3 protein levels [**Figure 4.7(i)**]. However, PARP proteolytic cleavage remained significantly elevated ($p \leq 0.001$) in Liraglutide and thapsigargin co-treated post-mitotic neurones, when compared to control conditions [**Figure 4.7(l)**]. Accordingly, the novel GLP-1/GIP Dual Agonist restored phosphorylated STAT3 to the baseline levels [**Figure 4.7(b)**] and significantly ameliorated the inhibitory effect of thapsigargin on Akt phosphorylation at Ser473 ($F_{1,28}$ =14.43, $p \leq 0.001$) [**Figure 4.7(c)**] and at Thr308 ($F_{1,28} = 5.521$, $p \leq 0.05$) [**Figure 4.7(d)**]. It additionally potentiated one- and an half-fold increase in the phosphorylated levels of PRAS40 [**Figure 4.7(j)**] and GSK3β [**Figure 4.7(e)**], respectively, to rescue the aberrant activity upon chronic disturbance of ER calcium homeostasis. Furthermore, the dual incretin significantly impacted mTOR [$F_{1,28} = 6.393$, $p \leq 0.05$] and rpS6 [$F_{1,28} = 4.507$, $p \leq 0.05$] signalling, potentiating an approximately 20% to 30% amelioration in the impaired phosphorylation patterns following chronic SERCA inhibition [**Figures 4.7(g)–4.7(h)**]. It further impacted p53 [$F_{1,28} = 5.054$, $p \leq 0.05$] and HSP27 [$F_{1,28} = 5.228$, $p \leq 0.05$] phosphorylation patterns, and specifically restored their activity to control levels, as shown in **Figures 4.7(k)–4.7(i)**. Intriguingly, novel GLP-1/GIP Dual Agonist co-treatment normalised the ectopic proteolytic cleavage of CASP3 [**Figure 4.7(i)**] and PARP [**Figure 4.7(l)**] in thapsigargin-treated post-mitotic neurones that signified neuroprotection upon unmitigated UPR and autophagy dysfunction.

The majority of pro-death signals emerging from the UPR regulated the expression and activity of pro- and anti-apoptotic proteins of BCL-2 family.[108,109] Consistently, herein, the persistent ER-localised blocking of calcium flux significantly altered the activity patterns of the pro-apoptotic BAD ($F_{(5,42)} = 10.13$, $p \leq 0.001$) and the pro-survival Bcl-2 [$F_{(5,42)} = 8.247$, $p \leq 0.001$], along with the protein expression levels of the pro-apoptotic BID [$F_{(5,42)} = 18.50$, $p \leq 0.001$]. Particularly, it diminished the inhibitory phosphorylation

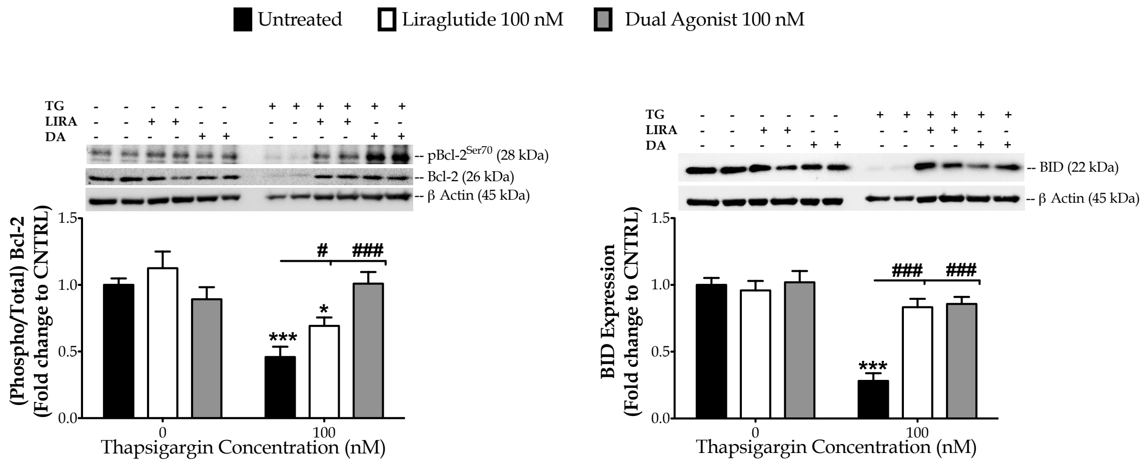

(a)

(b)

Figure 4.8: **Incretin mimetics ameliorate the suppressed Bcl-2 activity and BID protein expression in post-mitotic neurones upon persistent ER stress.** On d 5–6 of the differentiation period, post-mitotic neurones from the human LUHMES cell line were treated with 0 and 100 nM of thapsigargin (TG) in the presence or absence of 100 nM Liraglutide (LIRA) or of 100 nM novel GLP-1/GIP Dual Agonist (DA) for 16 h. Neurones were then harvested, and the expression of total and phosphorylated Bcl-2 [**(a)**] and of full-length BID [**(b)**] were determined by western blotting. β-Actin was used as the loading control to all western blot analyses. Each bar represents mean ± SEM from four independent experiments. Data is expressed as fold change to the control (CNTRL; unstressed/untreated conditions). Data was analysed by one- and two-way ANOVA, followed by *post hoc* Bonferroni's multiple comparison t-test ($^{*}p \leq 0.05$ & $^{***}p \leq 0.001$ compared to CNTRL; $^{\sharp}p \leq 0.05$& $^{\sharp\sharp\sharp}p \leq 0.001$ compared to the corresponding thapsigargin-treated neurones).

of BAD at Ser112 and the activating phosphorylation of Bcl-2 at Ser70 almost by half [**Figures 4.7(f) & 4.8(a)**]. It down-regulated the expression of the full-length BID by 70% [**Figure 4.8(b)**], which may have signalled for the proteolytic processing and activation of this pro-apoptotic factor.[309,310] *Post hoc* analysis demonstrated that Liraglutide co-treatment significantly attenuated the impairments in BAD ($p \leq 0.01$) [**Figure 4.7(f)**] and Bcl-2 ($p \leq 0.05$) [**Figure 4.8(a)**] phosphorylation patterns, and normalised the abnormal BID expression [**Figure 4.8(b)**]. Similarly, the GLP-1/GIP Dual Agonist significantly rescued BAD [two-way ANOVA; $F_{(1,28)} = 5.754$, $p \leq 0.05$] [**Figure 4.7(f)**] and Bcl-2 [two-way ANOVA; $F_{(1,28)} = 17.93$, $p \leq 0.001$] activity [**Figure 4.8(a)**] upon chronic thapsigargin treatment, and restored the suppressed BID expression back to control levels [**Figure 4.8(b)**].

4.8 Discussion

Chronic ER stress has emerged as a hub for the derailed proteostasis underlying the onset and progression of neuronal degeneration, with the UPR and autophagy dysregulation paralleling the temporal and spatial pattern of the pathologic protein deposition in the AD brain.[30,111,224,235,258] Mechanistically, chronic ER stress potentiates the disproportionate PERK, ATF6 and IRE1α signalling to determine cell fate.[109,169] It suppresses ATF6 and IRE1α signalling[164,169] to possibly attenuate the downstream survival signals and the neurotrophic effects of the spliced X-box binding protein 1(XBP-1).[109] Spliced XBP1 regulates the transcription of the brain-derived neurotrophic factor (BDNF) and other genes related to the BDNF signalling to fine-tune synaptic plasticity in the murine hippocampus.[193] Accordingly, herein, the chronic perturbation of ER calcium diminished the phosphorylation of IRE1α at Ser724 and the expression of ATF6 that correlated with a prominent decrease in the plasticity-related proteins, PSD95 and synaptophysin. Furthermore, IRE1α is a prerequisite, among the three UPR branches, for the induction of the pro-survival autophagy upon ER stress.[223] It mediates the phosphorylation of Bcl-2 to favour the dissociation of beclin-1 from its inhibitory complex with Bcl-2 at the ER membrane.[175] It stimulates the transcription factor XBP1 that in turn binds to the promoter of beclin-1 and induces its transcription.[192] Herein, human post-mitotic neurones featured the suppressed IRE1α and Bcl-2 activity following chronically persistent ER stress that may have accounted for the observed beclin-1 deficiency. A substantial loss of beclin-1 has been detected in the mid-frontal cortex of human AD brains that parallels disease progression.[239] Genetic depletion of beclin-1 exacerbates Aβ pathology and dampens the expression of synaptophysin, the dendrite-specific microtubule-associated protein 2 (MAP2) and of the calcium-binding protein, calbindin to potentiate synapse degeneration *in vivo*.[239]

In contrast, chronic ER stress augments the activity of PERK arm to amplify and sustain the transcription and translation of the short-lived pro-apoptotic transcription factor CHOP.[169] CHOP inhibits the expression of the pro-survival Bcl-2 factor whilst stimulating the transcription of the ERO1α to provoke the mitochondrial apoptotic machinery and neuronal damage,[109, 111] as prominent in our findings too. ERO1α harnesses the oxidising power of the molecular oxygen to oxidise the active cysteinyl-thiol groups in PDI, enabling the latter to introduce disulphide bonds to folding substrates and to maintain the thiol-disulphide exchange and PDI capacity for the bond isomerisation within nascent polypeptides.[27] The redox fidelity of the oxidoreductase and the detoxification of the hydrogen peroxide produced upon the formation of a disulphide bond relies on the glutathione metabolism[27] that is contingent on the Nrf2 activity.[230] Herein, the ERO1α excess correlated to the PDI deficiency and suppressed Nrf2 nuclear (active) content, signalling for defective oxidative folding. The latter along with the observed down-regulation of calnexin can exacerbate the abnormal protein load within the organelle lumen and hasten cell demise. Indeed, calnexin silencing has been previously reported to promote a CHOP/ERO1α-mediated ‘terminal’ UPR signalling to sensitise cadriomyocytes to ER stress.[24] Similarly, Nrf2 deficiency has been to shown to alter the glutathione ‘pool’ and favoured the accumulation of damaged proteins to impact ER stress magnitude.[322] Furthermore, CHOP-induced ERO1α up-regulation triggers the inositol-1,4,5-trisphosphate receptor (IP_3R)-mediated calcium efflux into cytosol[163] that can influence multiple pathways upstream of the core apoptosis machinery[144] and the proteolytic (activating) cleavage of CASP12.[211] Active CASP12 potentiates a downstream caspase cascade (*e.g.*, CASP3) that mediates synaptophysin depletion and executes PARP degradation to assure the fulfilment and irreversibility of the apoptotic process for synapse and neuronal toxicity,[147, 203, 207, 212, 247] as reflected in our results too.

Besides the modulation of redox signalling and core apoptosis machinery, CHOP can limit autophagy through the transcriptional regulation of Atg components for phagophore elongation and maturation into the autophagosome, including the Atg7 gene.[16,17] Atg7 deficiency potentiates a spontaneous accumulation of protein aggregates, neuronal degeneration and loss in mice.[150] Notably, Liraglutide and the dual incretin both alleviated the ectopic BiP and CHOP expressions, mitigated the aberrant IRE1α, Nrf2 and CASP12 activity, and restored the protein levels of ATF6, PDI, calnexin, ERO1α, beclin-1, Atg3, Atg7, and LC3. These biochemical traits corresponded to the normalisation of PSD95 and synaptophysin expression, as well as to a prominent amelioration of the neuronal toxicity in the XTT-assessed metabolic activity assay, LDH levels and the proteolysis of the executioner CASP3 and PARP. Taken together, the induction of GIP and/or GLP-1 receptors seemed to shift the 'terminal' UPR towards adaptive signals and thereby favoured the homeostasis of autophagy and quality control machinery, abetting proteostasis and neuronal repair following persistent ER stress.

Mechanistically, the incretin mimetics restored the suppressed STAT3 and Akt signalling to elicit neuroprotection upon irremediable ER stress. The induction of the GLP-1 receptor downstream stimulates the activating phosphorylation of the cytoplasmic STAT3 monomers at the tyrosine 705[272] that in turn favours conformational changes of STA3 central to the DNA target recognition and gene transcription.[52] Suppressed STAT3 activity occurs in the hippocampus of affected patients and animals of AD.[41] Mechanistically, Aβ inactivates the hippocampal JAK2 (Janus kinase 2)/STAT3 axis to compromise basal forebrain cholinergic function and induce spatial working memory deficits *in vivo*.[41] Subsequent work has further revealed that the ER stress perturbs the astrocytic STAT3 signalling to modulate acute-phase neuroinflammatory responses in a PERK-dependent fashion.[199] Although the mechanistic interplay between the UPR and STAT3 signalling in the context of neuronal functioning and fate remains elusive, STAT3 regulates the transcription of the pro-survival Bcl-2 protein and axonal outgrowth/branching programs to promote neuronal survival and axonal regeneration post oxygen-glucose deprivation and excitotoxicity.[37,233] Activated

STAT3 additionally induces the expression of synaptophysin that enhances synaptogenesis and synaptic plasticity in the hippocampus and cortex.[37,43] As such, the restoration of STA3 activation may offer a node through which GLP-1 and GIP receptors conferred trophic signals for the synapse homeostasis and neuronal repair following chronic ER stress.

Furthermore, Liraglutide and the dual incretin alleviated the suppressed phosphorylation of Akt at Thr308 and Ser473 sites that signified the restoration of the maximal kinase activity.[190] Akt (also known as protein kinase B – PKB) is a serine/threonine kinase member of the AGC protein kinase family with a profound function in neurotrophin (growth factor) signalling for neuronal survival[190] and the synaptic delivery of PSD95.[315] It possesses a wide spectrum of targets in the cytoplasm, nucleus, mitochondria, and the ER membrane to regulate adaptive responses and cell fate under stress conditions.[189,190] Among others, activated Akt phosphorylates and inhibits the death-agonist BAD that becomes rapidly de-phosphorylated upon apoptotic stimuli,[189] as prominent herein too. The active BAD enchains with the survival-agonist Bcl-x_L or Bcl-2 at the mitochondria and allows the Bax and Bak oligomerisation. The latter impacts the mitochondrial membrane permeabilisation and favours the point-of-no-return of apoptotic cell death.[40,306,328]However, the restoration of BAD phosphorylation, downstream of the growth-factor signalling, raises the mitochondrial threshold for apoptosis and renders the cells less vulnerable to death signals,[53] as reflected in our findings too.

In addition to BAD, Akt can phosphorylate the stress-responsive HSP27,[38] which in turn sequesters cytochrome c and/or pro-caspase 3 to preclude the apoptosome formation and downstream death signal transduction.[11,19,281] Furthermore, activated HSP27 phosphorylates p53 at Ser15 and induces its downstream target gene expression to prevent genotoxicity.[11,308] p53 is a transcription factor that orchestrates an array of cellular responses, including apoptosis, senescence, DNA repair or autophagy, depending on the nature and degree of stress insult, cell type, and 'environmental' context. The p53 regulation is complex and involves post-translational modifications (*e.g.,* phosphorylation and acetylation) at multiple sites that determine its cellular localisation, stability and transcriptional activity.[155] Herein, we monitored the phosphorylation of p53 at Ser15 that obstructs the interaction the E3 ubiquitin-protein ligase Mdm2 with the factor whilst facilitating the p53 nuclear accumulation and stabilisation.[270,324] In the findings presented here, irremediable ER stress suppressed p53 phosphorylation to favour its destabilisation that is in agreement with previously published reports.[12,245] As such, the restoration of HSP27 activation may offer a supplementary signalling node for the inhibition of the intrinsic apoptotic pathway and reinforce neuronal survival.

Phosphorylation of PRAS40 at Thr246 by Akt relieves PRAS40 inhibition of the mTOR signalling[98] that positively regulates protein synthesis, ribosomal biogenesis, oxidative metabolism and mitochondrial function.[157] ER stress derails mTOR activity that in turn renders neurones vulnerable to CHOP/ERO1α-mediated oxidative damage and facilitates the intrinsic apoptotic machinery,[60] as reflected in our findings too. Suppressed mTOR has been previously reported to underlie the down-regulated expression of the activity-regulated cytoskeleton associated protein (Arc) involved in synaptic memory process and the impaired long-term potentiation in primary cortical neurons and in hippocampal slices from the Tg2576 mouse model for AD, respectively, when exposed to Aβ.[106] Suppressed mTOR activity further abolishes the inhibitory phosphorylation of Atg13 and unc-51-like kinase 1 (ULK1) that in turn allows the ULK complex formation and autophagy initiation.[106,157] Excessive autophagic flux can exert detrimental effects by aberrantly degrading endogenous inhibitors of apoptosis and Atg components and lead to cell death.[106,274] Contrary to mTOR, Akt phosphorylates and inhibits GSK3β that pivotally drives neuronal degeneration in the AD brain[179] and neuronal apoptosis upon ER stress.[26,200,276,287] Indeed, accumulating evidence from diverse neuronal-like cell lines, primary neuronal cultures, and ER insults evinces that the UPR abrogates the inhibitory phosphorylation of GSK3β at Ser9[26, 200, 232, 276, 287] to facilitate CHOP expression and the dominance of pro-death signals during unmitigated ER stress,[200, 232] as evident herein too. In the AD brain, GSK3β immunoreactive granules occur in neurones with activated PERK signalling.[119, 216] Active PERK engages GSK3β activity through selective removal of the inactive (phosphorylated at Ser9) kinase form via the autosomal-lysosomal pathway.[216] GSK3β inhibits Nrf2 by nuclear exclusion and proteosomal degradation that could preclude the transcription of genes for oxidative folding and ER proteostasis.[230] Intriguingly, active (nuclear) Nrf2 induces the expression of regulatory proteins for the autophagy initiation, cargo recognition, autophagosome formation, elongation and autolysosome clearance[230, 231] whilst precluding the recruitment of ATF4 to the CHOP promoter and thereby CHOP transcription.[329] Taken together, the findings presented herein suggest that the stimulation of GIP and/or GLP-1 receptors rescued the impaired mTOR signalling and restored the exacerbated GSK3β activity, which may, in turn, normalise Nrf2 nuclear levels and thereby reinforce proteostasis upon chronic ER stress.

Akt may also phosphorylate and inhibit PERK kinase,[206] offering an additional mechanistic link for the neuroprotective and restorative effects of incretin mimetics upon persistent ER stress. Exacerbated PERK activity triggers general translation repression and down-regulation of the plasticity-related cyclic AMP response-element-binding protein (CREB), through its downstream targets eIF2α and ATF4 respectively, to provoke PSD95 deficiency, synapse damage and cognitive decline *in vivo*.[224] Although we did not assess the expression of phosphorylated PERK levels, transcriptional and translational regulation of Chop expression primarily lies downstream of the PERK arm.[169]

Despite these encouraging findings, we cannot exclude that incretin mimetics may restore calcium homeostasis to elicit neuroprotection following persistent SERCA inhibition. Previous studies have demonstrated that the GLP-1 receptor induction potentiates the cAMP production,[236] orchestrates calcium responses[91, 265] and thereby halts aberrant apoptosis of hippocampal neurones and SH-SY5Y neuroblastoma cells following excitotoxicity[91] and oxidative stress.[265] Downstream, the cAMP boosts the activity of the protein kinase A (PKA) that regulates SERCA function to favour cytoprotection in insulin-resistant macrophages[168] and high glucose-treated cardiomyocytes.[318] Pharmacological preclusion of PKA induction has been reported to block the anti-apoptotic effects mediated by the stimulation of the GLP-1 receptor. Contrarily, the adenylate cyclase potentiator, Forskolin mimics the GLP-1-induced cardioprotection upon hyperglycaemia.[318] The cAMP may additionally downstream activates cAMP-regulated guanine nucleotide exchange factors (also known as Epac) that in turn modulate calcium dynamics in response to GLP-1R stimulation.[117]

To sum up, the findings presented herein evinced the neuroprotective and restorative effects of Liraglutide and the novel GLP-1/GIP Dual Agonist following the unmitigated neuronal ER stress. They further unravelled an even more elaborate proteome through which the stimulation of GIP and/or GLP-1 receptors modulated the UPR, autophagy, protein quality control, and heat-shock response to elicit synapse homeostasis and neuronal survival following the chronic perturbation of ER calcium and proteostasis. Notably, in a recent pilot clinical trial in AD patients, Liraglutide attenuated impairments in cerebral glucose consumption, signifying improved neural energetics and activity in areas previously correlated with cognitive decline and disease progression.[86] These encouraging results have led to a randomised, placebo-controlled, double-blind phase II clinical trial of Liraglutide in AD that is currently ongoing (NCT01843075).[116] The present study endorsed the beneficial effects of incretin signalling in neurodegenerative disorders[116] and expanded our understanding of the incretin neuropharmacology.

Chapter 5

GLP-1/GIP Dual Agonist restored ER stress and autophagy impairments to attenuate Alzheimer's-like pathology in $APP_{swe}/PS1_{\triangle E9}$ mouse model

In preparation for submission

5.1 Introduction

Alzheimer's disease (AD) is an age-related neurodegenerative disorder that features the accumulation of two classes of highly insoluble, densely packed filaments – the extracellular amyloid plaques (also, termed as "senile" plaques) and the intracellular neurofibrillary tangles. Both the amyloid plaques and neurofibrillary tangles represent the pathognomonic signature of the disorder, required for diagnosis during the *post-mortem* examination.[246] In addition to these two lesions, multiple other structural and functional alterations ensue,[246] including oxidative stress, cell energy deprivation,[75, 238] deregulated calcium signalling,[20, 96] deficient proteasome-mediated and autophagy-mediated clearance of damaged proteins and organelles,[219, 220] aberrant gliosis, and abnormal inflammatory responses.[92, 188, 202] Suppressed expression and membranous distribution of the insulin receptor along with a defective insulin signalling occur in the AD brain, as well too.[254, 280, 288] The insulin signalling is essential to neuronal survival, the regulation of synapse population and post-synaptic plasticity.[54] Altogether, these pathologies contribute to the severe synaptic and neuronal damage in numerous brain areas, and particularly in those for high-order cognitive processing, such as basal forebrain and hippocampus.[54, 56, 75, 96, 202, 238, 246, 262]

Interestingly, recent evidence signals for the convergence of these pathologies in the occurrence of persistent endoplasmic reticulum (ER) stress and altered dynamics of proteostasis-related signalling.[30, 54, 111, 165, 224, 235, 258] The ER is a multifunctional signalling organelle central to calcium homeostasis and the biosynthesis of autophagosomes, as well as to the synthesis, maturation, quality control and delivery of secretory and membrane proteins,[108] including the amyloid precursor protein (APP)[301] and insulin.[173] Many physiological and pathological stimuli can alter the protein folding at the ER, triggering a rise in the unfolded or misfolded protein load in the organelle lumen, a cellular state referred to as ER stress. In turn, the cell activates an adaptive signalling network, known as the unfolded protein response (UPR). The UPR essentially engages the three ER-resident transmembrane stress transducers – protein kinase RNA-like ER kinase (PERK), activating transcription factor 6 (ATF6) and inositol-requiring enzyme 1 (IRE1) – to safeguard proteostasis through the attenuation of global protein synthesis and the transcriptional induction of genes functioning as ER chaperones, and to degrade the abnormal protein loal through the proteasome and lysosome-mediated autophagy.[108,109,111] Upon persistent or unsurmountable ER stress, the UPR adapts its dynamics towards apoptosis through diverse but often overlapping mechanisms, e.g. pro-inflammatory and apoptotic protease and kinase activity and the transcription of CAAT/enhancer-binding protein (C/EBP) homologous protein (Chop).[108,109] Therapeutic interventions which resolve the UPR towards a balance between protein generation and degradation may significantly benefit the Alzheimer's clinical outcome.[30,235,258] As such, herein, we have examined the neuroprotective effects of a novel dual incretin analogue on the AD-like pathology in the double transgenic $APP_{swe}/PS1_{\Delta E9}$ mouse model.

The incretin hormone, glucagon-like peptide 1 (GLP-1) is best known for regulating glucose homeostasis and the biosynthesis and signalling of insulin in response to food ingestion. GLP-1 mimetics are currently approved for the treatment of type 2 diabetes mellitus (T2DM).[10] Besides their glucose-dependent pancreatic effects, GLP-1 mimetics cross the blood-brain barrier and exert neurotrophic and cell survival signals, downstream of the stimulation of the GLP-1 receptors widely expressed in the human, primate and rodent brain.[6,115,116] For instance, chronic intraperitoneal administration of Liraglutide has preserved normal population and activity of cortical and hippocampal synapses, mitigated aberrant microglia reactivity and astrogliosis, and halted excessive Aβ accumulation and deposition to rescue spatial learning and memory deficits in young, middle-aged and aged $APP_{swe}/PS1_{\Delta E9}$ mice.[195,197,198] Similarly, chronic subcutaneous administration of Liraglutide impeded the hippocampal atrophy and spatial cognitive decline in the senescence accelerated mouse-prone 8 (SAMP8) model for age-related sporadic AD.[102] In line with the *in-vivo* findings, Liraglutide and other GLP-1 mimetics have favoured survival over apoptotic signalling to impede cytotoxicity and impaired viability of hippocampal and primary cortical neurones and neuronal-like cells chronically exposed to excitotoxic insults,[91,166,236,316] Aβ oligomers[237,244,316] and calcium-dependent ER stress.[232,316] Notably, in a pilot clinical trial, Liraglutide has rescued the decline of the cerebral glucose consumption in AD patients that signifies energy metabolism in brain areas previously correlated with cognitive decline and disease progression.[86]

Accordingly, the stable analogue of the glucose-dependent insulinotropic polypeptide (GIP), $_D$Ala^2-GIP has alleviated neuroinflammatory responses, oxidative stress and cerebral amyloid plaque load to attenuate the poor performance of the APP$_{swe}$/PS1$_{\Delta E9}$ mouse model in Morris water maze and novel object recognition paradigms.[63,70] These effects have been further correlated to enhanced synaptogenesis and restored synaptic plasticity events in the cortex and hippocampus of the middle-aged and aged APP$_{swe}$/PS1$_{\Delta E9}$ mice upon chronic $_D$Ala^2-GIP treatment.[70]

Recently, novel GLP-1/GIP Dual Agonist analogues have been developed and displayed superior anti-hyperglycaemic and insulinotropic efficacy compared to the GLP-1 mono-therapy, rendering them potent candidates for T2DM treatment.[76] Pilot pre-clinical studies have further demonstrated the neurotrophic and restorative effects of the dual incretin against hallmark, disease-related pathological lesions in a mouse model of mild traumatic brain injury (TBI),[289] a rat model of streptozotocin-induced diabetes and neurodegeneration,[269] and of the 1-methyl-4-phenyl-1,2,3,6-tetrahydropyridine (MPTP) and 6-hydroxydopamine (6-OHDA) rodent models of Parkinson's disease (PD).[31,133,136,320]

In the light of these encouraging findings, herein, the effects of the novel GLP-1/GIP Dual Agonist in the APP$_{swe}$/PS1$_{\Delta E9}$ mouse model at the age of 10 months old were assessed and further compared to the GLP-1 and GIP mono-therapy. Once-a-daily intraperitoneal administration of 25 nmol kg^{-1} of the Dual Agonist for two months halted the spatial cognitive decline and synapse damage of this murine model, as well as it decreased the plaque deposition and gliosis over the APP$_{swe}$/PS1$_{\Delta E9}$ cortex and hippocampus too. Attenuation of the AD-like pathology reflected the resolution of ER stress and restoration of autophagy impairments, both lying downstream of the rectified Akt signalling. The present study provided additional evidence for the beneficial effects of the incretins in neuronal degeneration management,[116] as outlined in the following sections.

5.2 Incretin mimetics had a neutral effect in the body weight of APP$_{swe}$/PS1$_{\Delta E9}$ mice

Incretin-based therapies have been previously shown to convey regulatory effects in satiety and appetite via the central nervous system, resulting in a reduced food intake and weight loss in patients and animal models of diabetes and obesity.[76,171,215] In this light, the body weight of the animals was monitored over the 8-week treatment administration period. Two-way ANOVA analysis demonstrated a non-significant effect both of the animal genotype ($F_{(1,25)} = 1.063$, $p = 0.312$) and assigned treatment ($F_{(3,41)} = 0.11$, $p = 0.955$), as illustrated in **Figure 5.1**.

5.3 APP$_{swe}$/PS1$_{\Delta E9}$ genotype was not accompanied by changes in the open-field behaviour

Eight weeks after the initiation of saline and incretin-based treatments, animals were subjected to the open field test. The total ambulatory distance that is arguably the most specific parameter for that behavioural paradigm[94] was evaluated over a 10-min session. In the experimental data presented here [**Figure 5.2**], wild type and APP$_{swe}$/PS1$_{\Delta E9}$ mice

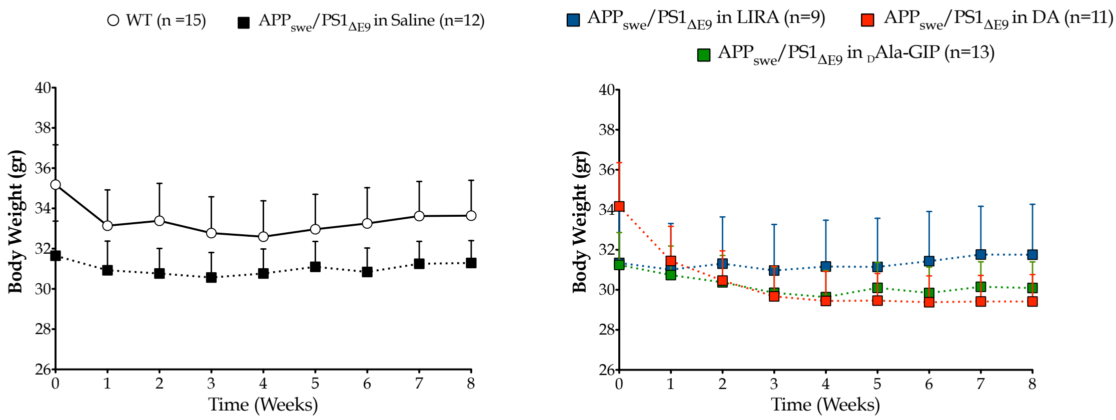

(a) (b)

Figure 5.1: **Incretin mimetics did not impact body weight of the APP$_{swe}$/PS1$_{\Delta E9}$ mouse model of Alzheimer's disease.** Each graph point represents mean ± SEM of wild-type (WT) or APP$_{swe}$/PS1$_{\Delta E9}$ mice treated with 10 mL kg^{-1} d^{-1} saline and APP$_{swe}$/PS1$_{\Delta E9}$ mice treated with 25 nmol kg^{-1} d^{-1} $_{D}$Ala^2-GIP, Liraglutide (LIRA) or GLP-1/GIP Dual Agonist (DA). Data was analysed by repeated measures two-way ANOVA.

displayed similar ambulatory ability in the arena, travelling a total path of 4400 ± 329.1 cm and 5834 ± 594.9 cm in length, respectively. To further evaluate locomotion motivated by exploration, the vertical activity (rearing incidents) and the frequency of grooming activity of each animal were monitored over the open field session. One-way ANOVA analysis revealed no significant differences in rearing incidents ($F_{(4.55)} = 1.449$, $p = 0.230$) and grooming sessions ($F_{(4.55)} = 0.566$, $p = 0.688$) among the animal groups. The activity in the centre of the open field arena that has been repeatedly validated as a measure of anxiogenic behaviour in mice.[243] As such, using a Python-based tracking/analyser system software, the generated animal tracks were partitioned into individual zones [**Figure 2.3(b)**]. The time spent along with the path travelled in the inner zone (centre) of the arena were calculated and presented as percentage of total time and path length in the open field [**Figure 5.2(b)**]. One-way ANOVA analysis demonstrated similar activity in the centre of the open field arena [**Figure 5.2(b)**] that further correlated to similar defecation among the animal groups ($F_{(4.55)} = 0.960$, $p = 0.437$). Overall, neither the APP$_{swe}$/PS1$_{\Delta E9}$

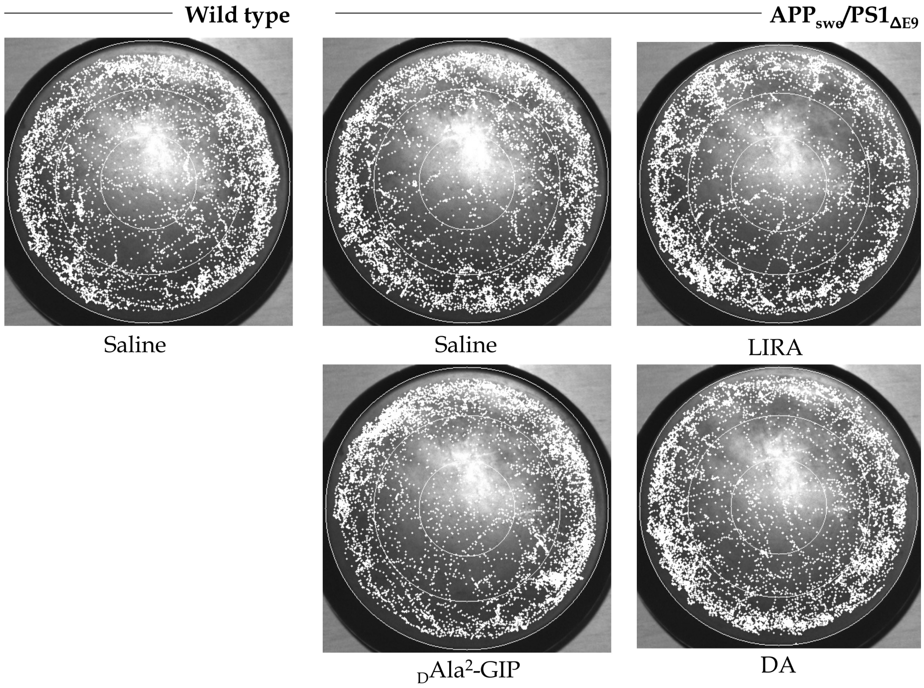

(a)

Behavioural Parameter ID	**Mean ± SEM**					**One-way ANOVA**	
	Wild type	$APP_{swe}/PS1_{\Delta E9}$				$F_{(4,55)}$	p
	Saline $n = 15$	Saline $n = 12$	LIRA $n = 9$	$_D$Ala^2-GIP $n = 13$	DA $n = 11$		
Rearing incidents	43.00 ± 3.489	43.50 ± 4.793	51.56 ± 6.083	40.00 ± 2.803	52.36 ± 5.759	1.449	0.230
Grooming sessions	3.467 ± 0.389	2.667 ± 0.449	3.333 ± 0.553	2.923 ± 0.265	3.182 ± 0.569	0.566	0.688
Total path length (cm)	4400 ± 329.1	5834 ± 594.9	5836 ± 585.4	6032 ± 510.7	5666 ± 260.7	2.400	0.061
%Path length in centre	7.134 ± 0.885	4.721 ± 0.618	5.074 ± 0.444	5.667 ± 0.473	5.390 ± 0.304	2.387	0.062
%Time spent in centre	4.612 ± 0.890	3.230 ± 0.633	3.315 ± 0.363	3.084 ± 0.416	3.175 ± 0.329	1.167	0.336
Faecal boli deposits	0.7333 ± 0.248	0.417 ± 0.229	0.556 ± 0.294	1.308 ± 0.511	0.909 ± 0.392	0.960	0.437

(b)

Figure 5.2: **$APP_{swe}/PS1_{\Delta E9}$ genotype was not accompanied by changes in exploratory behaviour and anxiety, as assessed in the open field test.** The open field test was conducted 8 weeks after the initiation of saline, $_D$Ala^2-GIP, Liraglutide (LIRA), and GLP-1/GIP Dual Agonist (DA) treatments. A Python-based video tracking/analyser system software interfaced with a monochrome digital camera was used to automatically detect, record and process mouse movements over a 10-min-session, as shown in the representative tracks [**(a)**]. Data was analysed by one way ANOVA, as summarised in the table [**(b)**].

genotype nor the treatments altered the exploratory locomotion and emotionality of the animals.

5.4 The novel GLP-1/GIP Dual Agonists alleviated spatial learning and memory deficits of the $APP_{swe}/PS1_{\Delta E9}$ mouse model

Numerous studies have previously reported spatial learning and reference memory deficits of the $APP_{swe}/PS1_{\Delta E9}$ mouse model in the Morris water-maze task.[71,156,305] The latter represents a cognitive paradigm highly specific for hippocampal function and thus particularly sensitive for examining age-related/AD-like impairments.[59] Consistently, herein, a significant effect of the animal genotype in the escape latency ($F_{1,25} = 17$, $p \leq 0.001$) and length of the swimming path ($F_{1,25} = 22.44$, $p \leq 0.001$) was apparent over the Morris water-maze acquisition phase. As illustrated in **Figures 5.3(a)** and **5.3(c)**, the $APP_{swe}/PS1_{\Delta E9}$ mice required longer sessions and swam longer paths to locate the escape platform, relative to wild-type counterparts. *Post hoc* analysis at each time point revealed that $APP_{swe}/PS1_{\Delta E9}$ mice displayed prominent spatial acquisition impairments at the 9^{th} ($p \leq 0.001$) and 10^{th} ($p \leq 0.01$) day of the training course.

Notably, the spatial acquisition impairments reflected a cognitive decline of the $APP_{swe}/PS1_{\Delta E9}$ mouse model, rather than defects in the locomotor coordination during swimming, visual acuity and/or in motivation. Indeed, $APP_{swe}/PS1_{\Delta E9}$ and wild type mice featured similar swim patterns in the Morris water maze visible-platform training [**Figure 5.4**], with an insignificant effect of the genotype over time in the repeated measures two-way ANOVA analysis of the swim time ($F_{3,75} = 0.20$, $p = 0.90$), path length to locate the cued escape platform ($F_{3,75} = 0.19$, $p = 0.90$), swim velocity ($F_{3,75} = 1.83$, $p = 0.15$), percentage of thigmotaxis ($F_{3,75} = 0.40$, $p = 0.75$). Similarly, $APP_{swe}/PS1_{\Delta E9}$

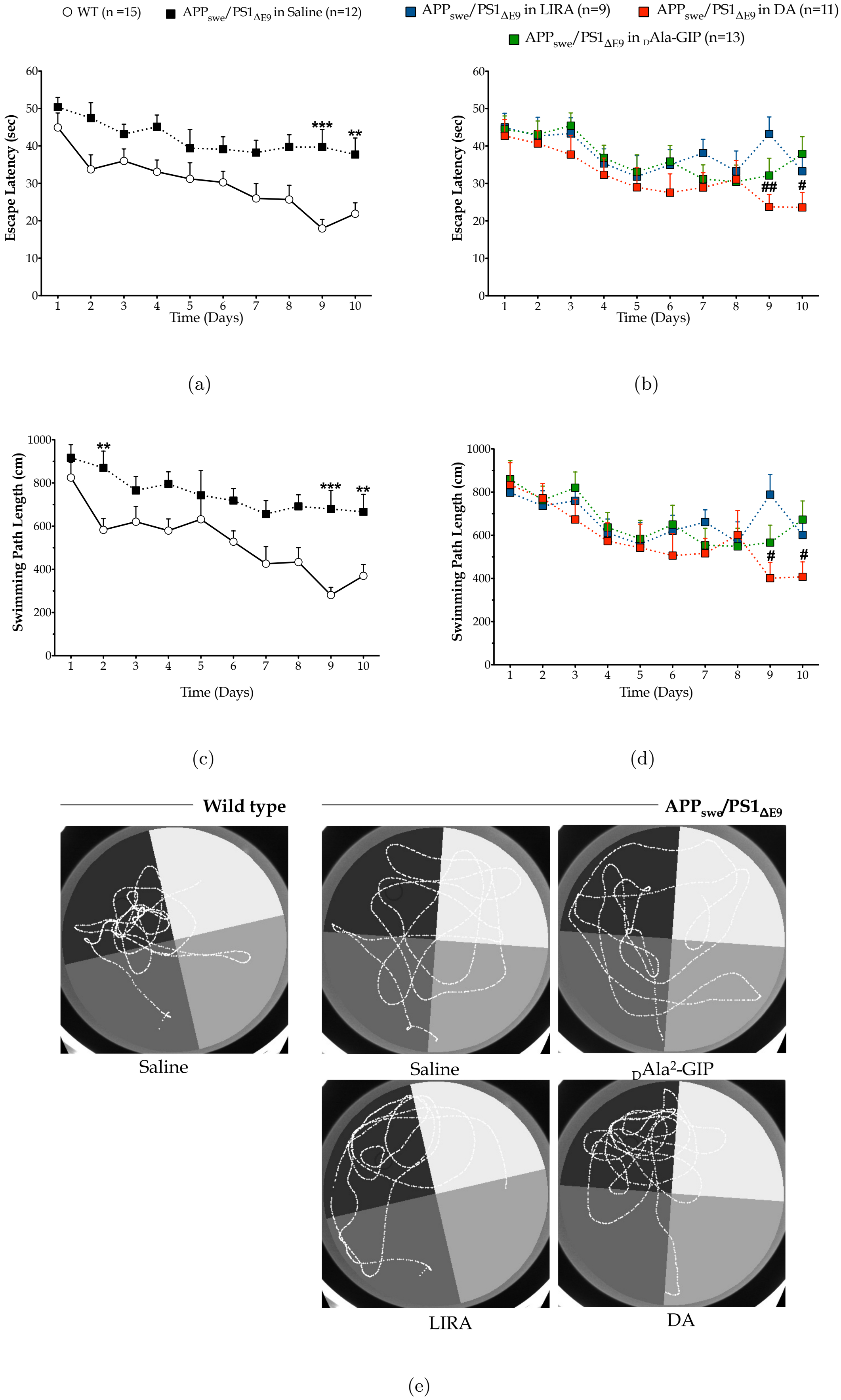
WT (n =15)
APPswe/PS1ΔE9 in Saline (n=12)
APPswe/PS1ΔE9 in LIRA (n=9)
APPswe/PS1ΔE9 in DA (n=11)
APPswe/PS1ΔE9 in DAla-GIP (n=13)
Escape Latency (sec)
Time (Days)
(a)
(b)
Swimming Path Length (cm)
(c)
(d)
Wild type
APPswe/PS1ΔE9
Saline
Saline
DAla2-GIP
LIRA
DA
(e)

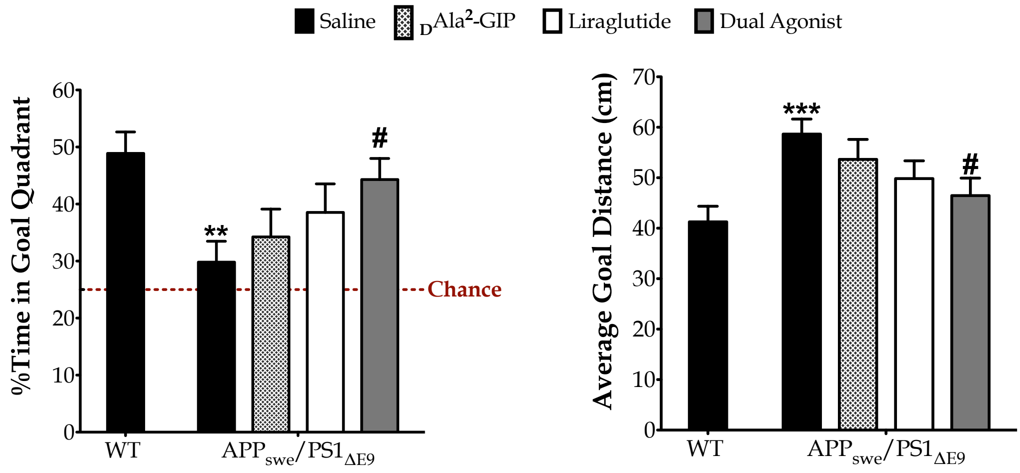

(f)

(g)

Figure 5.3: **The novel GLP-1/GIP Dual Agonist attenuated spatial acquisition and reference memory impairments of the APP$_{swe}$/PS1$_{\Delta E9}$ mouse model of Alzheimer's disease.** Nine weeks after the initiation of saline, $_D$Ala^2-GIP, Liraglutide (LIRA) and GLP-1/GIP Dual Agonist (DA) treatments, animals were trained to locate an invisible escape platform fixed on a target position in the northwest quadrant. Animals run 3 trials per day with an inter-trial interval of approximately 30 min for 10 consecutive days. The escape latency [**(a–b)**] along with the daily mean of length of the swimming path [**(c–d)**] to locate the platform were monitored to evaluate spatial learning. A retention probe trial was held on the 11$^{\text{th}}$ day, during the swimming pattern of each mouse was tracked in a single trial of 60 s in the absence of the escape platform, as illustrated in representative panel **(e)**. The percentage of the swim time spent in the quadrant that formerly contained the platform (goal quadrant) [**(f)**] along with the average distance of each mouse from the centre of platform [**(h)**] were considered as indexes of memory retention. Acquisition data was analysed by repeated measures two-way ANOVA, followed by *post hoc* Bonferroni's multiple comparison t-test at each time point. Probe trial data was analysed by one-way ANOVA, followed by *post hoc* Bonferroni's multiple comparison t-test ($^{**}p \leq 0.01$ &$^{***}p \leq 0.001$ compared to wild-type (WT); $^{\sharp}p \leq 0.05$ & $^{\sharp\sharp}p \leq 0.01$ compared to the saline-treated APP$_{swe}$/PS1$_{\Delta E9}$ group).

and wild type mice displayed comparable swim velocity and thigmotactic behaviour over the 10-d course of the Morris water-maze spatial acquisition, as shown in **Figure S3**. Spatial acquisition impairments accordingly compromised the performance of APP$_{swe}$/PS1$_{\Delta E9}$ mice in the Morris water-maze probe trial [**Figures 5.3(e)–5.3(g)**]. One way ANOVA demonstrated overall significant differences in the time spent in the quadrant that had formerly contained the escape platform (goal quadrant; $F_{(4,55)} = 3.579$, $p = 0.0115$) and the average goal distance ($F_{(4,55)} = 4.121$, $p = 0.005$) among groups. Wild type mice devoted

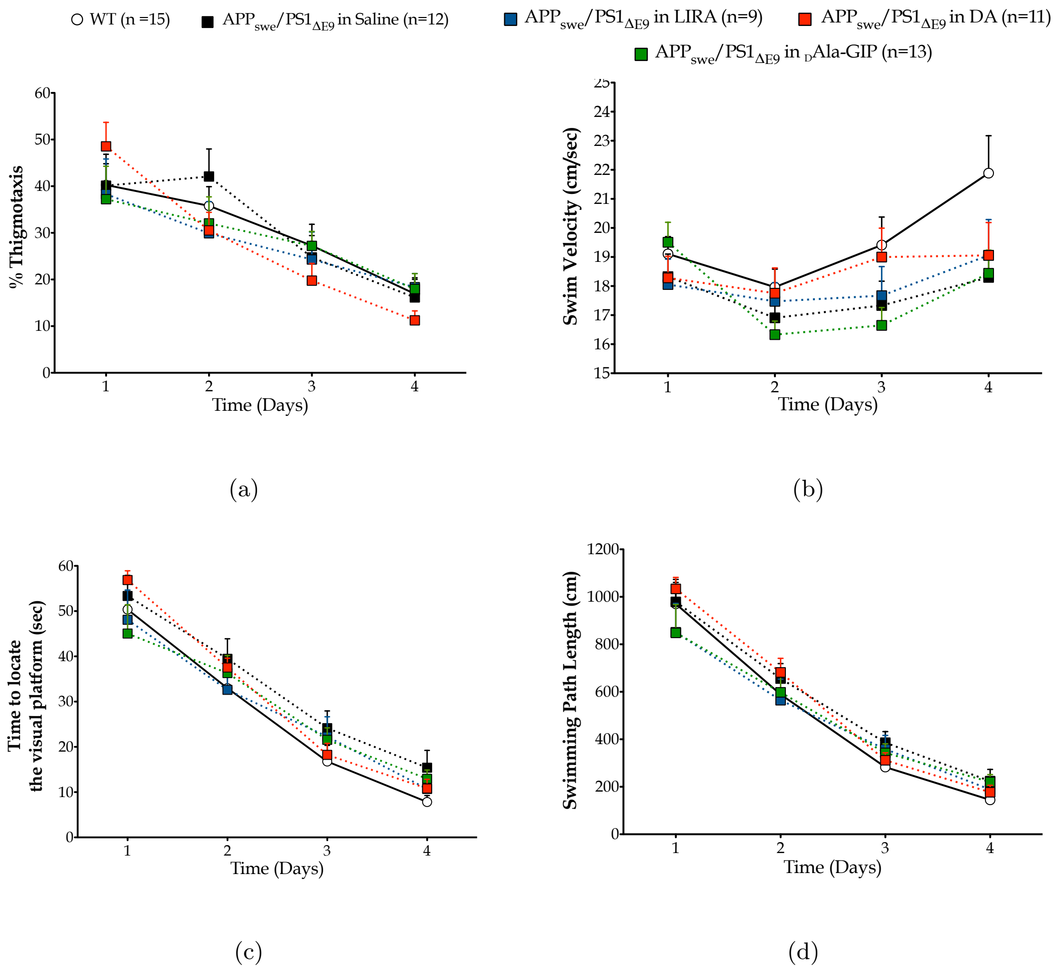

Figure 5.4: **APP$_{swe}$/PS1$_{\Delta E9}$ and wild-type mice showed comparable swim patterns to the cued escape platform in Morris water maze task.** A day after the completion of the open field test, animals were assigned to the visible-platform training for 4 consecutive days. The swim time along the perimeter of the pool – expressed as a percentage of the total swim time per animal (% thigmotaxis) [**(a)**], along with the swim velocity [**(b)**], swimming path length [**(d)**], and the amount of time required to locate the platform cued with a flag [**(c)**] were recorded over a 60-s trial. Each graph point represents the daily mean ± SEM of the aforementioned parameters from wild-type (WT) or APP$_{swe}$/PS1$_{\Delta E9}$ mice treated with 10 mL kg^{-1} d^{-1} saline and APP$_{swe}$/PS1$_{\Delta E9}$ mice treated with 25 nmol kg^{-1} d^{-1} $_D$Ala^2-GIP, Liraglutide (LIRA) or GLP-1/GIP Dual Agonist (DA). Data was analysed by repeated measures two-way ANOVA.

half of the allotted time in the goal quadrant, acquiring relative positions during the probe trial with an average distance of 41.26 ± 3.092 cm from the centre of the platform. Contrarily, APP$_{swe}$/PS1$_{\Delta E9}$ mice spent less than a third of the allotted time in the goal quadrant, having scored slightly above the chance level with an average distance from the centre of the platform of 58.65 ± 2.975 cm. As such, *post hoc* analysis demonstrated significant differences in the percentage of time spent in the goal quadrant ($p \leq 0.01$) [**Figure 5.3(f)**] and average goal distance ($p \leq 0.001$) [**Figure 5.3(g)**] between the two groups that signifies defective reference memory consolidation and recollection in $APP_{swe}/PS1_{\Delta E9}$ mice.

Intriguingly, GLP-1 and GIP co-administration reversed the spatial learning and reference memory defects of the $APP_{swe}/PS1_{\Delta E9}$ mouse model in Morris water-maze, as related to the individual administration of GLP-1 and GIP analogs and illustrated in **Figure 5.3**. During the spatial acquisition phase, GLP-1/GIP dual agonist-treated $APP_{swe}/PS1_{\Delta E9}$ mice required less time [**Figure 5.3(b)**] and swam shorter paths [**Figure 5.3(d)**] to locate the invisible escape platform as time progresses. Repeated measures two-way ANOVA analysis demonstrated a significant effect of the treatment in the escape latency ($F_{(1,21)} = 11.80$, $p = 0.0025$) and the length of the swimming path ($F_{(1,21)} = 7.77$, $p = 0.011$) during the the task acquisition phase. *Post hoc* analysis revealed that the restorative effects of the GLP-1/GIP dual agonist in spatial learning were prominent at the 9$^{\text{th}}$ (escape latency, $p \leq 0.05$; swimming path length, $p \leq 0.01$) and 10$^{\text{th}}$ ($p \leq 0.05$) day of the training course. The GLP-1/GIP dual agonist-treated $APP_{swe}/PS1_{\Delta E9}$ accordingly displayed a significantly improved recall of the escape platform position ($p \leq 0.05$) in the probe trial [**Figure 5.3(e)**], having spent approximately half of the allotted time in the goal quadrant [**Figure 5.3(f)**] with an average distance from the centre of the platform of 46.46 ± 3.465 cm [**Figure 5.3(g)**] and therefore scored similar to their wild type littermates.

Animals' cognitive flexibility was monitored in reversal spatial acquisition of the Morris water-maze task. Repeated measures two-way ANOVA analysis demonstrated significant effects of the genotype over time in the escape latency ($F_{(4,100)} = 4.51$, $p = 0.002$) and length of the swimming path ($F_{(4,100)} = 3.83$, $p = 0.006$). As illustrated in **Figure 5.5(a)**, $APP_{swe}/PS1_{\Delta E9}$ mice required longer sessions to locate the invisible escape platform, with their learning impairments becoming significantly prominent at 3$^{\text{rd}}$ ($p \leq 0.05$), 4$^{\text{th}}$ ($p \leq$

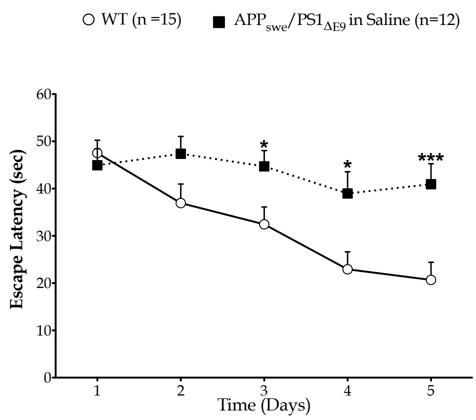
WT (n =15)
APPswe/PS1ΔE9 in Saline (n=12)
Escape Latency (sec)
Time (Days)
*
*
***

(a)

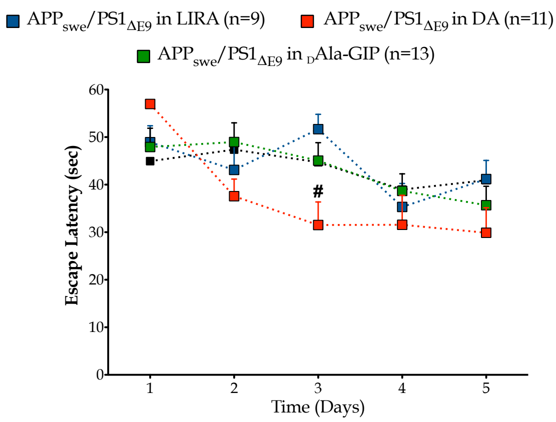
APPswe/PS1ΔE9 in LIRA (n=9)
APPswe/PS1ΔE9 in DA (n=11)
APPswe/PS1ΔE9 in DAla-GIP (n=13)
Escape Latency (sec)
Time (Days)
#

(b)

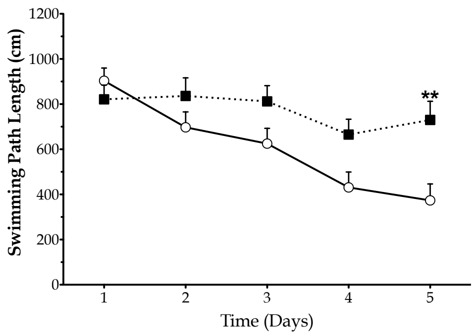
Swimming Path Length (cm)
Time (Days)
**

(c)

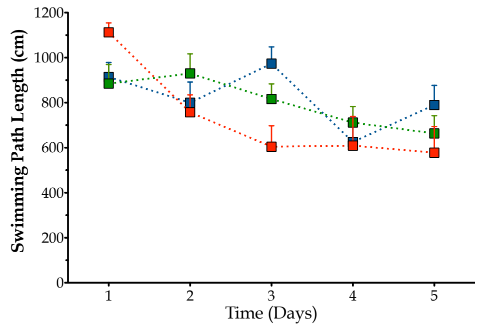
Swimming Path Length (cm)
Time (Days)

(d)

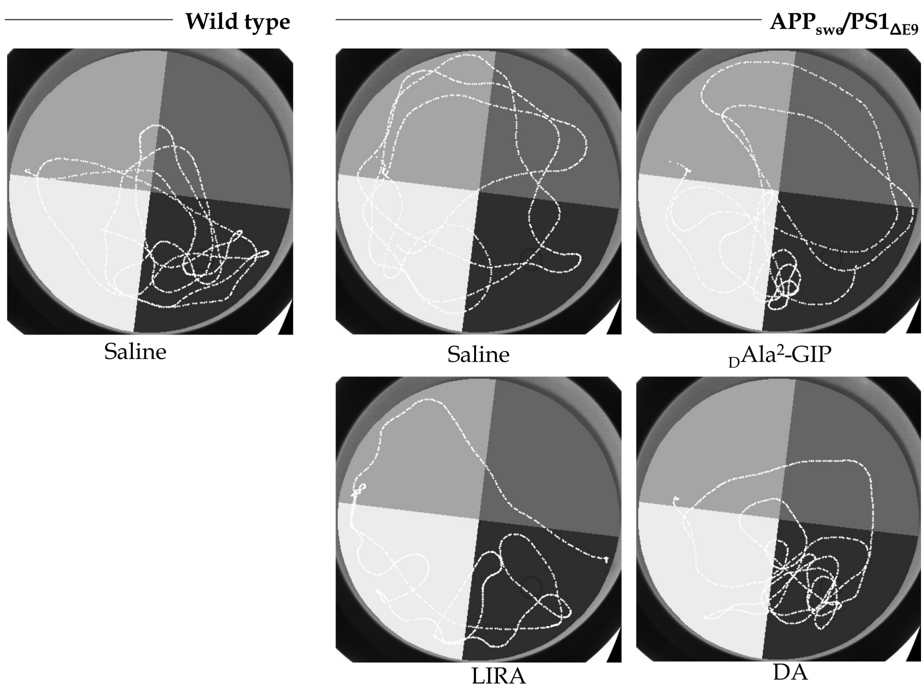
Wild type
APPswe/PS1ΔE9
Saline
Saline
DAla2-GIP
LIRA
DA

(e)

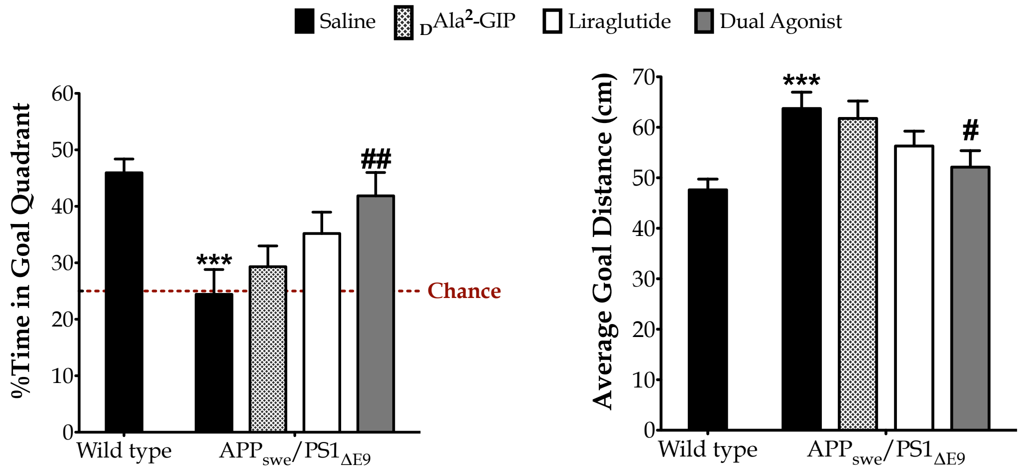

(f) (g)

Figure 5.5: **The novel GLP-1/GIP Dual Agonist promoted cognitive flexibility and restored reference memory impairments of the APP$_{swe}$/PS1$_{\Delta E9}$ mouse model of Alzheimer's disease.** Following the spatial acquisition phase, mice were assigned to the spatial reversal phase of Morris water maze task during which an invisible escape platform was fixed on a target position in the southeast quadrant. The escape latency [**(a–b)**] along with the daily mean of length of the swimming path [**(c–d)**] to locate the platform were monitored to evaluate spatial learning. A retention probe trial was held on the 6$^{\text{th}}$ day, during which the swimming pattern of each mouse was tracked in a single trial of 60 s in the absence of the escape platform, as illustrated in representative panel **(e)**. The percentage of the swim time spent in the quadrant that formerly contained the platform (goal quadrant) [**(f)**] along with the average distance of each mouse from the centre of platform [**(h)**] were considered as indexes of memory retention. Each graph point and bar represents the mean ± SEM of the corresponding parameter for wild type (WT) or APP$_{swe}$/PS1$_{\Delta E9}$ mice treated with 10 mL kg^{-1} d^{-1} saline and APP$_{swe}$/PS1$_{\Delta E9}$ mice treated with 25 nmol kg^{-1} d^{-1} $_D$Ala^2-GIP, Liraglutide (LIRA) or GLP-1/GIP Dual Agonist (DA). Acquisition data was analysed by repeated measures two-way ANOVA, followed by *post hoc* Bonferroni's multiple comparison t-test at each time point. Probe trial data was analysed by one-way ANOVA, followed by *post hoc* Bonferroni's multiple comparison t-test. ($^*p \leq 0.05$, $^{**}p \leq 0.01$ &$^{***}p \leq 0.001$ compared to wild-type (WT); $^\sharp p \leq 0.05$ & $^{\sharp\sharp}p \leq 0.01$ compared to the saline-treated APP$_{swe}$/PS1$_{\Delta E9}$ group).

0.05) and 5$^{\text{th}}$ day ($p \leq 0.001$). Accordingly, APP$_{swe}$/PS1$_{\Delta E9}$ mice acquired longer paths to the escape platform, particularly at the last day of the training course when their path was significantly longer to the corresponding of the wild type mice ($p \leq 0.01$) [**Figure 5.5(c)**]. Noteworthy is that the aforementioned spatial acquisition impairments correlated with an insignificant effect of the genotype over time in the repeated measures two-way ANOVA analysis of the swim velocity ($F_{4,100} = 2.45$, $p = 0.051$) and percentage of thigmotaxis ($F_{4,100} = 2.27$, $p = 0.066$) [**Figure S4**], which both indicated normal sensorimotor activity and emotionality of the APP$_{swe}$/PS1$_{\Delta E9}$ mice. In the retention probe trial, APP$_{swe}$/PS1$_{\Delta E9}$ mice spent approximately 24% of the allotted time to the goal quadrant, having performed at the chance level [**Figure 5.5(e)–5.5(f)**] with an average distance from the centre of the platform of 63.7 ± 3.25 cm [**Figure 5.5(g)**]. In contrast, wild type mice devoted half of the allotted in the quadrant that had formerly contained the escape platform [**Figure 5.5(e)–5.5(f)**] with an average goal distance of 47.6 ± 2.129 cm [**Figure 5.5(g)**]. As such, *post hoc* analysis demonstrated significant differences in percentage of time allotted in the goal quadrant ($p \leq 0.001$) and average goal distance ($p \leq 0.001$) between the two groups. Overall, these findings signalled for the cognitive inflexibility of the APP$_{swe}$/PS1$_{\Delta E9}$ mice to extinguish from the initial training and acquire a search strategy to the new goal.

Notably, GLP-1 and GIP co-administration promoted cognitive flexibility of the APP$_{swe}$/PS1$_{\Delta E9}$ mouse model in Morris water maze, as related to the individual administration of GLP-1 and GIP analogs and illustrated in **Figure 5.5**. During the reversal acquisition phase, repeated measures two-way ANOVA analysis demonstrated a significant effect of the GLP-1/GIP Dual Agonist treatment over time in the escape latency ($F_{(4,84)} = 4.98$, $p = 0.0012$) and the length of the swimming path ($F_{(4,84)} = 3.64$, $p = 0.009$) though *post hoc* analysis indicated a prominent restorative effect of the treatment solely in the escape latency at 3$^{\text{rd}}$ ($p \leq 0.05$) [**Figure 5.5(b)**]. The GLP-1/GIP dual agonist-treated APP$_{swe}$/PS1$_{\Delta E9}$ displayed significantly improved recall of the escape platform position ($p \leq 0.05$) in the reversal probe trial [**Figure 5.5(e)**], having spent approximately half of the allotted time in the goal quadrant [**Figure 5.5(f)**] with an average distance from the centre of the platform of 52.11 ± 3.27 cm [**Figure 5.5(g)**] and therefore scored similar to their wild type littermates.

5.5 APP$_{swe}$/PS1$_{\Delta E9}$ and wild type mice display comparable recognition memory

Intermediate-term recognition memory of the animals was evaluated in the novel object recognition paradigm. Eleven weeks after the initiation the treatments, animals were allowed to explore the familiar open field arena that had been enriched with two identical objects for 10 min. Animals displayed equal preference for the objects irrespective of their positioning in the arena, as well as comparable total exploration time over the training session [**Figure S5**]. Thus, neither the genotype nor the treatment impacted the task acquisition. After a retention interval of 3 h, wild type mice had a mean recognition index of 59.06% ± 2.868 and 40.94% ± 2.868 for the novel and familiar object, respectively, that indicated novelty preference ($t_{28} = 4.47$, $p = 0.0001$) and retrieval of the recognition memory. Similarly, APP$_{swe}$/PS1$_{\Delta E9}$ spent 57.15% ± 3.339 of the total exploration time in the novel object that significantly differed from the corresponding percent time ratio in the familiar object (42.85% ± 3.339; $t_{22} = 3.03$, $p = 0.006$). One way ANOVA analysis further demonstrated no significant differences in the novel object recognition index among the groups ($F_{(4,55)} = 1.111$, $p = 0.361$) that overall signalled for comparable recognition memory regardless of the animal genotype and assigned treatment [**Figure 5.6**].

5.6 The novel GLP-1/GIP Dual Agonist attenuates Aβ plaque deposition and aberrant neuroinflammation in the cortex and hippocampus of the APP$_{swe}$/PS1$_{\Delta E9}$ mouse model

Senile plaques – primarily composed of extracellular aggregates of the Aβ peptide – define the Alzheimer's pathological signature.[246] As such, coronal brain sections from

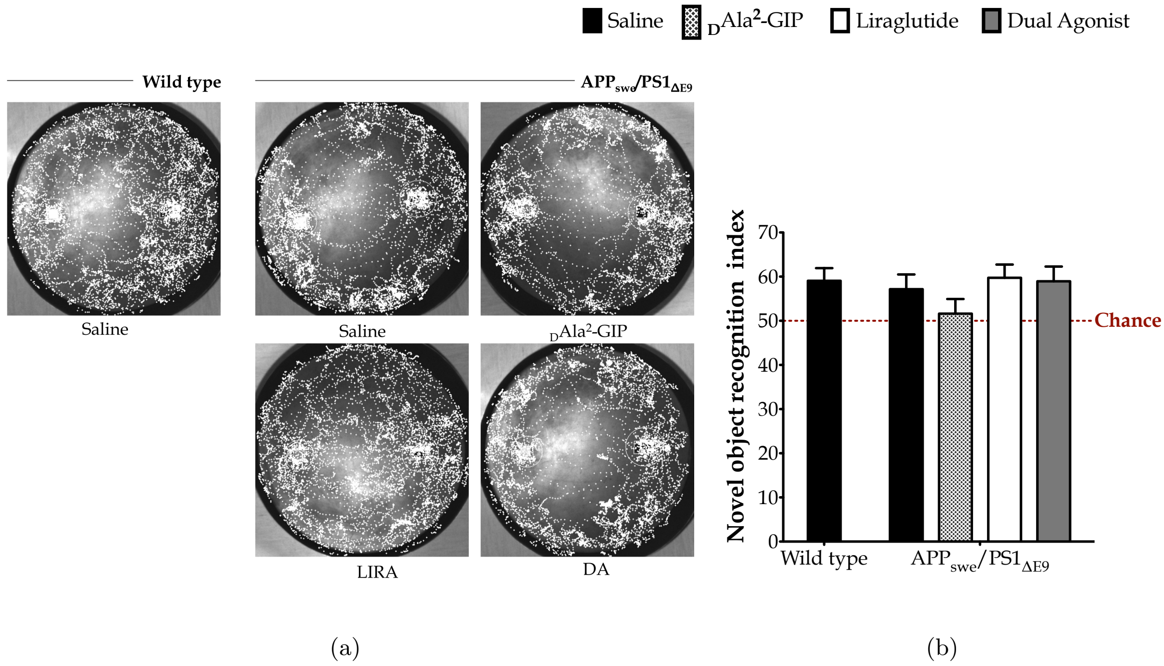

Figure 5.6: **APP$_{swe}$/PS1$_{\Delta E9}$ and wild type mice displayed comparable recognition memory in the novel object recognition task.** The novel object recognition task was conducted 11 weeks following the initiation of saline, $_D$Ala^2-GIP, Liraglutide (LIRA), and GLP-1/GIP Dual Agonist (DA) treatments. After a retention interval of 3 h from the acquisition, each mouse was assigned to re-explore the familiar arena in the presence of an object identical to previously encountered one and a novel object to evaluate its recognition memory over a 10-min session, as shown in the representative tracks [**(a)**]. Data was processed for the calculation of the *Recognition Index* that describes the percent ratio of the amount of time spent in exploring each (novel or familiar) object over the total time spent in object exploration during the retention trial course.[4] Each bar represents the mean ± SEM of the recognition index for the novel object for each animal group [**(b)**]. Data was analysed by one way ANOVA.

APP$_{swe}$/PS1$_{\Delta E9}$ mice were immunolabelled for Aβ to evaluate the cerebral β-plaque load. As illustrated in **Figures 5.7(a)** and **5.7(c)**, APP$_{swe}$/PS1$_{\Delta E9}$ mice featured a prominent β-amyloid plaque deposition over the cortex and hippocampus that remained intact after the individual administration of GLP-1 and GIP mono-therapy but notably lessened after the unimolecular GLP-1 and GIP co-administration. Indeed, the Kruskal-Wallis test indicated significant differences in the cortical (H_4 = 39.92, $p \leq 0.001$) and hippocampal (H_4 = 16.65, $p \leq 0.001$) Aβ load. The unimolecular GLP-1 and GIP co-administration almost halved the plaque pathology in the cortex [**Figure 5.7(b)**] and hippocampus [**Figure 5.7(d)**] of the APP$_{swe}$/PS1$_{\Delta E9}$ mouse model and rendered these

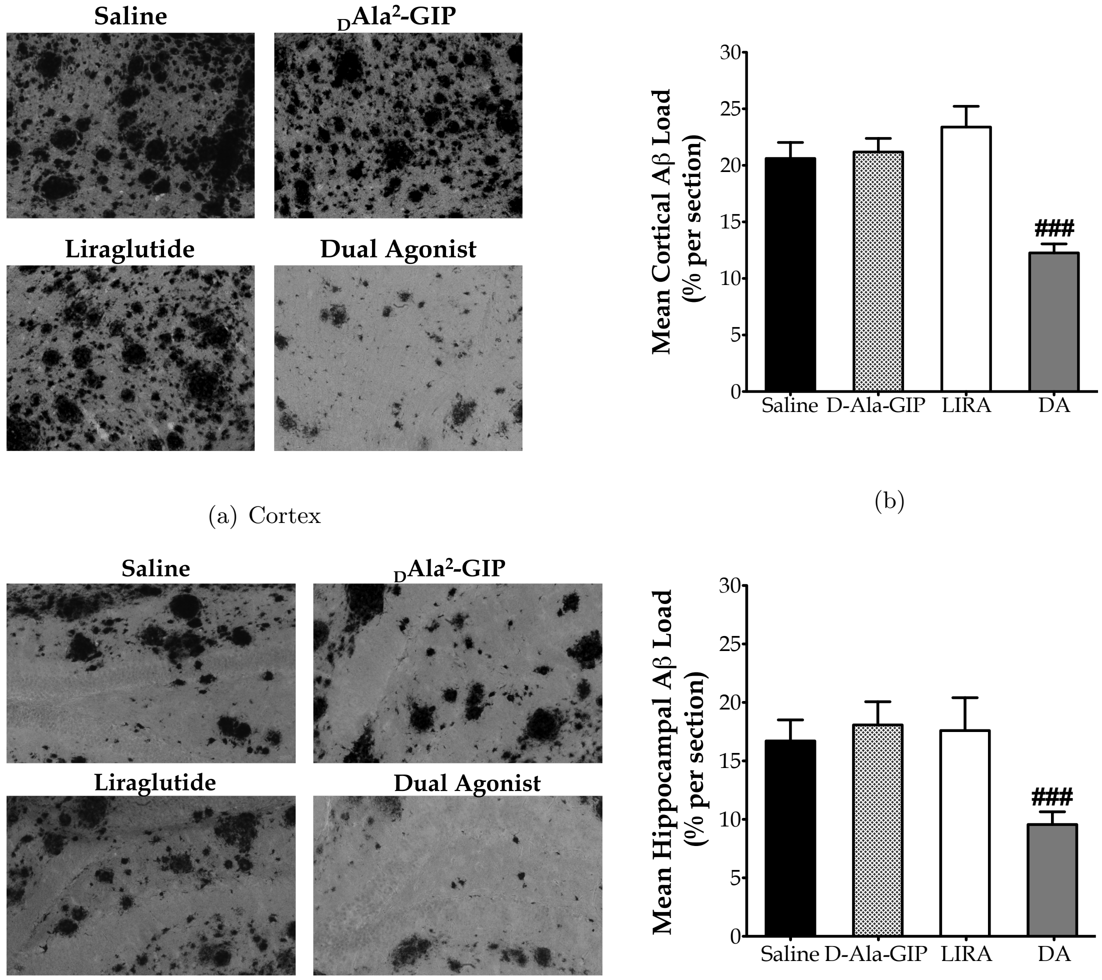

(a) Cortex

(b)

(c) Hippocampus

(d)

Figure 5.7: **The novel GLP-1/GIP Dual Agonist ameliorated β-amyloid (Aβ) plaque deposition in the cortex and hippocampus of the APP$_{swe}$/PS1$_{\triangle E9}$ mouse model of Alzheimer's disease.** Three micrographs over the cortex along with 2–3 micrographs over the hippocampus were captured per section per animal and converted in 8-bit black and white images, as shown in the representative micrograph panels **(a)** and **(c)**. Image J was used to segment each micrograph into stained and unstained surface areas and automatically measure the Aβ immunopositive load [**(b) & (d)**]. Each bar represents mean $\pm$ SEM of the percentage of stained area per section for APP$_{swe}$/PS1$_{\triangle E9}$ mice treated with $10\,\mathrm{mL\,kg^{-1}\,d^{-1}}$ saline ($n = 6$), $25\,\mathrm{nmol\,kg^{-1}\,d^{-1}}$ $_{D}$Ala^{2}-GIP ($n = 7$), $25\,\mathrm{nmol\,kg^{-1}\,d^{-1}}$ Liraglutide (LIRA; $n = 6$) or $25\,\mathrm{nmol\,kg^{-1}\,d^{-1}}$ GLP-1/GIP Dual Agonist (DA; $n = 6$). Data was analysed by Kruskal-Wallis test, followed by *post hoc* Dunn's multiple comparison test ($^{\sharp\sharp\sharp}p \leq 0.001$ compared to the saline-treated APP$_{swe}$/PS1$_{\triangle E9}$ group).

mice significantly different from the corresponding saline- treated mice ($p \leq 0.001$) in *post hoc* analysis with Dunn's multiple comparison test.

The formation of these deposits initiates a series of cellular events that can gradually elicit excessive gliosis and favour neuronal degeneration and death observed in AD patients.[202] Indeed, microglia from $APP_{swe}/PS1_{\Delta E9}$ cortex and hippocampus displayed an amoeboid morphology with decreased branching and enlarged soma [**Figure 5.8(a)**] that signifiedtheir activation.[202,295] Quantitative analysis revealed a more than three-fold increase in microglia load in the $APP_{swe}/PS1_{\Delta E9}$ cortex and hippocampus that significantly differed from the corresponding load in the retrospective brain areas from wild type mice (*post hoc*; $p \leq 0.001$), as illustrated in **Figures 5.8(c)–5.8(d)**. Accordingly, astrocytes in the $APP_{swe}/PS1_{\Delta E9}$ cortex and hippocampus assumed an immune-activated phenotype, with the processes emerging from their soma having been thicker and present in bundles. In contrast, the astrocytes from wild-type mice featured a stellate morphology with emerging processes at regular intervals [**Figure 5.8(b)**]. The Kruskal–Wallis test further demonstrated significant differences in the cortical ($H_5 = 152.6$, $p \leq 0.001$) and hippocampal ($H_5 = 80.46$, $p \leq 0.001$) astrocyte load. The $APP_{swe}/PS1_{\Delta E9}$ genotype nearly doubled the percentage of GFAP stained area in the cortex and hippocampus [**Figures 5.8(e)–5.8(f)**], having rendered it significantly different from the control in both examined brain areas ($p \leq 0.001$) in the *post hoc* Dunn's multiple comparison test. The latter along with the hypertrophy of cellular processes suggest the existence reactive astrocytes[114,275] in the $APP_{swe}/PS1_{\Delta E9}$ mouse brain.

Notably, the unimolecular GLP-1 and GIP co-administration attenuated abundant reactive microglia and excessive astrogliosis over the cortex and hippocampus of the $APP_{swe}/PS1_{\Delta E9}$ mouse model. In particular, the GLP-1/GIP Dual Agonist treatment decreased the amoeboid reactive microglia load in the cortex and hippocampus of the $APP_{swe}/PS1_{\Delta E9}$ mouse model [**Figure 5.8(a)**] that further corresponded to an approximately 50% drop in the percentage of IBA-1 stained area (*post hoc*; $p \leq 0.001$) in the

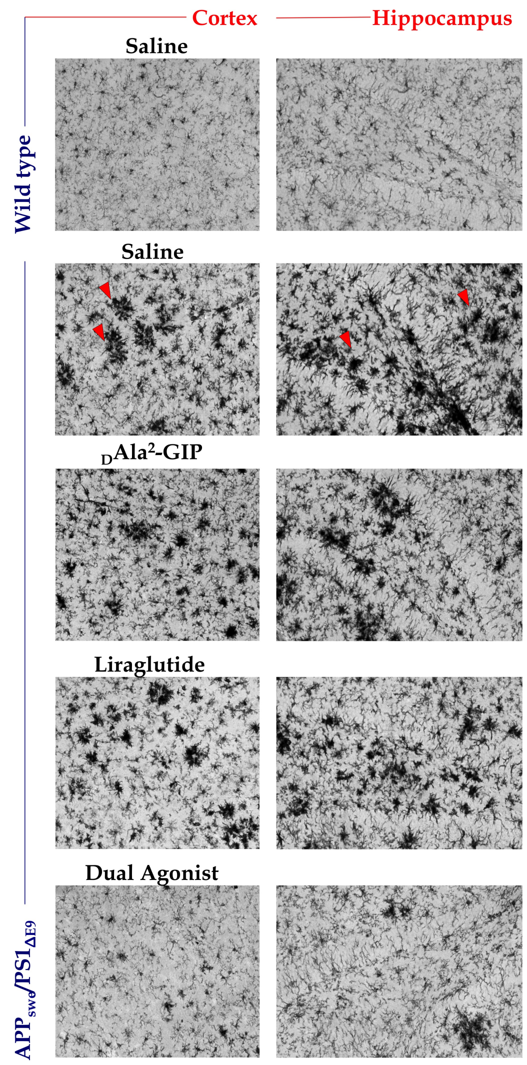

(a) IBA1

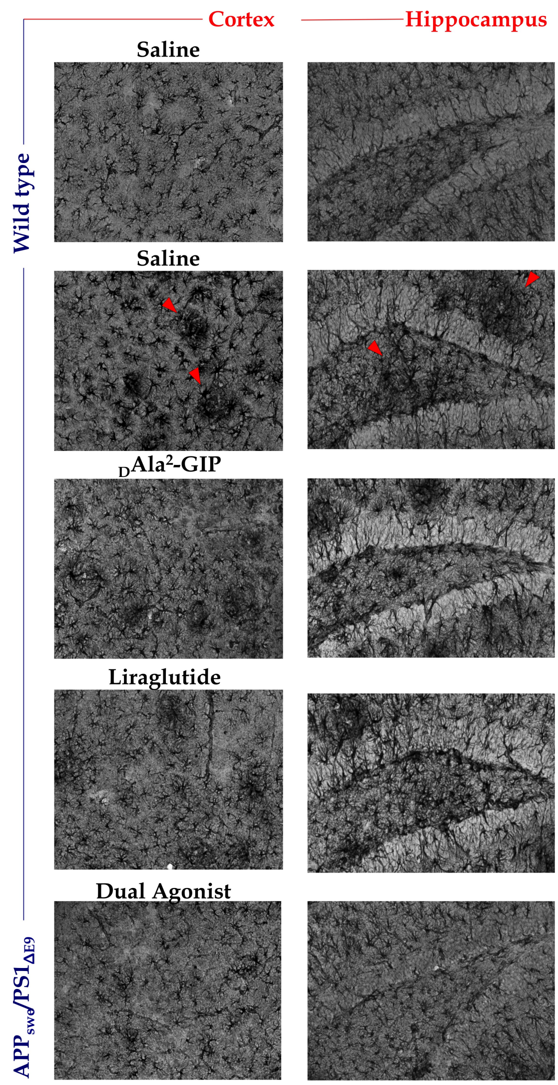

(b) GFAP

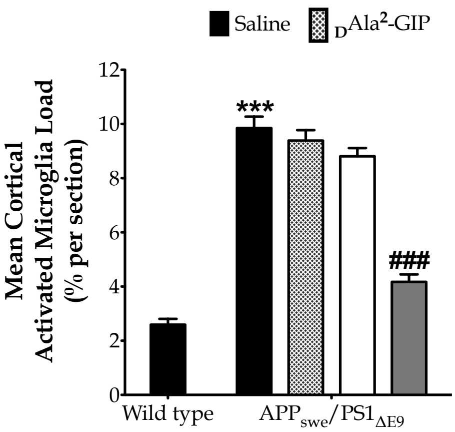

(c)

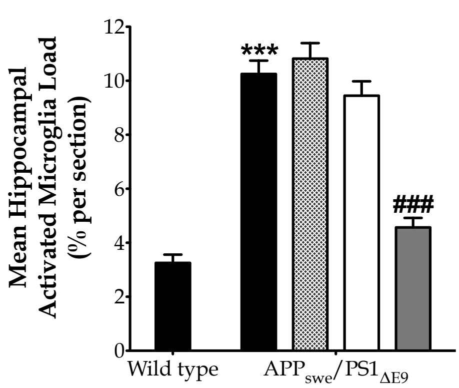

(d)

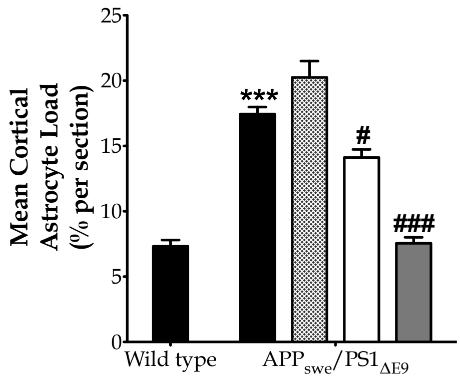

(e)

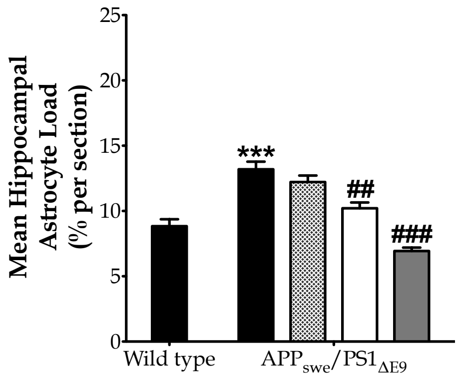

(f)

Figure 5.8: **The novel GLP-1/GIP Dual Agonist rescued aberrant neuroinflammation in the cortex and hippocampus of the APP$_{swe}$/PS1$_{\Delta E9}$ mouse model of Alzheimer's disease.** Three micrographs over the cortex along with 2–3 micrographs over the hippocampus were captured per section and converted in 8-bit black and white images, as shown in the representative micrograph panels **(a)** and **(b)**. Image J was used to segment each micrograph into stained and unstained surface areas and automatically measure the microglia [**(c) & (d)**] and astrocyte [**(e) & (f)**] immunopositive load. Each bar represents mean $\pm$ SEM of the percentage of stained area per section from wild-type ($n = 8$) or APP$_{swe}$/PS1$_{\Delta E9}$ ($n = 6$) mice treated with $10\,\mathrm{mL\,kg^{-1}\,d^{-1}}$ saline and APP$_{swe}$/PS1$_{\Delta E9}$ mice treated with $25\,\mathrm{nmol\,kg^{-1}\,d^{-1}}$ $_{D}$Ala^2-GIP ($n = 7$), Liraglutide ($n = 6$) or GLP-1/GIP Dual Agonist ($n = 6$). Data was analysed by Kruskal-Wallis test, followed by *post hoc* Dunn's multiple comparison test ($^{***}p \leq 0.001$ compared to wild-type; $^{\sharp}p \leq 0.05$, $^{\sharp\sharp}p \leq 0.01$ & $^{\sharp\sharp\sharp}p \leq 0.001$ compared to the saline-treated APP$_{swe}$/PS1$_{\Delta E9}$ group).

aforementioned brain areas [**Figures 5.8(c)–5.8(d)**]. Furthermore, the GLP-1/GIP Dual Agonist treatment restored the cortical [**Figure 5.8(e)**] and hippocampal [**Figure 5.8(f)**] load of the astrocytes, which mainly featured a normal stellate morphology [**Figure 5.8(b)**].

5.7 The novel GLP-1/GIP Dual Agonist promoted synapse homeostasis in the APP$_{swe}$/PS1$_{\Delta E9}$ mouse brain

Synapses are the earliest sites of neuropathology, with their loss being considered the best clinical correlate of dementia.[246,262] As such, immunoblotting analysis was performed to

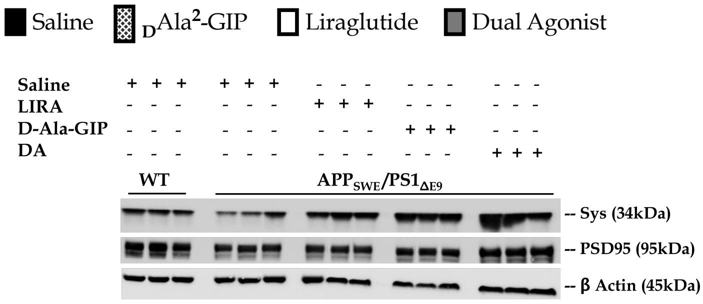

(a)

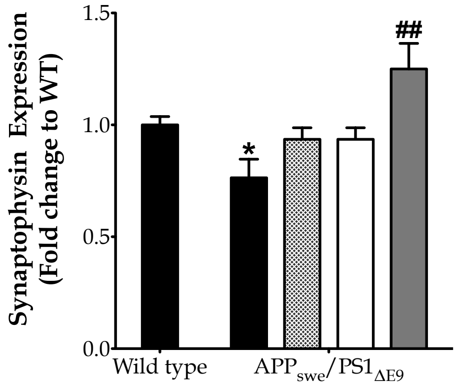

(b)

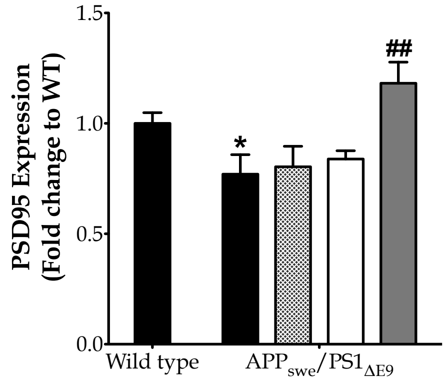

(c)

Figure 5.9: **The novel GLP-1/GIP Dual Agonist preserved synapse homeostasis in the APP$_{swe}$/PS1$_{\Delta E9}$ mouse brain.** Protein of mouse brain whole cell lysate (20 µg) were processed for western blotting where the expression of synaptophysin [Sys; **(a) & (b)**] and post-synaptic density protein 95 [PSD95; **(a) & (c)**] were assessed. β-Actin was used as the loading control to all western blot analyses. Each bar represents the mean ± SEM from wild-type (WT; $n = 8$) or APP$_{swe}$/PS1$_{\Delta E9}$ ($n = 6$) mice treated with $10\,\mathrm{mL\,kg^{-1}\,d^{-1}}$ saline and APP$_{swe}$/PS1$_{\Delta E9}$ mice treated with $25\,\mathrm{nmol\,kg^{-1}\,d^{-1}}$ $_D$Ala^2-GIP ($n = 7$), Liraglutide (LIRA; $n = 7$) or GLP-1/GIP Dual Agonist (DA; $n = 6$). Data was analysed by one-way ANOVA, followed by *post hoc* Bonferroni's multiple comparison t-test ($^*p \leq 0.05$ compared to WT; $^{\sharp\sharp}p \leq 0.01$ compared to the saline-treated APP$_{swe}$/PS1$_{\Delta E9}$ group).

quantify the *ex-vivo* expression levels of the pre-synaptic vesicle protein, synaptophysin and of the scaffolding protein involved in the assembly and function of the post-synaptic density complex, PSD95. One way ANOVA demonstrated significant differences in the synaptophysin ($F_{(4,48)} = 4.04$, $p = 0.007$) and PSD95 ($F_{(4,29)} = 5.03$, $p = 0.003$) protein expression among groups. The APP$_{swe}$/PS1$_{\Delta E9}$ genotype provoked a 25% drop in synaptophysin and PSD95 protein levels, as compared to wild type littermates and illustrated in **Figure 5.9**. GLP-1/GIP Dual Agonist significantly normalised the impairments in the aforementioned proteins (*post hoc*; $p \leq 0.01$) [**Figure 5.9**] to promote synapse homeostasis in the $\mathrm{APP}_{swe}/\mathrm{PS1}_{\Delta E9}$ mouse brain.

5.8 The novel GLP-1/GIP Dual Agonist resolved ER stress and autophagy dysfunction in the $\mathrm{APP}_{swe}/\mathrm{PS1}_{\Delta E9}$ mouse brain

It was pertinent to ask whether the novel GLP-1/GIP Dual Agonist could regulate mechanisms for proteostasis to attenuate Alzheimer's-like pathology in the $\mathrm{APP}_{swe}/\mathrm{PS1}_{\Delta E9}$ mouse model. One-way ANOVA analysis demonstrated overall significant differences in BiP ($F_{(4,29)} = 4.695$, $p = 0.005$), Chop ($F_{(4,28)} = 2.7$, $p = 0.05$) and caspase 12 (CASP12; $F_{(4,29)} = 2.73$, $p = 0.048$) protein expression. The $\mathrm{APP}_{swe}/\mathrm{PS1}_{\Delta E9}$ mouse brain featured a nearly one-fold increase in the protein levels of BiP [**Figure 5.10(a)**] that indicated ER stress,[159] as well as a significant up-regulation in protein expression of the pro-apoptotic UPR mediators Chop ($p \leq 0.05$) [**Figure 5.10(b)**] and active CASP12 fragment at 42 kDa ($p \leq 0.01$)[**Figure 5.10(c)**]. ER stress in the $\mathrm{APP}_{swe}/\mathrm{PS1}_{\Delta E9}$ mouse brain correlated to an approximate 25% decrease in the expression of the autophagy-related proteins beclin-1, Atg3 and LC3 when compared to the controls [**Figure 5.11**; **Table S3**].

Intriguingly, the unimolecular GLP-1 and GIP co-administration normalised the aberrant expressions of BiP and Chop and CASP12 activity [**Figure 5.10**]. It additionally rescued the suppressed beclin-1 ($p \leq 0.05$) [**Figure 5.11(a)**], Atg3 ($p \leq 0.001$) [**Figure 5.11(b)**] and LC3 ($p \leq 0.01$) [**Figure 5.11(d)**] protein expression to favour proteostasis in $\mathrm{APP}_{swe}/\mathrm{PS1}_{\Delta E9}$ mouse brain.

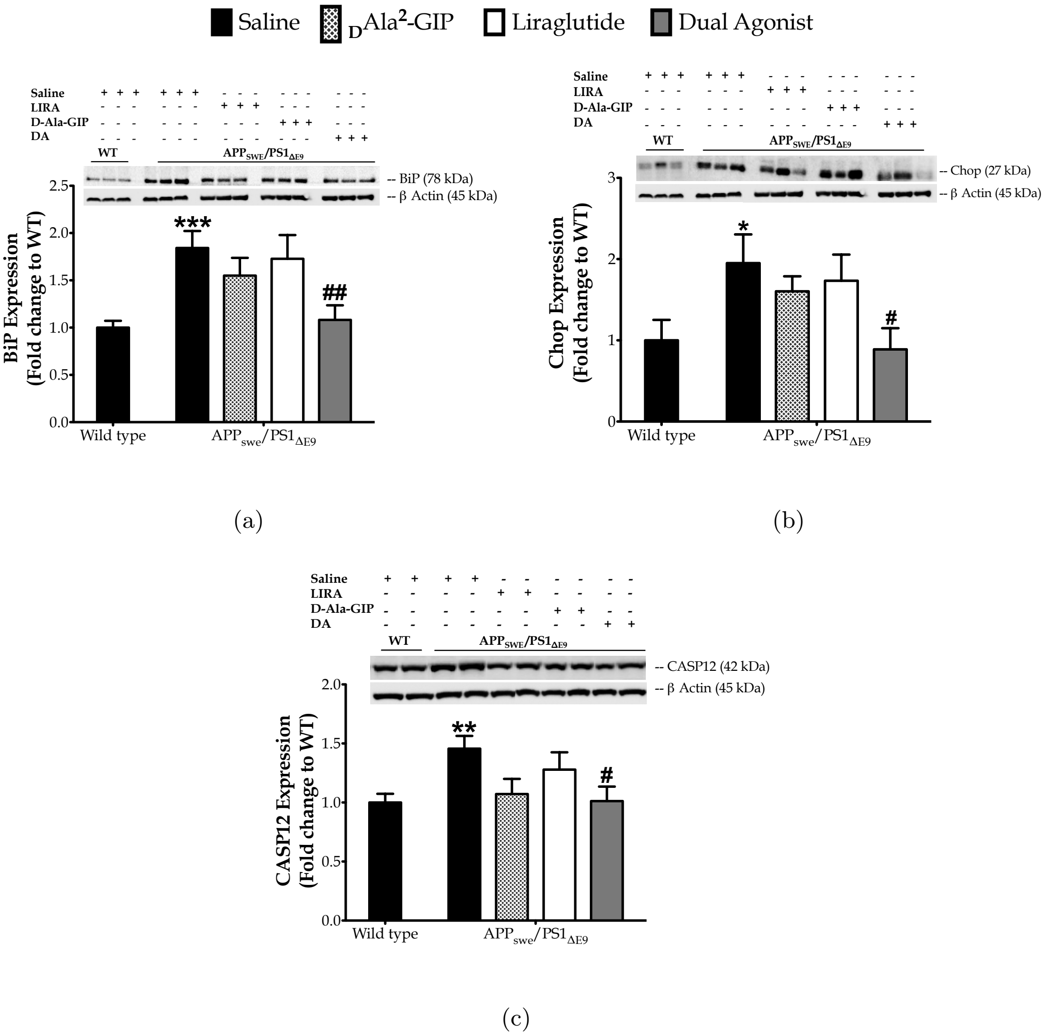

Figure 5.10: **The novel GLP-1/GIP Dual Agonist resolved ER stress in APP$_{swe}$/PS1$_{\Delta E9}$ mouse brain.** Protein of mouse brain whole cell lysate (20 µg) were processed for western blotting where the expression of BiP [**(a)**], Chop [**(b)**] of caspase 12 [CASP12; **(c)**] were assessed. β-Actin was used as the loading control to all western blot analyses. Each bar represents mean ± SEM from wild-type (WT; $n = 8$) or APP$_{swe}$/PS1$_{\Delta E9}$ ($n = 6$) mice treated with $10\,\mathrm{mL\,kg^{-1}\,d^{-1}}$ saline and APP$_{swe}$/PS1$_{\Delta E9}$ mice treated with $25\,\mathrm{nmol\,kg^{-1}\,d^{-1}}$ $_D$Ala^2-GIP ($n = 7$), Liraglutide (LIRA; $n = 7$) or GLP-1/GIP Dual Agonist (DA; $n = 6$). Data was analysed by one-way ANOVA, followed by *post hoc* Bonferroni's multiple comparison t-test ($^*p \leq 0.05$, $^{**}p \leq 0.01$ & $^{***}p \leq 0.001$compared to WT; $^{\sharp}p \leq 0.05$ & $^{\sharp\sharp}p \leq 0.01$ compared to the saline-treated APP$_{swe}$/PS1$_{\Delta E9}$ group).

5.9 The novel GLP-1/GIP Dual Agonist attenuated the impaired Akt signalling in the APP$_{swe}$/PS1$_{\Delta E9}$ mouse brain

GLP-1 and GIP receptors assume cellular responses through a downstream signalling cascade that converges into two main branches, the mitogen-associated protein kinase /

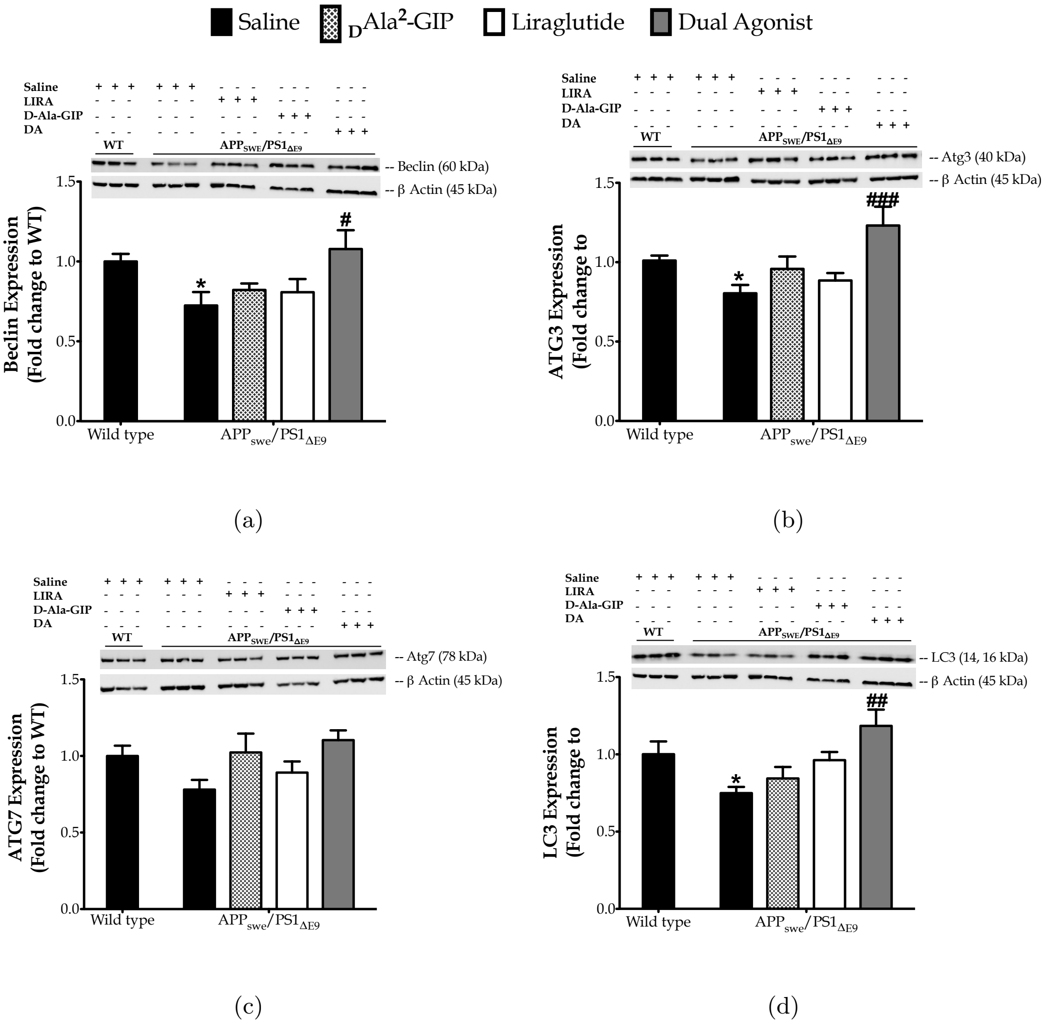

Figure 5.11: **The novel GLP-1/GIP Dual Agonist rectified the suppressed expression of "core" Atg proteins required for autophagosome formation in the $APP_{swe}/PS1_{\Delta E9}$ mouse brain.** Protein of mouse brain whole cell lysate (20 µg) were processed for western blotting where the expression of beclin-1 [**(a)**], ATG3 [**(b)**], ATG7 [**(c)**] and of LC3 [**(d)**] were assessed. β-Actin was used as the loading control to all western blot analyses. Each bar represents the mean ± SEM from wild-type (WT; $n = 8$) or $APP_{swe}/PS1_{\Delta E9}$ ($n = 6$) mice treated with $10\,\mathrm{mL\,kg^{-1}\,d^{-1}}$ saline and $APP_{swe}/PS1_{\Delta E9}$ mice treated with $25\,\mathrm{nmol\,kg^{-1}\,d^{-1}}$ ${}_{D}\mathrm{Ala}^2$-GIP ($n = 7$), Liraglutide (LIRA; $n = 7$) or GLP-1/GIP Dual Agonist (DA; $n = 6$). Data was analysed by one-way ANOVA, followed by *post hoc* Bonferroni's multiple comparison t-test ($^{*}p \leq 0.05$ compared to WT; $^{\sharp}p \leq 0.05$, $^{\sharp\sharp}p \leq 0.01$ & $^{\sharp\sharp\sharp}p \leq 0.001$ compared to the saline-treated $APP_{swe}/PS1_{\Delta E9}$ group).

extracellular signal-regulated kinase (MAPK / ERK) and the phosphatidylinositol 3-kinase / protein kinase B (PI3K / AKT) pathways.[6,10] Herein, one-way ANOVA analysis demonstrated overall significant differences in Akt phosphorylation at Thr308 ($F_{(4,44)} = 5.84$, $p = 0.0007$) [**Figure 5.12(a)**] but not in ERK1/2 phosphorylation at Thr202 and

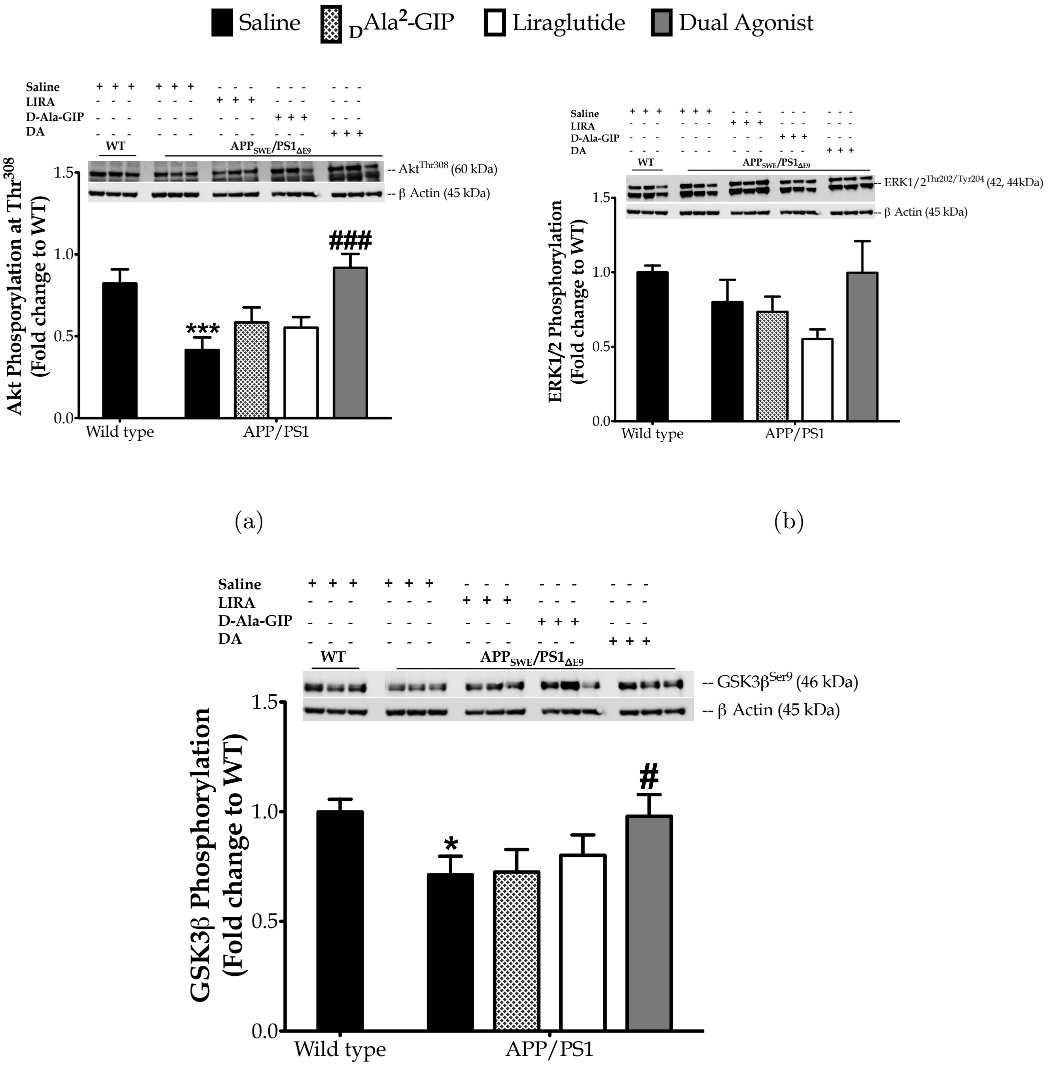

(a)

(b)

(c)

Figure 5.12: **The novel GLP-1/GIP Dual Agonist normalised the aberrant Akt and GSK3β activity in the APP$_{swe}$/PS1$_{\Delta E9}$ mouse brain.** Protein of mouse brain whole cell lysate (20 µg) were processed for western blotting where the expression of phosphorylated Akt at Thr308 [**(a)**], ERK1/2 at Thr202 and Tyr204 [**(b)**] of phosphorylated GSK3β at Ser9 [**(c)**] were assessed. β-Actin was used as the loading control to all western blot analyses. Each bar represents mean ± SEM from wild-type (WT; $n = 8$) or APP$_{swe}$/PS1$_{\Delta E9}$ ($n = 6$) mice treated with 10 mL kg^{-1} d^{-1} saline and APP$_{swe}$/PS1$_{\Delta E9}$ mice treated with 25 nmol kg^{-1} d^{-1} $_D$Ala^2-GIP ($n = 7$), Liraglutide (LIRA; $n = 7$) or GLP-1/GIP Dual Agonist (DA; $n = 6$). Data was analysed by one-way ANOVA, followed by *post hoc* Bonferroni's multiple comparison t-test ($^*p \leq 0.05$ & $^{***}p \leq 0.001$ compared to WT; $^\sharp p \leq 0.05$ & $^{\sharp\sharp\sharp}p \leq 0.001$ compared to the saline-treated APP$_{swe}$/PS1$_{\Delta E9}$ group).

Tyr204 residues ($F_{(4,44)} = 1.31$, $p = 0.28$) [**Figure 5.12(b)**]. *Post hoc* analysis showed a significant down-regulation of the Akt activation ($p \leq 0.001$) in APP$_{swe}$/PS1$_{\Delta E9}$ mouse brain that further correlated to a 30% drop in the inhibitory phosphorylation of GSK3β at the Ser9 residue [**Figure 5.12(c)**]. The unimolecular GLP-1 and GIP co-administration significantly reversed the suppressed Akt phoshporylation ($p \leq 0.001$) and exacerbated GSK3β activity in the APP$_{swe}$/PS1$_{\Delta E9}$ mouse brain [**Figure 5.12**].

5.10 Discussion

The present study demonstrated the neuroprotective and restorative effects of the novel GLP-1/GIP Dual Agonist in the APP$_{swe}$/PS1$_{\Delta E9}$ mouse model of AD along with the potential underlying mechanism for the first time. Ten-month old APP$_{swe}$/PS1$_{\Delta E9}$ mice were assigned to the incretin-based or saline treatment for 8 weeks before the initiation of the experiments. To determine whether GLP-1 and GIP co-administration would result in additive effects on cognitive function, cerebral Aβ load, neuroinflammation, ER stress, and autophagy, we have compared it to the individual administration of Liraglutide and $_D$Ala^2-GIP. Unlike the GLP-1 and GIP mono-therapy, the equimolar GLP-1 and GIP co-administration resolves the ER stress and autophagy impairments to attenuate cognitive decline and Alzheimer's-like pathology in middle-aged APP$_{swe}$/PS1$_{\Delta E9}$ mice.

The APP$_{swe}$/PS1$_{\Delta E9}$ mouse model over-expresses the Swedish mutation of APP together with the PS1 exon 9 deletion that both preferentially favour the generation of the highly fibrillogenic Aβ_{42} over Aβ_{40}. The latter progressively culminates in the parenchymal amyloid disposition[135, 248] surrounded by glial cytopathology in brain areas serving memory and cognition,[93, 248, 255] as evident in our histological assessment too. As such, these mice manifest spatial acquisition and reference memory impairments in the Morris water-maze task at the earliest test age of 7 months, which persist over the rest of the life of this murine model.[71, 305] Consistently, herein, quantitatively analysis of the Morris water-maze endpoints evinced a prominently poor performance of the 12-month old APP$_{swe}$/PS1$_{\Delta E9}$ mice in the cognitive paradigm, with longer latency and path lengths to the escape platform over the spatial acquisition phase along with shorter percentages of time in the correct quadrant and greater average distance from the centre of the platform over the retention probe trial as well. These deficits reflected a general cognitive decline of these mice, rather than defects in sensorimotor coordination and/or increased emotionality. Indeed, $APP_{swe}/PS1_{\Delta E9}$ mice have displayed a normal exploratory behaviour and total activity in the open field test, had similar performance in the visual platform training as their control littermates, and featured normal swim velocity and thigmotactic behaviour over the Morris water maze spatial acquisition phase. This general cognitive decline in turn restrained animals' executive function, as seen in AD patients.[305] Middle-aged $APP_{swe}/PS1_{\Delta E9}$ mice failed to develop a new spatial strategy to locate the escape platform over the Morris water maze reversal spatial acquisition phase that signified cognitive inflexibility and thus defects in higher cognitive processes.

$APP_{swe}/PS1_{\Delta E9}$ mice can additionally manifest declarative memory impairments in fear conditioning and novel object recognition tasks that start at the age of 7–8 months.[70,305] Herein, a comparable novel-object preference between the $APP_{swe}/PS1_{\Delta E9}$ and wild type mice at the age of 12 months was observed, which signalled for intact recognition memory irrespective of the animal genotype. Variations in the experimental design and setup, including arena size, object types, the time interval between the acquisition and test trials, animal housing conditions and handling may account for the divergent results. For instance, enriched housing conditions (as such in our experimental setup) have been previously shown to favour novelty preference in novel object recognition task *in vivo*, when compared to standard housing conditions.[145]

Intriguingly, chronic GLP-1/GIP Dual Agonist treatment restored learning and memory impairments of the $APP_{swe}/PS1_{\Delta E9}$ mouse model during the Morris water maze spatial acquisition phase. It additionally promoted cognitive flexibility in the spatial reversal phase of the Morris water maze task. The GLP-1/GIP Dual Agonist-treated $APP_{swe}/PS1_{\Delta E9}$ mice were able to extinguish from their initial training, developed a new spatial strategy to locate the escape platform – evident by the gradual decrease in the total duration of sessions and the swimming path length over the training period – and thereby scored similarly to their wild-type littermates at the reversal probe-trial endpoints. Histologically, the co-stimulation of GLP-1 and GIP receptors resulted in a prominent decrease of Aβ and reactive microglia loads in the cortex and hippocampus of the $APP_{swe}/PS1_{\Delta E9}$ mouse model. These histological traits further correlated to a restoration of the excessive astrogliosis in the aforementioned brain areas that serve learning and memory, and to the normalisation of synaptophysin and PSD95 protein expressions. It has been repeatedly shown that Aβ accumulation in the brain of mice and non-human primates potentiates the aberrant reactivity of microglia and astrocytes[77,93,158,248,255] that, in turn, stimulates pro-inflammatory signalling.[183,202] The latter, when persists, hampers Aβ clearance, exacerbates Aβ and tau pathologies, and compromised synapse homeostasis that ultimately altogether prompt cognitive defects.[92,188,202] Taken together, the unimolecular GLP-1 and GIP administration precluded excessive cerebral amyloid disposition and neuroinflammatory processes to rescue cognitive decline of this murine model. In accord with the observations of the present study, the co-stimulation of GLP-1 and GIP receptors has been previously reported to alleviate the exacerbated reactivity of glial cells and disorder-related pathognomonic features to restore cognitive or behavioural decrements of a mouse model of mild TBI,[289] a rat model of streptozotocin-induced diabetes and neurodegeneration[269] and of the neurotoxin-based rat models of PD.[31,133,136,320]

It was pertinent to ask at that point whether the GLP-1/GIP Dual Agonist could regulate mechanisms for proteostasis to attenuate AD-like pathology of the $APP_{swe}/PS1_{\Delta E9}$ mouse model. The UPR activation has repeatedly detected in the *post-mortem* brain samples from affected patients[99,119,120,160,283,314] and animal models of AD.[3,13,90,253,267] Increased

BiP expression and phosphorylation of IRE1α, PERK and eIF2α occur in morphologically intact neurones at the early disease stages,[99,119,120] preceding the overt amyloid deposition in AD brain.[99,121] Meanwhile, the up-regulation of pro-apoptotic UPR components, including Chop expression and CASP12 proteolysis occurs at the late disease stages (Braak stage *VI*), signifying the occurrence of persistent ER stress in the AD brain.[160,314] Similarly, the APP$_{swe}$/PS1$_{\Delta E9}$ mouse brain features elevated BiP and Chop expressions along with enhanced activity of the ER-resident CASP12,[13] as prominent in our findings too. CASP12 provokes a downstream caspase cascade to initiate programmed cell death (apoptosis)[203,212] that may serve a physiological role in eliminating cells unresponsive to the UPR.[111] However, in AD, the induction of apoptotic signallig is more likely to drive neuronal degeneration, in which synapse is the initiation point.[111,224,258] Indeed, Aβ potentiates an ER stress-dependent synaptosomal mitochondrial dysfunction and pre-synaptic vesicle depletion. These are accompanied by a decrease in the protein expression of synaptophysin and cytoskeletal components and mediated by local caspase activity.[207] Subsequent findings have revealed that Aβ requires CASP12 to induce pre-synapse toxicity in the triple transgenic mouse model for AD (3×Tg–AD).[247] Furthermore, Chop downstream inhibits the expression of the anti-apoptotic Bcl-2 protein and/or engages the p53 up-regulated modulator of apoptosis (PUMA) protein to signal to the mitochondrial apoptotic machinery and thus promote neuronal and astrocytic damage.[18,82] Herein, a 30% increase in the protein expression of the mitochondrial voltage-dependent anion channel (VDAC) noted in the APP$_{swe}$/PS1$_{\Delta E9}$ mouse brain [**Figure S6**]. VDAC interacts with Bcl-2 family members to regulate mitochondrial permeability and the subsequent release of pro-apoptotic factors.[273] Although the aforementioned enhanced expression has not reach the level of statistical significance, it may indicate an early mitochondrial dysfunction[51] in the middle-aged APP$_{swe}$/PS1$_{\Delta E9}$ mouse brain.

GLP-1/GIP Dual Agonist restored the excessive BiP and Chop expressions and aberrant CASP12 activity back to control levels that signalled for resolution of the UPR in the $APP_{swe}/PS1_{\Delta E9}$ mouse brain. GLP-1/GIP Dual Agonist additionally normalised the suppressed expression of the "core" Atg proteins beclin-1, ATG3 and LC3 that pivotally regulate the formation and maturation of the autophagosome.[30] In *post-mortem* brain samples from affected patients and animal models of AD, autophagic vacuoles accumulate in swollen dystrophic neurites that may reflect defective maturation and retrograde transport of the autophagosome.[219,220] A substantial suppression of beclin-1 protein levels has been found in the midfrontal cortex of human AD brains that parallels disease progression.[239] Mechanistically, beclin-1 determines the formation of the phagophore (that initiates autophagic process)[30] and regulates APP processing and turnover.[132] As such, the genetic reduction of beclin-1 compromises neuronal autophagy and exacerbates the intraneuronal Aβ accumulation and extracellular Aβ deposition in the brain of the transgenic APP_{sweInd} mouse model (J20) for AD.[239] Beclin-1 deficiency suppresses the expression of synaptophysin, the dendrite-specific microtubule-associated protein 2 (MAP2) and and of the calcium-binding protein, calbindin to provoke the degeneration of neuronal synapses[239] whilst eliciting phagocytic deficits in microglia to impair Aβ clearance *in vivo*.[185] Considering these, the co-stimulation of GLP-1 and GIP receptors appeared to favour the homeostasis of UPR and autophagy machinery, of which sustained dysregulation feeds a vicious circle of defective proteostasis and persistent ER stress, and thereby to rescue neuronal and glial dysfunction in the $APP_{swe}/PS1_{\Delta E9}$ mouse model.

Mechanistically, the GLP-1/GIP Dual Agonist rectified the suppressed Akt signalling to resolve ER stress and defective proteostasis in the $APP_{swe}/PS1_{\Delta E9}$ mouse brain. Akt (also known as protein kinase B – PKB) is a serine/threonine kinase member of the AGC protein kinase family with a profound function in neurotrophin (growth factor) signalling for neuronal survival[190] and synaptic delivery of PSD95,[315] as well as a pivotal effector of the neuroprotective signalling of the incretin mimetics too.[134,232,265] In response to the phosphoinositide 3-kinase (PI3K) stimulation, Akt is recruited to the cell membrane where it can undergo phosphorylation at the threonine 308 (Thr308) residue by PDK1 and at the serine 473 (Ser473) residue by mTORC2. Phosphorylation of the Thr308 site critically determines Akt activation while the phosphorylation of both aforementioned sites is required for the maximal kinase activity.[189,190] Herein, the GLP-1/GIP Dual Agonist significantly alleviated the impaired phosphorylating levels of Akt at Thr308 that signified the restoration of the kinase activation. Among others, activated Akt phosphorylates and inhibits the GSK3β,[189,190] a major protein kinase that drives neurodegenerative processes in AD[179] and neuronal apoptosis following ER stress.[26,200,276,287] Accumulating evidence from diverse neuronal cell lines, primary neuronal cultures, and ER insults has demonstrated that the UPR abolishes the inhibitory phosphorylation of GSK3β at Ser9[26,200,232,276,287] to promote Chop expression and switch from adaptive to pro-death signalling during ER stress.[200,232] In the AD brain, GSK3β immunoreactive granules occur in neurones with activated PERK signalling.[119,216] Active PERK engages GSK3β activity through selective removal of the inactive (phosphorylated at Ser9) kinase form via the autosomal-lysosomal pathway.[216] Exacerbated GSK3β activity has been previously shown to result in impaired performance in Morris water maze, excessive astrogliosis and aberrant microglia reactivity *in vivo*.[107,179] Restoring normal levels of GSK3β activity reverses spatial learning and reference memory deficits and precludes reactive gliosis,[107,179] as evident in our findings too.

Akt may also phosphorylate and inhibit PERK kinase,[206] offering an additional mechanistic link on how GLP-1/GIP Dual Agonist conferred its restorative effects on the $APP_{swe}/PS1_{\Delta E9}$ mouse model. Deregulated PERK signalling parallels the temporal and spatial pattern of pathologic protein accumulation and aggregation in AD brain. There, it triggers general translation repression and down-regulation of the plasticity-related cyclic AMP response-element-binding protein (CREB), through its downstream targets eIF2α and

ATF4 respectively, to provoke PSD95 deficiency, synapse damage and cognitive decline.[224] PERK over-activation can further elevate the expression of the β-site amyloid precursor protein cleaving enzyme 1 (BACE1) to accelerate amyloidogenesis.[57,222,224] Although the expression of phosphorylated PERK levels was not addressed herein, the transcriptional and translational regulation of Chop expression primarily lies downstream of PERK arm;[169] in support of it, no changes in IRE1α and ATF6 activation patterns characterised the middle-aged $APP_{swe}/PS1_{\Delta E9}$ mouse brain [**Figure S7**].

To sum up, the current study demonstrated the neuroprotective and restorative effects of the novel GLP-1/GIP Dual Agonist in the $APP_{swe}/PS1_{\Delta E9}$ mouse model for AD. It further unravelled mechanistic insights for the incretin-induced protection of synapse integrity, glial-cell homeostasis and cognitive functioning*in vivo*. Notably, in a pilot clinical trial, the GLP-1 analogue Liraglutide rescued the decline of cerebral glucose consumption in AD patients, which signified improved energy metabolism in brain areas that have been correlated with cognitive decline and disease progression.[86] These encouraging results have led to a randomised, placebo-controlled, double-blind phase II clinical trial of Liraglutide in AD that is currently ongoing (NCT01843075).[116] Herein, the GLP-1 and GIP mono-therapy surprisingly had no impact on the $APP_{swe}/PS1_{\Delta E9}$ phenotype. However, differences in the housing environment of laboratory animals should be considered (IVC cages herein *vs.* 'open' (conventional) cages in[63,70,195,197,198]) before interpreting inconsistencies among the studies.[28,140,268] Differences in the source from which Liraglutide was supplied for the in-vitro and in-vivo studies presented in the thesis may additionally have impacted upon the comparability and reproducibility of the peptide-induced neuroprotection. Nevertheless, the findings related to GLP-1/GIP Dual Agonist therapy endorsed the beneficial effects of incretin signalling in neurodegenerative disorders.[116]

Chapter 6

Perspectives

Alzheimer's afflicts more than 46.8 million people worldwide, with a newly-diagnosed case every 3 seconds[242] and no remission in the disease progression.[42,97,125] By the mid of the century, it will be a global epidemic with more than 130 million sufferers and will pose a public health crisis.[242] Therapeutic interventions able to delay or reverse the Alzheimer's pathology and cognitive decline will spare the AD patients and their families the debilitating emotional and financial burden of the disease. As such, the discovery of disease-modifying drugs is now on the summit of the neuropharmacological research priorities.[42,97,125]

Endogenous neurotrophic factors – long-ago considered central for the neuronal differentiation, survival, and connectivity during development – can restore the morphology and function of degenerating neurones during adulthood when administered exogenously. Over the last two to three decades with numerous pre-clinical studies in rodent and primate models of the AD-related β-amyloidosis or cholinergic lesions, an abundant research history has acquired regarding the therapeutic potential of the neurotrophins.[138,209,290] However, their efficacy and delivery to the brain remain significant disappointments at a clinical level.[14,15] The incretin mimetics currently approved for the type 2 Diabetes Mellitus management may offer an efficacious alternative for the neurotrophic support of the AD brain. They cross the blood-brain barrier and counteract an array of deleterious effects and memory decrements in AD animal models. Clinical trials for the efficacy of GLP-1 analogues in Alzheimer's and Parkinson's disease have revealed beneficial effects of these anti-diabetic agents in halting neuronal degeneration progression.[116]

The current thesis focused on incretin neuropharmacology. It demonstrated the incretin mimetics resolved the UPR and restored the homeostasis of the quality-control chaperones and autophagic machinery following persistent ER stress in proliferating SH-SY5Y neuroblastoma cells and post-mitotic neurones, as well following excessive β-amyloidosis, neuroinflammation, and aberrant cognitive functioning in the $APP_{swe}/PS1_{\Delta E9}$ mice too.

The significance of these findings lies on the multi-factorial involvement of the ER-stress signalling network in the Alzheimer's pathogenesis. As discussed in the previous chapters, the chronicity of the ER stress and UPR dysregulation can impact the β-amyloid cascade, τ phosphorylation, and synapse function via distinct mechanisms to drive the neuronal fate towards degeneration and apoptosis. Recent evidence further indicates that the UPR imbalance in the AD can favour neurodegenerative processes independent of the proteostasis regulation. For instance, the transcription XBP1 and ATF4 factors and the RIDD pathway can modulate lipid biosynthesis and the functional availability of insulin, insulin-like growth factors, their receptors and downstream signalling components. The insulin resistance and lipid dyshomeostasis are important contributors to the AD aetiology while in combination with unmitigated ER stress can exacerbate the accumulation of neurotoxic concentrations of lipids, such as ceramides.[85,88,104,321] Moreover, the UPR network regulates inflammatory signalling and cytokine production, rendering it an essential node for normal function of immune cells, including macrophages, dendritic cells and B lymphocytes.[88,258,293]

In addition to the restoration of the proteostasis capacity of the neurones, the present thesis revealed that the incretin mimetics rescued the aberrant activation of the 'core' antioxidant defence component, Nrf2, and Bcl-2 family members for the intrinsic apoptosis machinery to ameliorate defects in neuronal survival and function. Overall, the findings discussed herein point towards the pleiotropic effects of these anti-diabetic drastic agents, with a possible clinical relevance for the design of Alzheimer's disease-modifying therapeutic strategies. They further open up exciting avenues that may deepen our current understanding of the mechanism of action of the incretin mimetics on the proteostasis machinery and neuronal fate regulation. Specifically, future experimentation may address:

- **The autophagic flux, using the transmission electron microscopy.** Herein, the ER stress and UPR dysregulation coincided with decreased levels of autophagy-related proteins (Atg) both *in vitro* and *in vivo*. Among the proteins monitored, I quantified the expression of the microtubule-associated proteins 1A/1B light chain 3B (LC3) that functions in the autophagosome biogenesis.[30] The lack of detection of two district bands in the immunoblotting studies precluded the quantification of the ratio of the lipidated and autophagosome-recruited type II *vs.* the cytosolic type I of LC3 for the autophagy flux assessment. Electron microscopy is the most sensitive technique for the exact identification, morphological characterisation, and visualisation of autophagic structures in their complex cellular environments.[148] In combination with LC3 immunodetection methods, it may offer a more integrative approach for the evaluation of autophagy under ER stress conditions, as well as for clarification of the exact effect of the incretin mimetics on the degradative machinery too.

- **Calcium-dependency of the incretin mimetics for the UPR modulation and neuroprotection.** The cellular and animal models employed in the present thesis all featured persistent perturbation of the ER calcium stores. The proliferating neuroblastoma SH-SY5Y cells and the post-mitotic neurones from the human LUHMES cell line both received a 16-h treatment with thapsigargin that inhibits the SERCA channel.[292] The $PS1_{\Delta E9}$ mutation expressed *in vivo* enhances the IP_3R-mediated calcium release from the ER stores.[96] Although these models are advantageous for simulating the AD onset, partly due to the causative link between the ER calcium and the Aβ generation and aggregation,[95,96,130,240] they raise the question whether a calcium-dependency exists in the mechanism of action of incretin mimetics for proteostasis restoration and neuroprotection. Preliminary findings suggested that the incretin mimetics may modulate the UPR independently of calcium levels, as illustrated in **Figure S8**. Acquisition of biochemical data in additional cellular processes, such as autophagy, protein-quality control, and signalling components of the intrinsic apoptosis machinery, along with an assessment of the intracellular calcium content and functionality of calcium channels would provide a more concrete answer for the above.

- **NF-κB signalling for inflammatory responses.** In *Chapter 5*, the novel dual incretin resolved ER stress and ameliorated aberrant neuroinflammation in the $APP_{swe}/PS1_{\Delta E9}$ mouse brain. Chronically dysregulated UPR alters inflammatory signalling, including NF-κB, to exacerbate the cytokine release and thereby feedback neuronal degeneration processes in the AD brain. Notably, the PERK arm induces the NF-κB phosphorylation via its downstream target-kinases GSK3β and eIF2α to favour the expression of the tumour necrosis factor α (TNFα).[258] It would be of interest to examine in future whether the incretin signalling restores NF-kB pathway to attenuate astrogliosis and over-reactive microglia load in the cortex and hippocampus of the $APP_{swe}/PS1_{\Delta E9}$ mouse model.

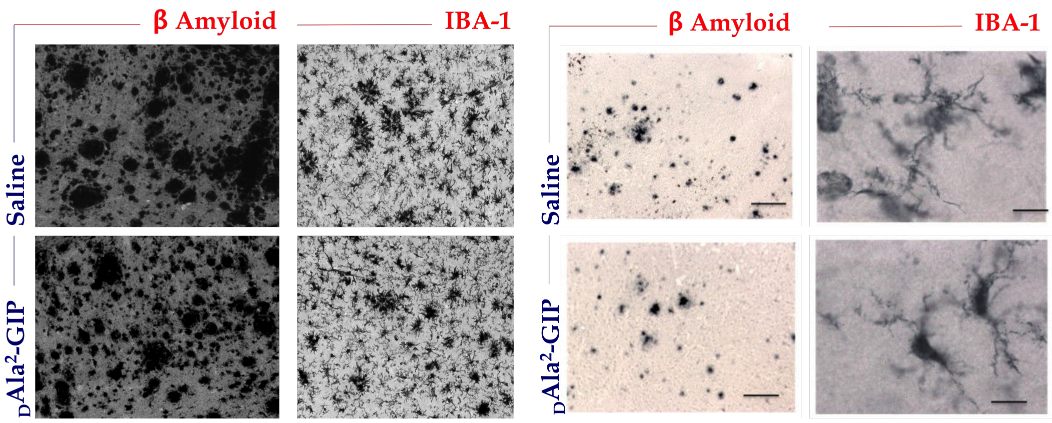

(a) (b)

Figure 6.1: **Comparison of the cortical amyloid and reactive microglia load between the $APP_{swe}/PS1_{\Delta E9}$ mouse brains processed in our study [(a)] and the study by *Faivre, E. & Hölscher, C.*[70] [(b)].** Scale bars for panel **(b)**: 880 µm, left-side micrographs; 80 µm, right-side micrographs.

- **Time - window for $_D$Ala^2-GIP-induced neuroprotection?** Previously studies from our group have demonstrated that the stable analogue of the glucose-dependent insulinotropic polypeptide (GIP), $_{D}$Ala^2-GIP has alleviated neuroinflammatory responses, oxidative stress and cerebral amyloid plaque load to attenuate the poor performance of the APP$_{swe}$/PS1$_{\Delta E9}$ mouse model in Morris water maze and novel object recognition paradigms.[63,70] These effects have been correlated to enhanced synaptogenesis and restored synaptic plasticity events in the cortex and hippocampus of the middle-aged and aged APP$_{swe}$/PS1$_{\Delta E9}$ mice upon chronic $_{D}$Ala^2-GIP treatment.[70] Surprisingly, the present thesis could not replicate the previously-reported neuroprotective effects in this murine model. Intriguingly, the comparison of histological analysis for pathognomonic features demonstrates prominent discrepancies in the cortical amyloid and reactive microglia load between the APP$_{swe}$/PS1$_{\Delta E9}$ mice used in our study and the study by *Faivre, E. & Hölscher, C.*[70] [**Figure 6.1**], albeit the similarities of the animal age, administration route and treatment dosage. These differences may signal for a time-window for the efficacy of $_{D}$Ala^2-GIP in neurodegenerative disorders. In other words, $_{D}$Ala^2-GIP may elicit neuroprotective and trophic effects at an intermediate stage for the severity of the amyloid aggregation and neuroinflammation in the brain. However, this hypothesis necessitates future experimentation and should be correlated to housing environment of the APP$_{swe}$/PS1$_{\Delta E9}$ mouse model. Conventional 'open' cages risk exposure of the animals to the microorganisms present in the room while IVC housing systems have been deployed to house the animals in a more 'protected' environment.[28] Considering that housing conditions significantly impact behavioural, physiological, developmental (brain and immune system) aspects of the animals housed within,[28,50,307] they may also shift the 'time-window' for the efficacy of the GIP mono-therapy against the Alzheimer's-like pathology *in vivo*.

Appendices

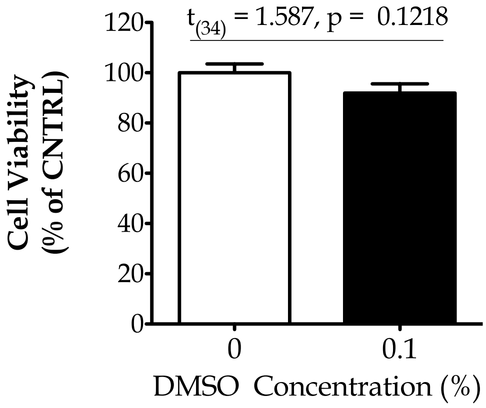

Figure S1: **0.1% DMSO did not impact SH-SY5Y cell viability.** Twenty-four hours post seeding, SH-SY5Y cells were serum starved for 8 h, treated with 0 or 0.1% DMSO for 16 h, and assayed for XTT metabolisation. Each bar represents the mean ± SEM from three independent experiments. Cell treatments were performed in sextuplicate in each experiment. Data is expressed as a percentage of the control (CNTRL; unstressed/untreated conditions). Data was analysed by unpaired two-sample *t* test.

Target	Modification Site	Mean ± SEM				One-way ANOVA	
		CNTRL	LIRA	TG	TG + LIRA	F	p
Stat1	Tyr 701	1.00 ± 0.178	1.36 ± 0.106	1.02 ± 0.162	1.38 ± 0.194	$(3, 28) = 1.619$	0.2072
Akt	Ser 4731	1.00 ± 0.214	1.42 ± 0.241	0.867 ± 0.151	1.23 ± 0.160	$(3, 28) = 1.575$	0.2174
AMPKα	Thr 172	1.00 ± 0.201	0.962 ± 0.191	0.666 ± 0.056	0.619 ± 0.052	$(3, 28) = 1.870$	0.1575
rpS6	Ser 235/236	1.00 ± 0.1664	0.813 ± 0.095	0.733 ± 0.096	0.958 ± 0.076	$(3, 28) = 1.203$	0.3268
mTOR	Ser 2448	1.00 ± 0.107	1.02 ± 0.122	0.70 ± 0.103	1.15 ± 0.190	$(3, 27) = 2.018$	0.1351
HSP27	Ser 78	1.00 ± 0.241	0.970 ± 0.145	0.609 ± 0.082	0.635 ± 0.128	$(3, 28) = 1.727$	0.1841
p70S6K	Thr 389	1.00 ± 0.103	0.863 ± 0.062	0.930 ± 0.122	0.807 ± 0.115	$(3, 28) = 0.6552$	0.5864
PRAS40	Thr 246	1.00 ± 0.176	0.925 ± 0.138	0.712 ± 0.077	0.798 ± 0.102	$(3, 28) = 0.9936$	0.4102
p38	Thr 180/Tyr 182	1.00 ± 0.212	1.03 ± 0.227	0.662 ± 0.140	1.16 ± 0.165	$(3, 28) = 1.261$	0.3068
SAPK/JNK	Thr 183/Tyr 185	1.00 ± 0.183	1.03 ± 0.164	0.89 ± 0.078	0.87 ± 0.111	$(3, 28) = 0.3143$	0.8149
Caspase 3	Asp 175	1.00 ± 0.0782	0.98 ± 0.119	1.35 ± 0.149	1.06 ± 0.047	$(3, 28) = 2.561$	0.0750

Table S1: **Protein expression of additional signalling targets included in the PathScan® Intracellular Signaling Array kit**. Twenty-four hours post seeding, SH-SY5Y cells were serum starved for 8 h and treated with 0 or 100 nM of thapsigargin (TG) for 16 h, in the presence or absence of 100 nM Liraglutide (LIRA). Cells were harvested, and 0.3 mg mL^{-1} protein of whole-cell lysate was processed with the PathScan® sandwich immunoassay. All samples per experiment were processed in duplicate. Data is expressed as fold change to the control (CNTRL; unstressed/untreated conditions) from four independent experiments. For the list of the abbreviations used, please refer to the corresponding **chapter** .

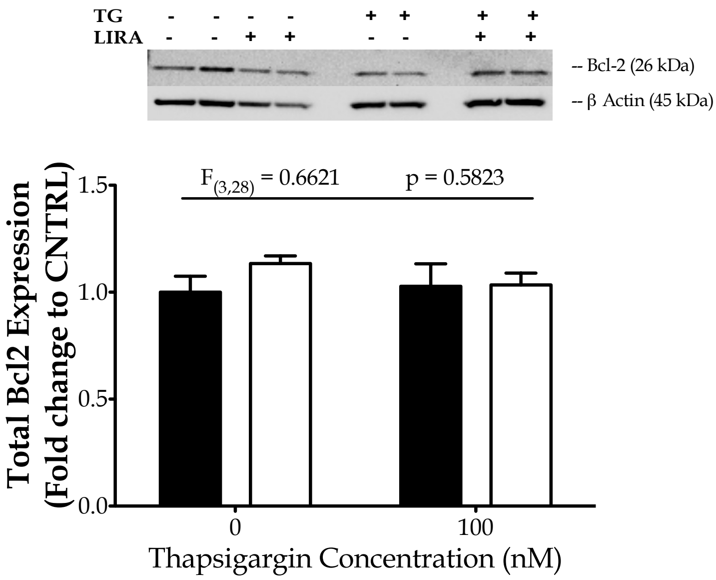

Figure S2: **Chronic disturbance of ER calcium homeostasis did not alter the expression levels of the pro-survival Bcl-2 protein.** Twenty-four hours post seeding, SH-SY5Y cells were serum starved for 8 h and treated with 0 or 100 nM of thapsigargin for 16 h, in the presence or absence of 100 nM Liraglutide. Cells were harvested, and Bcl-2 expression was determined by western blotting. β-Actin was used as the loading control to the western blot analysis. Each bar represents the mean $\pm$ SEM from four independent experiments. Data is expressed as fold change to the control (CNTRL; unstressed/untreated conditions). Data was analysed by one- and two-way ANOVA, followed by *post hoc* Bonferroni's multiple comparison t-test.

Target	Modification Site	Mean ± SEM						One-way ANOVA	
		CNTRL	LIRA	DA	TG	TG + LIRA	TG + DA	$F_{(5,42)}$	p
ERK1/2	Thr 202/Tyr 204	1.00 ± 0.129	1.00 ± 0.105	1.00 ± 0.108	0.638 ± 0.158	0.830 ± 0.131	1.10 ± 0.197	1.403	0.243
Stat1	Tyr 701	1.00 ± 0.205	0.891 ± 0.192	0.865 ± 0.212	0.855 ± 0.272	0.694 ± 0.160	1.05 ± 0.243	0.333	0.89
Stat3	**Tyr 705**	1.00 ± 0.060	0.880 ± 0.078	0.8325 ± 0.084	0.559 ± 0.086	0.839 ± 0.10	1.12 ± 0.077	**5.303**	$\leq$ **0.001**
Akt	**Thr 308**	1.00 ± 0.045	1.14 ± 0.103	0.947 ± 0.107	0.388 ± 0.068	0.620 ± 0.054	0.67 ± 0.045	**14.18**	$\leq$ **0.001**
Akt	**Ser 473**	1.00 ± 0.07	1.09 ± 0.077	0.946 ± 0.089	0.457 ± 0.065	0.798 ± 0.086	1.01 ± 0.092	**8.170**	$\leq$ **0.001**
AMPKα	Thr 172	1.00 ± 0.062	0.881 ± 0.162	0.997 ± 0.109	0.678 ± 0.059	0.704 ± 0.079	0.733 ± 0.065	2.181	0.074
rpS6	**Ser 235/236**	1.00 ± 0.034	0.781 ± 0.141	0.992 ± 0.096	0.401 ± 0.049	0.756 ± 0.1305	0.636 ± 0.017	**6.144**	$\leq$ **0.001**
mTOR	**Ser 2448**	1.00 ± 0.064	1.038 ± 0.104	0.956 ± 0.106	0.352 ± 0.041	0.588 ± 0.08	0.667 ± 0.055	**12.14**	$\leq$ **0.001**
HSP27	**Ser 78**	1.00 ± 0.044	1.08 ± 0.133	1.08 ± 0.120	0.432 ± 0.067	0.66 ± 0.058	0.72 ± 0.07	**9.022**	$\leq$ **0.001**
BAD	**Ser 112**	1.00 ± 0.05	1.13 ± 0.069	0.95 ± 0.09	0.60 ± 0.04	0.865 ± 0.03	0.83 ± 0.03	**10.13**	$\leq$ **0.001**
p70S6K	Thr 389	1.00 ± 0.081	0.869 ± 0.255	0.893 ± 0.142	0.508 ± 0.084	0.887 ± 0.171	0.670 ± 0.066	1.472	0.219
PRAS40	**Thr 246**	1.00 ± 0.05	1.10 ± 0.10	1.01 ± 0.11	0.33 ± 0.04	0.65 ± 0.07	0.69 ± 0.09	**13.20**	$\leq$ **0.001**
p53	**Ser 15**	1.00 ± 0.06	0.91 ± 0.16	0.99 ± 0.105	0.50 ± 0.05	0.84 ± 0.06	0.855 ± 0.08	**3.704**	$\leq$ **0.01**
p38	Thr 180/Tyr 182	1.00 ± 0.116	1.12 ± 0.107	0.882 ± 0.106	0.787 ± 0.045	0.851 ± 0.156	0.864 ± 0.108	1.187	0.332
SAPK/JNK	Thr 183/Tyr 185	1.00 ± 0.056	1.07 ± 0.102	0.911 ± 0100	0.848 ± 0.088	0.836 ± 0.04	0.763 ± 0.084	0.184	0.115
PARP	**Asp 214**	1.00 ± 0.09	1.19 ± 0.18	1.47 ± 0.16	3.31 ± 0.304	2.47 ± 0.40	1.69 ± 0.20	**13.04**	$\leq$ **0.001**
CASP3	**Asp 175**	1.00 ± 0.13	1.15 ± 0.150	1.54 ± 0.352	2.99 ± 0.425	1.61 ± 0.113	1.33 ± 0.095	**8.452**	$\leq$ **0.001**
GSK3β	**Ser 9**	1.00 ± 0.11	0.93 ± 0.082	0.88 ± 0.063	0.53 ± 0.06	0.72 ± 0.019	0.76 ± 0.034	**6.468**	$\leq$ **0.001**

Table S2: **One-way ANOVA results of the signalling targets included in the PathScan® Intracellular Signaling Array kit**. On d 5–6 of the differentiation period, post-mitotic neurones from the LUHMES cell line were treated with 0 and 100 nM of thapsigargin (TG) in the presence or absence of 100 nM Liraglutide (LIRA) or of 100 nM novel GLP-1/GIP Dual Agonist (DA) for 16 h. Neurones were then harvested, and 0.3 mg mL^{-1} protein of whole-cell lysate was processed with the PathScan® sandwich immunoassay. All samples per experiment were processed in duplicate. Data is expressed as fold change to the control (CNTRL; unstressed/untreated conditions) from four independent experiments. For the list of the abbreviations used, please refer to the corresponding **chapter** .

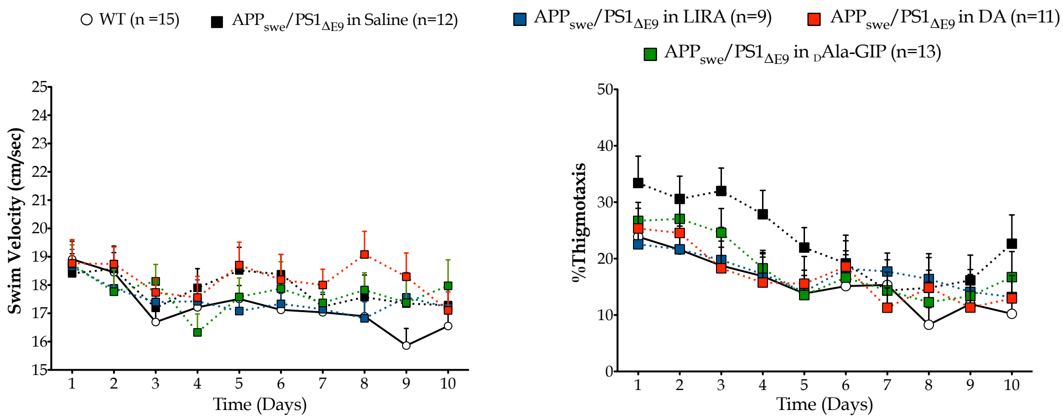

(a)

(b)

Figure S3: **APP$_{swe}$/PS1$_{\Delta E9}$ and wild-type (WT) mice displayed comparable swim velocity and thigmotactic behaviour over the course of Morris water maze acquisition phase.** Nine weeks after the initiation of saline, $_D$Ala^2-GIP, Liraglutide (LIRA) and GLP-1/GIP Dual Agonist (DA) treatments, animals were trained to locate an invisible escape platform fixed on a target position in the northwest quadrant. Animals run 3 trials per day with an inter-trial interval of approximately 30 min for 10 consecutive days. The swim velocity [**(a)**] along with the percentage of time spent in thigmotactic (wall hugging) swimming per trial [**(b)**] were monitored to evaluate animal locomotion and emotionality during the task. Each graph point represents the daily mean ± SEM of the aforementioned parameters. Data was analysed by repeated measures two-way ANOVA.

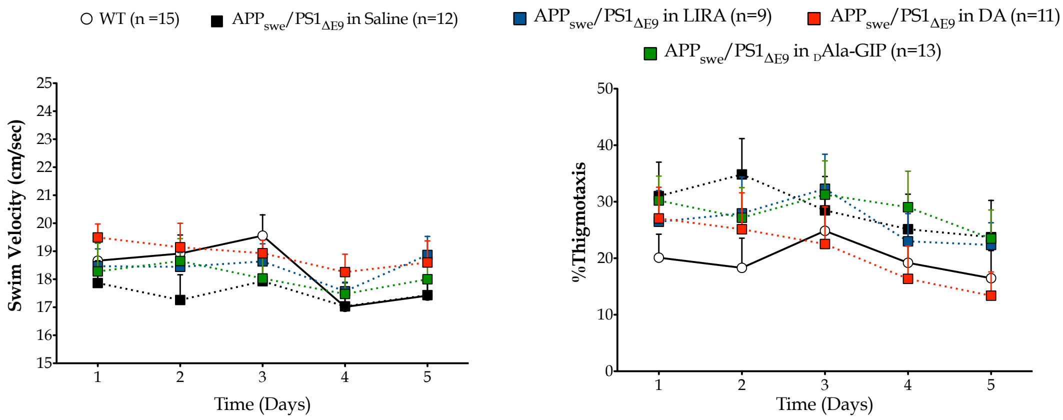

(a)

(b)

Figure S4: **APP$_{swe}$/PS1$_{\Delta E9}$ and wild type mice displayed comparable swim velocity and thigmotactic behaviour over the course of Morris water maze reversal acquisition phase.** Animals were trained to locate an invisible escape platform fixed on a target position in the southeast quadrant. Animals run 3 trials per day with an inter-trial interval of approximately 30 min for 5 consecutive days. The swim velocity [**(a)**] along with the percentage of time spent in thigmotactic (wall hugging) swimming per trial [**(b)**] were monitored to evaluate animal locomotion and emotionality during the task. Each graph point represents the daily mean ± SEM of the aforementioned parameters for wild type (WT) and APP$_{swe}$/PS1$_{\Delta E9}$ treated with 10 mL kg^{-1} d^{-1} saline and APP$_{swe}$/PS1$_{\Delta E9}$ mice treated with 25 nmol kg^{-1} d^{-1} $_D$Ala^2-GIP, Liraglutide (LIRA) or GLP-1/GIP Dual Agonist (DA). Data was analysed by repeated measures two-way ANOVA.

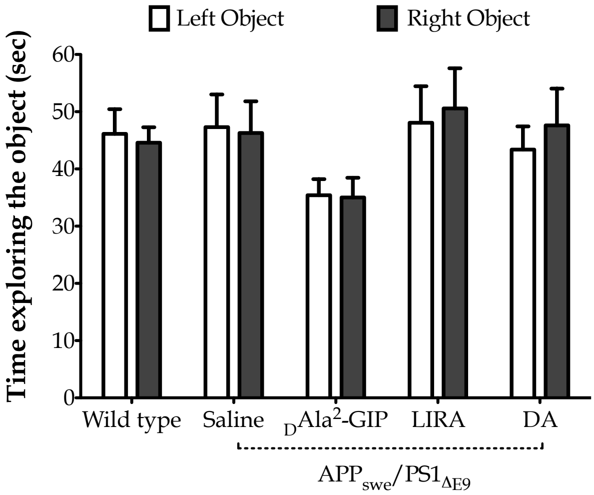

Genotype	Treatment	n	Student's t test	
			t	p
Wild-type	Saline	15	$t_{28} = 0.304$	0.764
APP$_{swe}$/PS1$_{\Delta E9}$	Saline	12	$t_{22} = 0.129$	0.899
APP$_{swe}$/PS1$_{\Delta E9}$	$_D$Ala^2-GIP	13	$t_{24} = 0.09$	0.932
APP$_{swe}$/PS1$_{\Delta E9}$	LIRA	9	$t_{16} = 0.263$	0.796
APP$_{swe}$/PS1$_{\Delta E9}$	DA	11	$t_{20} = 0.554$	0.586

(a)

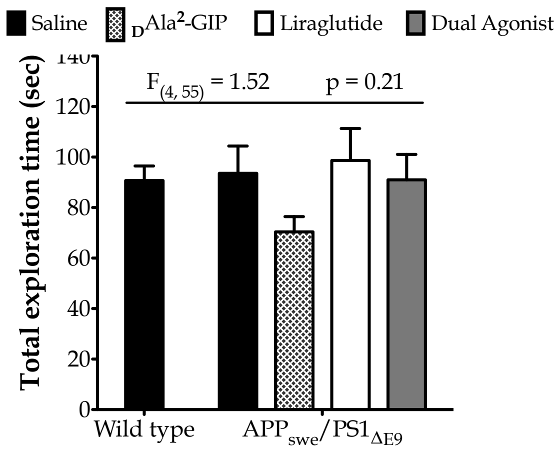

(b)

Figure S5: **Equal preference between the left and right object samples and comparable object exploration time among the animal groups over the acquisition session of the novel object recognition paradigm.** Animals were allowed to explore the familiar open field arena that had been enriched with two identical objects for 10 min. The exploration time allotted in each object was monitored [(a)] and processed for the computation of the total exploration time allotted in both objects [**(b)**] during the acquisition session. Each bar represents the mean ± SEM of the aforementioned parameters for wild type and APP$_{swe}$/PS1$_{\Delta E9}$ treated with 10 mL kg^{-1} d^{-1} saline and APP$_{swe}$/PS1$_{\Delta E9}$ mice treated with 25 nmol kg^{-1} d^{-1} $_D$Ala^2-GIP, Liraglutide (LIRA) or GLP-1/GIP Dual Agonist (DA). Data was analysed by Student's t test and one-way ANOVA.

Target	Mean ± SEM					One-way ANOVA	
	WT	$APP_{swe}/PS1_{\Delta E9}$	$APP_{swe}/PS1_{\Delta E9}$ in $_D$Ala^2-GIP	$APP_{swe}/PS1_{\Delta E9}$ in LIRA	$APP_{swe}/PS1_{\Delta E9}$ in DA	F	p
beclin-1	1.00 ± 0.05	0.72 ± 0.08	0.82 ± 0.04	0.81 ± 0.08	1.08 ± 0.12	$(4, 29) = 3.6$	0.017
ATG3	1.00 ± 0.03	0.80 ± 0.05	0.88 ± 0.05	0.95 ± 0.08	1.22 ± 0.12	$(4, 46) = 5.05$	0.002
ATG7	1.00 ± 0.07	0.78 ± 0.06	0.89 ± 0.07	1.02 ± 0.12	1.10 ± 0.06	$(4, 46) = 1.96$	0.12
LC3	1.00 ± 0.08	0.75 ± 0.04	0.96 ± 0.05	0.84 ± 0.07	1.18 ± 0.105	$(4, 29) = 4.38$	0.007

Table S3: **One-way ANOVA results of the *ex-vivo* protein expression of "core" Atg proteins required for autophagosome formation**. Protein of mouse brain whole cell lysate (20 µg) from wild-type (WT; $n = 8$) or $APP_{swe}/PS1_{\Delta E9}$ ($n = 6$) mice treated with $10\,\mathrm{mL\,kg^{-1}\,d^{-1}}$ saline and $APP_{swe}/PS1_{\Delta E9}$ mice treated with $25\,\mathrm{nmol\,kg^{-1}\,d^{-1}}$ $_D$Ala^2-GIP ($n = 7$), Liraglutide (LIRA; $n = 7$) or GLP-1/GIP Dual Agonist (DA; $n = 6$) was processed for western blotting. β-Actin was used as the loading control to all western blot analyses.

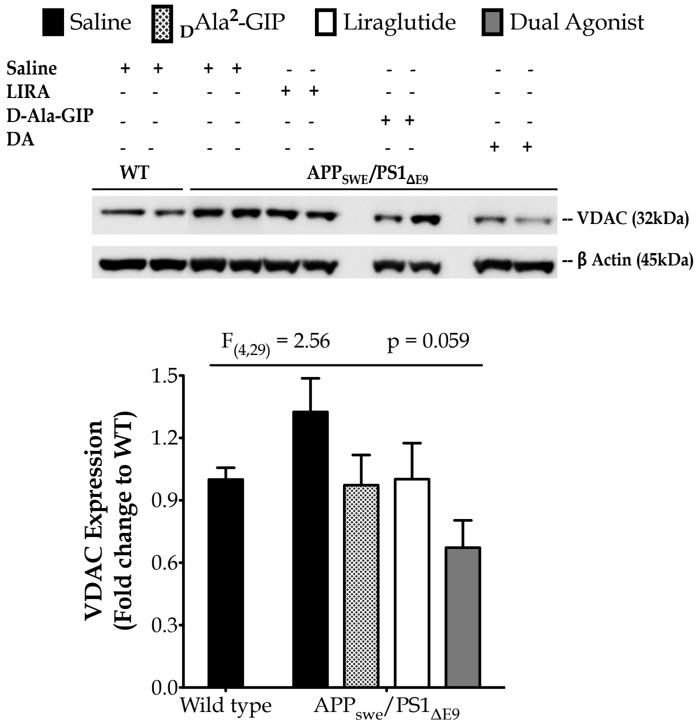

Figure S6: **A trend of enhanced VDAC protein expression in APP$_{swe}$/PS1$_{\Delta E9}$ mouse brain that seemed to get normalised upon GLP-1/GIP Dual Agonist treatment.** Protein of mouse brain whole cell lysate (20 µg) were processed for western blotting where the expression of the mitochondrial voltage-dependent anion channel (VDAC). β-Actin was used as the loading control to all western blot analyses. Each bar represents mean ± SEM from wild-type (WT; $n = 8$) or APP$_{swe}$/PS1$_{\Delta E9}$ ($n = 6$) mice treated with 10 mL kg^{-1} d^{-1} saline and APP$_{swe}$/PS1$_{\Delta E9}$ mice treated with 25 nmol kg^{-1} d^{-1} $_D$Ala^2-GIP ($n = 7$), Liraglutide (LIRA; $n = 7$) or GLP-1/GIP Dual Agonist (DA; $n = 6$). Data was analysed by one-way ANOVA.

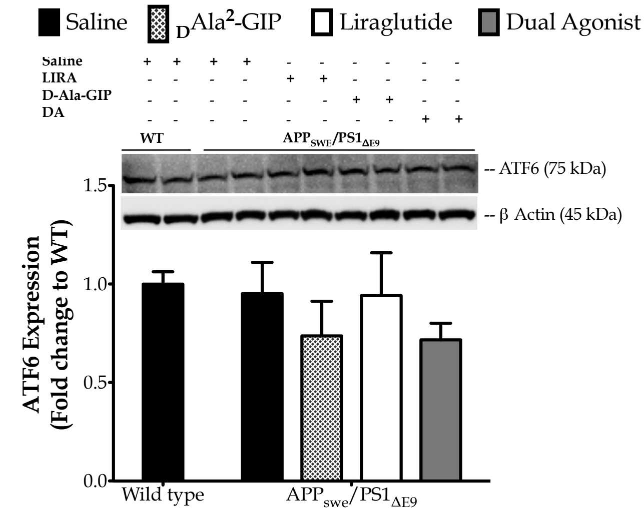

(a)

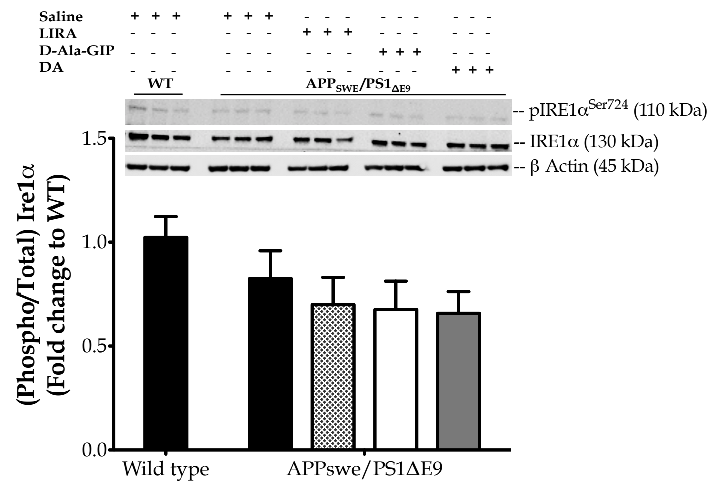

(b)

Figure S7: **UPR activation did not involve IRE1α and ATF6 signalling in the APP$_{swe}$/PS1$_{\Delta E9}$ mouse brain.** Protein of mouse brain whole cell lysate (20 µg) were processed for western blotting where the protein expression of ATF6 [**(a)**] along with the protein levels of total and phosphorylated IRE1α [**(b)**] were determined by western blotting. β-Actin was used as the loading control to all western blot analyses. Each bar represents mean ± SEM from wild-type (WT; $n = 8$) or APP$_{swe}$/PS1$_{\Delta E9}$ ($n = 6$) mice treated with 10 mL kg^{-1} d^{-1} saline and APP$_{swe}$/PS1$_{\Delta E9}$ mice treated with 25 nmol kg^{-1} d^{-1} $_{D}$Ala^{2}-GIP ($n = 7$), Liraglutide (LIRA; $n = 7$) or GLP-1/GIP Dual Agonist (DA; $n = 6$) [**(b)**]. Data was analysed by one-way ANOVA.

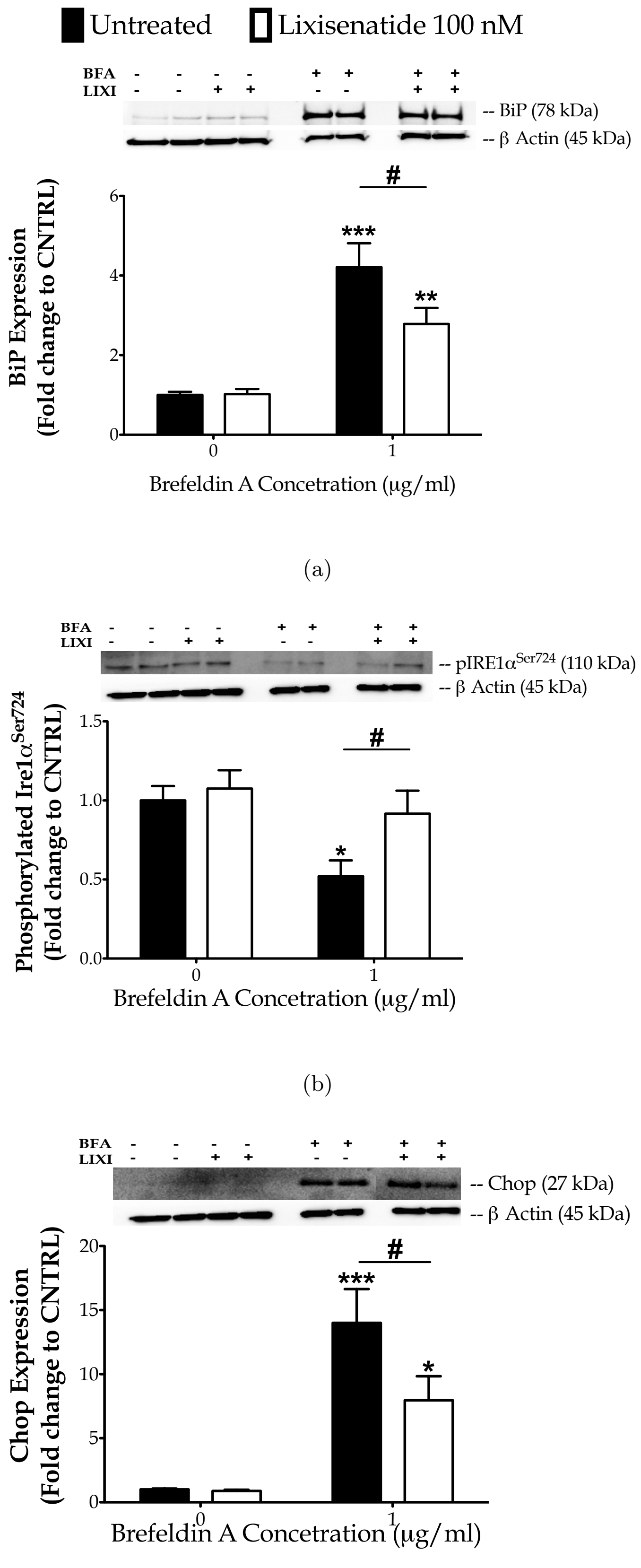
Untreated
Lixisenatide 100 nM
BFA
LIXI
-- BiP (78 kDa)
-- β Actin (45 kDa)
#
***
**
BiP Expression (Fold change to CNTRL)
Brefeldin A Concetration (μg/ml)
BFA
LIXI
-- pIRE1αSer724 (110 kDa)
-- β Actin (45 kDa)
#
*
Phosphorylated Ire1αSer724 (Fold change to CNTRL)
Brefeldin A Concetration (μg/ml)
BFA
LIXI
-- Chop (27 kDa)
-- β Actin (45 kDa)
#
***
*
Chop Expression (Fold change to CNTRL)
Brefeldin A Concetration (μg/ml)

(a)

(b)

(c)

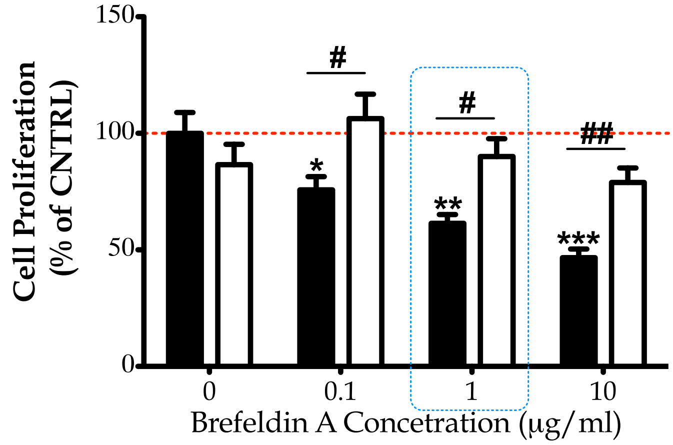

(d)

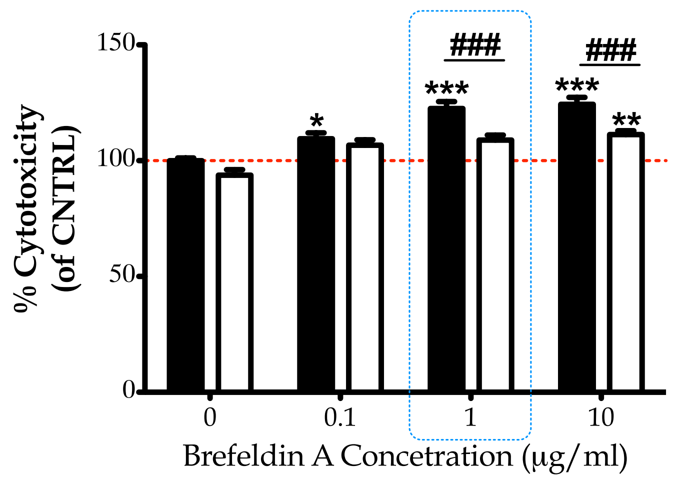

(e)

Figure S8: **Lixisenatide ameliorated ER stress to rescue aberrant cytotoxicity and proliferation impairments in the neuroblastoma SH-SY5Y cell line.** Twenty-four hours post seeding, SH-SY5Y cells were serum starved for 8 h and treated with Brefeldin A (BFA) for 16 h, in the presence or absence of 100 nM Lixisenatide (LIXI); BFA inhibits the anterograde protein transport from the ER to Golgi apparatus whilst enhancing the retrograde transport from Golgi apparatus to the ER and thereby culminating in abnormal protein load within the ER lumen.[261] Cells were harvested, and the expression of BiP [(**a**)] and Chop [(**c**)] along with the protein levels of phosphorylated IRE1α at the serine 724 [(**b**)] were determined by western blotting. β-Actin was used as the loading control to all western blot analyses. Alternatively, cells were assayed for the BrdU incorporation [(**d**)] to assess cell proliferation. Cell supernatant was collected and processed for the LDH activity [(**e**)] to determine cytotoxicity. Each bar represents mean ± SEM from four independent experiments. Data is expressed as fold change to the control (CNTRL; unstressed/untreated conditions). Data was analysed by one- and two-way ANOVA, followed by *post hoc* Bonferroni's multiple comparison t-test ($^{*}p \leq 0.05$, $^{**}p \leq 0.01$ & $^{***}p \leq 0.001$ compared to CNTRL; $^{\sharp}p \leq 0.05$, $^{\sharp\sharp}p \leq 0.01$ & $^{\sharp\sharp\sharp}p \leq 0.001$ compared to the corresponding BFA-treated cells)

Bibliography

[1] T. Abbas, E. Faivre, and C. Hölscher. Impairment of synaptic plasticity and memory formation in GLP-1 receptor KO mice: Interaction between type 2 diabetes and Alzheimer's disease. *Behavioural Brain Research*, 205(1):265–271, 2009.

[2] D. Acosta-Alvear, Y. Zhou, A. Blais, M. Tsikitis, N. H. Lents, C. Arias, C. J. Lennon, Y. Kluger, and B. D. Dynlacht. XBP1 controls diverse cell type- and condition-specific transcriptional regulatory networks. *Mol Cell*, 27(1):53–66, 2007.

[3] E. Alberdi, A. Wyssenbach, M. Alberdi, M. V. Sanchez-Gomez, F. Cavaliere, J. J. Rodriguez, A. Verkhratsky, and C. Matute. Ca^{2+}-dependent endoplasmic reticulum stress correlates with astrogliosis in oligomeric amyloid beta-treated astrocytes and in a model of alzheimer's disease. *Aging Cell*, 12(2):292–302, 2013.

[4] M. Antunes and G. Biala. The novel object recognition memory: neurobiology, test procedure, and its modifications. *Cognitive Processing*, 13(2):93–110, 2012.

[5] N. Arispe, E. Rojas, and H. B. Pollard. Alzheimer disease amyloid beta protein forms calcium channels in bilayer membranes: blockade by tromethamine and aluminum. *Proceedings of the National Academy of Sciences of the United States of America*, 90(2):567–571, 1993.

[6] D. Athauda and T. Foltynie. The glucagon-like peptide 1 (GLP) receptor as a therapeutic target in parkinson's disease: mechanisms of action. *Drug Discovery Today*,

21(5):802–818, 2016.

[7] D. Athauda, K. Maclagan, S. S. Skene, M. Bajwa-Joseph, D. Letchford, K. Chowdhury, S. Hibbert, N. Budnik, L. Zampedri, J. Dickson, Y. Li, I. Aviles-Olmos, T. T. Warner, P. Limousin, A. J. Lees, N. H. Greig, S. Tebbs, and T. Foltynie. Exenatide once weekly versus placebo in Parkinson's disease: a randomised, double-blind, placebo-controlled trial. *The Lancet*, 390(10103):1664–1667, 2017.

[8] I. Aviles-Olmos, J. Dickson, Z. Kefalopoulou, A. Djamshidian, P. Ell, T. Soderlund, P. Whitton, R. Wyse, T. Isaacs, A. Lees, P. Limousin, and T. Foltynie. Exenatide and the treatment of patients with Parkinson's disease. *The Journal of Clinical Investigation*, 123(6):2730–2736, 2013.

[9] I. Aviles-Olmos, J. Dickson, Z. Kefalopoulou, A. Djamshidian, J. Kahan, P. Ell, P. Whitton, R. Wyse, T. Isaacs, A. Lees, P. Limousin, and T. Foltynie. Motor and cognitive advantages persist 12 months after exenatide exposure in Parkinson's disease. *journal of Parkinson's Disease*, 4(3):337–344, 2014.

[10] L. L. Baggio and D. J. Drucker. Biology of Incretins: GLP-1 and GIP. *Gastroenterology*, 132(6):2131–2157, 2007.

[11] R. Bakthisaran, R. Tangirala, and C. M. Rao. Small heat shock proteins: Role in cellular functions and pathology. *Biochimica et Biophysica Acta (BBA) – Proteins and Proteomics*, 1854(4):291–319, 2015.

[12] D. Baltzis, O. Pluquet, A. I. Papadakis, S. Kazemi, L.-K. Qu, and A. E. Koromilas. The eif2α kinases PERK and PKR activate glycogen synthase kinase 3 to promote the proteasomal degradation of p53. *journal of Biological Chemistry*, 282(43):31675–31687, 2007.

[13] E. Barbero-Camps, A. Fernandez, A. Baulies, L. Martinez, J. C. Fernandez-Checa, and A. Colell. Endoplasmic reticulum stress mediates amyloid β neurotoxicity via mitochondrial cholesterol trafficking. *Am J Pathol*, 184(7):2066–81, 2010.

[14] R. T. Bartus and E. M. Johnson. Clinical tests of neurotrophic factors for human neurodegenerative diseases, part 1: Where have we been and what have we learned? *Neurobiology of Disease*, 97:156–168, 2017.

[15] R. T. Bartus and E. M. Johnson. Clinical tests of neurotrophic factors for human neurodegenerative diseases, part 2: Where do we stand and where must we go next? *Neurobiology of Disease*, 97:169–178, 2017.

[16] W. B'chir, C. Chaveroux, V. Carraro, J. Averous, A.-C. Maurin, C. Jousse, Y. Muranishi, L. Parry, P. Fafournoux, and A. Bruhat. Dual role for CHOP in the crosstalk between autophagy and apoptosis to determine cell fate in response to amino acid deprivation. *Cellular Signalling*, 26(7):1385–1391, 2014.

[17] W. B'chir, A.-C. Maurin, V. Carraro, J. Averous, C. Jousse, Y. Muranishi, L. Parry, G. Stepien, P. Fafournoux, and A. Bruhat. The eIF2α/ATF4 pathway is essential for stress-induced autophagy gene expression. *Nucleic Acids Research*, 41(16):7683, 2013.

[18] A. Benavides, D. Pastor, P. Santos, P. Tranque, and S. Calvo. CHOP plays a pivotal role in the astrocyte death induced by oxygen and glucose deprivation. *Glia*, 52(4):261–275, 2005.

[19] S. C. Benn, D. Perrelet, A. C. Kato, J. Scholz, I. Decosterd, R. J. Mannion, J. C. Bakowska, and C. J. Woolf. Hsp27 Upregulation and Phosphorylation Is Required for Injured Sensory and Motor Neuron Survival. *Neuron*, 36(1):45–56, 2002.

[20] I. Bezprozvanny and M. P. Mattson. Neuronal calcium mishandling and the pathogenesis of Alzheimer's disease. *Trends in Neurosciences*, 31(9):454–463, 2008.

[21] J. L. Biedler, L. Helson, and B. A. Spengler. Morphology and growth, tumorigenicity, and cytogenetics of human neuroblastoma cells in continuous culture. *Cancer Research*, 33(11):2643–2652, 1973.

[22] K. A. Boehme, R. Kulikov, and C. Blattner. p53 stabilization in response to dna damage requires akt/PKB and DNA-PK. *Proceedings of the National Academy of Sciences*, 105(22):7785–7790, 2008.

[23] L. Bondolfi, M. Calhoun, F. Ermini, H. G. Kuhn, K.-H. Wiederhold, L. Walker, M. Staufenbiel, and M. Jucker. Amyloid-associated neuron loss and gliogenesis in the neocortex of amyloid precursor protein transgenic mice. *Journal of Neuroscience*, 22(2):515–522, 2002.

[24] N. Bousette, C. Abbasi, R. Chis, and A. O. Gramolini. Calnexin silencing in mouse neonatal cardiomyocytes induces Ca^{2+} cycling defects, er stress, and apoptosis. *journal of Cellular Physiology*, 229(3):374–383, 2014.

[25] G. L. Bratthauer. The avidin-biotin complex (abc) method and other avidin-biotin binding methods. In L. C. Javois, editor, *Immunocytochemical Methods and Protocols*, pages 203–214. Humana Press, 1999.

[26] J. Brewster, D. Linseman, R. Bouchard, F. Loucks, T. Precht, E. Esch, and K. Heidenreich. Endoplasmic reticulum stress and trophic factor withdrawal activate distinct signaling cascades that induce glycogen synthase kinase-3β and a caspase-9-dependent apoptosis in cerebellar granule neurons. *Molecular and Cellular Neuroscience*, 32(3):242 –253, 2006.

[27] N. J. Bulleid and L. Ellgaard. Multiple ways to make disulfides. *Trends in Biochemical Sciences*, 36(9):485–492, 2011.

[28] O. Burman, L. Buccarello, V. Redaelli, and L. Cervo. The effect of two different Individually Ventilated Cage systems on anxiety-related behaviour and welfare in two strains of laboratory mouse. *Physiology & Behavior*, 124:92–99, 2014.

[29] H.-Y. Cai, Z.-J. Wang, C. Hölscher, L. Yuan, J. Zhang, P. Sun, J. Li, W. Yang, M.-N. Wu, and J.-S. Qi. Lixisenatide attenuates the detrimental effects of amyloid β protein on spatial working memory and hippocampal neurons in rats. *Behavioural Brain Research*, 318:28–35, 2017.

[30] Y. Cai, J. Arikkath, L. Yang, M.-L. Guo, P. Periyasamy, and S. Buch. Interplay of endoplasmic reticulum stress and autophagy in neurodegenerative disorders. *Autophagy*, 12(2):225–244, 2016.

[31] L. Cao, D. Li, P. Feng, L. Li, G.-F. Xue, G. Li, and C. Hölscher. A novel dual GLP-1 and GIP incretin receptor agonist is neuroprotective in a mouse model of Parkinson's disease by reducing chronic inflammation in the brain. *NeuroReport*, 27(6), 2016.

[32] G. Carpentier and E. Henault. Protein array analyzer for Image J. In *ImageJ User and Developer Conference*. Luxembourg Institute of Science and Technology, 2010.

[33] S. Casas-Tinto, Y. Zhang, J. Sanchez-Garcia, M. Gomez-Velazquez, D. E. Rincon-Limas, and P. Fernandez-Funez. The ER stress factor XBP1s prevents amyloid-β neurotoxicity. *Hum Mol Genet*, 20(11):2144–60, 2011.

[34] D. L. Castillo-Carranza, Y. Zhang, M. J. Guerrero-Munoz, R. Kayed, D. E. Rincon-Limas, and P. Fernandez-Funez. Differential activation of the ER stress factor XBP1 by oligomeric assemblies. *Neurochem Res*, 37(8):1707–17, 2012.

[35] S. M. Chafekar, J. J. Hoozemans, R. Zwart, F. Baas, and W. Scheper. Aβ_{1-42} induces mild endoplasmic reticulum stress in an aggregation state-dependent manner. *Antioxid Redox Signal*, 9(12):2245–54, 2007.

[36] S. M. Chafekar, R. Zwart, R. Veerhuis, H. Vanderstichele, F. Baas, and W. Scheper. Increased Aβ_{1-42} production sensitizes neuroblastoma cells for ER stress toxicity. *Curr Alzheimer Res*, 5(5):469–74, 2008.

[37] H. Chen, W. Lin, Y. Zhang, L. Lin, J. Chen, Y. Zeng, M. Zheng, Z. Zhuang, H. Du, R. Chen, and N. Liu. IL-10 Promotes Neurite Outgrowth and Synapse Formation in Cultured Cortical Neurons after the Oxygen-Glucose Deprivation via JAK1/STAT3 Pathway. *Scientific Reports*, 6(30459):1–16, 2016.

[38] H.-F. Chen, S.-J. Liu, and G. Chen. Heat shock protein 27 phosphorylation in the proliferation and apoptosis of human umbilical vein endothelial cells induced by high glucose through the phosphoinositide-3 kinase/Akt and extracellular signal regulated kinase 1/2 pathways. *Molecular medicine reports*, 11(2):1504–1508, 2015.

[39] K. H. Chen, E. A. Reese, H. W. Kim, S. I. Rapoport, and J. S. Rao. Disturbed neurotransmitter transporter expression in alzheimer's disease brain. *J Alzheimers Dis*, 26(4):755–66, 2011.

[40] E. H.-Y. Cheng, M. C. Wei, S. Weiler, R. A. Flavell, T. W. Mak, T. Lindsten, and S. J. Korsmeyer. BCL-2, BCL-$_X$L Sequester BH3 Domain-Only Molecules Preventing BAX- and BAK-Mediated Mitochondrial Apoptosis. *Molecular Cell*, 8(3):705–711, 2001.

[41] T. Chiba, M. Yamada, J. Sasabe, K. Terashita, M. Shimoda, M. Matsuoka, and S. Aiso. Amyloid-β causes memory impairment by disturbing the JAK2/STAT3 axis in hippocampal neurons. *Mol Psychiatry*, 14(2):206–222, 2008.

[42] M. Citron. Alzheimer's disease: strategies for disease modification. *Nat Rev Drug Discov*, 9(5):387–98, 2010.

[43] W. ClaireDominique, L. Hong, W. Sylvain, and R. Denis. Long?lasting effects of elevated neonatal leptin on rat hippocampal function, synaptic proteins and NMDA receptor subunits. *Journal of Neuroscience Research*, 85(4):816–828, 2007.

[44] E. Colla, P. Coune, Y. Liu, O. Pletnikova, J. C. Troncoso, T. Iwatsubo, B. L. Schneider, and M. K. Lee. Endoplasmic reticulum stress is important for the manifestations of α-synucleinopathy in vivo. *J Neurosci*, 32(10):3306–20, 2012.

[45] E. Colla, P. H. Jensen, O. Pletnikova, J. C. Troncoso, C. Glabe, and M. K. Lee. Accumulation of toxic α-synuclein oligomer within endoplasmic reticulum occurs in α-synucleinopathy in vivo. *journal of Neuroscience*, 32(10):3301–3305, 2012.

[46] R. O. Costa, E. Ferreiro, S. M. Cardoso, C. R. Oliveira, and C. M. Pereira. ER stress-mediated apoptotic pathway induced by Aβ peptide requires the presence of functional mitochondria. *J Alzheimers Dis*, 20(2):625–36, 2010.

[47] R. O. Costa, E. Ferreiro, I. Martins, I. Santana, S. M. Cardoso, C. R. Oliveira, and C. M. F. Pereira. Amyloid β-induced ER stress is enhanced under mitochondrial dysfunction conditions. *Neurobiology of Aging*, 33(4):824.e5–824.e16, 2012.

[48] R. O. Costa, E. Ferreiro, C. R. Oliveira, and C. M. F. Pereira. Inhibition of mitochondrial cytochrome C oxidase potentiates Aβ-induced ER stress and cell death in cortical neurons. *Molecular and Cellular Neuroscience*, 52(0):1–8, 2013.

[49] R. O. Costa, P. N. Lacor, I. L. Ferreira, R. Resende, Y. P. Auberson, W. L. Klein, C. R. Oliveira, A. C. Rego, and C. M. Pereira. Endoplasmic reticulum stress occurs downstream of GluN2B subunit of N-methyl-d-aspartate receptor in mature

hippocampal cultures treated with amyloid-β oligomers. *Aging Cell*, 11(5):823–33, 2012.

[50] J. C. Crabbe, D. Wahlsten, and B. C. Dudek. Genetics of Mouse Behavior: Interactions with Laboratory Environment. *Science*, 284(5420):1670–1672, 1999.

[51] M. Cuadrado-Tejedor, M. Vilariño, F. Cabodevilla, J. Del Río, D. Frechilla, and A. Pérez-Mediavilla. Enhanced expression of the voltage-dependent anion channel 1 (VDAC1) in Alzheimer's disease transgenic mice: an insight into the pathogenic effects of amyloid-β. *Journal of Alzheimer's disease*, 23(2):195–206, 2011.

[52] J. E. Darnell. STATs and Gene Regulation. *Science*, 277(5332):1630–1635, 1997.

[53] S. R. Datta, A. M. Ranger, M. Z. Lin, J. F. Sturgill, Y.-C. Ma, C. W. Cowan, P. Dikkes, S. J. Korsmeyer, and M. E. Greenberg. Survival factor-mediated bad phosphorylation raises the mitochondrial threshold for apoptosis. *Developmental Cell*, 3(5):631–643, 2002.

[54] F. G. De Felice. Alzheimer's disease and insulin resistance: translating basic science into clinical applications. *The Journal of Clinical Investigation*, 123(2):531–539, 2013.

[55] S. M. de la Monte. Therapeutic targets of brain insulin resistance in sporadic Alzheimer's disease. *Frontiers in bioscience (Elite edition)*, 4:1582–1605, 2012.

[56] B. De Strooper and E. Karran. The Cellular Phase of Alzheimer's Disease. *Cell*, 164(4):603–615, 2016.

[57] L. Devi and M. Ohno. Phospho-eIF2α Level Is Important for Determining Abilities of BACE1 Reduction to Rescue Cholinergic Neurodegeneration and Memory Defects in 5XFAD Mice. *PLOS ONE*, 5(9):e12974, 2010.

[58] L. Devi and M. Ohno. PERK mediates eIF2α phosphorylation responsible for BACE1 elevation, CREB dysfunction and neurodegeneration in a mouse model of Alzheimer's disease. *Neurobiology of Aging*, 35(10):2272–2281, 2014.

[59] R. D'Hooge and P. P. De Deyn. Applications of the Morris water maze in the study of learning and memory. *Brain Research Reviews*, 36(1):60–90, 2001.

[60] A. Di Nardo, I. Kramvis, N. Cho, A. Sadowski, L. Meikle, D. J. Kwiatkowski, and M. Sahin. Tuberous Sclerosis Complex Activity is Required to Control Neuronal Stress Responses in an mTOR-Dependent Manner. *The Journal of Neuroscience*, 29(18):5926–5937, 2009.

[61] K.-H. Diehl, R. Hull, D. Morton, R. Pfister, Y. Rabemampianina, D. Smith, J.-M. Vidal, and C. V. D. Vorstenbosch. A good practice guide to the administration of substances and removal of blood, including routes and volumes. *Journal of Applied Toxicology*, 21(1):15–23, 2001.

[62] K.-H. Ding, Q. Zhong, D. Xie, H.-X. Chen, M. A. Della-Fera, R. J. Bollag, W. B. Bollag, R. Gujral, B. Kang, S. Sridhar, C. Baile, W. Curl, and C. M. Lsales. Effects of glucose-dependent insulinotropic peptide on behavior. *Peptides*, 27(11):2750–2755, 2006.

[63] A. M. Duffy and C. Hölscher. The incretin analogue D-Ala^{2}GIP reduces plaque load, astrogliosis and oxidative stress in an APP/PS1 mouse model of Alzheimer's disease. *Neuroscience*, 228:294–300, 2013.

[64] M. J. During, L. Cao, D. S. Zuzga, J. S. Francis, H. L. Fitzsimons, X. Jiao, R. J. Bland, M. Klugmann, W. A. Banks, D. J. Drucker, and C. N. Haile. Glucagon-like peptide-1 receptor is involved in learning and neuroprotection. *Nature Medicine*, 9(9):1173–1179, 2003.

[65] F. J. Ekinci, K. U. Malik, and T. B. Shea. Activation of the L Voltage-sensitive Calcium Channel by Mitogen-activated Protein (MAP) Kinase following Exposure of Neuronal Cells to β-Amyloid: MAP KINASE MEDIATES β-AMYLOID-INDUCED NEURODEGENERATION . *Journal of Biological Chemistry*, 274(42):30322–30327, 1999.

[66] F. Elisabete and P. C. MF. Endoplasmic reticulum stress: a new player in tauopathies. *The journal of Pathology*, 226(5):687–692, 2012.

[67] N. Engedal, M. L. Torgersen, G. I. J, S. J. Barfeld, D. Bakula, F. Sætre, L. K. Hagen, J. B. Patterson, T. Proikas-Cezanne, P. O. Seglen, A. Simonsen, and I. G. Mills. Modulation of intracellular calcium homeostasis blocks autophagosome formation. *Autophagy*, 9(10):1475–1490, 2013.

[68] S. Facchin, M. Ruzzene, C. Peggion, G. Sartori, G. Carignani, O. Marin, F. Brustolon, R. Lopreiato, and L. A. Pinna. Phosphorylation and activation of the atypical kinase p53-related protein kinase (PRPK) by akt/PKB. *Cellular and Molecular Life Sciences*, 64(19):2680, 2007.

[69] E. Faivre, A. Hamilton, and C. Hölscher. Effects of acute and chronic administration of GIP analogues on cognition, synaptic plasticity and neurogenesis in mice. *European Journal of Pharmacology*, 674(2):294–306, 2012.

[70] E. Faivre and C. Hölscher. Neuroprotective effects of D-Ala^{2}GIP on Alzheimer's disease biomarkers in an APP/PS1 mouse model. *Alzheimer's Research & Therapy*, 5(2):20, 2013.

[71] S. A. Ferguson, S. Sarkar, and L. C. Schmued. Longitudinal behavioral changes in the app/ps1 transgenic alzheimer's disease model. *Behavioural Brain Research*, 242:125–134, 2013.

[72] E. Ferreiro, I. Baldeiras, I. L. Ferreira, R. O. Costa, A. C. Rego, C. F. Pereira, and C. R. Oliveira. Mitochondrial- and endoplasmic reticulum-associated oxidative stress in alzheimer's disease: from pathogenesis to biomarkers. *Int J Cell Biol*, 2012(735206):1–23, 2012.

[73] E. Ferreiro, C. R. Oliveira, and C. Pereira. Involvement of endoplasmic reticulum Ca^{2+} release through ryanodine and inositol-1,4,5-triphosphate receptors in the neurotoxic effects induced by the amyloid-β peptide. *Journal of Neuroscience Research*, 76(6):872–880, 2004.

[74] E. Ferreiro, R. Resende, R. Costa, C. R. Oliveira, and C. M. Pereira. An endoplasmic-reticulum-specific apoptotic pathway is involved in prion and amyloid-β peptides neurotoxicity. *Neurobiol Dis*, 23(3):669–78, 2006.

[75] I. Ferrer. Altered mitochondria, energy metabolism, voltage-dependent anion channel, and lipid rafts converge to exhaust neurons in alzheimer's disease. *journal of Bioenergetics and Biomembranes*, 41(5):425–431, 2009.

[76] B. Finan, T. Ma, N. Ottaway, T. D. Müller, K. M. Habegger, K. M. Heppner, H. Kirchner, J. Holland, J. Hembree, C. Raver, S. H. Lockie, D. L. Smiley, V. Gelfanov, B. Yang, S. Hofmann, D. Bruemmer, D. J. Drucker, P. T. Pfluger, D. Perez-Tilve, J. Gidda, L. Vignati, L. Zhang, J. B. Hauptman, M. Lau, M. Brecheisen, S. Uhles, W. Riboulet, E. Hainaut, E. Sebokova, K. Conde-Knape, A. Konkar, R. D. DiMarchi, and M. H. Tschöp. Unimolecular dual incretins maximize metabolic benefits in rodents, monkeys, and humans. *Science Translational Medicine*, 5(209):1–8, 2013.

[77] L. Forny-Germano, N. M. Lyra e Silva, A. F. Batista, J. Brito-Moreira, M. Gralle, S. E. Boehnke, B. C. Coe, A. Lablans, S. A. Marques, A. M. B. Martinez, W. L. Klein, J.-C. Houzel, S. T. Ferreira, D. P. Munoz, and F. G. De Felice. Alzheimer's

Disease-Like Pathology Induced by Amyloid-β Oligomers in Nonhuman Primates. *The Journal of Neuroscience*, 34(41):13629LP–13643, 2014.

[78] H. Förstl and A. Kurz. Clinical features of alzheimer's disease. *European Archives of Psychiatry and Clinical Neuroscience*, 249(6):288–290, 1999.

[79] O. J. Freeman and G. R. Mallucci. The UPR and synaptic dysfunction in neurodegeneration. *Brain Research*, 1648(Part B):530–537, 2016.

[80] L. Funke, S. Dakoji, and D. S. Bredt. Membrane-associated guanylate kinases regulate adhesion and plasticity at cell junctions. *Annual Review of Biochemistry*, 74(1):219–245, 2005.

[81] S. C. Gad, C. B. Spainhour, C. Shoemake, D. R. Stackhouse Pallman, A. Stricker-Krongrad, R. E. Downing, Philip A.and Seals, L. A. Eagle, K. Polhamus, and J. Daly. Tolerable levels of nonclinical vehicles and formulations used in studies by multiple routes in multiple species with notes on methods to improve utility. *International Journal of Toxicology*, 35(2):95–178, 2016.

[82] Z. Galehdar, P. Swan, B. Fuerth, S. M. Callaghan, D. S. Park, and S. P. Cregan. Neuronal Apoptosis Induced by Endoplasmic Reticulum Stress Is Regulated by ATF4–CHOP-Mediated Induction of the Bcl-2 Homology 3-Only Member PUMA. *The Journal of Neuroscience*, 30(50):16938LP–16948, 2010.

[83] M. Gallagher, R. Burwell, and M. Burchinal. Severity of spatial learning impairment in aging: development of a learning index for performance in the morris water maze. *Behav Neurosci*, 107(4):618–626, 1993.

[84] I. G. Ganley, P.-M. Wong, N. Gammoh, and X. Jiang. Distinct autophagosomal-lysosomal fusion mechanism revealed by thapsigargin-induced autophagy arrest. *Molecular Cell*, 42(6):731–743, 2011.

[85] P. Garcia-Huerta, P. Troncoso-Escudero, C. Jerez, C. Hetz, and R. L. Vidal. The intersection between growth factors, autophagy and ER stress: A new target to treat neurodegenerative diseases? *Brain Research*, 1649(PART B):173–180, 2016.

[86] M. Gejl, A. Gjedde, L. Egefjord, A. Møller, S. B. Hansen, K. Vang, A. Rodell, H. Brændgaard, H. Gottrup, A. Schacht, N. Møller, B. Brock, and J. Rungby. In Alzheimer's Disease, 6-Month Treatment with GLP-1 Analog Prevents Decline of Brain Glucose Metabolism: Randomized, Placebo-Controlled, Double-Blind Clinical Trial. *Frontiers in Aging Neuroscience*, 8:108, 2016.

[87] S. Gengler, P. L. McClean, R. McCurtin, V. A. Gault, and C. Hölscher. Val$^{(8)}$GLP-1 rescues synaptic plasticity and reduces dense core plaques in APP/PS1 mice. *Neurobiology of Aging*, 33(2):265–276, 2012.

[88] Y. Gerakis and C. Hetz. Emerging roles of ER stress in the etiology and pathogenesis of Alzheimer's disease. *The FEBS Journal*, 285(6):995–1011, 2017.

[89] A. K. Ghosh, T. Mau, M. O'Brien, S. Garg, and R. Yung. Impaired autophagy activity is linked to elevated ER-stress and inflammation in aging adipose tissue. *Aging (Albany NY)*, 8(10):2525–2536, 2016.

[90] O. Ghribi, M. M. Herman, P. Pramoonjago, N. K. Spaulding, and J. Savory. GDNF regulates the Aβ-induced endoplasmic reticulum stress response in rabbit hippocampus by inhibiting the activation of GADD153 and the JNK and ERK kinases. *Neurobiol Dis*, 16(2):417–27, 2004.

[91] C. P. Gilman, T. Perry, K. Furukawa, N. H. Grieg, J. M. Egan, and M. P. Mattson. Glucagon-like peptide 1 modulates calcium responses to glutamate and membrane depolarization in hippocampal neurons. *journal of Neurochemistry*, 87(5):1137–1144, 2003.

[92] R. E. González-Reyes, M. O. Nava-Mesa, K. Vargas-Sánchez, D. Ariza-Salamanca, and L. Mora-Muñoz. Involvement of Astrocytes in Alzheimer's Disease from a Neuroinflammatory and Oxidative Stress Perspective. *Frontiers in Molecular Neuroscience*, 10(427):1–20, 2017.

[93] M. N. Gordon, L. A. Holcomb, P. T. Jantzen, G. DiCarlo, D. Wilcock, K. W. Boyett, K. Connor, J. Melachrino, J. P. O'Callaghan, and D. Morgan. Time Course of the Development of Alzheimer-like Pathology in the Doubly Transgenic PS1+APP Mouse. *Experimental Neurology*, 173(2):183–195, 2002.

[94] T. D. Gould, D. T. Dao, and C. E. Kovacsics. The open field test. In T. D. Gould, editor, *Mood and Anxiety Related Phenotypes in Mice: Characterization Using Behavioral Tests*, pages 1–20. Humana Press, 2009.

[95] K. N. Green, A. Demuro, Y. Akbari, B. D. Hitt, I. F. Smith, I. Parker, and F. M. LaFerla. Serca pump activity is physiologically regulated by presenilin and regulates amyloid beta production. *J Cell Biol*, 181(7):1107–16, 2008.

[96] K. N. Green and F. M. LaFerla. Linking calcium to aβ and alzheimer's disease. *Neuron*, 59(2):190–4, 2008.

[97] J. D. Grill and J. L. Cummings. Current therapeutic targets for the treatment of alzheimer's disease. *Expert Rev Neurother*, 10(5):711–28, 2010.

[98] E. V. Haar, S.-i. Lee, S. Bandhakavi, T. J. Griffin, and D.-H. Kim. Insulin signalling to mTOR mediated by the Akt/PKB substrate PRAS40. *Nature Cell Biology*, 9(3):316–323, 2007.

[99] J. E. Hamos, B. Oblas, D. Pulaski-Salo, W. J. Welch, D. G. Bole, and D. A. Drachman. Expression of heat shock proteins in Alzheimer's disease. *Neurology*, 41(3):345–50, 1991.

[100] J. Han, S. H. Back, J. Hur, Y.-H. Lin, R. Gildersleeve, J. Shan, C. L. Yuan, D. Krokowski, S. Wang, M. Hatzoglou, M. S. Kilberg, M. A. Sartor, and R. J. Kaufman. ER-stress-induced transcriptional regulation increases protein synthesis leading to cellÊdeath. *Nature Cell Biology*, 15:481–490, 2013.

[101] H. H. Hansen, P. Barkholt, K. Fabricius, J. Jelsing, D. Terwel, C. Pyke, L. B. Knudsen, and N. Vrang. The GLP-1 receptor agonist liraglutide reduces pathology-specific tau phosphorylation and improves motor function in a transgenic htaup301l mouse model of tauopathy. *Brain Research*, 1634:158–170, 2016.

[102] H. H. Hansen, K. Fabricius, P. Barkholt, M. L. Niehoff, J. E. Morley, J. Jelsing, C. Pyke, L. B. Knudsen, S. A. Farr, and N. Vrang. The GLP-1 Receptor Agonist Liraglutide Improves Memory Function and Increases Hippocampal CA1 Neuronal Numbers in a Senescence-Accelerated Mouse Model of Alzheimer's Disease. *Journal of Alzheimer's Disease*, 46(4):877–888, 2015.

[103] A. Harkavyi, A. Abuirmeileh, R. Lever, A. E. Kingsbury, C. S. Biggs, and P. S. Whitton. Glucagon-like peptide 1 receptor stimulation reverses key deficits in distinct rodent models of parkinson's disease. *journal of Neuroinflammation*, 5(1):1–9, 2008.

[104] N. J. Haughey, V. V. R. Bandaru, M. Bae, and M. P. Mattson. Roles for dysfunctional sphingolipid metabolism in Alzheimer's disease neuropathogenesis. *Biochimica et Biophysica Acta (BBA) - Molecular and Cell Biology of Lipids*, 1801(8):878–886, 2010.

[105] Q. He, S. Sha, L. Sun, J. Zhang, and M. Dong. Glp-1 analogue improves hepatic lipid accumulation by inducing autophagy via ampk/mtor pathway. *Biochemical and Biophysical Research Communications*, 476(4):196–203, 2016.

[106] D. Heras-Sandoval, J. M. Pérez-Rojas, J. Hernández-Damián, and J. Pedraza-Chaverri. The role of PI3K/AKT/mTOR pathway in the modulation of autophagy and the clearance of protein aggregates in neurodegeneration. *Cellular Signalling*, 26(12):2694–2701, 2014.

[107] F. Hernández, J. Borrell, C. Guaza, J. Avila, and J. J. Lucas. Spatial learning deficit in transgenic mice that conditionally over-express GSK-3β in the brain but do not form tau filaments. *Journal of neurochemistry*, 83(6):1529–1533, 2002.

[108] C. Hetz. The unfolded protein response: controlling cell fate decisions under ER stress and beyond. *Nat Rev Mol Cell Biol*, 13(2):89–102, 2012.

[109] C. Hetz, E. Chevet, and S. A. Oakes. Proteostasis control by the unfolded protein response. *Nat Cell Biol*, 17:829–838, 2015.

[110] C. Hetz, F. Martinon, D. Rodriguez, and L. H. Glimcher. The unfolded protein response: integrating stress signals through the stress sensor ire1α. *Physiol Rev*, 91(4):1219–43, 2011.

[111] C. Hetz and B. Mollereau. Disturbance of endoplasmic reticulum proteostasis in neurodegenerative diseases. *Nat Rev Neurosci*, 15(4):233–49, 2014.

[112] S. A. Hinke, R. W. Gelling, R. A. Pederson, S. Manhart, C. Nian, H.-U. Demuth, and C. H. McIntosh. Dipeptidyl peptidase iv-resistant [$_D$-ala^2] glucose-dependent insulinotropic polypeptide (gip) improves glucose tolerance in normal and obese diabetic rats. *Diabetes*, 51(3):652–661, 2002.

[113] G. U. Hoglinger, N. M. Melhem, D. W. Dickson, P. M. Sleiman, L. S. Wang, L. Klei, R. Rademakers, R. de Silva, I. Litvan, D. E. Riley, J. C. van Swieten, P. Heutink, Z. K. Wszolek, R. J. Uitti, J. Vandrovcova, H. I. Hurtig, R. G. Gross, W. Maetzler, S. Goldwurm, E. Tolosa, B. Borroni, P. Pastor, L. B. Cantwell, M. R. Han, A. Dill-

man, M. P. van der Brug, J. R. Gibbs, M. R. Cookson, D. G. Hernandez, A. B. Singleton, M. J. Farrer, C. E. Yu, L. I. Golbe, T. Revesz, J. Hardy, A. J. Lees, B. Devlin, H. Hakonarson, U. Muller, and G. D. Schellenberg. Identification of common variants influencing risk of the tauopathy progressive supranuclear palsy. *Nat Genet*, 43(7):699–705, 2011.

[114] E. M. Hol and M. Pekny. Glial fibrillary acidic protein (gfap) and the astrocyte intermediate filament system in diseases of the central nervous system. *Current Opinion in Cell Biology*, 32(Supplement C):121–130, 2015.

[115] C. Hölscher. The incretin hormones glucagonlike peptide 1 and glucose-dependent insulinotropic polypeptide are neuroprotective in mouse models of alzheimer's disease. *Alzheimer's & Dementia: The journal of the Alzheimer's Association*, 10(1):S47–S54, 2014.

[116] C. Hölscher. Novel dual GLP-1/GIP receptor agonists show neuroprotective effects in Alzheimer's and Parkinson's disease models. *Neuropharmacology*, *In Press*, 2018.

[117] G. G. Holz. Epac: A new camp-binding protein in support of glucagon-like peptide-1 receptor-mediated signal transduction in the pancreatic ?-cell. *Diabetes*, 53(1):5–13, 2003.

[118] J. J. Hoozemans and W. Scheper. Endoplasmic reticulum: the unfolded protein response is tangled in neurodegeneration. *Int J Biochem Cell Biol*, 44(8):1295–8, 2012.

[119] J. J. Hoozemans, E. S. van Haastert, D. A. Nijholt, A. J. Rozemuller, P. Eikelenboom, and W. Scheper. The unfolded protein response is activated in pretangle neurons in alzheimer's disease hippocampus. *Am J Pathol*, 174(4):1241–51, 2009.

[120] J. J. Hoozemans, R. Veerhuis, E. S. Van Haastert, J. M. Rozemuller, F. Baas, P. Eikelenboom, and W. Scheper. The unfolded protein response is activated in alzheimer's disease. *Acta Neuropathol*, 110(2):165–72, 2005.

[121] J. J. M. Hoozemans, E. S. van Haastert, D. A. T. Nijholt, A. J. M. Rozemuller, and W. Scheper. Activation of the Unfolded Protein Response Is an Early Event in Alzheimer's and Parkinson's Disease. *Neurodegenerative Diseases*, 10:1–4, 2012.

[122] T. Hosoi, K. Hyoda, Y. Okuma, Y. Nomura, and K. Ozawa. Akt up- and down-regulation in response to endoplasmic reticulum stress. *Brain Research*, 1152:27–31, 2007.

[123] T. Hosoi, M. Sasaki, T. Miyahara, C. Hashimoto, S. Matsuo, M. Yoshii, and K. Ozawa. Endoplasmic reticulum stress induces leptin resistance. *Molecular Pharmacology*, 74(6):1610–1619, 2008.

[124] P. Hu, Z. Han, A. D. Couvillon, and J. H. Exton. Critical role of endogenous akt/iaps and mek1/erk pathways in counteracting endoplasmic reticulum stress-induced cell death. *journal of Biological Chemistry*, 279(47):49420–49429, 2004.

[125] Y. Huang and L. Mucke. Alzheimer Mechanisms and Therapeutic Strategies. *Cell*, 148(6):1204–1222, 2010.

[126] K. Hunter and C. Hölscher. Drugs developed to treat diabetes, liraglutide and lixisenatide, cross the blood brain barrier and enhance neurogenesis. *BMC Neurosci*, 13:33, 2012.

[127] C. Hyun Lee, B. Yan, K.-Y. Yoo, J. H. Choi, S.-H. Kwon, S. Her, Y. Sohn, I. K. Hwang, J. H. Cho, Y.-M. Kim, and M.-H. Won. Ischemia-induced changes in glucagon-like peptide-1 receptor and neuroprotective effect of its agonist, exendin-

4, in experimental transient cerebral ischemia. *Journal of Neuroscience Research*, 89(7):1103–1113, 2011.

[128] T. Imai, Y. Kosuge, K. Ishige, and Y. Ito. Amyloid β-protein potentiates tunicamycin-induced neuronal death in organotypic hippocampal slice cultures. *Neuroscience*, 147(3):639–51, 2007.

[129] S. Inoue. In situ Aβ pores in AD brain are cylindrical assembly of Aβ protofilaments. *Amyloid*, 15(4):223–233, 2008.

[130] A. M. Isaacs, D. B. Senn, M. Yuan, J. P. Shine, and B. A. Yankner. Acceleration of Amyloid β-Peptide Aggregation by Physiological Concentrations of Calcium. *Journal of Biological Chemistry*, 281(38):27916–27923, 2006.

[131] D. Ito, Y. Imai, K. Ohsawa, K. Nakajima, Y. Fukuuchi, and S. Kohsaka. Microglia-specific localisation of a novel calcium binding protein, iba1. *Molecular Brain Research*, 57(1):1–9, 1998.

[132] P. A. Jaeger, F. Pickford, C.-H. Sun, K. M. Lucin, E. Masliah, and T. Wyss-Coray. Regulation of Amyloid Precursor Protein Processing by the Beclin 1 Complex. *PLOS ONE*, 5(6):e11102, 2010.

[133] J. Jalewa, M. K. Sharma, S. Gengler, and C. Hölscher. A novel GLP-1/GIP dual receptor agonist protects from 6-OHDA lesion in a rat model of Parkinson's disease. *Neuropharmacology*, 117:238–248, 2017.

[134] J. Jalewa, M. K. Sharma, and C. Hölscher. Novel incretin analogues improve autophagy and protect from mitochondrial stress induced by rotenone in SH-SY5Y cells. *journal of Neurochemistry*, 139(1):55–67, 2016.

[135] J. L. Jankowsky, D. J. Fadale, J. Anderson, G. M. Xu, V. Gonzales, N. A. Jenkins, N. G. Copeland, M. K. Lee, L. H. Younkin, S. L. Wagner, S. G. Younkin, and

D. R. Borchelt. Mutant presenilins specifically elevate the levels of the 42 residue β-amyloid peptide *in vivo*: evidence for augmentation of a 42-specific γ secretase. *Human molecular genetics*, 13(2):159–170, 2004.

[136] C. Ji, G.-F. Xue, C. Lijun, P. Feng, D. Li, L. Li, G. Li, and C. Hölscher. A novel dual GLP-1 and GIP receptor agonist is neuroprotective in the MPTP mouse model of Parkinson's disease by increasing expression of BNDF. *Brain Research*, 1634:1–11, 2016.

[137] J. Jing Yin, Y. bo Li, M. ming Cao, and Y. Wang. Liraglutide improves the survival of ins-1 cells by promoting macroautophagy. *International journal of Endocrinology and Metabolism*, 11(3):184–190, 2013.

[138] M. E. Jönhagen. Nerve Growth Factor Treatment in Dementia. *Alzheimer Disease & Associated Disorders*, 14(1), 2000.

[139] C. Kakiuchi, K. Iwamoto, M. Ishiwata, M. Bundo, T. Kasahara, I. Kusumi, T. Tsujita, Y. Okazaki, S. Nanko, H. Kunugi, T. Sasaki, and T. Kato. Impaired feedback regulation of xbp1 as a genetic risk factor for bipolar disorder. *Nat Genet*, 35(2):171–5, 2003.

[140] M. Kallnik, R. Elvert, N. Ehrhardt, D. Kissling, E. Mahabir, G. Welzl, T. Faus-Kessler, M. H. de Angelis, W. Wurst, J. Schmidt, and S. M. Hölter. Impact of IVC housing on emotionality and fear learning in male C3HeB/FeJ and C57BL/6J mice. *Mammalian Genome*, 18(3):173–186, 2007.

[141] F. Kamenetz, T. Tomita, H. Hsieh, G. Seabrook, D. Borchelt, T. Iwatsubo, S. Sisodia, and R. Malinow. App processing and synaptic function. *Neuron*, 37(6):925–37, 2003.

[142] M. Kaneko, H. Koike, R. Saito, Y. Kitamura, Y. Okuma, and Y. Nomura. Loss of hrd1-mediated protein degradation causes amyloid precursor protein accumulation and amyloid-β generation. *J Neurosci*, 30(11):3924–32, 2010.

[143] T. Katayama, K. Imaizumi, T. Manabe, J. Hitomi, T. Kudo, and M. Tohyama. Induction of neuronal death by er stress in alzheimer's disease. *J Chem Neuroanat*, 28(1-2):67–78, 2004.

[144] R. J. Kaufman and J. D. Malhotra. Calcium trafficking integrates endoplasmic reticulum function with mitochondrial bioenergetics. *Biochimica et Biophysica Acta (BBA) - Molecular Cell Research*, 1843(10):2233–2239, 2014.

[145] V. Kazlauckas, N. Pagnussat, S. Mioranzza, E. Kalinine, F. Nunes, L. Pettenuzzo, D. O.Souza, L. V. Portela, L. O. Porciúncula, and D. R. Lara. Enriched environment effects on behavior, memory and BDNF in low and high exploratory mice. *Physiology & Behavior*, 102(5):475–480, 2011.

[146] K. Kimura, T. Yamada, M. Matsumoto, Y. Kido, T. Hosooka, S.-i. Asahara, T. Matsuda, T. Ota, H. Watanabe, Y. Sai, K. Miyamoto, S. Kaneko, M. Kasuga, and H. Inoue. Endoplasmic reticulum stress inhibits stat3-dependent suppression of hepatic gluconeogenesis via dephosphorylation and deacetylation. *Diabetes*, 61(1):61–73, 2011.

[147] Y. Kitamura, A. Miyamura, K. Takata, M. Inden, D. Tsuchiya, K. Nakamura, and T. Taniguchi. Possible involvement of both endoplasmic reticulum-and mitochondria-dependent pathways in thapsigargin-induced apoptosis in human neuroblastoma sh-sy5y cells. *journal of Pharmacological Sciences*, 92(3):228–236, 2003.

[148] D. J. Klionsky, K. Abdelmohsen, A. Abe, M. J. Abedin, H. Abeliovich, and Abraham, A.A. *et. al*. Guidelines for the use and interpretation of assays for monitoring

autophagy (3^{rd} edition). *Autophagy*, 12(1):1–222, 2016.

[149] M. Komatsu, H. Kurokawa, S. Waguri, K. Taguchi, A. Kobayashi, Y. Ichimura, Y.-S. Sou, I. Ueno, A. Sakamoto, K. I. Tong, M. Kim, Y. Nishito, S.-i. Iemura, T. Natsume, T. Ueno, E. Kominami, H. Motohashi, K. Tanaka, and M. Yamamoto. The selective autophagy substrate p62 activates the stress responsive transcription factor nrf2 through inactivation of keap1. *Nat Cell Biol*, 12(3):213–223, 2010.

[150] M. Komatsu, S. Waguri, T. Chiba, S. Murata, J.-i. Iwata, I. Tanida, T. Ueno, M. Koike, Y. Uchiyama, E. Kominami, and K. Tanaka. Loss of autophagy in the central nervous system causes neurodegeneration in mice. *Nature*, 441:880–884, 2006.

[151] T. Kondo, M. Asai, K. Tsukita, Y. Kutoku, Y. Ohsawa, Y. Sunada, K. Imamura, N. Egawa, N. Yahata, K. Okita, K. Takahashi, I. Asaka, T. Aoi, A. Watanabe, K. Watanabe, C. Kadoya, R. Nakano, D. Watanabe, K. Maruyama, O. Hori, S. Hibino, T. Choshi, T. Nakahata, H. Hioki, T. Kaneko, M. Naitoh, K. Yoshikawa, S. Yamawaki, S. Suzuki, R. Hata, S. Ueno, T. Seki, K. Kobayashi, T. Toda, K. Murakami, K. Irie, W. L. Klein, H. Mori, T. Asada, R. Takahashi, N. Iwata, S. Yamanaka, and H. Inoue. Modeling alzheimer's disease with ipscs reveals stress phenotypes associated with intracellular aβ and differential drug responsiveness. *Cell Stem Cell*, 12(4):487–96, 2013.

[152] E. Korkotian and M. Segal. Fast confocal imaging of calcium released from stores in dendritic spines. *European Journal of Neuroscience*, 10(6):2076–2084, 1998.

[153] Y. Kosuge, T. Sakikubo, K. Ishige, and Y. Ito. Comparative study of endoplasmic reticulum stress-induced neuronal death in rat cultured hippocampal and cerebellar granule neurons. *Neurochem Int*, 49(3):285–93, 2006.

[154] N. J. Kruger. The Bradford method for protein quantitation. In J. M. Walker, editor, *The Protein Protocols Handbook*, pages 17–24. Humana Press, 2009.

[155] J.-P. Kruse and W. Gu. Modes of p53 regulation. *Cell*, 137(4):609–622, 2009.

[156] R. Lalonde, H. D. Kim, J. A. Maxwell, and K. Fukuchi. Exploratory activity and spatial learning in 12-month-old $APP_{(695)}$SWE/co+PS1/Δ E9 mice with amyloid plaques. *Neuroscience Letters*, 390(2):87–92, 2005.

[157] M. Laplante and D. M. Sabatini. mTOR signaling at a glance. *Journal of Cell Science*, 122(20):3589–3594, 2009.

[158] J. H. Ledo, E. P. Azevedo, J. R. Clarke, F. C. Ribeiro, C. P. Figueiredo, D. Foguel, F. G. De Felice, and S. T. Ferreira. Amyloid-β oligomers link depressive-like behavior and cognitive deficits in mice. *Molecular Psychiatry*, 18:1053–1054, 2012.

[159] A. S. Lee. The ER chaperone and signaling regulator GRP78/BiP as a monitor of endoplasmic reticulum stress. *Methods*, 35(4):373–381, 2005.

[160] J. Lee, S. Won, J. Suh, S. Son, G. Moon, U. Park, and B. Gwag. Induction of the unfolded protein response and cell death pathway in alzheimer's disease, but not in aged tg2576 mice. *Experimental & Molecular Medicine*, 42:386–394, 2010.

[161] Y. Lee do, K. S. Lee, H. J. Lee, H. Kim do, Y. H. Noh, K. Yu, H. Y. Jung, S. H. Lee, J. Y. Lee, Y. C. Youn, Y. Jeong, D. K. Kim, W. B. Lee, and S. S. Kim. Activation of perk signaling attenuates aβ-mediated er stress. *PLoS ONE*, 5(5):e10489, 2010.

[162] A. G. Lerner, J.-P. Upton, P. V. K. Praveen, R. Ghosh, Y. Nakagawa, A. Igbaria, S. Shen, V. Nguyen, B. J. Backes, M. Heiman, N. Heintz, P. Greengard, S. Hui, Q. Tang, A. Trusina, S. A. Oakes, and F. R. Papa. IRE1α induces thioredoxin-interacting protein to activate the NLRP3 inflammasome and promote programmed cell death during endoplasmic reticulum stress. *Cell metabolism*, 16(2):250–264, 2012.

[163] G. Li, M. Mongillo, K.-T. Chin, H. Harding, D. Ron, A. R. Marks, and I. Tabas. Role of ero1-α mediated stimulation of inositol 1,4,5-triphosphate receptor activity in endoplasmic reticulum stress-induced apoptosis. *The journal of Cell Biology*, 186(6):783–792, 2009.

[164] H. Li, A. V. Korennykh, S. L. Behrman, and P. Walter. Mammalian endoplasmic reticulum stress sensor ire1 signals by dynamic clustering. *Proceedings of the National Academy of Sciences*, 107(37):16113–16118, 2010.

[165] J. Q. Li, J. T. Yu, T. Jiang, and L. Tan. Endoplasmic reticulum dysfunction in alzheimer's disease. *Mol Neurobiol*, 51(1):383–95, 2014.

[166] Y. Li, M. Bader, I. Tamargo, V. Rubovitch, D. Tweedie, C. G. Pick, and N. H. Greig. Liraglutide is neurotrophic and neuroprotective in neuronal cultures and mitigates mild traumatic brain injury in mice. *journal of Neurochemistry*, 135(6):1203–1217, 2015.

[167] Y. Li, T. Perry, M. S. Kindy, B. K. Harvey, D. Tweedie, H. W. Holloway, K. Powers, H. Shen, J. M. Egan, K. Sambamurti, A. Brossi, D. K. Lahiri, M. P. Mattson, B. J. Hoffer, Y. Wang, and N. H. Greig. GLP-1 receptor stimulation preserves primary cortical and dopaminergic neurons in cellular and rodent models of stroke and parkinsonism. *Proceedings of the National Academy of Sciences*, 106(4):1285–1290, 2009.

[168] C.-P. Liang, S. Han, G. Li, I. Tabas, and A. R. Tall. Impaired MEK signaling and SERCA expression promote ER stress and apoptosis in insulin-resistant macrophages and are reversed by exenatide treatment. *Diabetes*, 61(10):2609–2620, 2012.

[169] J. H. Lin, H. Li, D. Yasumura, H. R. Cohen, C. Zhang, B. Panning, K. M. Shokat, M. M. LaVail, and P. Walter. IRE1 signaling affects cell fate during the unfolded

protein response. *Science*, 318(5852):944–949, 2007.

[170] Q. Lin, Y. Cao, and J. Gao. Serum Calreticulin Is a Negative Biomarker in Patients with Alzheimer's Disease. *International Journal of Molecular Sciences*, 15(12):21740–21753, 2014.

[171] M. Lind. Incretin therapy and its effect on body weight in patients with diabetes. *Primary Care Diabetes*, 6(3):187–191, 2012.

[172] M. M. Lipinski, G. Hoffman, A. Ng, W. Zhou, B. F. Py, E. Hsu, X. Liu, J. Eisenberg, J. Liu, J. Blenis, R. J. Xavier, and J. Yuan. A genome-wide siRNA screen reveals multiple mTORC1 independent signaling pathways regulating autophagy under normal nutritional conditions. *Developmental Cell*, 18(6):1041–1052, 2010.

[173] K. L. Lipson, S. G. Fonseca, S. Ishigaki, L. X. Nguyen, E. Foss, R. Bortell, A. A. Rossini, and F. Urano. Regulation of insulin biosynthesis in pancreatic beta cells by an endoplasmic reticulum-resident protein kinase IRE1. *Cell metabolism*, 4(3):245–254, 2006.

[174] B. Liu, Y. Zhu, J. Zhou, Y. Wei, C. Long, M. Chen, Y. Ling, J. Ge, and Y. Zhuo. Endoplasmic reticulum stress promotes amyloid-β peptides production in RGC-5 cells. *Cell Stress Chaperones*, 19(6):827–35, 2014.

[175] D. Liu, X. Liu, T. Zhou, W. Yao, J. Zhao, Z. Zheng, W. Jiang, F. Wang, F. O. Aikhionbare, D. L. Hill, N. Emmett, Z. Guo, D. Wang, X. Yao, and Y. Chen. IRE1–RACK1 axis orchestrates ER stress preconditioning-elicited cytoprotection from ischemia/reperfusion injury in liver. *journal of Molecular Cell Biology*, 8(2):144, 2016.

[176] S.-Y. Liu, W. Wang, Z.-Y. Cai, L.-F. Yao, Z.-W. Chen, C.-Y. Wang, B. Zhao, and K.-S. Li. Polymorphism –116c/g of human x-box-binding protein 1 promoter is associated

with risk of alzheimer's disease. *CNS Neuroscience & Therapeutics*, 19(4):229–234, 2013.

[177] W. Liu, J. Jalewa, M. Sharma, G. Li, L. Li, and C. Hölscher. Neuroprotective effects of lixisenatide and liraglutide in the 1-methyl-4-phenyl-1,2,3,6-tetrahydropyridine mouse model of Parkinson's disease. *Neuroscience*, 303:42–50, 2015.

[178] Z. C. Liu, Z. Q. Fu, J. Song, J. Y. Zhang, Y. P. Wei, J. Chu, L. Han, N. Qu, J. Z. Wang, and Q. Tian. Bip enhanced the association of GSK-3β with tau during ER stress both in vivo and in vitro. *J Alzheimers Dis*, 29(4):727–40, 2012.

[179] M. Llorens-Marítin, J. Jurado, F. Hernández, and J. Ávila. GSK-3β, a pivotal kinase in Alzheimer's disease. *Frontiers in Molecular Neuroscience*, 7(46):1–11, 2014.

[180] C. A. Loewen and M. B. Feany. The unfolded protein response protects from tau neurotoxicity in vivo. *PLoS ONE*, 5(9):e13084, 2010.

[181] J. Lotharius, S. Barg, P. Wiekop, C. Lundberg, H. K. Raymon, and P. Brundin. Effect of mutant α-synuclein on dopamine homeostasis in a new human mesencephalic cell line. *Journal of Biological Chemistry*, 277(41):38884–38894, 2002.

[182] J. Lotharius, J. Falsig, J. van Beek, S. Payne, R. Dringen, P. Brundin, and M. Leist. Progressive degeneration of human mesencephalic neuron-derived cells triggered by dopamine-dependent oxidative stress is dependent on the mixed-lineage kinase pathway. *Journal of Neuroscience*, 25(27):6329–6342, 2005.

[183] M. Lourenco, J. Clarke, R. Frozza, T. Bomfim, L. Forny-Germano, A. Batista, L. Sathler, J. Brito-Moreira, O. Amaral, C. Silva, L. Freitas-Correa, S. Espírito-Santo, P. Campello-Costa, J.-C. Houzel, W. Klein, C. Hölscher, J. Carvalheira, A. Silva, L. Velloso, D. Munoz, S. Ferreira, and F. De Felice. TNF-α Mediates PKR-Dependent

Memory Impairment and Brain IRS-1 Inhibition Induced by Alzheimer's β-Amyloid Oligomers in Mice and Monkeys. *Cell Metabolism*, 18(6):831–843, 2013.

[184] M. Lu, D. A. Lawrence, S. Marsters, D. Acosta-Alvear, P. Kimmig, A. S. Mendez, A. W. Paton, J. C. Paton, P. Walter, and A. Ashkenazi. Opposing unfolded-protein-response signals converge on death receptor 5 to control apoptosis. *Science*, 345(6192):98–101, 2014.

[185] K. Lucin, C. O'Brien, G. Bieri, E. Czirr, K. Mosher, R. Abbey, D. Mastroeni, J. Rogers, B. Spencer, E. Masliah, and T. Wyss-Coray. Microglial Beclin 1 Regulates Retromer Trafficking and Phagocytosis and Is Impaired in Alzheimer’s Disease. *Neuron*, 79(5):873–886, 2013.

[186] Q. Ma. Role of nrf2 in oxidative stress and toxicity. *Annual review of pharmacology and toxicology*, 53:401–426, 2013.

[187] X. Ma, W. Lin, Z. Lin, M. Hao, X. Gao, Y. Zhang, and H. Kuang. Liraglutide alleviates h2o2-induced retinal ganglion cells injury by inhibiting autophagy through mitochondrial pathways. *Peptides*, 92(Supplement C):1–8, 2017.

[188] T. M. Malm, T. R. Jay, and G. E. Landreth. The Evolving Biology of Microglia in Alzheimer's Disease. *Neurotherapeutics*, 12(1):81–93, 2015.

[189] B. D. Manning and L. C. Cantley. AKT/PKB signaling: Navigating downstream. *Cell*, 129(7):1261–1274, 2007.

[190] B. D. Manning and A. Toker. AKT/PKB Signaling: Navigating the Network. *Cell*, 169(3):381–405, 2017.

[191] S. J. Marciniak, C. Y. Yun, S. Oyadomari, I. Novoa, Y. Zhang, R. Jungreis, K. Nagata, H. P. Harding, and D. Ron. Chop induces death by promoting protein syn-

thesis and oxidation in the stressed endoplasmic reticulum. *Genes & Development*, 18(24):3066–3077, 2004.

[192] A. Margariti, H. Li, T. Chen, D. Martin, G. Vizcay-Barrena, S. Alam, E. Karamariti, Q. Xiao, A. Zampetaki, Z. Zhang, W. Wang, Z. Jiang, C. Gao, B. Ma, Y.-G. Chen, G. Cockerill, Y. Hu, Q. Xu, and L. Zeng. Xbp1 mrna splicing triggers an autophagic response in endothelial cells through BECLIN-1 transcriptional activation. *journal of Biological Chemistry*, 288(2):859–872, 2013.

[193] G. Martínez, R. Vidal, P. Mardones, F. Serrano, A. Ardiles, C. Wirth, P. Valdés, P. Thielen, B. Schneider, B. Kerr, J. Valdés, A. Palacios, N. Inestrosa, L. Glimcher, and C. Hetz. Regulation of Memory Formation by the Transcription Factor XBP1. *Cell Reports*, 14(6):1382–1394, 2016.

[194] E. V. Maytin, M. Ubeda, J. C. Lin, and J. F. Habener. Stress-Inducible Transcription Factor CHOP/gadd153 Induces Apoptosis in Mammalian Cells via p38 Kinase-Dependent and -Independent Mechanisms. *Experimental Cell Research*, 267(2):193–204, 2001.

[195] P. L. McClean and C. Hölscher. Liraglutide can reverse memory impairment, synaptic loss and reduce plaque load in aged APP/PS1 mice, a model of Alzheimer's disease. *Neuropharmacology*, 76, Part A(0):57–67, 2014.

[196] P. L. McClean and C. Hölscher. Lixisenatide, a drug developed to treat type 2 diabetes, shows neuroprotective effects in a mouse model of Alzheimer's disease. *Neuropharmacology*, 86(0):241–258, 2014.

[197] P. L. McClean, J. Jalewa, and C. Hölscher. Prophylactic liraglutide treatment prevents amyloid plaque deposition, chronic inflammation and memory impairment in APP/PS1 mice. *Behavioural Brain Research*, 293(Supplement C):96–106, 2015.

[198] P. L. McClean, V. Parthsarathy, E. Faivre, and C. Hölscher. The diabetes drug liraglutide prevents degenerative processes in a mouse model of Alzheimer's disease. *The journal of Neuroscience*, 31(17):6587–6594, 2011.

[199] G. P. Meares, Y. Liu, R. Rajbhandari, H. Qin, S. E. Nozell, J. A. Mobley, J. A. Corbett, and E. N. Benveniste. PERK-dependent activation of JAK1 and STAT3 contributes to endoplasmic reticulum stress-induced inflammation. *Molecular and Cellular Biology*, 34(20):3911–3925, 2014.

[200] G. P. Meares, M. A. Mines, E. Beurel, T.-Y. Eom, L. Song, A. A. Zmijewska, and R. S. Jope. Glycogen synthase kinase-3 regulates endoplasmic reticulum (ER) stress-induced CHOP expression in neuronal cells. *Experimental Cell Research*, 317(11):1621–1628, 2011.

[201] B. Mellström and J. R. Naranjo. Mechanisms of Ca^{2+}-dependent transcription. *Current Opinion in Neurobiology*, 11(3):312–319, 2001.

[202] M. A. Meraz-Ríos, D. Toral-Rios, D. Franco-Bocanegra, J. Villeda-Hernández, and V. Campos-Peña. Inflammatory process in Alzheimer's Disease. *Front Integr Neurosci*, 7(59):1–15, 2013.

[203] N. Morishima, K. Nakanishi, H. Takenouchi, T. Shibata, and Y. Yasuhiko. An endoplasmic reticulum stress-specific caspase cascade in apoptosis: Cytochrome c-independent activation of caspase-9 by caspase-12. *journal of Biological Chemistry*, 277(37):34287–34294, 2002.

[204] R. Morris. Developments of a water-maze procedure for studying spatial learning in the rat. *Journal of Neuroscience Methods*, 11(1):47–60, 1984.

[205] D. B. Morton, M. Jennings, A. Buckwell, R. Ewbank, C. Godfrey, B. Holgate, I. Inglis, R. James, C. Page, I. Sharman, R. Verschoyle, L. Westall, and A. B. Wilson. Refining

procedures for the administration of substances. *Laboratory Animals*, 35(1):1–41, 2001.

[206] Z. Mounir, J. L. Krishnamoorthy, S. Wang, B. Papadopoulou, S. Campbell, W. J. Muller, M. Hatzoglou, and A. E. Koromilas. Akt determines cell fate through inhibition of the PERK-eIF2α phosphorylation pathway. *Science Signaling*, 4(192):ra62, 2011.

[207] X. Mungarro-Menchaca, P. Ferrera, J. Morán, and C. Arias. β-Amyloid peptide induces ultrastructural changes in synaptosomes and potentiates mitochondrial dysfunction in the presence of ryanodine. *Journal of Neuroscience Research*, 68(1):89–96, 2002.

[208] V. Muresan and Z. Muresan. A persistent stress response to impeded axonal transport leads to accumulation of amyloid-β in the endoplasmic reticulum, and is a probable cause of sporadic alzheimer's disease. *Neurodegener Dis*, 10(1–4):60–3, 2012.

[209] A. H. Nagahara, D. A. Merrill, G. Coppola, S. Tsukada, B. E. Schroeder, G. M. Shaked, L. Wang, A. Blesch, A. Kim, J. M. Conner, E. Rockenstein, M. V. Chao, E. H. Koo, D. Geschwind, E. Masliah, A. A. Chiba, and M. H. Tuszynski. Neuroprotective effects of brain-derived neurotrophic factor in rodent and primate models of Alzheime's disease. *Nature Medicine*, 15:331–337, 2009.

[210] N. Naidoo. Er and aging — protein folding and the er stress response. *Ageing Research Reviews*, 8(3):150–159, 2009.

[211] T. Nakagawa and J. Yuan. Cross-Talk between Two Cysteine Protease Families. *The Journal of Cell Biology*, 150(4):887–894, 2000.

[212] T. Nakagawa, H. Zhu, N. Morishima, E. Li, J. Xu, B. A. Yankner, and J. Yuan. Caspase-12 mediates endoplasmic-reticulum-specific apoptosis and cytotoxicity by amyloid-β. *Nature*, 403(6765):98–103, 2000.

[213] V. P. Nakka, P. Prakash-babu, and R. Vemuganti. Crosstalk between endoplasmic reticulum stress, oxidative stress and autophagy: Potential therapeutic targets for acute CNS injuries. *Molecular Neurobiology*, 53(1):532–544, 2016.

[214] C. S. Nicolas, M. Amici, Z. A. Bortolotto, A. Doherty, Z. Csaba, A. Fafouri, P. Dournaud, P. Gressens, G. L. Collingridge, and S. Peineau. The role of JAK-STAT signaling within the CNS. *JAK-STAT*, 2(1):e22925, 2013.

[215] L. L. Nielsen, A. A. Young, and D. G. Parkes. Pharmacology of exenatide (synthetic exendin-4): a potential therapeutic for improved glycemic control of type 2 diabetes. *Regulatory Peptides*, 117(2):77–88, 2004.

[216] D. A. T. Nijholt, A. Nölle, E. S. van Haastert, H. Edelijn, R. F. Toonen, J. J. M. Hoozemans, and W. Scheper. Unfolded protein response activates glycogen synthase kinase-3 via selective lysosomal degradation. *Neurobiology of Aging*, 34(7):1759–1771, 2013.

[217] D. A. T. Nijholt, E. S. van Haastert, A. J. M. Rozemuller, W. Scheper, and J. J. M. Hoozemans. The unfolded protein response is associated with early tau pathology in the hippocampus of tauopathies. *The journal of Pathology*, 226(5):693–702, 2012.

[218] K. Nishitsuji, T. Tomiyama, K. Ishibashi, K. Ito, R. Teraoka, M. P. Lambert, W. L. Klein, and H. Mori. The E693δ mutation in amyloid precursor protein increases intracellular accumulation of amyloid β oligomers and causes endoplasmic reticulum stress-induced apoptosis in cultured cells. *The American journal of Pathology*, 174(3):957–969, 2009.

[219] R. A. Nixon. Autophagy, amyloidogenesis and Alzheimer disease. *Journal of Cell Science*, 120(23):4081LP–4091, 2007.

[220] R. A. Nixon, J. Wegiel, A. Kumar, W. H. Yu, C. Peterhoff, A. Cataldo, and A. M. Cuervo. Extensive Involvement of Autophagy in Alzheimer Disease: An Immuno-Electron Microscopy Study. *Journal of Neuropathology & Experimental Neurology*, 64(2):113–122, 2005.

[221] J. Nyberg, M. F. Anderson, B. Meister, A.-M. Alborn, A.-K. Ström, A. Brederlau, A.-C. Illerskog, O. Nilsson, T. J. Kieffer, M. A. Hietala, A. Ricksten, and P. S. Eriksson. Glucose-Dependent Insulinotropic Polypeptide Is Expressed in Adult Hippocampus and Induces Progenitor Cell Proliferation. *The Journal of Neuroscience*, 25(7):1816–1825, 2005.

[222] T. O'Connor, K. R. Sadleir, E. Maus, R. A. Velliquette, J. Zhao, S. L. Cole, W. A. Eimer, B. Hitt, L. A. Bembinster, S. Lammich, S. F. Lichtenthaler, S. S. Hebert, B. De Strooper, C. Haass, D. A. Bennett, and R. Vassar. Phosphorylation of the translation initiation factor eif2α increases bace1 levels and promotes amyloidogenesis. *Neuron*, 60(6):988–1009, 2008.

[223] M. Ogata, S.-i. Hino, A. Saito, K. Morikawa, S. Kondo, S. Kanemoto, T. Murakami, M. Taniguchi, I. Tanii, K. Yoshinaga, S. Shiosaka, J. A. Hammarback, F. Urano, and K. Imaizumi. Autophagy is activated for cell survival after endoplasmic reticulum stress. *Molecular and Cellular Biology*, 26(24):9220–9231, 2006.

[224] M. Ohno. PERK as a hub of multiple pathogenic pathways leading to memory deficits and neurodegeneration in Alzheimer's disease. *Brain Research Bulletin*, *In Press*, 2017.

[225] K. Ohsawa, Y. Imai, H. Kanazawa, Y. Sasaki, and S. Kohsaka. Involvement of iba1 in membrane ruffling and phagocytosis of macrophages/microglia. *Journal of Cell Science*, 113(17):3073–3084, 2000.

[226] K. Ohta, A. Mizuno, S. Li, M. Itoh, M. Ueda, E. Ohta, Y. Hida, M. X. Wang, M. Furoi, Y. Tsuzuki, M. Sobajima, Y. Bohmoto, T. Fukushima, M. Kobori, T. Inuzuka, and T. Nakagawa. Endoplasmic reticulum stress enhances gamma-secretase activity. *Biochem Biophys Res Commun*, 416(3-4):362–6, 2011.

[227] T. Okuno, M. Matsuoka, T. Sumizawa, and H. Igisu. Involvement of the extracellular signal-regulated protein kinase pathway in phosphorylation of p53 protein and exerting cytotoxicity in human neuroblastoma cells (sh-sy5y) exposed to acrylamide. *Archives of Toxicology*, 80(3):146–153, 2006.

[228] F. J. Oliver, G. de la Rubia, V. Rolli, M. C. Ruiz-Ruiz, G. de Murcia, and J. M.-d. Murcia. Importance of poly(ADP-ribose) polymerase and its cleavage in apoptosis: Lesson from an uncleavable mutant. *journal of Biological Chemistry*, 273(50):33533–33539, 1998.

[229] S. Paillusson, P. Gomez-Suaga, R. Stoica, D. Little, P. Gissen, M. J. Devine, W. Noble, D. P. Hanger, and C. C. J. Miller. α-synuclein binds to the ER–mitochondria tethering protein VAPB to disrupt Ca^{2+} homeostasis and mitochondrial ATP production. *Acta Neuropathologica*, 134(1):129–149, 2017.

[230] M. Pajares, A. Cuadrado, and A. I. Rojo. Modulation of proteostasis by transcription factor NRF2 and impact in neurodegenerative diseases. *Redox Biology*, 11:543–553, 2017.

[231] M. Pajares, N. Jiménez-Moreno, Á. J. García-Yagüe, M. Escoll, M. L. de Ceballos, F. Van Leuven, A. Rábano, M. Yamamoto, A. I. Rojo, and A. Cuadrado. Tran-

scription factor NFE2L2/NRF2 is a regulator of macroautophagy genes. *Autophagy*, 12(10):1902–1916, 2016.

[232] T. Panagaki, M. Michael, and C. Hölscher. Liraglutide restores chronic ER stress, autophagy impairments and apoptotic signalling in SH-SY5Y cells. *Scientific Reports*, 7(1):16158, 2017.

[233] K. W. Park, S. E. Nozell, and E. N. Benveniste. Protective Role of STAT3 in NMDA and Glutamate-Induced Neuronal Death: Negative Regulatory Effect of SOCS3. *PLOS ONE*, 7(11):e50874, 2012.

[234] C. G. Parsons, A. Stoffler, and W. Danysz. Memantine: a NMDA receptor antagonist that improves memory by restoration of homeostasis in the glutamatergic system–too little activation is bad, too much is even worse. *Neuropharmacology*, 53(6):699–723, 2007.

[235] C. M. Pereira. Crosstalk between endoplasmic reticulum stress and protein misfolding in neurodegenerative diseases. *ISRN Cell Biology*, 2013:22, 2013.

[236] T. Perry, N. J. Haughey, M. P. Mattson, J. M. Egan, and N. H. Greig. Protection and reversal of excitotoxic neuronal damage by glucagon-like peptide-1 and exendin-4. *journal of Pharmacology and Experimental Therapeutics*, 302(3):881–888, 2002.

[237] T. Perry, D. K. Lahiri, K. Sambamurti, D. Chen, M. P. Mattson, J. M. Egan, and N. H. Greig. Glucagon-like peptide-1 decreases endogenous amyloid-β peptide (Aβ) levels and protects hippocampal neurons from death induced by Aβ and iron. *Journal of Neuroscience Research*, 72(5):603–612, 2003.

[238] T. Persson, B. O. Popescu, and A. Cedazo-Minguez. Oxidative stress in alzheimer's disease: why did antioxidant therapy fail? *Oxid Med Cell Longev*, 2014:318–427, 2014.

[239] F. Pickford, E. Masliah, M. Britschgi, K. Lucin, R. Narasimhan, P. A. Jaeger, S. Small, B. Spencer, E. Rockenstein, B. Levine, and T. Wyss-Coray. The autophagy-related protein beclin 1 shows reduced expression in early Alzheimer disease and regulates amyloid β accumulation in mice. *The Journal of Clinical Investigation*, 118(6):2190–2199, 2008.

[240] N. Pierrot, P. Ghisdal, A.-S. Caumont, and J.-N. Octave. Intraneuronal amyloid-β_{1-42} production triggered by sustained increase of cytosolic calcium concentration induces neuronal death. *Journal of Neurochemistry*, 88(5):1140–1150, 2004.

[241] F. Pietrocola, V. Izzo, M. Niso-Santano, E. Vacchelli, L. Galluzzi, M. C. Maiuri, and G. Kroemer. Regulation of autophagy by stress-responsive transcription factors. *Seminars in Cancer Biology*, 23(5):310–322, 2013.

[242] M. Prince, A. Wimo, M. Guerchet, A. Gemma–Claire, W. Yu–Tzu, and M. Prina. World Alzheimer Report 2015: The Global Impact of Dementia. *Alzheimer's Disease International (ADI)*, pages 1–92, 2015.

[243] L. Prut and C. Belzung. The open field as a paradigm to measure the effects of drugs on anxiety-like behaviors: a review. *European Journal of Pharmacology*, 463(1):3–33, 2003.

[244] C. Qiu, Y.-P. Wang, X.-D. Pan, X.-Y. Liu, Z. Chen, and L.-B. Liu. Exendin-4 protects A$\beta_{(1-42)}$ oligomer-induced PC12 cell apoptosis. *American Journal of Translational Research*, 8(8):3540–3548, 2016.

[245] L. Qu, S. Huang, D. Baltzis, A.-M. Rivas-Estilla, O. Pluquet, M. Hatzoglou, C. Koumenis, Y. Taya, A. Yoshimura, and A. E. Koromilas. Endoplasmic reticulum stress induces p53 cytoplasmic localization and prevents p53-dependent apop-

tosis by a pathway involving glycogen synthase kinase-3β. *Genes & Development*, 18(3):261–277, 2004.

[246] H. W. Querfurth and F. M. LaFerla. Alzheimer's disease. *The New England Journal of Medicine*, 362(4):329–44, 2010.

[247] R. Quiroz-Baez, P. Ferrera, R. Rosendo-Gutierrez, J. Moran, F. Bermudez-Rattoni, and C. Arias. Caspase-12 activation is involved in amyloid-β protein-induced synaptic toxicity. *J Alzheimers Dis*, 26(3):467–76, 2011.

[248] R. Radde, T. Bolmont, S. A. Kaeser, J. Coomaraswamy, D. Lindau, L. Stoltze, M. E. Calhoun, F. Jäggi, H. Wolburg, S. Gengler, C. Haass, B. Ghetti, C. Czech, C. Hölscher, P. M. Mathews, and M. Jucker. Aβ_{42}–driven cerebral amyloidosis in transgenic mice reveals early and robust pathology. *EMBO reports*, 7(9):940–946, 2006.

[249] O. A. Ramírez and A. Couve. The endoplasmic reticulum and protein trafficking in dendrites and axons. *Trends Cell Biol*, 21(4):219–227, 2011.

[250] C. P. Ramsey, C. A. Glass, M. B. Montgomery, K. A. Lindl, G. P. Ritson, L. A. Chia, R. L. Hamilton, C. T. Chu, and K. L. Jordan-Sciutto. Expression of Nrf2 in neurodegenerative diseases. *J Neuropathol Exp Neurol*, 66(1):75–85, 2007.

[251] S. Reinhardt, F. Schuck, S. Grosgen, M. Riemenschneider, T. Hartmann, R. Postina, M. Grimm, and K. Endres. Unfolded protein response signalling by transcription factor XBP-1 regulates ADAM10 and is affected in alzheimer's disease. *FASEB J*, 28(2):978–97, 2014.

[252] R. Resende, E. Ferreiro, C. Pereira, and C. R. Oliveira. Er stress is involved in Aβ-induced GSK-3β activation and tau phosphorylation. *J Neurosci Res*, 86(9):2091–9, 2008.

[253] A. Ricobaraza, M. Cuadrado-Tejedor, S. Marco, I. Perez-Otano, and A. Garcia-Osta. Phenylbutyrate rescues dendritic spine loss associated with memory deficits in a mouse model of alzheimer disease. *Hippocampus*, 22(5):1040–50, 2012.

[254] E. J. Rivera, A. Goldin, N. Fulmer, R. Tavares, J. R. Wands, and S. M. de la Monte. Insulin and insulin-like growth factor expression and function deteriorate with progression of Alzheimer's disease: link to brain reductions in acetylcholine. *Journal of Alzheimer's Disease*, 8(3):247–268, 2005.

[255] L. Ruan, Z. Kang, G. P. Le, and Yingying. Amyloid Deposition and Inflammation in $APP_{swe}/PS1\Delta$ E9 Mouse Model of Alzheimer's Disease. *Current Alzheimer Research*, 6(6):531–540, 2009.

[256] P. K. Sahoo, S. Soltani, and A. K. C. Wong. A survey of thresholding techniques. *Computer Vision, Graphics, and Image Processing*, 41(2):233–260, 1988.

[257] X. Sai, Y. Kawamura, K. Kokame, H. Yamaguchi, H. Shiraishi, R. Suzuki, T. Suzuki, M. Kawaichi, T. Miyata, T. Kitamura, B. De Strooper, K. Yanagisawa, and H. Komano. Endoplasmic reticulum stress-inducible protein, herp, enhances presenilin-mediated generation of amyloid β-protein. *J Biol Chem*, 277(15):12915–20, 2002.

[258] L. E. Santos and S. T. Ferreira. Crosstalk between endoplasmic reticulum stress and brain inflammation in Alzheimer's disease. *Neuropharmacology*, *In Press*, 2017.

[259] K. Sato, M. Kameda, T. Yasuhara, T. Agari, T. Baba, F. Wang, A. Shinko, T. Wakamori, A. Toyoshima, H. Takeuchi, T. Sasaki, S. Sasada, A. Kondo, C. V. Borlongan, M. Matsumae, and I. Date. Neuroprotective effects of liraglutide for stroke model of rats. *International journal of Molecular Sciences*, 14(11):21513–21524, 2013.

[260] D. Scholz, D. Pöltl, A. Genewsky, M. Weng, T. Waldmann, S. Schildknecht, and M. Leist. Rapid, complete and large-scale generation of post-mitotic neurons from the human LUHMES cell line. *Journal of Neurochemistry*, 119(5):957–971, 2011.

[261] M. Schroder and R. J. Kaufman. The mammalian unfolded protein response. *Annu Rev Biochem*, 74:739–89, 2005.

[262] D. J. Selkoe. Alzheimer's disease is a synaptic failure. *Science*, 298(5594):789–91, 2002.

[263] S. P. Selwood, S. Parvathy, B. Cordell, H. S. Ryan, F. Oshidari, V. Vincent, J. Yesavage, L. C. Lazzeroni, and J. Murphy, G. M. Gene expression profile of the pdapp mouse model for alzheimer's disease with and without apolipoprotein e. *Neurobiol Aging*, 30(4):574–90, 2009.

[264] K. I. Seyb, S. Ansar, J. Bean, and M. L. Michaelis. β-Amyloid and endoplasmic reticulum stress responses in primary neurons: effects of drugs that interact with the cytoskeleton. *J Mol Neurosci*, 28(2):111–23, 2006.

[265] M. K. Sharma, J. Jalewa, and C. Hölscher. Neuroprotective and anti-apoptotic effects of liraglutide on SH-SY5Y cells exposed to methylglyoxal stress. *journal of Neurochemistry*, 128(3):459–471, 2014.

[266] S. Sharma, J. E. Mells, P. P. Fu, N. K. Saxena, and F. A. Anania. Glp-1 analogs reduce hepatocyte steatosis and improve survival by enhancing the unfolded protein response and promoting macroautophagy. *PLOS ONE*, 6(9):1–13, 2011.

[267] H. Shen, X.-D. Pan, J. Zhang, Y.-Q. Zeng, M. Zhou, L.-M. Yang, B. Ye, X.-M. Dai, Y.-G. Zhu, and X.-C. Chen. Endoplasmic Reticulum Stress Induces the Early Appearance of Pro-apoptotic and Anti-apoptotic Proteins in Neurons of Five Familial Alzheimer's Disease Mice. *Chinese Medical Journal*, 129(23):2845–2852, 2016.

[268] C. M. Sherwin. The influences of standard laboratory cages on rodents and the validity of research data. *Animal Welfare*, 13(SUPPL.):S9–S15, 2004.

[269] L. Shi, Z. Zhang, L. Li, and C. Hölscher. A novel dual GLP-1/GIP receptor agonist alleviates cognitive decline by re-sensitizing insulin signaling in the Alzheimer icv. STZ rat model. *Behavioural Brain Research*, 327:65–74, 2017.

[270] S.-Y. Shieh, M. Ikeda, Y. Taya, and C. Prives. DNA damage-induced phosphorylation of p53 alleviates inhibition by MDM2. *Cell*, 91(3):325–334, 1997.

[271] T. Shinichiro, M. Nobukazu, Y. Kenji, T. Yasutaka, O. Hidenori, A. Hajime, H. Nobutaka, and U. Takao. Exendin-4, a glucagon-like peptide-1 receptor agonist, provides neuroprotection in mice transient focal cerebral ischemia. *journal of Cerebral Blood Flow & Metabolism*, 31(8):1696–1705, 2011.

[272] D. Shiraishi, Y. Fujiwara, Y. Komohara, H. Mizuta, and M. Takeya. Glucagon-like peptide-1 (GLP-1) induces M2 polarization of human macrophages via STAT3 activation. *Biochemical and Biophysical Research Communications*, 425(2):304–308, 2012.

[273] V. Shoshan-Barmatz, V. De Pinto, M. Zweckstetter, Z. Raviv, N. Keinan, and N. Arbel. VDAC, a multi-functional mitochondrial protein regulating cell life and death. *Molecular Aspects of Medicine*, 31(3):227–285, 2010.

[274] S. Shuling, T. Jin, M. Yuyang, L. Mengmeng, and Z. Qiang. Crosstalk of autophagy and apoptosis: Involvement of the dual role of autophagy under ER stress. *Journal of Cellular Physiology*, 232(11):2977–2984, 2017.

[275] M. V. Sofroniew and H. V. Vinters. Astrocytes: biology and pathology. *Acta Neuropathologica*, 119(1):7–35, 2010.

[276] L. Song, P. De Sarno, and R. S. Jope. Central role of glycogen synthase kinase-3β in endoplasmic reticulum stress-induced caspase-3 activation. *J Biol Chem*, 277(47):44701–8, 2002.

[277] S. Song, H. Lee, T. I. Kam, M. L. Tai, J. Y. Lee, J. Y. Noh, S. M. Shim, S. J. Seo, Y. Y. Kong, T. Nakagawa, C. W. Chung, D. Y. Choi, H. Oubrahim, and Y. K. Jung. E2-25k/hip-2 regulates caspase-12 in er stress-mediated aβ neurotoxicity. *J Cell Biol*, 182(4):675–84, 2008.

[278] T. L. Spires-Jones and B. T. Hyman. The intersection of amyloid β and tau at synapses in alzheimer's disease. *Neuron*, 82(4):756–771, 2014.

[279] L. R. Squire, J. T. Wixted, and R. E. Clark. Recognition memory and the medial temporal lobe: a new perspective. *Nature reviews. Neuroscience*, 8(11):872–883, 2007.

[280] E. Steen, B. M. Terry, E. J. Rivera, J. L. Cannon, T. R. Neely, R. Tavares, X. J. Xu, J. R. Wands, and S. M. de la Monte. Impaired insulin and insulin-like growth factor expression and signaling mechanisms in Alzheimer's disease–is this type 3 diabetes? *Journal of Alzheimer's Disease*, 7(1):63–80, 2005.

[281] R. A. Stetler, Y. Gao, L. Zhang, Z. Weng, F. Zhang, X. Hu, S. Wang, P. Vosler, G. Cao, D. Sun, S. H. Graham, and J. Chen. Phosphorylation of HSP27 by Protein Kinase D is Essential for Mediating Neuroprotection Against Ischemic Neuronal Injury. *The Journal of Neuroscience*, 32(8):2667–2682, 2012.

[282] N. V. Stiegler, A. K. Krug, F. Matt, and M. Leist. Assessment of Chemical-Induced Impairment of Human Neurite Outgrowth by Multiparametric Live Cell Imaging in High-Density Cultures. *Toxicological Sciences*, 121(1):73–87, 2011.

[283] L. D. Stutzbach, S. X. Xie, A. C. Naj, R. Albin, S. Gilman, V. M. Y. Lee, J. Q. Trojanowski, B. Devlin, and G. D. Schellenberg. The unfolded protein response

is activated in disease-affected brain regions in progressive supranuclear palsy and Alzheimer's disease. *Acta Neuropathologica Communications*, 1(31):1–13, 2013.

[284] G. E. Stutzmann and M. P. Mattson. Endoplasmic Reticulum Ca^{2+} Handling in Excitable Cells in Health and Disease. *Pharmacological Reviews*, 63(3):700–727, 2011.

[285] H. Sun, S. Knippenberg, N. Thau, D. Ragancokova, S. Körner, D. Huang, R. Dengler, K. Döhler, and S. Petri. Therapeutic potential of N-acetyl-glucagon-like peptide-1 in primary motor neuron cultures derived from non-transgenic and SOD1-G93A ALS mice. *Cellular and Molecular Neurobiology*, 33(3):347–357, 2013.

[286] M. Suzuki, Y. Nagai, K. Wada, and T. Koike. Calcium leak through ryanodine receptor is involved in neuronal death induced by mutant huntingtin. *Biochemical and biophysical research communications*, 429(1–2):18—23, 2012.

[287] T. Takadera, M. Fujibayashi, H. Kaniyu, N. Sakota, and T. Ohyashiki. Caspase-dependent apoptosis induced by thapsigargin was prevented by glycogen synthase kinase-3 inhibitors in cultured rat cortical neurons. *Neurochemical Research*, 32(8):1336–1342, 2007.

[288] K. Talbot, H.-Y. Wang, H. Kazi, L.-Y. Han, K. P. Bakshi, A. Stucky, R. L. Fuino, K. R. Kawaguchi, A. J. Samoyedny, R. S. Wilson, Z. Arvanitakis, J. A. Schneider, B. A. Wolf, D. A. Bennett, J. Q. Trojanowski, and S. E. Arnold. Demonstrated brain insulin resistance in Alzheimer's disease patients is associated with IGF-1 resistance, IRS-1 dysregulation, and cognitive decline. *The Journal of clinical investigation*, 122(4):1316–1338, 2012.

[289] I. A. Tamargo, M. Bader, Y. Li, S.-J. Yu, Y. Wang, K. Talbot, R. D. DiMarchi, C. G. Pick, and N. H. Greig. Novel GLP-1R/GIPR co-agonist "twincretin" is neu-

roprotective in cell and rodent models of mild traumatic brain injury. *Experimental Neurology*, 288:176–186, 2017.

[290] H. Tanila. The role of BDNF in Alzheimer's disease. *Neurobiology of Disease*, 97:114–118, 2017.

[291] J. Terry, A. V. and J. J. Buccafusco. The cholinergic hypothesis of age and alzheimer's disease-related cognitive deficits: recent challenges and their implications for novel drug development. *J Pharmacol Exp Ther*, 306(3):821–7, 2003.

[292] O. Thastrup, P. J. Cullen, B. K. Drobak, M. R. Hanley, and A. P. Dawson. Thapsigargin, a tumor promoter, discharges intracellular Ca^{2+} stores by specific inhibition of the endoplasmic reticulum Ca^{2+}-ATPase. *Proc Natl Acad Sci U S A*, 87(7):2466–2470, 1990.

[293] D. J. Todd, A.-H. Lee, and L. H. Glimcher. The endoplasmic reticulum stress response in immunity and autoimmunity. *Nature Reviews Immunology*, 8:663–674, 2008.

[294] W. Tong, L. Ju, M. Qiu, Q. Xie, Y. Chen, W. Shen, W. Sun, W. Wang, and J. Tian. Liraglutide ameliorates non-alcoholic fatty liver disease by enhancing mitochondrial architecture and promoting autophagy through the SIRT1/SIRT3–FOXO3α pathway. *Hepatology Research*, 46(9):933–943, 2016.

[295] T. Town, V. Nikolic, and J. Tan. The microglial "activation" continuum: from innate to adaptive responses. *Journal of Neuroinflammation*, 2(24):1–10, 2005.

[296] T. Uehara, T. Nakamura, D. Yao, Z. Q. Shi, Z. Gu, Y. Ma, E. Masliah, Y. Nomura, and S. A. Lipton. S-nitrosylated protein-disulphide isomerase links protein misfolding to neurodegeneration. *Nature*, 441(7092):513–7, 2011.

[297] T. Umeda, T. Tomiyama, N. Sakama, S. Tanaka, M. P. Lambert, W. L. Klein, and H. Mori. Intraneuronal amyloid β oligomers cause cell death via endoplasmic retic-

ulum stress, endosomal/lysosomal leakage, and mitochondrial dysfunction in vivo. *journal of Neuroscience Research*, 89(7):1031–1042, 2011.

[298] F. Urano, X. Wang, A. Bertolotti, Y. Zhang, P. Chung, H. P. Harding, and D. Ron. Coupling of Stress in the ER to Activation of JNK Protein Kinases by Transmembrane Protein Kinase IRE1. *Science*, 287(5453):664– 666, 2000.

[299] R. Vidal, B. Caballero, A. Couve, and C. Hetz. Converging pathways in the occurrence of endoplasmic reticulum (ER) stress in huntington's disease. *Current Molecular Medicine*, 11(1):1–12, 2011.

[300] C. V. Vorhees and M. T. Williams. Morris water maze: procedures for assessing spatial and related forms of learning and memory. *Nature protocols*, 1(2):848–858, 2006.

[301] J. Walter and C. Haass. Chapter 10 – posttranslational modifications of amyloid precursor protein. In *Alzheimer's Disease*, volume 32 of *Methods in Molecular Medicine*^{TM}, pages 149–168. Humana Press, 2000.

[302] J. Wang, J. Wu, H. Wu, X. Liu, Y. Chen, J. Wu, C. Hu, and D. Zou. Liraglutide protects pancreatic β-cells against free fatty acids in vitro and affects glucolipid metabolism in apolipoprotein E(−/−) mice by activating autophagy. *Molecular Medicine Reports*, 12(3):4210–4218, 2015.

[303] M. Wang and R. J. Kaufman. Protein misfolding in the endoplasmic reticulum as a conduit to human disease. *Nature*, 529:326–335, 2016.

[304] X. Wang and D. Ron. Stress-induced phosphorylation and activation of the transcription factor CHOP (GADD153) by p38 MAP kinase. *Science*, 272(5266):1347–1349, 1996.

[305] S. J. Webster, A. D. Bachstetter, P. T. Nelson, F. A. Schmitt, and L. J. Van Eldik. Using mice to model Alzheimer's dementia: an overview of the clinical disease and the preclinical behavioral changes in 10 mouse models. *Frontiers in Genetics*, 5(88):1–23, 2014.

[306] M. C. Wei, W.-X. Zong, E. H.-Y. Cheng, T. Lindsten, V. Panoutsakopoulou, A. J. Ross, K. A. Roth, G. R. MacGregor, C. B. Thompson, and S. J. Korsmeyer. Proapoptotic bax and bak: A requisite gateway to mitochondrial dysfunction and death. *Science*, 292(5517):727–730, 2001.

[307] H. Würbel. Ideal homes? Housing effects on rodent brain and behaviour. *Trends in Neurosciences*, 24(4):207–211, 2001.

[308] Y. Xu, Y. Diao, S. Qi, X. Pan, Q. Wang, Y. Xin, X. Cao, J. Ruan, Z. Zhao, L. Luo, C. Liu, and Z. Yin. Phosphorylated Hsp27 activates ATM-dependent p53 signaling and mediates the resistance of MCF-7 cells to doxorubicin-induced apoptosis. *Cellular Signalling*, 25(5):1176–1185, 2013.

[309] H. Yamaguchi, K. Bhalla, and H.-G. Wang. Bax plays a pivotal role in thapsigargin-induced apoptosis of human colon cancer HCT116 cells by controlling Smac/Diablo and Omi/HtrA2 release from mitochondria. *Cancer Research*, 63(7):1483–1489, 2003.

[310] H. Yamaguchi and H.-G. Wang. CHOP is involved in endoplasmic reticulum stress-induced apoptosis by enhancing DR5 expression in human carcinoma cells. *Journal of Biological Chemistry*, 279(44):45495–45502, 2004.

[311] Y. Yang, R. S. Turner, and J. R. Gaut. The chaperone bip/grp78 binds to amyloid precursor protein and decreases aβ_{40} and aβ_{42} secretion. *J Biol Chem*, 273(40):25552–5, 1998.

[312] Y. Yin, G. Sun, E. Li, K. Kiselyov, and D. Sun. ER stress and impaired autophagy flux in neuronal degeneration and brain injury. *Ageing Research Reviews*, 34:3–14, 2017.

[313] B. C. Yoo, S. H. Kim, N. Cairns, M. Fountoulakis, and G. Lubec. Deranged Expression of Molecular Chaperones in Brains of Patients with Alzheimer's Disease. *Biochemical and Biophysical Research Communications*, 280(1):249–258, 2001.

[314] S. O. Yoon, D. J. Park, J. C. Ryu, H. G. Ozer, C. Tep, Y. J. Shin, T. H. Lim, L. Pastorino, A. J. Kunwar, J. C. Walton, A. H. Nagahara, K. P. Lu, R. J. Nelson, M. H. Tuszynski, and K. Huang. Jnk3 perpetuates metabolic stress induced by aβ peptides. *Neuron*, 75(5):824–37, 2012.

[315] A. Yoshii and M. Constantine-Paton. BDNF induces transport of PSD-95 to dendrites through PI3K-AKT signaling after NMDA receptor activation. *Nature Neuroscience*, 10(6):702–711, 2007.

[316] Y. Yoshino, M. Ishisaka, S. Tsujii, M. Shimazawa, and H. Hara. Glucagon-like peptide-1 protects the murine hippocampus against stressors via Akt and ERK1/2 signaling. *Biochemical and Biophysical Research Communications*, 458(2):274–279, 2015.

[317] L. You, Z. Wang, H. Li, J. Shou, Z. Jing, J. Xie, X. Sui, H. Pan, and W. Han. The role of stat3 in autophagy. *Autophagy*, 11(5):729–739, 2015.

[318] C. W. Younce, M. A. Burmeister, and J. E. a. Ayala. Exendin-4 attenuates high glucose-induced cardiomyocyte apoptosis via inhibition of endoplasmic reticulum stress and activation of SERCA2a. *American journal of Physiology - Cell Physiology*, 304(6):C508–C518, 2013.

[319] M. S. Yu, K. C. Suen, N. S. Kwok, K. F. So, J. Hugon, and R. C. Chang. β-amyloid peptides induces neuronal apoptosis via a mechanism independent of unfolded protein responses. *Apoptosis*, 11(5):687–700, 2006.

[320] Z. Yuan, D. Li, P. Feng, G. Xue, C. Ji, G. Li, and C. Hölscher. A novel GLP-1/GIP dual agonist is more effective than liraglutide in reducing inflammation and enhancing GDNF release in the MPTP mouse model of Parkinson's disease. *European Journal of Pharmacology*, 812:82–90, 2017.

[321] K. Yuyama, S. Mitsutake, and Y. Igarashi. Pathological roles of ceramide and its metabolites in metabolic syndrome and Alzheimer's disease. *Biochimica et Biophysica Acta (BBA) - Molecular and Cell Biology of Lipids*, 1841(5):793–798, 2014.

[322] A. Zanotto-Filho, V. P. Masamsetti, E. Loranc, S. S. Tonapi, A. Gorthi, X. Bernard, R. M. Gonçalves, J. C. F. Moreira, Y. Chen, and A. J. R. Bishop. Alkylating AgentÐInduced NRF2 Blocks Endoplasmic Reticulum StressÐMediated Apoptosis via Control of Glutathione Pools and Protein Thiol Homeostasis. *Molecular Cancer Therapeutics*, 15(12):3000–3014, 2016.

[323] Y. Zhang, Y. Chen, L. Li, and C. Hölscher. Neuroprotective effects of $(Val^8)GLP-1-Glu-PAL$ in the MPTP parkinson's disease mouse model. *Behavioural Brain Research*, 293:107–113, 2015.

[324] Y. Zhang and Y. Xiong. A p53 amino-terminal nuclear export signal inhibited by DNA damage-induced phosphorylation. *Science*, 292(5523):1910–1915, 2001.

[325] X. Zhao, G. Liu, H. Shen, B. Gao, X. Li, J. Fu, J. Zhou, and Q. Ji. Liraglutide inhibits autophagy and apoptosis induced by high glucose through glp-1r in renal tubular epithelial cells. *International journal of Molecular Medicine*, 35(3):684–692, 2015.

[326] S.-W. Zhou, M. Zhang, and M. Zhu. Liraglutide reduces lipid accumulation in steatotic l-02 cells by enhancing autophagy. *Molecular Medicine Reports*, 10(5):2351–2357, 2014.

[327] H. Zhu, Y. Zhang, Z. Shi, D. Lu, T. Li, Y. Ding, Y. Ruan, and A. Xu. The neuroprotection of liraglutide against ischaemia-induced apoptosis through the activation of the PI3K/AKT and MAPK pathways. *Scientific Reports*, 6:26859, 2016.

[328] W.-X. Zong, T. Lindsten, A. J. Ross, G. R. MacGregor, and C. B. Thompson. Bh3-only proteins that bind pro-survival bcl-2 family members fail to induce apoptosis in the absence of bax and bak. *Genes & Development*, 15(12):1481–1486, 2001.

[329] Z.-H. Zong, Z.-X. Du, N. Li, C. Li, Q. Zhang, B.-Q. Liu, Y. Guan, and H.-Q. Wang. Implication of Nrf2 and ATF4 in differential induction of CHOP by proteasome inhibition in thyroid cancer cells. *Biochimica & Biophysica Acta (BBA) – Molecular Cell Research*, 1823(8):1395–1404, 2012.

Acknowledgements

Joining the Division of Biomedical and Life Sciences of Lancaster University for my PhD studies has been so far a valuable and unforgettable experience for me. I seize this opportunity to express my deep regards and sincere gratitude to all those people that have constantly supported me over that period and contributed to making this assignment possible.

I would like to express my deep sense of gratitude to Prof. Christian Hölscher who has offered me the opportunity to work on such an interesting research project. Thank you for your exemplary guidance, insightful comments, and constant encouragement. I would like to extend my sincere gratitude to the funding bodies Rosetrees Trust (UK) and the Alzheimer's Society (UK) for kindly supporting my research. .

A big thank to Dr. Simon Gengler for sharing his knowledge about animal breeding, animal handling and behavioural assessment with such a patience. Your valuable advice and constant support have helped me in expanding my knowledge and developing my skills in *in-vivo* regulated procedures and aspects. I am additionally indebted to Dr. Mohit K. Sharma and Jaishree Jalewa for teaching the art of ELISAs and immunoblotting. Thank for your immense encouragement and willingness to support me.

I am particularly thankful to Maria Michael for being a great neighbour, colleague and collaborator! I always enjoy our discussions over expensive cappuccinos. Your optimism and cheerfulness have been a source of hope in times of need. Many many thanks to all of my officemates and lab colleagues for the fruitful discussions and joyful breaks.

Lastly, I would like to thank my parents and siblings for all their love, encouragement and support in all my pursuits. And most of all, an immense appreciation is for my beloved, supportive, encouraging, and patient husband, Andreas, whose faith and endless support during this assignment got me this far.